ΕΘΝΙΚΟ ΜΕΤΣΟΒΙΟ ΠΟΛΥΤΕΧΝΕΙΟ

ΣΧΟΛΗ ΜΗΧΑΝΟΛΟΓΩΝ ΜΗΧΑΝΙΚΩΝ

ΑΝΑΠΤΥΞΗ ΠΑΡΕΜΒΑΤΙΚΩΝ ΚΑΙ ΜΗ, ΔΙΑΓΝΩΣΤΙΚΩΝ ΜΕΘΟΔΩΝ ΚΑΙ ΑΞΙΟΛΟΓΗΣΗ ΣΕ ΣΥΣΤΗΜΑΤΑ ΚΑΥΣΗΣ ΠΡΟΑΝΑΜΙΞΗΣ. ΕΦΑΡΜΟΓΗ ΣΕ ΚΑΥΣΤΗΡΑ ΠΟΡΩΔΟΥΣ ΑΔΡΑΝΟΥΣ ΜΕΣΟΥ

ΔΙΔΑΚΤΟΡΙΚΗ ΔΙΑΤΡΙΒΗ

ΧΡΗΣΤΟΥ Ν. ΚΕΡΑΜΙΩΤΗ

Διπλωματούχου Μηχανολόγου & Αεροναυπηγού Μηχανικού, ΜΔΕ ΕΜΠ

ΕΠΙΒΛΕΠΟΥΣΑ:
Μ. ΦΟΥΝΤΗ
Καθηγήτρια Ε.Μ.Π.

Αθήνα, Ιανουάριος 2013

ΕΘΝΙΚΟ ΜΕΤΣΟΒΙΟ ΠΟΛΥΤΕΧΝΕΙΟ

ΣΧΟΛΗ ΜΗΧΑΝΟΛΟΓΩΝ ΜΗΧΑΝΙΚΩΝ

ΑΝΑΠΤΥΞΗ ΠΑΡΕΜΒΑΤΙΚΩΝ ΚΑΙ ΜΗ ΔΙΑΓΝΩΣΤΙΚΩΝ ΜΕΘΟΔΩΝ ΚΑΙ ΑΞΙΟΛΟΓΗΣΗ ΣΕ ΣΥΣΤΗΜΑΤΑ ΚΑΥΣΗΣ ΠΡΟΑΝΑΜΙΞΗΣ. ΕΦΑΡΜΟΓΗ ΣΕ ΚΑΥΣΤΗΡΑ ΠΟΡΩΔΟΥΣ ΑΔΡΑΝΟΥΣ ΜΕΣΟΥ

ΔΙΔΑΚΤΟΡΙΚΗ ΔΙΑΤΡΙΒΗ

ΧΡΗΣΤΟΥ Ν. ΚΕΡΑΜΙΩΤΗ
Διπλωματούχου Μηχανολόγου & Αεροναυπηγού Μηχανικού, MSc.

ΤΡΙΜΕΛΗΣ ΣΥΜΒΟΥΛΕΥΤΙΚΗ ΕΠΙΤΡΟΠΗ:
1. Μ. ΦΟΥΝΤΗ, Καθ. Ε.Μ.Π. (Επιβλέπουσα)
2. Κ. ΡΑΚΟΠΟΥΛΟΣ, Καθ. Ε.Μ.Π.
3. Δ. ΧΟΥΝΤΑΛΑΣ, Καθ. Ε.Μ.Π.

ΕΠΤΑΜΕΛΗΣ ΕΞΕΤΑΣΤΙΚΗ ΕΠΙΤΡΟΠΗ:
1. Σ. ΚΑΡΕΛΛΑΣ, Επικ. Καθ. Ε.Μ.Π.
2. Δ. ΜΑΘΙΟΥΛΑΚΗΣ, Αν. Καθ. Ε.Μ.Π.
3. Ν. ΟΡΦΑΝΟΥΔΑΚΗΣ Καθ. Α.Τ.Ε.Ι. Χ.
4. Κ. ΡΑΚΟΠΟΥΛΟΣ, Καθ. Ε.Μ.Π.
5. Εμ. ΡΟΓΔΑΚΗΣ, Καθ. Ε.Μ.Π.
6. Μ.ΦΟΥΝΤΗ, Καθ. Ε.Μ.Π. (Επιβλέπουσα)
7. Δ. ΧΟΥΝΤΑΛΑΣ, Καθ. Ε.Μ.Π.

Αθήνα, Ιανουάριος 2013

Ανάπτυξη παρεμβατικών και μη, διαγνωστικών μεθόδων και αξιολόγηση σε συστήματα καύσης προανάμιξης. Εφαρμογή σε καυστήρα πορώδους αδρανούς μέσου

Development of intrusive and nonintrusive combustion diagnostic methodologies and assessment of premixed combustion systems. Implementation on a porous inert medium burner

Σύμφωνα με απόφαση της Γ.Σ.Ε.Σ. της Σχολής Μηχανολόγων Μηχανικών του Ε.Μ. Πολυτεχνείου στις 13/02/2012 η παρούσα Διατριβή γίνεται αποδεκτή στην Αγγλική γλώσσα, συνοδευόμενη από εκτενή περίληψη στην ελληνική.

....

Κεραμιώτης Ν. Χρήστος

Διπλωματούχος Μηχανολόγος και Αεροναυπηγός Μηχανικός της Πολυτεχνικής Σχολής του Πανεπιστημίου Πατρών (2006)

Μεταπτυχιακό Δίπλωμα Ειδίκευσης του Διατμηματικού Προγράμματος Μεταπτυχιακών Σπουδών Συστημάτων Αυτοματισμού του Ε.Μ.Π. (2008)

Στους γονείς μου,

την αδερφή μου Ελένη

και τους ανθρώπους που με τιμούν θεωρώντας με φίλο τους

***Προμηθεύς**[*]*	βραχεῖ δὲ μύθῳ πάντα συλλήβδην μάθε, πᾶσαι τέχναι βροτοῖσιν ἐκ Προμηθέως.	Και μ' ένα λόγο σύντομο σου λέω να ξέρεις· στον Προμηθέα χρωστούν οι άνθρωποι όλες τις τέχνες.
Χορός	μή νυν βροτοὺς μὲν ὠφέλει καιροῦ πέρα, σαυτοῦ δ' ἀκήδει δυστυχοῦντος. ὡς ἐγὼ εὔελπίς εἰμι τῶνδέ σ' ἐκ δεσμῶν ἔτι	Μα ενώ ωφελείς τον άνθρωπο πέρ' απ' το μέτρο, στη δυστυχία μην παρατάς μονάχα εσένα· μα εγώ έχω ελπίδα να λυθείς απ' τα δεσμά σου
(510)	λυθέντα μηδὲν μεῖον ἰσχύσειν Διός.	κι όχι πιο λίγη δύναμη απ' το Δία να πάρεις.
Προμηθεύς	οὔ ταῦτα ταύτῃ μοῖρά πω τελεσφόρος κρᾶναι πέπρωται, μυρίαις δὲ πημοναῖς δύαις τε καμφθεὶς ὧδε δεσμὰ φυγγάνω· τέχνη δ' ἀνάγκης ἀσθενεστέρα μακρῷ.	Δεν είν' γραφτό απ' τη μοίρα τέτοιο ακόμα τέλος αυτά να λάβουν, μα αφού δαμαστώ από μύρια βάσανα, τότε θα λυθώ, γιατί έχει η τέχνη πολύ πιο λίγη δύναμη απ' την ανάγκη.
Χορός	τίς οὖν ἀνάγκης ἐστὶν οἰακοστρόφος;	Και ποιος να κυβερνά το δοιάκι της ανάγκης;
Προμηθεύς	Μοῖραι τρίμορφοι μνήμονές τ' Ἐρινύες	Μοίρες οι τρεις κι οι Ερινύες που δεν ξεχνούνε.
Χορός	τούτων ἄρα Ζεύς ἐστιν ἀσθενέστερος;	Ώστε είναι πιο απ' αυτές αδύνατος ο Δίας;
Προμηθεύς	οὔκουν ἂν ἐκφύγοι γε τὴν πεπρωμένην.	Βέβαια να φύγει απ' το γραφτό δε θα ήταν τρόπος.
Χορός	τί γὰρ πέπρωται Ζηνὶ πλὴν ἀεὶ κρατεῖν;	Και τι άλλο του γραφτό παρά εξουσία αιώνια;
Προμηθεύς	τοῦτ' οὐκέτ' ἂν πύθοιο μηδὲ λιπάρει.	Μ' όλα τα παρακάλια αυτό δε θα το μάθεις.
Χορός	ἦ πού τι σεμνόν ἐστιν ὃ ξυναμπέχεις.	Μυστήριο θα 'ναι βέβαια που έτσι τα κρύβεις.
Προμηθεύς	ἄλλου λόγου μέμνησθε, τόνδε δ' οὐδαμῶς καιρὸς γεγωνεῖν, ἀλλὰ συγκαλυπτέος ὅσον μάλιστα· τόνδε γὰρ σῴζων ἐγὼ	Άλλη ομιλία ας αλλάζαμε, γιατί δεν είναι καιρός γι' αυτό το λόγο, που όσο πιο κρυμμένος πρέπει να μένει·κι έτσι μόνο αν τον φυλάγω,
(525)	δεσμοὺς ἀεικεῖς καὶ δύας ἐκφυγγάνω.	απ' τ' άπρεπα δεσμά και πάθη θα γλιτώσω.

The pioneering experiments in combustion research, some 600000 years ago, were concerned with flame propagation. The initial ignition source was provided by Mother Nature in the form of the electrical discharge plasma of a thunderstorm or as volcanic lava, depending on location (Weinberg, 1975[†]). *Prometheus has been identified as the mythological deliverer of combustion science to mankind* (Williams, 1992[‡]). *Since sciences have been traditionally divided into experimental and theoretical, a question arises naturally: Was Prometheus more nearly an experimenter or a theoretician?*

---

[*] Αἰσχύλου Προμηθεὺς Δεσμώτης, Β' Επεισόδιο, μετάφραση: Ι. Γρυπάρη.

[†] Weinberg FJ. The first half-million years of combustion research and today's burning problems. *15th Symposium (International) on Combustion* 1975;15:1–17.

[‡] Williams FA. The role of theory in combustion science. *24th Symposium (International) on Combustion* 1992;24: 1-17.

Ευχαριστίες

Περίληψη

Η παρούσα διατριβή στοχεύει στην ανάπτυξη διαγνωστικών εργαλείων για τη μέτρηση εκπομπών από φαινόμενα καύσης και την εφαρμογή τους σε συστήματα καύσης προανάμιξης βαθμωτής πολυπλοκότητας. Αρχικά, αναδεικνύεται η αναγκαιότητα και το πεδίο εφαρμογής των διαγνωστικών μεθόδων καύσης και οι χρησιμοποιούμενες τεχνικές αναλύονται και σχολιάζονται. Το πρώτο μέρος της διατριβής επεξηγεί τις αρχές λειτουργίας, τη θεμελιώδη θεωρία και τα βασικά συστατικά των χρησιμοποιηθέντων τεχνικών. Σε αυτές περιλαμβάνονται το σύστημα της αέριας χρωματογραφίας, το σύστημα συνεχούς ανάλυσης καυσαερίων, καθώς επίσης και το σύστημα για φασματοσκοπία φθορισμού επαγόμενου από διέγερση με χρήση ακτινοβολίας laser. Το πρώτο μέρος της διατριβής παρέχει το απαραίτητο υπόβαθρο για το σχεδιασμό, την εκτέλεση και την κατανόηση των αποτελεσμάτων κι υπό αυτό το πρίσμα, καθίσταται απαραίτητο συστατικό της.

Στο δεύτερο σκέλος της διατριβής, τα διαγνωστικά εργαλεία χρησιμοποιούνται για τη μελέτη διατάξεων χαμηλής πολυπλοκότητας, στοχεύοντας αφενός στην αξιολόγηση των διαγνωστικών μεθόδων και αφετέρου στη διεξαγωγή πρωτότυπης έρευνας, συνδεόμενης με υπαρκτά ζητήματα στο πεδίο των συστημάτων καύσης. Υπό αυτό το πρίσμα, η τεχνική της αέριας χρωματογραφίας επιστρατεύτηκε για την ποσοτικοποίηση αερίων αλλά και επιλεγμένων πολυκυκλικών αρωματικών υδρογονανθράκων, που ευρίσκονται στα προϊόντα της πυρόλυσης μιγμάτων μεθανίου σε αντιδραστήρα εμβολικής ροής. Τα αποτελέσματα αναπαρήχθησαν με δυο μηχανισμούς λεπτομερούς χημείας, για την πληρέστερη κατανόηση των διεργασιών, με ικανοποιητική συμφωνία υπολογιστικών προλέξεων και πειραματικών δεδομένων. Εν συνεχεία, η τεχνική της φασματοσκοπίας φθορισμού επαγόμενου από διέγερση laser εφαρμόστηκε για τη μελέτη φλόγας προανάμιξης εγκάρσιας ροής. Η ψυχρή ροή μελετήθηκε ιχνηλατώντας μόρια ακετόνης στη ροή του καυσίμου και τα χαρακτηριστικά του σχήματος της φλόγας αναλύθηκαν μέσω της παρακολούθησης της ρίζας του υδροξυλίου στη ζώνη καύσης.

Μέσω της εκμετάλλευσης συμβατικών πηγών ενέργειας, όπως το φυσικό αέριο και ο γαιάνθρακας, δύνανται μέσω της διεργασίας Fischer-Tropsch να προκύψουν εναλλακτικά καύσιμα, συμβατά με τις υπαρκτές υποδομές. Στο έκτο κεφάλαιο της διατριβής, αεροπορικά καύσιμα της ανωτέρω προέλευσης, εξετάζονται με τη χρήση ενός εργαστηριακού καυστήρα προανάμιξης. Μετρήσεις θερμοκρασίας και καυσαερίων, σε συνδυασμό με μια αναλυτική μεθοδολογία για τον υπολογισμό των θερμοχημικών ιδιοτήτων βάσει της αναλυτικής χημικής σύστασης, κατέστησαν εφικτή την αξιολόγηση των καυσίμων και τη συσχέτιση της απόδοσης, με τα περιεχόμενα συστατικά τους.

Τελικώς, οι προαναφερθείσες παρεμβατικές και μη τεχνικές, συνδυάστηκαν για τον χαρακτηρισμό ενός καυστήρα υψηλής πολυπλοκότητας (καυστήρας πορώδους αδρανούς μέσου). Η οπτικοποίηση της φλόγας μέσα στο πορώδες, μέσω της τεχνικής φασματοσκοπίας φθορισμού επαγόμενου από διέγερση laser και συγκεκριμένα της παρακολούθησης της ρίζας του υδροξυλίου στη ζώνη καύσης, ανέδειξε της περιοχές λειτουργίας του συναρτήσει του θερμικού φορτίου και της στοιχειομετρίας. Εν κατακλείδι, διεξήχθη πλήρης πολυπαραμετρικός χαρακτηρισμός του πορώδους καυστήρα και αναλύθηκε η ικανότητα του για λειτουργία με συμβατικά και εναλλακτικά καύσιμα.

Abstract

The present thesis aims at the development and validation of intrusive and nonintrusive combustion diagnostic techniques and their implementation in premixed combustion systems. The work may be divided in three main directions. Firstly, the necessity and applicability of combustion diagnostics is discussed and the developed methodologies are presented. This part, presented in the 1st, 2nd and 3rd chapter, describes the operating principles, the fundamental theory and the basic components of gas chromatographic and continuous analysis systems, as well as the fundamentals of laser spectroscopy and the theoretical considerations for laser induced fluorescence measurements. The latter diagnostic tools were utilized to investigate combustion phenomena of varying complexity. The scope of the first part is to provide a comprehensive support to the experimental investigations presented in the next chapters and it is an essential part of the thesis that assists the planning, execution and interpretation of experiments.

In the second part of the thesis the developed diagnostic tools are firstly implemented in configurations with generally moderate degree of complexity. The research work implements the discussed diagnostic tools focusing on the evaluation of their performance, and at the same time innovative research is conducted pertaining to practical combustion problems. Gas chromatographic measurements were conducted in a plug flow reactor; gaseous products up to toluene were quantified for methane mixtures pyrolysis. The results were reproduced by two detailed chemical kinetic models, with satisfactory agreement. In addition, soot and selected polycyclic aromatic hydrocarbons were monitored in order to obtain a more complete picture of the underlying processes. The laser induced fluorescence system was utilized for the study of a simple premixed laminar cross-flow flame, whereby its shape characteristics were discussed using hydroxyl radical and acetone-tracer measurements.

As the work mainly focuses on the investigation of flames produced by conventional fuels, a chapter is devoted in examining potential drop-in fuels, which may originate from natural gas or coal feedstock through the Fischer-Tropsch process. In this context, a simple premixed laboratory flame burner was utilized in order to investigate the performance of virtually similar aviation fuels of high complexity. Aviation fuels have to meet strict criteria with respect to physico-chemical properties and this induces additional challenge to the work. Temperature and emission measurements were combined with an analytical methodology that aimed at the systematic evaluation of the different fuels, facilitating the assignment of combustion trends to the constituent compounds.

Finally, intrusive and nonintrusive tools were combined in order to fully characterize stable species as well as radical concentrations from a complex combustor, as is the porous burner. Initially, hydroxyl radical – laser induced fluorescence imaging experiments were performed in order to parametrically examine the burner operating regimes, through the visualization of the flame zone inside the porous media. Subsequently, the burner stability, emission characterization and fuel interchangeability with conventional as well as alternative fuels, was thoroughly tested with respect to nominal thermal loads and stoichiometries.

Prologue

The present thesis focuses on the development and implementation of diagnostic techniques in combustion research. The carried out experimental campaigns, took place mainly in the laboratory of Heterogeneous Mixtures and Combustion Systems of the National Technical University of Athens (HMCS-NTUA), under the supervision of Prof. Dr. Maria Founti. Nonetheless, an important part of the work was undertaken in other institutes which ought to be acknowledged.

The experiments on the flow reactor, presented in the 4th chapter were carried out at the Aragon institute of Engineering research of the University of Saragossa in Spain (Instituto de Investigación en Ingeniería de Aragón, Universidad de Zaragoza) under the supervision of Prof. Dr. Maria Uxue Alzueta. Moreover, the supplemental investigation of PAH species was performed at the same Institute with the valuable assistance of Ms. Nazly Sánchez. The Cooperation in Science and Technology–COST Project is acknowledged for supporting this scientific mission.

The experimental campaign concerning laser induced fluorescence measurements, presented in the 5th and partially in the 7th chapter, was realized at the chair of Gas and Heat Technology of the Institute of Thermal Engineering, (Institut für Wärmetechnik und Thermodynamik Lehrstuhl für Gas- und Wärmetechnische Anlagen), of the T.U. Bergakademie Freiberg in Germany, under the supervision of Prof. Dr-Ing Demosthenes Trimis. During this experimental mission, Dipl-Ing Björn Stelzner, Dipl-Ing Martin Werner and Dipl-Ing Stefan Voß provided indispensable assistance.

Finally, the fuel blends and the burner assembly presented in the 6th chapter were provided by Shell Global Solutions. The contribution of the laboratory of Thermal Turbomachines of the National Technical University of Athens (LTT-NTUA) and Prof. Dr. K. Mathioudakis is also acknowledged.

Table of Contents

List of Figures

5

List of tables

Περίληψη εκτενούς περιεχομένου στην Ελληνική γλώσσα

Το παρόν αποτελεί εκτενή περίληψη του κυρίως στελέχους στην ελληνική γλώσσα και αποτελεί ενιαίο και αναπόσπαστο κομμάτι της διατριβής. Η αρίθμηση σχημάτων, πινάκων και εξισώσεων, τα οποία για λόγους οικονομίας χώρου δεν επαναλαμβάνονται, έχει πλήρως διατηρηθεί μεταξύ κυρίως κειμένου και περίληψης. Επιπροσθέτως οι βιβλιογραφικές παραπομπές αντιστοιχούν, προς ευκολία του αναγνώστη, στη συνολική βιβλιογραφία όπως παρατίθεται στο τέλος της διατριβής.

Κεφάλαιο 1ο – Δομή, περιεχόμενο και καινοτομία της διατριβής

Ο άνθρωπος αναγκάστηκε να τιθασεύσει την τέχνη της φλόγας από τις πρώτες στιγμές που άρχισε να ζει σε οργανωμένες κοινωνίες. Έκτοτε, η επιστήμη της καύσης χρησιμοποιείται κατεξοχήν για την εκμετάλλευση των συμβατικών πηγών ενέργειας. Για αρκετές δεκαετίες η ενεργειακή ζήτηση και οι τιμές των καυσίμων ήταν αρκετά χαμηλές. Η μείωση των συμβατικών ενεργειακών αποθεμάτων και η αύξηση του παγκόσμιου πληθυσμού οδηγεί στην όξυνση του ενεργειακού ζητήματος. Προς επίλυση του ενεργειακού ζητήματος, ένα μεγάλο κομμάτι της παγκόσμιας ερευνητικής δραστηριότητας επικεντρώνεται στην αναζήτηση και βελτιστοποίηση τεχνολογιών ανανεώσιμων πηγών ενέργειας. Παρόλα αυτά, η πλειονότητα των εφαρμογών παραγωγής ηλεκτρικής ενέργειας βιομηχανικών εφαρμογών και μεταφορών, που στηρίζουν τα θεμέλια της σύγχρονης οικονομικής και κοινωνικής ζωής, εξακολουθεί και θα εξακολουθεί (*Σχήμα* 1.1 – *σελ.* 50) να στηρίζεται στην τεχνολογία της καύσης. Στις ανωτέρω εφαρμογές η χημική ενέργεια των ορυκτών καυσίμων όπως ο γαιάνθρακας, το πετρέλαιο ή το φυσικό αέριο, μετατρέπεται σε θερμότητα ή έργο, μέσω της οξείδωσης με το περιεχόμενο στον αέρα οξυγόνο. Καθώς η διαθεσιμότητα των ορυκτών καυσίμων είναι πεπερασμένη, είναι αναγκαία η ανάπτυξη εναλλακτικών καυσίμων (είτε προέλευσης ανανεώσιμων πηγών ή συνθετικών καυσίμων) και νέων τεχνολογιών όπως οι κυψέλες καυσίμου. Ωσότου όμως οι νέες τεχνολογίες φτάσουν σε ώριμο επίπεδο, κρίνεται αναγκαία η συντήρηση, ανάπτυξη και βελτιστοποίηση των υπαρχουσών τεχνολογιών καύσης. Αναμφισβήτητα, για την επίτευξη αυτών των στόχων είναι αναγκαία η βαθύτερη κατανόηση των φαινομένων καύσης. Η εις βάθος κατανόηση των πολύπλοκων φαινομένων που διέπουν τις χημικά αντιδρώσες ροές, οδηγεί στη βελτιστοποίηση των σύγχρονων συστημάτων καύσης και κατά συνέπεια στη μείωση του περιβαλλοντικού τους αποτυπώματος. Αυτό αναλύεται πλην των αερίων του θερμοκηπίου, όπως το διοξείδιο του άνθρακα, σε οξείδια του θείου και του αζώτου, πολυκυκλικούς αρωματικούς υδρογονάνθρακες και αιθάλη, τα οποία είναι ιδιαιτέρως επιβλαβή για την υγεία του ατόμου.

Η καύση είναι το αποτέλεσμα χωροχρονικά δυναμικών αλληλεπιδράσεων σε μοριακό κι ατομικό επίπεδο, που καθορίζουν την ενεργειακή απόδοση, τους ρύπους, την κατανάλωση καυσίμου και την εν γένει λειτουργία και αξιοπιστία ενός συστήματος καύσης. Ο σχεδιασμός σύγχρονων συστημάτων καύσης βασίζεται ολοένα και περισσότερο στην υπολογιστική προσομοίωση. Τα υπολογιστικά εργαλεία αναπτύσσονται αξιοποιώντας τα πειραματικά δεδομένα μετρήσεων

πεδίων ταχύτητας, θερμοκρασίας, συγκέντρωσης χημικών ενώσεων και μεγέθους σωματιδίων παρεχόμενα από την εφαρμογή πληθώρας διαγνωστικών εργαλείων. Τα υπολογιστικά εργαλεία τροφοδοτούνται συνεχώς με δεδομένα για τη ροή και τη χημεία της καύσης μέσω των αντίστοιχων πειραματικών διερευνήσεων, πράγμα που οδηγεί στην αποδοτικότερη, με όρους χρόνου και κόστους, λειτουργία τους. Προφανώς, η ανάπτυξη και βελτιστοποίηση των υπολογιστικών εργαλείων είναι αλληλένδετα συνδεδεμένη με την πρόοδο των αντίστοιχων πειραματικών διαγνωστικών μεθόδων. Ωστόσο, τα υπολογιστικά εργαλεία σήμερα δε δύνανται να μοντελοποιήσουν σε πλήρη έκταση τη αλληλουχία των σύνθετων φαινομένων που λαμβάνουν χώρα λ.χ στις σύγχρονες μηχανές[62]. Συνεπώς, η εκτενής πειραματική διερεύνηση αποτελεί μονόδρομο για την περεταίρω ανάπτυξη και βελτιστοποίηση των συστημάτων καύσης καθώς επίσης και τη βαθύτερη κατανόηση των θεμελιωδών φαινομένων που διέπουν τη διεργασία της καύσης. Σε αυτά τα πλαίσια η παρούσα διατριβή στοχεύει στην ανάπτυξη διαγνωστικών εργαλείων για φαινόμενα καύσης και κατ' επέκταση την εφαρμογή τους σε συστήματα καύσης προανάμιξης βαθμωτής πολυπλοκότητας.

Καύση, καύσιμα και συστήματα καυστήρες προανάμιξης

Η επιλογή καυσίμου είναι μια πολυεπίπεδη διαδικασία καθώς ιδεατά οφείλει να πληροί αλληλοσυγκρουόμενες απαιτήσεις. Οι απαιτήσεις αυτές είναι το υψηλό ενεργειακό περιεχόμενο, ο υψηλός ρυθμός έκλυσης ενέργειας, η ευκολία αεριοποίησης, η σταθερότητα αποθήκευσης και το μειωμένο περιβαλλοντικό αποτύπωμα. Αντιστοίχως, το υποψήφιο καύσιμο οφείλει να παρουσιάζει υψηλή θερμογόνο ικανότητα και ενεργειακή πυκνότητα, ικανοποιητική θερμική ευστάθεια, χαμηλή τάση ατμών, χωρίς ταυτόχρονα να είναι τοξικό[196]. Τα αέρια καύσιμα, εν γένει πλεονεκτούν υπό τη σκοπιά της προαναμεμιγμένης και πιο ομογενοποιημένης προσαγωγής στο θάλαμο καύσης, που υπό της κατάλληλες συνθήκες λειτουργίας παράγει μειωμένους ρύπους και επικαθήσεις, μειονεκτώντας ταυτόχρονα σε ζητήματα αποθήκευσης και μεταφοράς, τα οποία είναι αναγκαία λόγου χάριν στην αυτοκινητοβιομηχανία. Απεναντίας, τα ευρέως διαδεδομένα υγρά καύσιμα, παρουσιάζουν υψηλό κατ' όγκο ενεργειακό περιεχόμενο, όντας ταυτόχρονα ασφαλή στη μεταφορά και αποθήκευση, εισάγοντας όμως περεταίρω απαιτήσεις για την ανάμιξη και ατμοποίηση τους. Τα στερεά καύσιμα συμπεριλαμβάνουν είδη ξυλείας, βιομάζας και γαιανθράκων και αποτελούν φθηνή και άμεσα διαθέσιμη πηγή ενέργειας, αλλά ως επί το πλείστον προορίζονται για μεγάλης κλίμακας εγκαταστάσεις. Επιπλέον, περιέχουν τέφρα, υγρασία και θειούχες, αζωτούχες και οξυγονούχες ενώσεις, οι οποίες συμβάλουν στη δημιουργία ρύπων και άλλων επιβλαβών ενώσεων για την εγκατάσταση[205].

Η άνοδος των τιμών των συμβατικών καυσίμων και η μείωση των διαθέσιμων αποθεμάτων, στρέφουν το ενδιαφέρον της επιστημονικής έρευνας στην ανάπτυξη εναλλακτικών καυσίμων που θα υποκαθιστούν τα υπάρχοντα, με ελάχιστες μετατροπές στην υπάρχουσα υποδομή. Συνεπώς, τα εναλλακτικά καύσιμα οφείλουν να υπακούν στις ίδιες προδιαγραφές με τα συμβατικά σε ότι αφορά στις φυσικές αλλά και θερμοχημικές τους ιδιότητες. Ωστόσο, τα σύγχρονα εναλλακτικά καύσιμα περιέχουν εν δυνάμει πολύπλοκες ενώσεις όπως ακόρεστοι και οξυγονωμένοι υδρογονάνθρακες, αλκοόλες κι εστέρες. Αυτό συνεπάγεται ότι οι χημικές διαδρομές αυτών των καυσίμων πρέπει να προσδιοριστούν με ακρίβεια, για την ανάπτυξη, το σχεδιασμό και τη βελτιστοποίηση των συστημάτων καύσης. Υπό αυτό το πρίσμα, οι πειραματικές διερευνήσεις εναλλακτικών καυσίμων πραγματώνονται σε δύο κυρίως άξονες: αφενός για να επιβεβαιώσουν ότι

10

το υποψήφιο καύσιμο είναι λειτουργικό στα υπάρχοντα συστήματα και μηχανές (μηχανές εσωτερικής καύσης, στροβιλομηχανές κ.α.) και αφετέρου για τη μελέτη θεμελιωδών χαρακτηριστικών του υποψήφιου καυσίμου σε πρότυπες διατάξεις εργαστηριακού περιβάλλοντος, όπως αντιδραστήρες εμβολικής ροής ή τέλειας ανάδευσης. Η παρούσα διατριβή αφιερώνει το 6ο κεφάλαιο για τη μελέτη εναλλακτικών αεροπορικών καυσίμων, τα οποία είναι τα πιο απαιτητικά από πλευράς φυσικο-χημικών ιδιοτήτων, με τα ανεπτυγμένα διαγνωστικά εργαλεία.

Οι σύγχρονη νομοθεσία απαιτεί μειωμένες τιμές ρύπων από τα συστήματα καύσης χωρίς όμως να διακυβεύεται η απόδοση τους, όπως επιτάσσει η οικονομική βιωσιμότητα τους. Η ταυτόχρονη μείωση του μονοξείδιου του άνθρακα και των οξειδίων του αζώτου, όντας αυτοί οι κυριότεροι ρύποι, είναι πρακτικά δύσκολη διαδικασία καθώς οι απαιτούμενες υψηλές θερμοκρασίας για πληρέστερη καύση με χαμηλότερα επίπεδα μονοξείδιου του άνθρακα, δρουν καταλυτικά για το σχηματισμό θερμικών οξειδίων του αζώτου. Οι δύο τύποι φλογών, κατ' επέκταση και καυστήρων, είναι οι φλόγες διάχυσης και προανάμιξης. Οι καυστήρες προανάμιξης παρέχοντας πιο ομογενοποιημένο μίγμα καυσίμου-οξειδωτικού, ενδείκνυνται για εφαρμογές ήπιου περιβάλλοντος καύσης[55], σε πιο χαμηλές θερμοκρασίες. Στις φλόγες προανάμιξης, το καύσιμο και το οξειδωτικό εισάγονται στο θάλαμο καύσης προαναμεμιγμένα κι αυτό καθιστά τη φλόγα προανάμιξης μια ταχεία, ουσιαστικά ισοβαρή, εξώθερμη αντίδραση μεταξύ καυσίμου και οξειδωτικού[42]. Οι καυστήρες προανάμιξης χρίζουν ιδιαιτέρου σχεδιασμού, ιδιαιτέρως σε περιπτώσεις προθέρμανσης, καθώς υπάρχει εν δυνάμει αναφλέξιμο μίγμα πριν από το θάλαμο καύσης. Ωστόσο, οι εφαρμογές των καυστήρων προανάμιξης σε περιβάλλον μη εκτεθειμένης φλόγας[339] δίδει την ευκαιρία για υψηλούς βαθμούς απόδοσης και ταυτόχρονα χαμηλές εκπομπές ρύπων. Σε αυτό το πλαίσιο η παρούσα διατριβή εξετάζει ένα σύστημα πορώδους καυστήρα προανάμιξης (κεφάλαιο 7), συνδυάζοντας τις διαγνωστικές μεθόδους που αναλύονται στα επόμενα κεφάλαια, με σκοπό τον πλήρη χαρακτηρισμό της λειτουργίας, συναρτήσει του επιβαλλόμενου θερμικού φορτίου, της στοιχειομετρίας και του καυσίμου.

Διαγνωστική φαινομένων καύσης. Παρεμβατικές και μη τεχνικές για μετρήσεις κύριων και δευτερευουσών προϊόντων καύσης

Η καύση είναι το σύνολο σύνθετων, πολυδιάστατων αλληλεπιδράσεων φαινομένων χημικής κινητικής και ρευστομηχανικής. Η διαγνωστική των φαινομένων καύσης συμβάλει στη θεμελιώδη κατανόηση της λειτουργίας ενός συστήματος και κατ' επέκταση των κύριων μηχανισμών παραγωγής ρύπων. Η επιστήμη της διαγνωστικής φαινομένων καύσης απαιτεί υψηλό θεωρητικό υπόβαθρο και υψηλά επίπεδα σχεδιασμού και λειτουργικότητας, καλύπτοντας από απλές εφαρμογές εργαστηριακής κλίμακας έως μηχανές εσωτερικής καύσης, αεροστρόβιλους και εγκαταστάσεις βιομηχανικής κλίμακας και υψηλών πιέσεων[157]. Πρωτίστως, οι λεπτομερείς μετρήσεις χημικών ειδών, θερμοκρασιακών και ροϊκών πεδίων και σωματιδίων παρέχουν την αναγκαία πληροφορία για τις υποβόσκουσες διεργασίες και τροφοδοτούν τα υπολογιστικά μοντέλα με δεδομένα για την επικύρωση τους. Η κατανόηση των διεργασιών που διέπουν τα φαινόμενα καύσης, οδηγούν στη βελτιστοποίηση της απόδοσης με την ελάχιστη δυνατή κατανάλωση καυσίμου και σημαντικά μειωμένους ρύπους. Υπό αυτή την έννοια, η διαγνωστική σε φαινόμενα καύσης είναι απαράμιλλος κρίκος της αλυσίδας του σχεδιασμού και της ανάπτυξης νέων και καθαρότερων τεχνολογιών καύσης. Επιπροσθέτως, τεχνικά ζητήματα που προκύπτουν από τη σύζευξη καινοτόμων μηχανών και καυσίμων κατανοούνται και λύνονται σχεδόν

11

αποκλειστικά με την εφαρμογή διαγνωστικών μεθόδων. Επίσης, ένα σημαντικό κομμάτι των εφαρμογών της διαγνωστικής των συστημάτων καύσης είναι ταυτίζεται με την επίβλεψη και τον έλεγχο θερμικών διεργασιών προς αποφυγή και εξάλειψη των συνεπειών της αστάθειας της καύσης[81]. Ο έλεγχος της διεργασίας της καύσης είναι αναγκαίος για τη μείωση των ρύπων, ειδικότερα όταν ενσωματώνονται τεχνολογίες ανακυκλοφορίας και εκμετάλλευσης των καυσαερίων ή όταν η λειτουργία του συστήματος γίνεται σε καθεστώτα κοντά στα όρια αναφλεξιμότητας, όπως στην περίπτωση της εξαιρετικά πτωχής σε καύσιμο καύσης.

Οι παρεμβατικές διαγνωστικές μέθοδοι χρησιμοποιούν μία γραμμής δειγματοληψίας, για να οδηγήσουν το δείγμα στον αναλυτή, η απόληξη της οποίας διαταράσσει αεροδυναμικά, θερμικά και χημικά σε τοπικό επίπεδο τα υπό μελέτη φαινόμενα[173]. Οι παρεμβατικές μέθοδοι, εφόσον απομονώνουν το δείγμα, συνδυάζουν εν δυνάμει μία πληθώρα αρχών ανίχνευσης όπως της αέριας χρωματογραφίας, ή της φασματοσκοπίας μάζας, η οποίες αποτελούν μονόδρομο στην ανάλυση πολύπλοκων ενώσεων, αλλά μειονεκτούν παρέχοντας περιορισμένη χωρική και χρονική διακριτική ικανότητα. Αναλόγως της αρχής λειτουργίας του ανιχνευτή οι μέθοδοι χαρακτηρίζονται σε καταστρεπτικές ή μη, κατηγοριοποίηση που δεν πρέπει να συγχέεται με τους όρους παρεμβατικός ή μη, αντίστοιχα. Στον αντίποδα, στις οπτικές ή μη παρεμβατικές μεθόδους, μια ακτίνα λέιζερ διεισδύει στη φλόγα, ή τον όγκο ελέγχου γενικότερα, και το παραγόμενο σήμα συλλέγεται και αντιστοίχως αναλύεται. Οι οπτικές μέθοδοι βρίσκουν εφαρμογή σε αντιδρώσες ροές με ολοένα αυξανόμενους ρυθμούς, ακολουθώντας την εξέλιξη της επιστήμης της φασματοσκοπίας με χρήση λέιζερ[243], με σημαντικότερο πρόβλημα στις μέρες μας, την καθεαυτή οπτική πρόσβαση σε πρακτικές εφαρμογές. Οι μη παρεμβατικές μέθοδοι με χρήση λέιζερ πλεονεκτούν στην υψηλή χρονική και χωρική διακριτική τους ικανότητα, παρέχοντας άμεσα τη δυνατότητα δισδιάστατων μετρήσεων[125]. Οι μετρήσεις με χρήση λέιζερ πλεονεκτούν ιδιαιτέρως στην ανίχνευση χημικών ειδών σε μικρές συγκεντρώσεις, όπως ρίζες και άλλες ασταθείς ενώσεις[86], πράγμα που οφείλεται στη συγκέντρωση υψηλών ενεργειακών επιπέδων ακτινοβολίας στον όγκο ελέγχου.

Η πειραματική διερεύνηση και παρακολούθηση των κύριων χημικών προϊόντων ενός συστήματος καύσης είναι αναγκαία για τον έλεγχο και τη βελτιστοποίηση της λειτουργίας του. Επίσης η μελέτη των κύριων χημικών ειδών σε πρότυπες διατάξεις όπως οι αντιδραστήρες εμβολικής ροής (όπως επιχειρείται στο 4ο κεφάλαιο της διατριβής) προσφέρει τα αναγκαία δεδομένα για την αξιολόγηση και βαθμονόμηση των υπολογιστικών εργαλείων. Η πλήρης κατανόηση των φαινομένων καύσης, απαιτεί τη μελέτη ασταθών χημικών ενώσεων, που δεν επιζούν εύκολα σε γραμμές δειγματοληψίας, όπως οι ρίζες των χημικών ενώσεων. Οι ρίζες αυτές συμμετέχουν στις στοιχειώδεις αντιδράσεις οξείδωσης, πυρόλυσης και κατανάλωσης καυσίμου, λαμβάνοντας εξαιρετικά σημαντικό ρόλο στην έκλυση θερμότητας, διάδοσης και σβέσης της φλόγας και του σχηματισμού ρύπων. Η πιο πολυδιερευνημένη είναι η ρίζα του υδροξυλίου (OH) καθώς παρουσιάζεται σε υψηλές συγκεντρώσεις στις φλόγες, παίζει σημαντικό ρόλο στις αντιδράσεις των υδρογονανθράκων και ως εκ τούτου η μοριακές-φασματοσκοπικές μεταβάσεις της είναι ευρέως γνωστές. Οι ρίζες OH και CH, χρησιμοποιούνται κατεξοχήν για την οπτικοποίηση του πεδίου της φλόγας, όπως επιχειρείται στα κεφάλαια 5 και 7.2 της παρούσας διατριβής. Επίσης, το CH και το CN επηρεάζουν έντονα το σχηματισμό οξειδίων του αζώτου και υπάρχουν αντίστοιχες μελέτες με μη παρεμβατικές μεθόδους[216]. Επιπροσθέτως, συνδυασμένες πειραματικές μελέτες OH και HCHO αντικατοπτρίζουν την έκλυση θερμότητας[97] από τη φλόγα ή χρησιμοποιούνται εμμέσως για τον

προσδιορισμό της ταχύτητας της καύσης[343]. Τέλος χαρακτηριστικό παράδειγμα για τη χρησιμότητα των πειραματικών διερευνήσεων των ριζών αντί των αντίστοιχων ενώσεων, αποτελεί το παράδειγμα της ρίζας CHO έναντι της φορμαλδεΰδης (HCHO), για μελέτες απεικόνισης του πεδίου της φλόγας. Η φορμαλδεΰδη εν δυνάμει σχηματίζεται και εν συνεχεία καταναλώνεται σε σχετικά πρώιμο στάδιο της χημικής μετατροπής των υδρογονανθράκων[41], ενώ το CHO σχηματίζεται μέσω αντιδράσεων όπου λαμβάνει χώρα η μέγιστη έκλυση θερμότητας, απεικονίζοντας με μεγαλύτερη ακρίβεια κατ' αυτόν τον τρόπο, την πραγματική περιοχή της φλόγας[208].

<u>Δομή και καινοτομία της διατριβής</u>

Το εισαγωγικό κεφάλαιο της διατριβής αναλύει την αναγκαιότητα της ανάπτυξης και εφαρμογής διαγνωστικών εργαλείων για συστήματα καύσης και τοποθετεί το παρόν πόνημα σε αυτό το πλαίσιο, παρουσιάζοντας τη δομή της διατριβής (*Σχήμα 1.2 – σελ. 59*). Το πρώτο μέρος της διατριβής παρέχει το απαραίτητο υπόβαθρο για το σχεδιασμό, την εκτέλεση και την κατανόηση των αποτελεσμάτων, επεξηγώντας τις αρχές λειτουργίας, τη θεμελιώδη θεωρία και τα βασικά συστατικά των χρησιμοποιηθέντων τεχνικών. Σε αυτές περιλαμβάνονται το σύστημα της αέριας χρωματογραφίας, το σύστημα συνεχούς ανάλυσης καυσαερίων, καθώς επίσης και το σύστημα για φασματοσκοπία φθορισμού επαγόμενου από διέγερση με χρήση ακτινοβολίας λέιζερ.

Στο δεύτερο σκέλος της διατριβής, κεφάλαια 4 έως 6, τα διαγνωστικά εργαλεία χρησιμοποιούνται για τη μελέτη διατάξεων χαμηλής πολυπλοκότητας, στοχεύοντας αφενός στην αξιολόγηση καθαυτών των διαγνωστικών μεθόδων και αφετέρου στη διεξαγωγή πρωτότυπης έρευνας, συνδεόμενης με υπαρκτά ζητήματα στο πεδίο των συστημάτων καύσης. Υπό αυτό το πρίσμα, η τεχνική της αέριας χρωματογραφίας επιστρατεύτηκε για την ποσοτικοποίηση αέριων ρύπων και επιλεγμένων πολυκυκλικών αρωματικών υδρογονανθράκων, από τα προϊόντα της πυρόλυσης μιγμάτων μεθανίου σε αντιδραστήρα εμβολικής ροής. Τα αποτελέσματα αναπαρήχθησαν με δυο μηχανισμούς λεπτομερούς χημείας, για την πληρέστερη κατανόηση των διεργασιών, με ικανοποιητική συμφωνία υπολογιστικών προλέξεων και πειραματικών δεδομένων. Εν συνεχεία, η τεχνική της φασματοσκοπίας φθορισμού επαγόμενου από διέγερση λέιζερ εφαρμόστηκε για τη μελέτη φλόγας προανάμιξης εγκάρσιας ροής. Η ψυχρή ροή μελετήθηκε ιχνηλατώντας μόρια ακετόνης στη ροή του καυσίμου και τα χαρακτηριστικά του σχήματος της φλόγας αναλύθηκαν μέσω της παρακολούθησης της ρίζας του υδροξυλίου στη ζώνη καύσης. Στο έκτο κεφάλαιο η διατριβή επεκτείνεται στη μελέτη μη συμβατικών καυσίμων, εξετάζοντας σύνθετα αεροπορικά καύσιμα, με τη χρήση ενός εργαστηριακού καυστήρα προανάμιξης. Οι μετρήσεις θερμοκρασίας και καυσαερίων, σε συνδυασμό με την προτεινόμενη αναλυτική μεθοδολογία για τον υπολογισμό των θερμοχημικών ιδιοτήτων βάσει της αναλυτικής χημικής τους σύστασης, καθιστούν εφικτή την αξιολόγηση των καυσίμων και τη συσχέτιση της απόδοσης, με τα περιεχόμενα συστατικά τους.

Τελικώς, οι προαναφερθείσες παρεμβατικές και μη τεχνικές, συνδυάζονται για τον χαρακτηρισμό ενός καυστήρα υψηλής περιπλοκότητας και εν προκειμένω ενός καυστήρα πορώδους αδρανούς μέσου. Η επιλογή του καυστήρα πορώδους αδρανούς μέσου έγινε καθώς αυτή η τεχνολογία υπόσχεται από υψηλή λειτουργική ευελιξία προσφέροντας παράλληλα υψηλή απόδοση και χαμηλά επίπεδα ρύπων. Η οπτικοποίηση της φλόγας μέσα στο πορώδες, μέσω της τεχνικής φασματοσκοπίας φθορισμού επαγόμενου από διέγερση λέιζερ και συγκεκριμένα της

παρακολούθησης της ρίζας του υδροξυλίου στη ζώνη καύσης, ανέδειξε της περιοχές λειτουργίας του συναρτήσει του θερμικού φορτίου και της στοιχειομετρίας. Εν κατακλείδι, διεξάγεται πλήρης πολυπαραμετρικός χαρακτηρισμός του πορώδους καυστήρα συναρτήσει του επιβαλλόμενου φορτίου, της στοιχειομετρίας και αναλύεται η ικανότητα του καυστήρα για λειτουργία με συμβατικά και εναλλακτικά καύσιμα.

Καινοτόμα σημεία έρευνας και προοπτικές της διατριβής

Η διατριβή αρχικά μελετά διατάξεις χαμηλής πολυπλοκότητας, στοχεύοντας στην αξιολόγηση καθαυτών των διαγνωστικών μεθόδων, αποσκοπώντας όμως παράλληλα στη διεξαγωγή πρωτότυπης εφαρμοσμένης έρευνας. Σε αυτό το πλαίσιο, στα κεφάλαια 4 και 5 (εκτός του ότι παρέχουν πειραματικά δεδομένα προς ανάλυση και βαθμονόμηση των αντίστοιχων υπολογιστικών εργαλείων) διερευνώνται πειραματικά δύο συστήματα με προεκτάσεις στο πεδίο έρευνας και εφαρμογής των σύγχρονων κυψελών καυσίμων[138]. Οι κυψέλες καυσίμου στερεού οξειδίου είναι μία από τις πιο ελκυστικές νέες τεχνολογίες για αποκεντρωμένα (υβριδικά) συστήματα μικροσυμπαραγωγής θερμότητας και ηλεκτρικής ενέργειας[288]. Οι κυψέλες καυσίμου δύνανται να λειτουργήσουν με υδρογονάνθρακες[115] ή ακόμη και μονοξείδιο του άνθρακα[159], ωστόσο η πιο συνήθης λύση είναι η παραγωγή αερίου σύνθεσης ή υδρογόνου[316], μέσω της αναμόρφωσης του φυσικού αερίου ή του βιοαερίου. Η διάταξη αναμορφωτή καυσίμου και στήλης της κυψέλης καυσίμου δύναται μακροσκοπικά να προσομοιωθεί μέσω διάταξης αντιδραστήρα εμβολικής ροής[19]. Στο 4ο κεφάλαιο μελετάται η πυρόλυση μιγμάτων με κύριο συστατικό το μεθάνιο σε διατάξεις αντιδραστήρα εμβολικής ροής. Τα εξεταζόμενα μίγματα προσομοιώνουν τη σύσταση του φυσικού αερίου και διερευνούν την επίδραση του διοξειδίου του άνθρακα, αποσκοπώντας στην εκτίμηση της επίδρασης της χρήσης του βιοαερίου στο σύστημα της κυψέλης καυσίμου, σε σύγκριση με το καθαρό μεθάνιο ή το φυσικό αέριο. Επίσης, οι κυψέλες καυσίμου ανταλλαγής πρωτονίων με καύσιμο υδρογόνο[28] ή χρήση αναμορφωτών βιοκαυσίμων[99] είναι, προφανώς μετά της μηχανές εσωτερικής καύσης, η πιο υποσχόμενη εναλλακτική λύση για το μέλλον της αυτοκινητοβιομηχανίας[116]. Για την επιτυχή λειτουργία ενός τέτοιου συστήματος είναι απαραίτητη η χρήση βοηθητικών συστημάτων παραγωγής θερμότητας[270]. Στο 5ο κεφάλαιο μελετάται η λειτουργικότητα ενός τέτοιου βοηθητικού συστήματος[318], βασιζόμενου στην τεχνολογία του καυστήρα πορώδους αδρανούς μέσου (η οποία αναλύεται στο 7ο κεφάλαιο) μίας πιο απλοποιημένης φλόγας που αναπαριστά τη διάταξη του σταδίου προανάμιξης του καυστήρα[319].

Όσον αφορά στην επιλογή καυσίμου η διατριβή εξετάζει ως επί το πλείστον συμβατικά και εναλλακτικά αέρια καύσιμα. Παρόλα αυτά, μέσω της εκμετάλλευσης συμβατικών πηγών ενέργειας, όπως το φυσικό αέριο, δύνανται μέσω της διεργασίας Fischer-Tropsch να προκύψουν εναλλακτικά καύσιμα, συμβατά με τις υπαρκτές υποδομές. Σε αυτό το πλαίσιο, το 6ο κεφάλαιο εξετάζει τη λειτουργία ενός καυστήρα εργαστηριακής κλίμακας, με καύσιμα Fischer-Tropsch για αεροπορική εφαρμογή, τα οποία καλούνται να πληρούν απαιτητικές προδιαγραφές όσον αφορά στις φυσικοχημικές τους ιδιότητες. Τα καύσιμα αυτά παρουσιάζουν σημαντική διαφοροποίηση ως προς τη σύσταση τους, κάτι που καθιστά δύσκολη την αντιστοίχιση της συμπεριφοράς τους σε συστήματα καύσης με το συστατικά που τα απαρτίζουν. Οι περισσότερες μελέτες στη βιβλιογραφία ασχολούνται με την απόδοση αυτών των καυσίμων σε πρακτικά συστήματα, όπως στροβιλομηχανές[309] και μηχανές εσωτερικής καύσης[5]. Το 6ο κεφάλαιο ακολουθεί μία αναλυτική

μεθοδολογία υπολογισμού των θερμοχημικών ιδιοτήτων των καυσίμων, τα οποία διαφοροποιούνται συστηματικά σε παραφινικούς, ναφθενικούς και αρωματικούς υδρογονάνθρακες. Συνεπώς, μέσω λεπτομερών θερμοκρασιακών μετρήσεων και των μετρήσεων καυσαερίων αξιολογούνται οι αποκλίσεις της συμπεριφοράς των διαφόρων καυσίμων αναφορικά με τα περιεχόμενα σε αυτά συστατικά. Εν κατακλείδι, το κεφάλαιο παρέχει πρωτογενή πειραματικά δεδομένα για το χαρακτηρισμό καυσίμων Fischer-Tropsch, τα οποία βρίσκονται στην αιχμή της έρευνας της τεχνολογίας καυσίμων.

Στο 7ο κεφάλαιο της διατριβής οι προαναφερθείσες παρεμβατικές και μη τεχνικές συνδυάζονται για τον πλήρη χαρακτηρισμό ενός καυστήρα υψηλής περιπλοκότητας, όπως ο καυστήρας πορώδους αδρανούς μέσου). Αρχικά η λειτουργία του καυστήρα διερευνάται μέσω της τεχνικής φασματοσκοπίας φθορισμού επαγόμενου από διέγερση λέιζερ και συγκεκριμένα της παρακολούθησης της ρίζας του υδροξυλίου ως ιχνηθέτη της ζώνης καύσης. Η μελέτη αυτή παρουσιάζει υψηλό βαθμό δυσκολίας αναφορικά με την οπτική πρόσβαση διαμέσου της πορώδους δομής. Η διάνοιξη της οπτικής διαδρομής πραγματοποιήθηκε κατόπιν ενδελεχούς πολυπαραμετρικής μελέτης, καταλήγοντας σε ένα βέλτιστο σχήμα, το οποίο διαταράσσει κατά το ελάχιστο δυνατόν τη λειτουργία του καυστήρα. Η μελέτη αναδεικνύει της περιοχές σταθερής λειτουργίας του καυστήρα συναρτήσει του θερμικού φορτίου και της επικρατούσας στοιχειομετρίας. Στη συνέχεια, πραγματοποιείται πλήρης πολυπαραμετρικός χαρακτηρισμός του πορώδους καυστήρα και αναλύεται η λειτουργία του με συμβατικά και εναλλακτικά καύσιμα.

Κεφάλαιο 2ο – Παρεμβατικές μέθοδοι διαγνωστικής φαινομένων καύσης που εφαρμόστηκαν στα πλαίσια της διατριβής

Οι λεπτομερείς μετρήσεις χημικών ειδών, θερμοκρασιών και ροϊκών πεδίων παρέχουν την αναγκαία πληροφορία για τις διεργασίες που διέπουν τα φαινόμενα καύσης. Παραδοσιακά οι πρώτες διαγνωστικές μέθοδοι ήταν παρεμβατικές. Οι παρεμβατικές διαγνωστικές μέθοδοι χρησιμοποιούν μία γραμμής δειγματοληψίας, για να οδηγήσουν το ερέθισμα/δείγμα στον αναλύτη, η απόληξη της οποίας διαταράσσει σε τοπικό επίπεδο τη φλόγα. Αρκετά διαδεδομένες παρεμβατικές μέθοδοι είναι τα θερμοζεύγη για μετρήσεις θερμοκρασίας και τα ανεμόμετρα θερμού νήματος για μετρήσεις ταχυτήτων.

Όσον αφορά στις μετρήσεις συγκεντρώσεων χημικών ειδών οι διαγνωστικές μέθοδοι ποικίλουν από σχετικά απλά συστήματα συνεχούς ανάλυσης μέχρι πολύπλοκες διατάξεις χρωματογραφίας και φασματοσκοπίας μάζας. Εν προκειμένω η μέθοδος της αέριας χρωματογραφίας βρίσκει εφαρμογή σε ευρύ ερευνητικό πεδίο που άπτεται της διαγνωστικής των συστημάτων καύσης. Συγκεκριμένα αναλύσεις απλής ή δισδιάστατης αέριας χρωματογραφίας, όπως αυτές που παρουσιάζονται στην παράγραφο 6.2, πραγματοποιούνται συχνά για το χαρακτηρισμό σύνθετων καυσίμων, όπως μίγματα ανώτερων υδρογονανθράκων[27], πετρελαίου[198] και κηροζίνης[74]. Επίσης η τεχνική της αέριας χρωματογραφίας εφαρμόζεται για το λεπτομερή χαρακτηρισμό των προϊόντων φλογών και καυστήρων προανάμιξης[218], συχνά συνδυαζόμενες με άλλες τεχνικές[314] λ.χ. συνεχείς αναλυτές, όπως στην παράγραφο 7.3. Επιπροσθέτως, η αέρια χρωματογραφία σε συνδυασμό με τη φασματοσκοπία μάζας αποτελεί ένα από τα ακριβέστερα συστήματα για την ανάλυση μακρομορίων όπως οι πολυκυκλικοί αρωματικοί υδρογονάνθρακες[252], όπως παρουσιάζεται στην υποπαράγραφο 4.4.2.1. Τέλος, η αέρια χρωματογραφία παραμένει, σε μεγάλο

βαθμό, ένα από τα πιο αξιόπιστα εργαλεία για την παροχή λεπτομερών πειραματικών δεδομένων συγκεντρώσεων χημικών ειδών με σκοπό την ανάπτυξη και βαθμονόμηση υπολογιστικών εργαλείων[69], όπως καθίσταται προφανές στην παράγραφο 4.3 της παρούσας διατριβής.

<u>Αέρια χρωματογραφία – Θεμελιώδης θεωρία και βασικά συστατικά του συστήματος</u>

Η αέρια χρωματογραφία ενδείκνυται για αναλύσεις μονίμων αερίων και πτητικών υγρών, καλύπτοντας ένα ευρύ φάσμα εφαρμογών από τη χημική βιομηχανία φαρμάκων και τροφίμων έως τη βιομηχανία καυσίμων[101]. Η αέρια χρωματογραφία, προσφέρει με σχετικά απλές διατάξεις ανιχνευτών υψηλή ευαισθησία και επιλεκτικότητα καθώς επίσης και βέλτιστη απόδοση σε χρόνο και κόστος λόγω εύκολης αυτοματοποίησης της διαδικασίας ανάλυσης[118]. Ο όρος χρωματογραφία αναφέρεται την τεχνική του διαχωρισμού των συστατικών ενός μίγματος βάσει της κατανομής τους μεταξύ μίας κινητής και μίας στατικής φάσης. Η γενική αρχή που εφαρμόζεται είναι ότι το αδρανές φέρον αέριο, συνήθως ήλιο ή άζωτο, είναι η κινητή φάση η οποία εκλούει τα συστατικά ενός μίγματος σε μία στήλη που περιέχει την σταθερή φάση. Το μίγμα κατανέμεται μεταξύ στατικής και κινητής φάσης και μετακινείται με τη βοήθεια της κινητής με ένα ρυθμό, που εξαρτάται από τη σχετική έλξη κάθε συστατικού για τις δύο φάσεις. Ανάλογα με το μηχανισμό διαχωρισμού διακρίνονται η χρωματογραφία προσρόφησης, κατανομής, διαχωρισμού, συγγένειας και ιοντο-εναλλαγής[150]. Η αέρια χρωματογραφία είναι ένας κλάδος της χρωματογραφικής επιστήμης στον οποίο η κινητή φάση είναι αέρια. Το αποτέλεσμα του διαχωρισμού ήτοι η συνάρτηση της απόκρισης του ανιχνευτή σε σχέση με το χρόνο καλείται χρωματογράφημα, ενώ η καμπύλη συγκέντρωσης των συστατικών του υπό διαχωρισμό μίγματος, λέγεται καμπύλη έκλουσης και είναι αποτέλεσμα της διεύρυνσης που υφίστανται τα μόρια του ίδιου του συστατικού στη στήλη εξαιτίας φαινομένων διάχυσης. Η σχετική απόσταση δύο συστατικών ενός μίγματος σε ένα σύστημα χρωματογραφίας εκφράζεται από τους διαφορετικούς χρόνους έκλουσης και καθορίζει την ποιότητα διαχωρισμού και για την ποσότητα του συστατικού που εκλούεται.

Οι διεργασίες που χαρακτηρίζουν ένα σύστημα αέριας χρωματογραφίας προσεγγίζονται από κυρίως δύο θεωρίες. Αφενός ,η θεωρία των δίσκων/κελίων, η οποία προσεγγίζει το σύστημα ως μία ασυνεχή διεργασία διύλισης αποτελούμενη από έναν ευρύ αριθμό ισοδύναμων σταδίων και αφετέρου η θεωρία ρυθμού που υπολογίζει τους ρυθμούς έκλυσης βάσει φαινομένων μεταφοράς μάζας και διάχυσης. Αναλυτικότερα η θεωρία των κελίων υποθέτει ο αναλύτης καθώς διέρχεται της χρωματογραφικής στήλης βρίσκεται σε ισορροπία μεταξύ στατικής και κινητής φάσης και συνεπώς η διεργασία χωρίζεται σε κελία ικανού μήκους να εξασφαλίσει τον απαιτούμενο χρόνο παραμονής για την επίτευξη της ισορροπίας. Όσο μικρότερο μήκος κελίου απαιτείται για την ισορροπία, τόσο περισσότερα κελία αντιστοιχούν στη στήλη ώστε ο θεωρητικός απαιτούμενος αριθμός κελίων να αντιστοιχίζεται με τις σταθερές ισορροπίας της στήλης. Η επίλυση της εξίσωσης μεταφοράς μάζας σε κάθε κελίο οδηγεί στην σχέση που συνδέει τη συγκέντρωση του αναλύτη σε κάθε κελίο με τη ροή του φέροντος από αυτό και κατ' επέκταση της τελικής καμπύλης έκλουσης[56]. Η θεωρία των κελίων είναι μία χρήσιμη ημιεμπειρική μέθοδος που παρόλα αυτά δεν καθορίζει το μηχανισμό του διαχωρισμού σε μια χρωματογραφικής στήλη. Το κενό αυτό καλύπτει η αναλυτική προσέγγιση της θεωρίας του ρυθμού, η οποία λαμβάνει υπόψη τη δυναμική αλληλεπίδραση ανάμεσα στο συστατικό με τη στατική και κινητή φάση, προσδιορίζοντας ποιοτικά και ποσοτικά το ρυθμό έκλουσης της σε αυτές. Συμπερασματικά, οι δύο προσεγγίσεις καταλήγουν στο βασικό

συμπέρασμα ότι το σχήμα της καμπύλης έκλουσης ακολουθεί την κανονική κατανομή με διεύρυνση ζώνης ανάλογη της τετραγωνικής ρίζας του μήκους της χρωματογραφικής στήλης[117].

Βασικά συστατικά και λειτουργία του συστήματος της χρωματογραφίας

Τα βασικά μέρη του συστήματος της αέριας χρωματογραφίας συμπεριλαμβάνουν συσκευές παροχής και ελέγχου της ροής το φέροντος αερίου και του δείγματος, δειγματολήπτες, χρωματογραφικές στήλες, ανιχνευτές, θερμοκρασιακά ελεγχόμενες ζώνες και συστήματα συλλογής και επεξεργασίας δεδομένων (*Σχήμα* 2.1 – *σελ.* 74). Η λειτουργία του συστήματος έχει εν ολίγοις ως εξής. Το φέρον αέριο κυκλοφορεί διαμέσου του συστήματος ενώ η ροή ελέγχεται με ακρίβεια καθώς είναι καθοριστικός παράγοντας για την επαναληψιμότητα των μετρήσεων και τη μείωση του επιπέδου θορύβου. Πριν από τη στήλη, το φέρον αέριο διέρχεται από φίλτρα που αποκρίνουν υγρασία και λοιπές ενώσεις. Το φέρον αέριο δεν επηρεάζει την κατανομή του δείγματος στις δύο χρωματογραφικές φάσεις, παρόλα αυτά επηρεάζει τη διασπορά καθώς με την αύξηση της θερμοκρασίας αυξάνεται το ιξώδες και συνεπώς επηρεάζεται η ροή μέσα στη στήλη. Το δείγμα εισέρχεται μέσω της διάταξης δειγματοληψίας στο σύστημα. Οι συνηθέστερες μέθοδοι για την πραγματοποίηση της δειγματοληψίας είναι η χρήση σύριγγας (για υγρής φάσης δείγματα), οι αυτόματοι δειγματολήπτες και οι βαλβίδες δειγματοληψίας. Ο εισαγωγέας διατηρείται σε θερμοκρασία υψηλότερη της στήλης και συνήθως 50 ^{o}C πάνω από τη θερμοκρασία βρασμού του πιο πτητικού στοιχείου του μίγματος ούτως ώστε όταν το δείγμα βρίσκεται σε υγρή φάση, να αεριοποιείται ταχύτατα και εξ' ολοκλήρου. Το δείγμα οδηγείται στη χρωματογραφική στήλη, η οποία βρίσκεται σε θερμοκρασιακά ελεγχόμενο θάλαμο όπου διαχωρίζεται στα συστατικά που αλληλεπιδρούν με την κινητή και τη σταθερή φάση στη στήλη. Κατόπιν, το δείγμα διέρχεται στη διάταξη του ανιχνευτή όπου τα συστατικά του αναγνωρίζονται ποιοτικά και ποσοτικοποιούνται. Στο τελευταίο βήμα της ανάλυσης τα δεδομένα συγκεντρώνονται και η σύσταση του υπό μελέτη δείγματος γίνεται γνωστή άμεσα.

Η διαδικασία εισαγωγής του δείγματος στο σύστημα είναι ουσιώδους σημασίας για την επιτυχή του ανάλυση. Για τα υγρής φάσης δείγματα, χρησιμοποιούνται στις περισσότερες εφαρμογές αυτόματοι δειγματολήπτες υψηλής ακρίβειας. Για αέρια δείγματα, όπως στην παρούσα διατριβή, η δειγματοληψία πραγματοποιείται μέσω βαλβίδων, που στην πλειονότητα τους είναι δύο θέσεων (*Σχήμα* 2.2 – *σελ.* 75). Μια τυπική βαλβίδα δειγματοληψίας αποτελείται από έξι θέσεις στις οποίες συνδέονται οι εισαγωγές και εξαγωγές της δειγματοληψίας, του φέροντος αερίου και της στήλης. Οι βαλβίδες εν δυνάμει ενώνουν δύο διαδρομές, βραχυκυκλώνοντας συμπληρωματικές θύρες. Αρχικά το δείγμα διοχετεύεται σε ένα κύκλωμα δειγματοληψίας και κατόπιν αποβάλλεται, ενώ ταυτόχρονα η δεύτερη διαδρομή πληρώνεται με φέρον αέριο. Όταν η βαλβίδα αλλάξει θέση, το δείγμα που βρίσκεται εγκλωβισμένο στο κύκλωμα οδηγείτε στη χρωματογραφική στήλη, ενώ η είσοδος του δείγματος βραχυκυκλώνεται με την έξοδο του από τη βαλβίδα. Πιο σύνθετες διατάξεις βαλβίδων δειγματοληψίας δέκα θέσεων δίνουν τη δυνατότητα αποβολής από το σύστημα ανεπιθύμητων ουσιών παγιδεύοντας τις αρχικά σε μία βοηθητική χρωματογραφική στήλης[280]. Επίσης, για πληρωμένες στήλες οι ροές στη στήλη είναι μεγαλύτερες συνεπώς το δείγμα εισάγεται όλο στη στήλη. Όταν χρησιμοποιούνται τριχοειδείς στήλες ο κίνδυνος κορεσμού της στήλης είναι μεγαλύτερος συνεπώς χρησιμοποιούνται δύο είδη λειτουργίες των εισαγωγέων, με ή χωρίς διαχωρισμό ροής.

Χρωματογραφικές στήλες

Η χρωματογραφική στήλη αποτελεί την καρδιά της χρωματογραφικής ανάλυσης. Στη στήλη διαχωρίζονται τα επιμέρους συστατικά του δείγματος, ώστε κατόπιν να ποσοτικοποιηθούν στη διάταξη του ανιχνευτή. Η θερμοκρασία λειτουργίας της στήλης είναι παράγοντας μεγάλης σημασίας για τον διαχωρισμό. Οι χρωματογραφικές στήλες διατηρούνται και θερμαίνονται σε φούρνο είτε με σταθερή θερμοκρασία είτε με θερμο-προγραμματισμό, ήτοι άνοδο της θερμοκρασίας με σταθερό ρυθμό επιτυγχάνοντας μείωση του χρόνου των μετρήσεων καθώς η αύξηση της θερμοκρασίας συνεπάγεται αύξηση της διαχωριστότητας[147]. Οι δύο βασικές κατηγορίες χρωματογραφικών στηλών είναι οι στήλες πλήρωσης και οι τριχοειδείς. Οι πληρωμένες στήλες περιέχουν αδρανή, στερεά υποστρώματα τα οποία η στατική φάση διαβρέχει ή προσδένεται σε αυτά. Οι πληρωμένες στήλες είναι μεγαλύτερης διαμέτρου, κατασκευασμένες από ανοξείδωτο χάλυβα ή γυαλί και περιέχουν αδρανή και στερεά σώματα. Οι τριχοειδείς στήλες κατασκευάζονται ως επί το πλείστον από διοξείδιο του πυριτίου και περιέχουν ένα λεπτό στρώμα από υψηλού μοριακού βάρους πολυμερές το οποίο αποτελεί τη στατική φάση. Οι τριχοειδείς ή ανοιχτού σωλήνα στήλες έχουν εσωτερική διατομή της τάξης των μερικών μικρομέτρων και ανάλογα με τον τρόπο πλήρωσης διακρίνονται σε πορώδους στρώματος, επιτοίχιας επικάλυψης και υποστηρικτικής επικάλυψης ανοιχτού σωλήνα στήλες. Οι τριχοειδείς στήλες παρέχουν αποδοτικότερο διαχωρισμό από τις πληρωμένες στήλες, ωστόσο υπερφορτώνονται ευκολότερα από μεγάλες ποσότητες δείγματος[30]. Ωστόσο η σύγκριση μεταξύ των κατηγοριών στηλών δεν είναι τόσο απλή. Οι τριχοειδείς στήλες έχουν σημαντικά μεγαλύτερο μήκος αλλά η πληρωμένες περιέχουν μεγαλύτερες ποσότητες στατικής φάσης. Η απόδοση του διαχωρισμού αυξάνεται με την απομάκρυνση των κορυφών έκλουσης των επιμέρους των συστατικών. Στις πληρωμένες στήλες ο κυρίαρχος μηχανισμός διαχωρισμού είναι η ευρεία διασπορά των συστατικών στη στατική φάση, ενώ ένεκα της περιορισμένης στατικής φάσης στις τριχοειδείς στήλες, ο κύριος μηχανισμός είναι κίνηση τους καθ' όλο το μήκος της στήλης. Η κατάλληλη επιλογή στήλης και συνθηκών λειτουργίας είναι κρίσιμη επιλογή για την επίτευξη του καλύτερου χρωματογραφήματος. Η επιλογή κατάλληλης στατικής φάσης γίνεται βάσει της πολικότητας και της πτητικότητας των αναλυτών και του θερμο-προγραμματισμού που ακολουθείται. Οι συνηθέστερες στατικές φάσεις είναι οι πολυσιλοξάνες γνωστές ως σιλικονούχα έλαια, οι οποίες παρουσιάζουν θερμοκρασιακή και χημική αδρανή σε ευρεία περιοχή λειτουργίας.

Χρωματογραφικοί ανιχνευτές

Η ευελιξία της τεχνικής της χρωματογραφίας οφείλεται εν πολλοίς στην ποικιλομορφία ανιχνευτών που συνδυάζει, συμπεριλαμβάνοντας από απλούς ανιχνευτές μέχρι σύνθετες φασματοσκοπικές διατάξεις. Οι ανιχνευτές κυρίως διακρίνονται σε καθολικούς και εκλεκτικούς ανάλογα με το αν ανταποκρίνονται σε κάθε είδους ουσίες ή όχι. Οι ανιχνευτές αέριας χρωματογραφίας παρουσιάζουν έως και πέντε τάξεις μεγέθους μεγαλύτερη ακρίβεια από τους αντίστοιχους της υγρής χρωματογραφίας, γεγονός που τους καθιστά ιδανικούς για μετρήσεις περιβαλλοντικών παραγόντων[281]. Η στήλη που χρησιμοποιείται, η θερμοκρασία λειτουργίας της και εν γένει τα χαρακτηριστικά του χρωματογραφικού συστήματος, οφείλουν να λαμβάνονται υπόψη κατά την επιλογή κατάλληλου ανιχνευτή, ώστε το τελικό χρωματογράφημα να είναι αξιόπιστο (*Σχήμα* 2.3 – *σελ.* 81). Τα κύρια χαρακτηριστικά του ανιχνευτή είναι η ευαισθησία σε συνδυασμό με τη δυναμική του περιοχή, καθορίζοντας όσο ευδιάκριτα μία αλλαγή στη συγκέντρωση του μετρούμενου μεγέθους προκαλεί διαφορετική απόκριση στον ανιχνευτή, καθώς

18

επίσης και η γραμμική περιοχή, στην οποία η ανωτέρω διέγερση συσχετίζεται γραμμικά με την απόκριση του ανιχνευτή. Οι συνηθέστεροι ανιχνευτές, οι οποίοι και χρησιμοποιήθηκαν στο πλαίσιο της παρούσας διατριβής, είναι ο ανιχνευτής φλόγας ιονισμού και ο ανιχνευτής θερμικής αγωγιμότητας. Ο ανιχνευτής θερμικής αγωγιμότητας είναι ικανός να ανιχνεύσει οποιοδήποτε συστατικό έχει διαφορετική θερμοχωρητικότητα από το φέρον αέριο στη θερμοκρασία του ανιχνευτή, ενώ ο ανιχνευτής φλόγας ιονισμού είναι πιο ευαίσθητος και κυρίως κατάλληλος για υδρογονάνθρακες. Εκτός των δύο προαναφερθέντων ανιχνευτών αρκετά διαδεδομένοι είναι ο ανιχνευτής σύλληψης ηλεκτρονίων, ο ανιχνευτής αζώτου φωσφόρου, ο φωτομετρικός ανιχνευτής και ο ανιχνευτής φωτοϊονισμού.

Ο ανιχνευτής φλόγας ιονισμού (*Σχήμα* 2.4 – *σελ.* 83) είναι ο πιο διαδεδομένος αναλυτής για εφαρμογές αέριας χρωματογραφίας λόγω της υψηλής αξιοπιστίας του, των χαμηλών ορίων ανίχνευσης, της ευρείας δυναμικής περιοχής με γραμμικότητα της τάξης του 10^7 και της εξαιρετικής χρηστικότητας για εφαρμογές οργανικών ενώσεων. Επίσης η απόκριση του ανιχνευτή φλόγας ιονισμού δεν είναι ευαίσθητη σε μικροαλλαγές στη ροή του φέροντος ή περιεχόμενο στο δείγμα νερό ή διοξείδιο του άνθρακα. Ο ανιχνευτής φλόγας ιονισμού μειονεκτεί στο ότι δεν ανταποκρίνεται σε αέρια που δεν καίγονται, όπως θειούχα ή νιτρικά οξείδια, και ότι είναι καταστροφικός για το δείγμα. Ο ανιχνευτής φλόγας ιονισμού αποτελείται από δύο ηλεκτρόδια εκ των οποίων το ένα λειτουργεί ως καυστήρας και το άλλο ως συλλέκτης. Καθώς το δείγμα εισέρχεται στον ανιχνευτή καίγεται και σχηματίζονται φορτισμένα σωματίδια, τα οποία δημιουργούν ρεύμα μικρής έντασης μεταξύ των δύο ηλεκτροδίων στα οποία υπάρχει διαφορά τάσης. Το φορτισμένο θετικά ηλεκτρόδιο λειτουργεί ως συλλέκτης του ρεύματος που δημιουργείται και κατόπιν ενίσχυσης το σήμα μετατρέπεται σε μετρήσιμη διαφορά δυναμικού[140]. Σημαντική είναι η παρατήρηση ότι όσο μεγαλύτερος είναι ο αριθμός ατόμων άνθρακα μίας οργανικής ένωσης, τόσο ο αριθμός των ιόντων που προέρχονται από τον ιονισμό τους είναι μεγαλύτερος συνεπάγοντας αύξηση στο σήμα του ανιχνευτή. Στην ουσία ο ανιχνευτής φλόγας ιονισμού είναι ένας μετρητής ατόμων άνθρακα της ουσίας και η σχέση που συνδέει τον αισθητό από τον ανιχνευτή αριθμό ατόμων άνθρακα μίας ουσίας συνδέεται με τις ομόλογες σειρές ενώσεων[154], το μοριακό της βάρος[155] και τις συνθήκες λειτουργίας[156]. Ωστόσο, ο επακριβής μηχανισμός του σχηματισμού των ιόντων σε μία διάταξη ανιχνευτή φλόγας ιονισμού δεν είναι πλήρως γνωστός[282] χωρίς αυτό να τον εμποδίζει να είναι ο πιο διαδεδομένος τα τελευταία χρόνια.

Ο ανιχνευτής θερμικής αγωγιμότητας είναι καθολικός και χαρακτηρίζεται από σχετικά χαμηλά όρια ανίχνευσης και μικρή γραμμική περιοχή. Ο ανιχνευτής θερμικής αγωγιμότητας στηρίζεται στη θερμική αγωγιμότητα των αέριων μιγμάτων και αποτελείται από δύο ζεύγη θερμικών νημάτων συνδεδεμένα σε γέφυρα Wheatstone (*Σχήμα* 2.5 – *σελ.* 84), η διάταξη της οποίας βοηθά στην επίλυση προβλημάτων θερμοκρασιακής διαφοράς ανάμεσα στους κλάδους της. Στο πρώτο ζεύγος διοχετεύεται καθαρό φέρον αέριο το οποίο είναι συνήθως ήλιο εξαιτίας της υψηλής θερμικής αγωγιμότητας και στο δεύτερο ζεύγος διοχετεύεται η έξοδος της στήλης. Όταν μία ουσία εξέρχεται από τη στήλη έχει υποστεί αλλαγή στη σύνθεση της κινητής φάσης και ως εκ τούτου στη θερμική αγωγιμότητα με συνέπεια να διαταράσσεται η ισορροπία της γέφυρας. Το ρεύμα που απαιτείται για την αποκατάσταση της ισορροπίας, αποτελεί το σήμα του ανιχνευτή και είναι ανάλογο με την συγκέντρωση της ουσίας.

Ανάπτυξη χρωματογραφικής μεθόδου για ανάλυση καυσαερίων

Ο συνδυασμός κατάλληλων χρωματογραφικών στηλών, ανιχνευτών, εισαγωγέων και η επιλογή των αντίστοιχων ρυθμίσεων θερμοκρασιών και παροχών φέροντος αερίου καλείται χρωματογραφική μέθοδος. Στα πλαίσια της διατριβής αναπτύχθηκαν και χρησιμοποιήθηκαν δύο εναλλακτικές διατάξεις. Οι δύο μέθοδοι στοχεύουν στην αναγνώριση και ποσοτικοποίηση των κύριων προϊόντων της καύσης καθώς και των σημαντικότερων ενδιάμεσων χημικών ειδών. Το κύριο κοινό χαρακτηριστικό των δύο μεθόδων είναι ότι εμπεριέχουν από δύο κανάλια ανάλυσης, που αντίστοιχα οδηγούν σε έναν ανιχνευτή θερμικής αγωγιμότητας κι έναν φλόγας ιονισμού.

Η πρώτη μέθοδος που χρησιμοποιείται στα κεφάλαια 6 και 7, συνδυάζει μία τριχοειδή στήλη διμέθυλο-πολυσιλοξάνης που οδηγεί στον ανιχνευτή φλόγας ιονισμού και τρεις πληρωμένες στήλες εν σειρά, οι οποίες καταλήγουν στον ανιχνευτή θερμικής αγωγιμότητας (*Πίνακας 2.1 – σελ. 87*). Η ανάλυση είναι ισοθερμοκρασιακή με τη στήλη του ανιχνευτή φλόγας ιονισμού να αναγνωρίζει ισομερείς υδρογονάνθρακες περιεκτικότητας μέχρι τεσσάρων ατόμων άνθρακα. Το κανάλι του ανιχνευτή θερμικής αγωγιμότητας αναγνωρίζει όλα τα κύρια προϊόντα της καύσης και είναι συνδεδεμένο με δύο βαλβίδες. Η πρώτη βαλβίδα είναι η εισαγωγής και η δεύτερη είναι εναλλαγής στηλών (*Σχήμα 2.6 – σελ. 87*). Η πρώτη βαλβίδα ενσωματώνει δέκα θέσεις στις οποίες είναι συνδεδεμένες οι πρώτη και η δεύτερη στήλη του καναλιού του ανιχνευτή θερμικής αγωγιμότητας δίνοντας τη δυνατότητα αντιστροφής της ροής για την αποφυγή της εισόδου βαρέων ενώσεων και υδρατμών στο σύστημα. Η τρίτη στήλη διαχωρίζει το οξυγόνο από το άζωτο χρησιμοποιώντας ένα μοριακό πλέγμα της τάξης των 5Å. Για την προστασία της στήλης τα στοιχεία αυτά απομονώνονται ωσότου διέρθουν τα υπόλοιπα από το σύστημα και εν συνεχεία επαναφέρονται με τη χρήση της βαλβίδας εναλλαγής. Συνολικά, το δεύτερο κανάλι ποσοτικοποιεί υδρογόνο, οξυγόνο, άζωτο, μονοξείδιο και διοξείδιο του άνθρακα περιεχόμενα στα καυσαέρια.

Η δεύτερη χρωματογραφική μέθοδος που χρησιμοποιήθηκε στα πλαίσια της διατριβής και ειδικότερα στο τέταρτο κεφάλαιο, έχει δοκιμαστεί σε πλείστες πειραματικές μελέτες κατά το παρελθόν[90], με μόνη διαφορά τα δοκιμαζόμενα καύσιμα. Η δεύτερη μέθοδος δεν έχει τη δυνατότα αντιστροφής της ροής στις στήλες και απλώς ενσωματώνει δύο κανάλια που οδηγούν σε έναν ανιχνευτή θερμικής αγωγιμότητας κι έναν φλόγας ιονισμού, αντίστοιχα συνδεδεμένα σε δύο βαλβίδες εισαγωγής. Στον αντίποδα η ανάλυση είναι αρχικά ισοθερμοκρασιακή ενώ ακολούθως αυξάνεται με ρυθμό 20 °C το λεπτό έως τους 210 °C διευκολύνοντας την ανάλυση των βαρέων υδρογονανθράκων στο κανάλι του ανιχνευτή φλόγας ιονισμού[128]. Συνολικά, η μέθοδος αναλύει μέσω του ανιχνευτή θερμικής αγωγιμότητας όλα τα κύρια και ενδιάμεσα χημικά προϊόντα της καύσης καθώς επίσης βενζόλιο, αιθυλο-βενζόλιο, τολουένιο και ξυλένιο στον ανιχνευτή φλόγας ιονισμού (*Πίνακας 2.2 – σελ. 89*).

Βαθμονόμηση και ανάλυση αβεβαιότητας της χρωματογραφικής μεθόδου

Η αέρια χρωματογραφία χρησιμοποιείται τόσο για ποιοτική ταυτοποίηση μίας ουσίας στο υπό ανάλυση δείγμα όσο και για ποσοτική ανάλυση της περιεχόμενης σε αυτό ποσότητας. Δεδομένου ότι οι συνθήκες λειτουργίας του συστήματος είναι σταθερές, ο χρόνος έκλουσης ενός συστατικού του μίγματος αποτελεί χαρακτηριστικό του και συνεπώς δύναται να οδηγήσει στην ταυτοποίηση του. Η ποσοτική ανάλυση πραγματοποιείται μέσω της μέτρησης του ύψους και του εμβαδού της καμπύλης έκλουσης του συστατικού. Η μέτρηση του εμβαδού της καμπύλης έκλουσης είναι

ακριβέστερη μέθοδος καθώς υπερβαίνει δυσκολίες λόγω ασυμμετρίας η εν γένει ανομοιομορφίας της καμπύλης έκλουσης. Η ποσοτικοποίηση της ανάλυσης απαιτεί ακρίβεια στη δειγματοληψία και μετρήσεις στη γραμμική περιοχή του ανιχνευτή. Η συνηθέστερη μέθοδος βαθμονόμησης είναι η εισαγωγή δεδομένης ποσότητας της υπό ανάλυση ουσίας και η εν συνεχεία μέτρηση της απόκρισης του ανιχνευτή σε μία ή πολλαπλές συγκεντρώσεις, ώστε να αποκτάται ανωτέρου βαθμού καμπύλη βαθμονόμησης. Η βαθμονόμηση του συστήματος της κύριας χρωματογραφικής μεθόδου που αναπτύχθηκε στα πλαίσια της διατριβής (*Πίνακας* 2.3 – *σελ.* 91) παρουσιάζει αβεβαιότητα της τάξης του ±1%, με ολική αβεβαιότητα των μετρήσεων της τάξης του ±5%, λαμβάνοντας υπόψη παραμέτρους όπως η εσωτερική ακρίβεια και η μη γραμμικότητα των ανιχνευτών η διασπορά των μετρήσεων και τα σφάλματα ολοκλήρωσης της καμπύλης έκλουσης.

Σύστημα συνεχούς ανάλυσης αέριων ρύπων – Αρχές λειτουργίας και χαρακτηριστικά

Το σύστημα της αέριας χρωματογραφίας είναι εξαιρετικά ευέλικτο όσον αφορά στις δυνατότητες ανάλυσης πλείστων χημικών ειδών, χωρίς όμως να δίνει τη δυνατότητα συνεχούς παρακολούθησης των παραγόμενων καυσαερίων. Την αναγκαιότητα τούτη καλύπτουν αναλυτές συνεχούς ποσοτικοποίησης των αέριων ρυπαντών, οι οποίοι με τη σειρά τους δύνανται να συνδυάσουν διαφορετικές τεχνικές μέτρησης[192]. Οι τεχνικές αυτές βρίσκουν εφαρμογή τόσο στη μελέτη της μεταβατικής λειτουργίας πρακτικών εφαρμογών[108], όσο και την συμπληρωματική με άλλα κύρια συστήματα παρακολούθηση ρύπων όπως τα οξείδια του θείου[102]. Στο πλαίσιο της διατριβής η προαναφερθείσες μέθοδοι αέριας χρωματογραφίας συνδυάστηκαν με συστήματα συνεχούς ανάλυσης, ούτως ώστε ή λεπτομερής ανάλυση χημικών ειδών να συνδυάζεται με τη συνεχή ποσοτικοποίηση σημαντικών αέριων ρύπων όπως τα οξείδια του αζώτου. Οι αναλυτές που χρησιμοποιήθηκαν βασίζονται στο νόμο των Beer-Lambert, σύμφωνα με τον οποίο η συγκέντρωση μίας ένωσης διερχόμενης από γνωστού μήκους κοιλότητα είναι ανάλογη του κλάσματος της εισερχόμενης προς την εξερχόμενη ακτινοβολία στην κοιλότητα αυτή. Απαραίτητη προϋπόθεση για την ορθή ανίχνευση και ταυτοποίηση μίας ουσίας αποτελεί η σωστή ρύθμιση του συντελεστή απορρόφησης αναλόγως του μήκους κύματος απορρόφησης της επιθυμητής ουσίας. Εν προκειμένω, για την ανάλυση του μονοξειδίου και του διοξειδίου του άνθρακα χρησιμοποιήθηκε αναλυτής απορρόφησης υπερύθρου ακτινοβολίας χωρίς διασπορά, ενώ τα οξείδια του αζώτου και του θείου ταυτοποιήθηκαν στην υπεριώδη περιοχή του ηλεκτρομαγνητικού φάσματος. Τέλος για τη συνεχή ανίχνευση και ποσοτικοποίηση του περιεχόμενου στα καυσαέρια οξυγόνου χρησιμοποιήθηκαν, εκτός των προαναφερθέντων συστημάτων, και παραμαγνητικοί αναλυτές.

Κεφάλαιο 3ο – Μη παρεμβατικές μέθοδοι διαγνωστικής φαινομένων καύσης που εφαρμόστηκαν στα πλαίσια της διατριβής

Τις τελευταίες δεκαετίες, η ανάπτυξη ποικίλων πηγών ακτινοβολίας λέιζερ και αξιοποίηση τους σε διαγνωστικές μεθόδους, έχει ωθήσει σημαντικά την έρευνα αφενός στη διαγνωστική καθ' αυτή και αφετέρου στα εφαρμοζόμενα πρακτικά συστήματα καύσης. Οι μη παρεμβατικές μέθοδοι είναι ως επί το πλείστον οπτικές μέθοδοι οι οποίες χρησιμοποιούν τη διέγερση που προκαλεί η ακτινοβολία λέιζερ για να φωτίσουν πτυχές της ροής, αντιδρώσας ή μη. Τα βασικά χαρακτηριστικά του φωτός λέιζερ που συνέδραμαν την αλματώδη βελτίωση των διαγνωστικών μεθόδων είναι η μονοχρωματικότητα ήτοι το γεγονός ότι τα φωτόνια της δέσμης έχουν όλα την ίδια συχνότητα, η κατευθυντικότητα, καθώς τα φωτόνια της δέσμης έχουν όλα την ίδια διεύθυνση, η συμφωνία φάσης και η μεγάλη ένταση, ήτοι πολλά φωτόνια σε μικρή επιφάνεια. Με τις τεχνικές αυτές η

άμεση μέτρηση χημικών ειδών, θερμοκρασιών και ροϊκών πεδίων σε φαινόμενα καύσης κατέστη δυνατή σε πραγματικό χρόνο, με ελάχιστη διατάραξη των τοπικών συνθηκών. Επίσης, κατέστη δυνατή η διενέργεια πειραματικών μετρήσεων ριζών χημικών ειδών και κατ' επέκταση των στοιχειωδών αντιδράσεων που είναι σε μεγάλο βαθμό υπεύθυνες για τον έλεγχο του μηχανισμού έκλυσης θερμότητας και σχηματισμού ρύπων κατά την καύση[334]. Οι συνηθέστερες οπτικές μέθοδοι για τη μέτρηση πεδίων ταχυτήτων είναι η ανεμομετρία φάσης Doppler με χρήση λέιζερ[272] και η τεχνική της ανεμομετρίας ιχνηλάτησης σωματιδίων[315]. Όσον αφορά στις θερμοκρασιακές μετρήσεις, οι τεχνικές με χρήση λέιζερ εμφανίζουν ευρεία ποικιλομορφία από μεθόδους βασιζόμενες σε ελαστική[178], ανελαστική[246] ή συνδυαζόμενη[200] σκέδαση της ακτινοβολίας, έως τεχνικές θερμομετρίας ατομικής διάσπασης μέσω λέιζερ[164] και διχρωματικής φασματοσκοπίας φθορισμού[51]. Ακόμη περισσότερες τεχνικές, σε συνδυασμό με τις προαναφερθείσες, έχουν εφαρμοστεί για μη παρεμβατικές μετρήσεις χημικών ειδών, είτε με γραμμικές οπτικές μεθόδους όπως η χημειοφωταύγεια[233] και η φασματομετρία απορρόφησης κοιλότητας[113], είτε με μη γραμμικές μεθόδους όπως η συμφασική αντί-Stokes ανελαστική σκέδαση[82], η τεχνική της εκφυλιστικής τετραχρωματικής ανάμιξης[283] και η φασματομετρία πόλωσης[301].

Μια από τις πιο ευέλικτες, μη παρεμβατικές μεθόδους διαγνωστικής συστημάτων καύσης στηρίζεται στην τεχνική της επιλεκτικής διέγερσης στοχευόμενων ενεργειακών μεταπτώσεων της υπό μελέτη χημικής ένωσης ή ρίζας, ήτοι η τεχνική της ανίχνευσης του φάσματος φθορισμού επαγόμενου από ακτινοβολία λέιζερ. Τα κύρια πλεονεκτήματα της μεθόδου είναι ότι δεν απαιτεί εξαιρετικά πολύπλοκες οπτικές διατάξεις, δίνοντας υψηλής επιλεκτικότητας, ακόμη και τρισδιάστατα, αποτελέσματα λόγω του υψηλού χρονισμού διέγερσης-ανίχνευσης, της τάξης των μερικών νανοδευτερολέπτων. Επίσης, η ανίχνευση του φάσματος φθορισμού που επάγεται από ακτινοβολία λέιζερ είναι εξαιρετικά επιλεκτική αναφορικά με τα υποπροϊόντα της καύσης, προσδίδοντας πολύτιμη πειραματική πληροφορία για τη χημεία της καύσης. Η υψηλή διακριτική ικανότητα της τεχνικής προϋποθέτει τον ακριβή προσδιορισμό του φάσματος διέγερσης και ανίχνευσης, πράγμα που αφενός απαιτεί τη χρήση σύνθετων διατάξεων λέιζερ ρυθμιζόμενου μήκους κύματος και αφετέρου καθιστά την ποσοτικοποίηση των αποτελεσμάτων μία εξαιρετικά δύσκολή διαδικασία. Οι παραπάνω λόγοι καθιστούν την τεχνική της φασματοσκοπίας φθορισμού επαγόμενου από λέιζερ ιδιαιτέρως διαδεδομένη ανάμεσα στις πειραματικές μελέτες φαινομένων καύσης, για την ανίχνευση ποικίλων χημικών ειδών και κατά συνέπεια πλείστων παραμέτρων που ελέγχουν την καύση. Τα πιο συχνά υπαντώμενα χημικά είδη σε πειραματικές μελέτες με την τεχνική της φασματοσκοπίας φθορισμού επαγόμενου από λέιζερ καθώς και τα πρώτα που μελετήθηκαν είναι η ρίζα του υδροξειλίου[83] και ακολούθως τα οξείδια του αζώτου. Το επιστημονικό βάθος των μελετών τις τελευταίες δεκαετίες έχει σήμερα οδηγήσει στην ανάπτυξη λογισμικών πακέτων προσομοίωσης των ενεργειακών μεταβάσεων σε μοριακό επίπεδο για τα παραπάνω χημικά είδη, οδηγώντας στην πιο εύκολη ποσοτικοποίηση των αποτελεσμάτων. Εξίσου σημαντικές για το πεδίο της έρευνας που σχετίζεται με την καύση είναι πειραματικές μελέτες που πραγματοποιούνται με την τεχνική της φασματοσκοπίας φθορισμού επαγόμενου από λέιζερ αναφορικά τις ρίζες όπως το CH[107], ή ενώσεις όπως η φορμαλδεΰδη[114] και το NCN[300], παρέχοντας κρίσιμα πειραματικά δεδομένα για την μορφή και τη γεωμετρία της φλόγας, των ρυθμών έκλυσης θερμότητας σε αυτήν και το σχηματισμό ρύπων όπως τα οξείδια του αζώτου[171]. Στα πλαίσια της παρούσας διατριβής η τεχνική της φασματοσκοπίας φθορισμού επαγόμενου από λέιζερ χρησιμοποιήθηκε για την απεικόνιση του μετώπου της φλόγας μέσω της παρακολούθησης

της ρίζας του υδροξυλίου. Το τρίτο κεφάλαιο επεξηγεί την πειραματική μεθοδολογίας, παρουσιάζει τα βασικά συστατικά του συστήματος διέγερσης του υδροξυλίου και ανίχνευσης του αντίστοιχου φθορισμού και παρέχει το απαραίτητο υπόβαθρο για την κατανόηση των αποτελεσμάτων που πραγματοποιήθηκαν με φασματοσκοπικές, μη παρεμβατικές τεχνικές.

Θεμελιώδης θεωρία φασματοσκοπικών μετρήσεων

Σύμφωνα με την κβαντομηχανική θεωρία, ένα χημικό μόριο δύναται να παρουσιάζει διακριτές και κβαντισμένες στάθμες ενέργειας, που οφείλονται λόγου χάριν, στην περιστροφική ενέργεια όταν το μόριο κινείται γύρω από το κέντρο βαρύτητας του, στην ενέργεια δόνησης λόγω περιοδικής μετατόπισης των ατόμων από το κέντρο ισορροπίας, την ηλεκτρονική ενέργεια λόγω αέναης κίνησης των ηλεκτρονίων και ούτω καθεξής (*Σχήμα 3.1 – σελ.* 103). Ομοίως, οι ενεργειακές μεταπτώσεις σε ένα μόριο είναι αντιστοίχως κβαντισμένες[203]. Κατ' αναλογία, χρησιμοποιώντας το απλό και πασίγνωστο μοντέλο του Bohr, τα παραπάνω σημαίνουν ότι τα ηλεκτρόνια κινούνται σε ορισμένες επιτρεπτές τροχιές γύρω από τον πυρήνα και η μετάβαση τους σε άλλη τροχιά συνοδεύεται από την απορρόφηση ή εκπομπή ηλεκτρομαγνητικής ακτινοβολίας ίσης ενεργειακά με τη διαφορά δυναμικού των εμπλεκόμενων τροχιακών. Η αλληλεπίδραση της ηλεκτρομαγνητικής ακτινοβολίας με την ύλη και οι κβαντικές μεταβολές ενέργειας κατά την απορρόφηση ή εκπομπή ακτινοβολίας είναι το κύριο χαρακτηριστικό της φασματοσκοπίας. Οι φασματοσκοπικές μέθοδοι είναι τεχνικές που επιτρέπουν την ακριβή μέτρηση της ποσότητας ηλεκτρομαγνητικής ακτινοβολίας που απορροφάται ή εκπέμπεται από τις διάφορες χημικές ενώσεις σε μεγάλη ποικιλία περιοχών συχνοτήτων ή μηκών κύματος.

Η ολική ενέργεια ενός μορίου και αντίστοιχα οι δυνατές ενεργειακές μεταπτώσεις, προέρχονται από τέσσερις βασικές πηγές: *α*) Την ηλεκτρονική ενέργεια, η οποία οφείλεται στην ηλεκτροστατική αλληλεπίδραση των ηλεκτρονίων και των πρωτονίων του μορίου, *β*) τη μεταφορική κινητική ενέργεια η οποία οφείλεται στην μεταφορική κίνηση του κέντρου μάζας του μορίου στο χώρο, *γ*) την κινητική ενέργεια εκ περιστροφής, που οφείλεται στην περιστροφή του μορίου γύρω από το κέντρο μάζας του και *δ*) την ενέργεια ταλάντωσης που οφείλεται στις ταλαντώσεις των ατόμων του μορίου ως προς το κέντρο μάζας του μορίου[99]. Παράγοντες που επιδρούν στην ένταση των φασματικών γραμμών είναι κατά βάση η πιθανότητα μετάβασης, ο πληθυσμός των καταστάσεων και η συγκέντρωση και πάχος του δείγματος. Η ακριβής γνώση των κβαντικο-κυματομηχανικών συναρτήσεων μεταξύ δύο ενεργειακών καταστάσεων όπου θα γίνει μετάβαση και οι κανόνες επιλογής, εάν δηλαδή μια μετάβαση είναι δυνατή ή όχι, βοηθά στη θεωρητική πρόγνωση της θέσης και της έντασης των φασματικών γραμμών, χωρίς αυτό να είναι πάντοτε δυνατό. Επίσης εάν υπάρχουν δύο ισοπίθανες ενεργειακές μεταβάσεις η πιο έντονη φασματική γραμμή θα προκύψει από την ενεργειακή στάθμη με το μεγαλύτερο πληθυσμό μορίων. Η κατανομή πληθυσμών μορίων με δύο διαφορετικές καταστάσεις δίνεται από το νόμο κατανομής του Boltzmann.

Όταν η μονοχρωματική ακτινοβολία λέιζερ προσπέσει πάνω σε μόρια μιας ένωσης τότε αυτά εν δυνάμει υπόκεινται ελαστικές διαθλάσεις, χωρίς απώλεια ενέργειας, και ένας ανιχνευτής σε ορθή γωνία ως προς την κατεύθυνση της προσπίπτουσας ακτινοβολίας, μπορεί να δεχθεί τα διαθλώμενα φωτόνια. Στην περίπτωση που υφίσταται ανταλλαγή ενέργειας κατά τη διάρκεια ανελαστικών συγκρούσεων μεταξύ φωτονίων και μορίων, τότε τα μόρια είτε κερδίζουν ή χάνουν ποσότητα ενέργειας και το φάσμα καλείται αντίστοιχα Stokes ή αντι-Stokes[348]. Η διαφορά ενέργειας, μεταξύ

δύο επιτρεπόμενων καταστάσεων αντιπροσωπεύει αλλαγές στη δονητική και/ή περιστροφική ενέργεια του μορίου (*Σχήμα 3.2 – σελ. 104*). Στην περίπτωση του φαινομένου Raman οι κβαντικές ενεργειακές μεταβολές οφείλονται στη δυνατότητα πόλωσης του χημικού μορίου, δηλαδή την ικανότητα ενός ατόμου ή μορίου να υποστεί διαχωρισμό των κέντρων θετικού και αρνητικού φορτίου μέσα σε ένα ηλεκτρικό πεδίο.

Η τεχνική της φασματοσκοπίας φθορισμού επαγόμενου από λέιζερ

Ο φθορισμός ενός ατόμου είναι η προϊούσα εκπεμπόμενη ηλεκτρομαγνητική ακτινοβολία κατόπιν θερμικής, ηλεκτρονικής ή χημικής διέγερσης, ή απορρόφησης φωτονίου από το άτομο αυτό. Στη δεδομένη μεθοδολογία στα πλαίσια της διατριβής, ο φθορισμός επάγεται από μονοχρωματική ακτινοβολία λέιζερ, συντονισμένη κατάλληλα ώστε να διεγείρει τα υπό μελέτη στοιχεία. Κατά αυτόν τον τρόπο ο φθορισμός προέρχεται από επιλεγμένες ενεργειακές μεταβάσεις που υπό κανονικές συνθήκες θα είχαν μικρή πιθανότητα μετάβασης και κατά συνέπεια χαμηλά επίπεδα σήματος. Επιπροσθέτως, κατά την ακολουθούμενη τεχνική η προϊούσα ακτινοβολία εντοπίζεται σε πλείστα μήκη κύματος εκτός αυτών της διεγείροντος ακτινοβολίας, δίνοντας τη δυνατότητα αποφυγής φαινομένων ελαστικής σκέδασης κατά την ανίχνευση του σήματος. Ωστόσο, τα ίδια φαινόμενα αλληλεπίδρασης σε μοριακό επίπεδο που παρέχουν τη δυνατότητα υψηλού σήματος σε διαφορετικά εύρη συχνοτήτων, εισάγουν υψηλή δυσκολία στην ποσοτικοποίηση των αποτελεσμάτων.

Ανάλογα με το κυρίαρχο είδος μοριακής αλληλεπίδρασης διαχωρίζονται οι αντίστοιχες στρατηγικές μεθοδολογίες διέγερσης-ανίχνευσης (*Σχήμα 3.3 – σελ. 106*). Η πρώτη πιθανή αποδιέγερση είναι το διεγερμένο μόριο να επανέρθει στην αρχική ενεργειακή στάθμη με εκπομπή ακτινοβολίας στη συχνότητα της ακτινοβολούσας δέσμης λέιζερ. Δευτερευόντως, το μόριο δύναται να απορροφήσει την ακτινοβολία φτάνοντας στα επίπεδα ιονισμού ή διάστασης του[125]. Σε περιβάλλον φλόγας, λόγω των υψηλών θερμοκρασιών και της χημικά ενεργής σύστασης του όγκου ελέγχου, το υπό μελέτη μόριο υπόκειται σε δονητική και περιστροφική ενεργειακή μετάπτωση με ή χωρίς αντίστοιχη εκπομπή ακτινοβολίας και αυτό ακριβώς το φαινόμενο προκαλεί τις μεγαλύτερες δυσκολίες ποσοτικοποίησης των αποτελεσμάτων[61]. Μία στρατηγική που απαλλάσσει την εξάρτηση του σήματος από τις μοριακές συγκρούσεις είναι η τεχνική της διέγερσης σε επίπεδα κορεσμού[132], ούτως ώστε ο πληθυσμός που μεταβαίνει από τη βασική στη διεγερμένη στάθμη εξαρτάται κυρίως από την εξαναγκασμένη ακτινοβολία και την ένταση της δέσμης λέιζερ. Στα πλαίσια της διατριβής, η διέγερση επετεύχθη σε επίπεδα όπου διατηρείται γραμμική συσχέτιση μεταξύ της έντασης της εφαρμοζόμενης ακτινοβολίας και του πληθυσμού της στάθμης διέγερσης και κατ' επέκταση του πληθυσμού βάσης. Με την τεχνική της φασματοσκοπίας γραμμικώς επαγόμενου φθορισμού από λέιζερ, τα απαιτούμενα επίπεδα ενέργειας της δέσμης διέγερσης είναι σχετικά χαμηλά και συνεπώς είναι δυνατή η παραγωγή επίπεδης δέσμης για άμεση δισδιάστατη απεικόνιση της ζώνης έκτασης του μελετώμενου στοιχείου, εξυπηρετώντας τους στόχους που θέτει η διατριβή.

Βασικά συστατικά του συστήματος φθορισμού επαγόμενου από λέιζερ

Η παρακολούθηση των σύνθετων φαινομένων που περιγράφηκαν νωρίτερα και η ορθή μεθοδολογία για την ανίχνευση του επιθυμητού στοιχείου, απαιτεί υψηλά επίπεδα λειτουργικότητας από το διαγνωστικό σύστημα ενσωματώνοντας τη βαθειά επιστημονική γνώση

που τα διέπουν. Το τελικό αποτέλεσμα του συστήματος διέγερσης που επάγει το φθορισμό της υπό μελέτη χημικής ένωσης, οφείλει να είναι μία ομοιόμορφη δέσμη η οποία διασφαλίζει επαρκή ισχύ στην επιθυμητή περιοχή συχνοτήτων. Οι περισσότερες διατάξεις φθορισμού επαγόμενου από λέιζερ θυσιάζουν το μεγαλύτερο μέρος της αρχικής ισχύος τους ώστε να παράγουν την απολύτως επαρκή ισχύ στο επιθυμητό μήκος κύματος. Χαρακτηριστικά, στο σύστημα που χρησιμοποιήθηκε στα πλαίσια της διατριβής (*Σχήμα* 3.4 – *σελ.* 109), παράγει αρχική ισχύ της τάξης του ενός Joule ανά παλμό στα 1064 nm καταλήγοντας περίπου στα 10 mJ ανά παλμό στα 280 nm, απαραίτητο για τη διέγερση τις ρίζας του υδροξυλίου ή τα περίπου 2 mJ ανά παλμό στα 220 nm για τη διέγερση του μονοξειδίου του αζώτου, όπως επεξηγείται παρακάτω.

Συνοπτικά, το σύστημα αποτελείται από ένα παλμικό λέιζερ γρανάτη αργιλίου-υττρίου ενισχυμένου με νεοδήμιο (Nd: YAG) το οποίο παράγει ακτινοβολία στα 1064 nm, ισχύος της τάξης του ενός Joule ανά παλμό. Το νεοδήμιο είναι ένα τρισθενές λανθανίδιο, συχνά χρησιμοποιούμενο σε προσμίξεις με κρυστάλλους, ο γνωστότερος των οποίων είναι ο γρανάτης υττρίου αργιλίου. Τα άτομα του νεοδημίου αντικαθιστούν μερικώς τα άτομα του υττρίου στο συνθετικό γρανάτη, με συνέπεια τα ενεργειακά επίπεδα να διευρύνονται ελαφρώς διατηρώντας την κατάσταση πολλαπλής ενέργειας, η οποία είναι σημαντική για την αναστροφή πληθυσμών και τελικά την εκπομπή ακτίνας λέιζερ (*Σχήμα* 3.5 – *σελ.* 110). Το σύστημα με χρήση μεταβλητού εξασθενητή του οπτικού συντονιστή σε παλμική λειτουργία (Q-switch) παρέχει υψηλά επίπεδα ισχύος με χρονισμό της τάξης των 10 ns[310]. Επιπροσθέτως, με χρήση μη γραμμικής οπτικής ανάμιξης το σύστημα παράγει ακτινοβολία λέιζερ στα 532 nm, 355 nm και 266 nm, τα οποία καλούνται αντίστοιχα δεύτερη, τρίτη και τέταρτη αρμονική γεννήτρια του Nd: YAG[240].

Εν συνεχεία, η παραγόμενη από τη δεύτερη αρμονική γεννήτρια του Nd: YAG ακτινοβολία στα 532 nm, χρησιμοποιείται αφενός για να τροφοδοτήσει ένα σύστημα ταλαντωτή για τη ρύθμιση του τελικού μήκους κύματος στα 560 nm και αφετέρου να διεγείρει τη φέρουσα ουσία ενός λέιζερ χρωστικής. Η επίτευξη του ακριβούς μήκους κύματος διέγερσης του υπό μελέτη στοιχείου είναι ουσιώδους σημασίας για την επαγωγή του φθορισμού μέσω της δέσμης λέιζερ. Τα συστήματα λέιζερ με χρήση χρωστικής ουσίας φθορισμού[296], χρησιμοποιούν ως ενεργό μέσο υγρά διαλύματα αλκοολών με σύνθετες οργανικές ενώσεις, που παρουσιάζουν φωτοχημική σταθερότητα και ελάχιστη επικάλυψη φάσματος εκπομπής απορρόφησης και συνεπώς υψηλά επίπεδα κβαντικής απόδοσης (*Σχήμα* 3.6 – *σελ.* 112). Για τη μελέτη της ρίζας του υδροξυλίου χρησιμοποιήθηκε διάλυμα αιθανόλης με ροδαμίνη, το οποίο παρουσιάζει μέγιστη απόδοση του φάσματος εκπομπής στα 590 nm, κατόπιν διέγερσης από τη δεύτερη αρμονική γεννήτρια του Nd: YAG. Τελικά, η προϊούσα ακτίνα υπόκειται οπτικό διπλασιασμό συχνότητας, παράγοντας νέα ακτίνα με μήκος κύματος ίσο με το μισό της αρχικής, ήτοι περίπου 280 nm, ιδανικό για τη διέγερση του υδροξυλίου (*Σχήμα* 3.7 – *σελ.* 113).

Για τη συλλογή του επαγόμενου φθορισμού χρησιμοποιήθηκε ανιχνευτής με διάταξη σύζευξης φορτίου σε συνδυασμό με κατάλληλα φίλτρα φάσματος (*Σχήμα* 3.8 – *σελ.* 115). Εν προκειμένω, για την ανίχνευση του φθορισμού κατά τη μετάβαση της ρίζας του υδροξυλίου από και προς τη βασική ενεργειακή στάθμη, ήτοι OH (0,0), χρησιμοποιήθηκε φίλτρο με μέγιστη οπτική απόδοση στα 313 nm και τυπική απόκλιση της κατανομής περίπου 10 nm. Η επιμέρους λεπτομέρειες της διέγερσης και ανίχνευσης του υδροξυλίου παρατίθενται στη συνέχεια. Όσον αφορά στη μελέτη της

ψυχρής ροής φλόγας προανάμιξης εγκάρσιας ροής που πραγματοποιήθηκε στην παράγραφο 5.2.1.1, μέσω της διερεύνησης του φθορισμού ίχνους ακετόνης, η διαδικασία μπορεί να περιγραφεί εν συντομία ως εξής. Το ευρύ φάσμα απορρόφησης που παρουσιάζει η ακετόνη από τα 225 έως τα 320 nm δίνει τη δυνατότητα διέγερσης με χρήση της τέταρτης αρμονικής γεννήτριας του Nd: YAG στα 266 nm[191], με επίπεδα ισχύος περί τα 90 mJ ανά παλμό και ακόλουθη ανίχνευση του επαγόμενου φθορισμού με χρήση φίλτρου ευρείας φασματικής απόδοσης που καλύπτει την εκπεμπόμενη ακτινοβολία σε μήκη κύματος από 350 έως περίπου 470 nm.

Η μεθοδολογία διέγερσης και ανίχνευσης του επαγόμενου φθορισμού της ρίζας του υδροξυλίου

Η ρίζα του υδροξυλίου σχηματίζεται κυρίως από την προσκόλληση ατόμων οξυγόνου στα μόρια των περιεχόμενων στο καύσιμο υδρογονανθράκων και τελικώς ανασυντάσσονται προς το σχηματισμό νερού. Η αλληλουχία αυτή καθιστά την μελέτη της ρίζας του υδροξυλίου ουσιώδους σημασίας για την κατανόηση της χημείας της καύσης, των χαρακτηριστικών της φλόγας και την επαλήθευση και βελτιστοποίηση των θεωρητικών και υπολογιστικών εργαλείων. Ως αποτέλεσμα της πολύχρονης μελέτης του υδροξυλίου, υπάρχουν σήμερα εκτενείς θεωρητικές μελέτες[171] για τις ενεργειακές μεταπτώσεις του μορίου σε περιβάλλον φλόγας, οι οποίες είναι εξαιρετικής σημαντικότητας για την εκτέλεση ακριβών πειραματικών μελετών με χρήση οπτικών μεθόδων και τανάπαλιν. Στα πλαίσια της διατριβής, παρακολούθηση της ρίζας του υδροξυλίου στη ζώνη καύσης μέσω της τεχνικής της φασματοσκοπίας φθορισμού επαγόμενου από διέγερση laser χρησιμοποιείται για την οπτικοποίηση της φλόγας και την παραμετρική μελέτη των χαρακτηριστικών της ζώνης καύσης[170]. Προκειμένου η ζώνη της φλόγας να οπτικοποιείται κατά το δυνατόν σαφέστερα, η δισδιάστατη δέσμη διέγερσης οφείλει να παρουσιάζει ομοιόμορφη κατανομή ισχύος. Επιπροσθέτως, η δέσμη λέιζερ οφείλει να έχει ικανή ενεργειακή ισχύος, ώστε να μην εξασθενεί κατά τη διείσδυση στη φλόγα, χωρίς συνάμα να είναι υπερβολικά υψηλή, για την αποφυγή του φαινομένου του κορεσμού.

Η κύρια ενεργειακή μετάβαση που επιλέχθηκε προς διέγερση αφορά στη μετάπτωση από τη βασική ενεργειακή στάθμη στην αντίστοιχη πρώτη διεγερμένη, η οποία συμβολίζεται ως $A^2\Sigma^+ - X^2\Pi_i$. Περαιτέρω, για την αποφυγή φαινομένων σκέδασης μεταξύ διεγείρουσας και εκπεμπόμενης ακτινοβολίας (*Σχήμα 3.9 – σελ. 117*), η δευτερεύουσα ενεργειακή μετάβαση που παρακολουθήθηκε ήταν η δονητική μετάπτωση OH (0,0)[151], ενώ η αντίστοιχη διέγερση έγινε προς τη δονητική μετάπτωση OH (1,0)[169]. Η μεθοδολογία αυτή είναι εφικτή, καθώς κατόπιν της διέγερσης στο πρώτο δονητικό επίπεδο, οι μοριακές αλληλεπιδράσεις ακτινοβολούν φθορισμό σε όλες τις υπόλοιπες δονητικές στάθμες[173]. Τελικώς, η επιλογή κατάλληλης περιστροφικής ενεργειακής μετάβασης μέσα στο μόριο, είναι εξαιρετικά σημαντική για την ορθή απεικόνιση του πληθυσμού στις στάθμης. Σε κάθε μία δονητική μετάπτωση αντιστοιχούν πολλές αντίστοιχες περιστροφικές, Οι περιστροφικές μεταπτώσεις παρουσιάζουν ποικιλόμορφη εξάρτηση από τη θερμοκρασία της κάθε στάθμης και της επικρατούσας θερμοκρασίας. Μέσω κατάλληλων υπολογιστικών προσομοιώσεων[52] η εξάρτηση της προς διέγερση περιστροφικής μετάπτωσης με τον πληθυσμό στάθμης και τη θερμοκρασία μπορεί να υπολογιστεί. Εφόσον ο στόχος των πειραματικών μελετών στα πλαίσια της διατριβής είναι η απεικόνιση της ζώνης της φλόγας και συνεπώς του πληθυσμού της ρίζας του υδροξυλίου (και όχι η θερμοκρασιακή μέτρηση όπου θα ακολουθούταν η ακριβώς αντίστροφη διαδικασία επιλογής διεγείρουσας περιστροφικής ενεργειακής μετάπτωσης), η προς

26

διέγερση περιστροφική ενεργειακή μετάπτωση οφείλει να είναι κατά το δυνατόν θερμοκρασιακά ανεξάρτητη. Συνεπώς, η περιστροφική ενεργειακή μετάβαση της αντίστοιχης πρώτης δονητικής που επιλέχθηκε προς διέγερση ήταν η $Q_1(6)$ (*Σχήμα 3.10 – σελ.* 119), η οποία εξασφαλίζει ότι ο προϊόν φθορισμός πηγάζει ως επί το πλείστον από τον πληθυσμό ριζών υδροξυλίου στην αντίστοιχη διεγερμένη ενεργειακή στάθμη και όχι από την επίδραση της θερμοκρασίας.

Η περιγραφείσα μεθοδολογία για την ανίχνευση του φθορισμού της ρίζας του υδροξυλίου κατόπιν διέγερσης από το έκτο περιστροφικό του αντίστοιχου πρώτου δονητικού ενεργειακού επιπέδου της μετάβασης $A^2\Sigma^+ – X^2\Pi_i$, σε συνδυασμό με τη λήψη πολλαπλών στατιστικά ανεξάρτητων μετρήσεων, οδηγεί στην επαρκή περιγραφή της ζώνης αντίδρασης στη φλόγα. Επιπροσθέτως, η ομοιογενής ενεργειακή κατανομή της ισχύος στη διεγείρουσα δέσμη, προσδίδει σαφή δισδιάστατη απεικόνιση των χαρακτηριστικών της φλόγας, όπως παρουσιάζεται στα κεφάλαια 5 και 7.

Κεφάλαιο 4ο – Εφαρμογή και αξιολόγηση παρεμβατικών διαγνωστικών τεχνικών σε βασικές διατάξεις φαινομένων καύσης στα πλαίσια της διατριβής

Τα διαγνωστικά εργαλεία που περιγράφηκαν νωρίτερα, εφαρμόζονται αρχικά σε διατάξεις μικρής πολυπλοκότητας, προτού εφαρμοστούν σε σύνθετα συστήματα καύσης. Στα πλαίσια του παρόντος κεφαλαίου, επιχειρείται η εφαρμογή του συστήματος της αέριας χρωματογραφίας που περιγράφηκε στο 2ο κεφάλαιο, σε μία διάταξη αντιδραστήρα εμβολικής ροής. Ο αντιδραστήρας εμβολικής ροής προσομοιάζεται υπολογιστικά με τη βασική παραδοχή ότι δεν υπάρχει ανάμιξη στην αξονική διάσταση ενώ υπάρχει πλήρης ανάμιξη στην διάσταση που είναι εγκάρσια της κατεύθυνσης της ροής. Η απουσία ανάμιξης στην αξονική διάσταση επιτρέπει τη μεγιστοποίηση της εφικτής μετατροπής των αντιδρώντων, ενώ η έλλειψη εγκάρσιων διανυσμάτων διασφαλίζει την απουσία των περιορισμών που τίθενται λόγω της μεταφοράς μάζας με αποτέλεσμα την αύξηση των υπολογιστικών επιδόσεων του ιδανικού αντιδραστήρα. Καθίσταται προφανές ότι η διάταξη του αντιδραστήρα εμβολικής ροής είναι ιδανική για την εφαρμογή εργαλείων που παρέχουν λεπτομερείς μετρήσεις χημικών ειδών, όπως η αέρια χρωματογραφία, με σκοπό την βελτιστοποίηση υπολογιστικών μοντέλων αναλυτικής χημικής κινητικής. Επιπροσθέτως, η επιλογή αρχικών συνθηκών, μιγμάτων καυσίμου και εύρους δοκιμών σχετίζεται άμεσα με τη διεργασία αναμόρφωσης καυσίμου για κυψέλες καυσίμου, όπως επεξηγείται στην εισαγωγή της διατριβής. Η παραγωγή υδρογόνου κατά την αναμόρφωση ευνοείται από τις πλούσιες σε καύσιμο συνθήκες, και έτσι αναμένεται ότι θεωρητικά θα μεγιστοποιείται σε συνθήκες πυρόλυσης[220], στις οποίες ωστόσο, μεγιστοποιείται και ο σχηματισμός μη αέριων ανθρακικών ενώσεων και αιθάλης.

Η μελέτη της πυρόλυσης μιγμάτων με βάση το μεθάνιο έχει πραγματοποιηθεί κατά το παρελθόν σε πρότυπες, βασικές διατάξεις όπως θαλάμους κρουστικού κύματος[7], αντιδραστήρες τέλειας ανάμιξης[305] και αντιδραστήρες εμβολικής ροής[238]. Παρόλα αυτά η συνθήκες και τα μίγματα που εξετάζονται στο παρόν κεφάλαιο, καλύπτουν ένα θερμοκρασιακό εύρος για το οποίο δεν υπάρχουν ενδελεχή πειραματικά δεδομένα[211]. Ακόμη, η μελέτη περιπτώσεων (*Πίνακας 4.1 – σελ.* 130) στα πλαίσια του κεφαλαίου, σχετίζεται με μίγματα των οποίων η συμπεριφορά αναδεικνύει τη διαφορετικότητα ενός μίγματος συνθετικού φυσικού αερίου και ενός μίγματος βιοαερίου σε σχέση με την πυρόλυση του καθαρού μεθανίου. Εν προκειμένω, η αναγκαιότητα της μελέτης του μίγματος CH_4/CO_2, έγκειται σε δύο παράγοντες. Αφενός, στο γεγονός ότι τέτοια μίγματα συναντώνται ολοένα και περισσότερο σε πρακτικές εφαρμογές που χρησιμοποιούν προϊόντα

αεριοποίησης βιομάζας[340], και αφετέρου από την σκοπιά της χημείας καύσης, όπου η διερεύνηση του ρόλου του CO_2 σαν διαλύτης δρώντας όμοια με το αδρανές περιβάλλον N_2, ή σαν οξειδωτικό, αποτελεί προϋπόθεση για την αξιολόγηση της περαιτέρω χρήσης παρόμοιων μιγμάτων σε πρακτικές εφαρμογές.

Τα πειράματα που πραγματοποιήθηκαν, μοντελοποιούνται και αναλύονται στο παρόν κεφάλαιο με σκοπό την διερεύνηση της χημείας που σχετίζεται με την παραγωγή του αερίων ρύπων, καθώς και των προϊόντων μεγάλου μοριακού βάρους, αφορούν στην πυρόλυση μεθανίου, φυσικού αερίου και βιοαερίου σε αντιδραστήρα εμβολικής ροής. Τα πειράματα πυρόλυσης πραγματοποιήθηκαν σε ισοθερμοκρασιακό αντιδραστήρα εμβολικής ροής (*Σχήμα 4.1 – σελ. 130*) για T = 1000 ^{o}C έως T = 1200 ^{o}C υπό αυστηρώς ελεγχόμενες συνθήκες. Τα παραγόμενα χημικά είδη στην έξοδο του αντιδραστήρα μετρήθηκαν με σύστημα αέριας χρωματογραφίας σε πραγματικό χρόνο ενώ η συνολικά παραγόμενη αιθάλη προσδιορίστηκε με συλλογή της από όλα τα μέρη του αντιδραστήρα και διεξαγωγή κατάλληλης ζύγισή της. Επιπρόσθετα, οι βασικοί παραγόμενοι πολυκυκλικοί αρωματικοί υδρογονάνθρακες μετρήθηκαν επιλεκτικά με σύστημα αέριας χρωματογραφίας συνδυαζόμενο με φασματοσκοπίας μάζας, βοηθώντας στη βαθύτερη κατανόηση των διεργασιών που διέπουν την πυρόλυση αλλά και τους μηχανισμούς παραγωγής ρύπων.

Τα πειραματικά δεδομένα που συλλέχτηκαν, αναπαρήχθησαν υπολογιστικά με χρήση εμπορικού εργαλείου, κάνοντας χρήση δύο διαφορετικών εργαλείων αναλυτικής χημικής κινητικής. Το πρώτο εργαλείο έχει χρησιμοποιηθεί κατά το παρελθόν για την πρόλεξη πειραμάτων πυρόλυσης από τον ακριβώς ίδιο αντιδραστήρα[14] και το δεύτερο αναπτύσσεται τα τελευταία χρόνια στο Ε.Μ.Π.[320]. Για τις ανάγκες τις προσομοίωσης των συνθηκών πυρόλυσης ο υπάρχων C_1-C_6 λεπτομερής μηχανισμός[322] εμπλουτίστηκε με αντιδράσεις, θερμοδυναμική και δεδομένα διάχυσης/μεταφοράς, από υπό-μηχανισμό της βιβλιογραφίας[289], ώστε να καλύπτει την περιοχή των πολυκυκλικών αρωματικών υδρογονανθράκων μέχρι το βενζο-πυρένιο. Η απόδοση του μηχανισμού ενάντια δεδομένων από πλούσιες φλόγες προανάμιξης φυσικού αερίου (*Σχήμα 4.2 – σελ. 131*) και βενζολίου (*Σχήμα 4.3 – σελ. 132*) είναι πολύ ικανοποιητική, πράγμα που συνηγορεί στο ότι ο μηχανισμός ενδείκνυται για την πρόλεξη των πειραματικών αποτελεσμάτων της πυρόλυσης στα πλαίσια του κεφαλαίου.

Μετατροπή καυσίμου και κύρια παράγωγα της πυρόλυσης

Το υδρογόνο αποτελεί κύριο προϊόν της πυρόλυσης των μιγμάτων μεθανίου, πράγμα που καθιστά και τη διεργασία αυτή σημαντική μεθοδολογία για την παραγωγή υδρογόνου ή/και αερίου σύνθεσης[95]. Το επίπεδα μετατροπής καυσίμου και παραγόμενου υδρογόνου κατά την πυρόλυση του μεθανίου και του φυσικού αερίου (*Σχήμα 4.4 – σελ. 133*) καθώς και τα επίπεδα μετατροπής καυσίμου και παραγόμενου υδρογόνου και μονοξειδίου του άνθρακα σε περιβάλλον διοξειδίου του άνθρακα και αζώτου (*Σχήμα 4.5 – σελ. 134*), έρχονται σε εξαιρετική συμφωνία με τις αντίστοιχες υπολογιστικές προλέξεις. Γενικά τα αποτελέσματα επιβεβαιώνουν την πιο αυξημένη αντιδραστικότητα του μίγματος μεθανίου/αιθανίου, σε συμφωνία με την βιβλιογραφία[38]. Αυτό οφείλεται στο γεγονός ότι, στις χαμηλότερες και ενδιάμεσες θερμοκρασίες, τα σχετικά πιο ασταθή μόρια αιθανίου αποσυντίθεται αφήνοντας αιθυλικές ρίζες και ρίζες υδρογόνου. Το υδρογόνο τροφοδοτεί στη συνέχεια την αντίδραση R 4.4 και έτσι επιταχύνεται η μετατροπή του μεθανίου. Σε υψηλότερες θερμοκρασίες, η αντίδραση R 4.1 γίνεται σημαντικά βραδύτερη από την θερμική

28

διάσπαση του αιθανίου (R 4.2) και, ως αποτέλεσμα, η παραγωγή ριζών υδρογόνου μειώνεται. Από την άλλη πλευρά, η προσθήκη διοξειδίου του άνθρακα δεν έχει ευδιάκριτη επίδραση επί της μετατροπής του μεθανίου σε χαμηλές θερμοκρασίες. Καθώς η θερμοκρασία αυξάνεται, ρίζες υδρογόνου παράγονται από την πυρόλυση του μεθανίου και ευνοούν την αντίδραση παραγωγής μονοξειδίου του άνθρακα και υδροξυλίου από διοξείδιο του άνθρακα και ρίζες υδρογόνου, η οποία οδηγεί σε αυξημένο ρυθμό σχηματισμού ριζών υδροξυλίου. Οι τελευταίες ξεκινούν αντιδράσεις αφαίρεση ρίζας υδρογόνου από το μεθάνιο, ενισχύοντας έτσι τη μετατροπή του. Παρά τις διαφορές στους αντίστοιχους ρυθμούς κατανάλωσης καυσίμου μεταξύ μεθανίου και φυσικού αερίου, τα επίπεδα υδρογόνου είναι τα παρόμοια. Από την άλλη, η παραγωγή H_2 μειώνεται σημαντικά όταν προστίθεται CO_2 στο αρχικό καύσιμο μίγμα. Ωστόσο, τα συνολικά επίπεδα H_2 και CO, διατηρούνται σε όρους γραμμομοριακού κλάσματος, αλλά όχι από την άποψη του ενεργειακού περιεχομένου, λόγω της χαμηλότερης ενθαλπίας σχηματισμού του μονοξειδίου του άνθρακα.

Για την περεταίρω διερεύνηση των χημικών διεργασιών που λαμβάνουν χώρα κατά την διάρκεια της πυρόλυσης των υπό μελέτη μιγμάτων, πραγματοποιήθηκε υπολογιστική ανάλυση του ρυθμού παραγωγής. Σε όλες τις περιπτώσεις, η συνολική αντίδραση ξεκινά με την θερμική διάσπαση του μεθανίου για την παράγωγη ριζών μεθυλίου και ριζών υδρογόνου (R 4.3). Κατόπιν, η επίθεση ριζών H στο μεθάνιο (R 4.4), τροφοδοτεί το σύστημα με περισσότερο CH_3. Η παραπάνω αλληλουχία συμβάλλει επίσης σχεδόν κατά 50% στην συνολική παραγωγή μοριακού υδρογόνου κατά την πυρόλυση του μεθανίου. Η μεθυλική ρίζα καταναλώνεται αποκλειστικά στο αιθάνιο, μέσω της αντίδρασης αυτο-ανασυνδυασμού του (R 4.2), ξεκινώντας έτσι την C_2 αλυσίδα. Στην συνέχεια, οι ρίζες υδρογόνου προκαλούν αλληλουχία αντιδράσεων αφαίρεσης H που οδηγεί από το αιθάνιο στο ακετυλένιο μέσω της αποβολής μορίων υδρογόνου. Είναι ενδιαφέρον να σημειωθεί ότι η παραπάνω αλληλουχία δεν είναι μια αλληλουχία παραγωγής ριζών H, αφού όσες ρίζες H σχηματίζονται από τις αντιδράσεις (R 4.6) και (R 4.8), καταναλώνονται σε ίσα ποσοστά στις αντιδράσεις (R 4.5) και (R 4.7). Οι παραπάνω χημικές διαδρομές σχετίζονται με την παραγωγή H_2, ωστόσο ο μηχανισμός τείνει να υπο-εκτιμά τα επίπεδα του παραγόμενου υδρογόνου στις υψηλότερες θερμοκρασίες (T > 1100 °C), και ιδίως στα πειράματα πυρόλυσης σε περιβάλλον αζώτου, με αποκλίσεις της τάξης του 30%. Τέτοιες διαφορές δεν μπορούν εύκολα να αποδοθούν σε παραλείψεις στις δύο μεγάλες διαδρομές παραγωγής H_2 που περιγράφονται παραπάνω (R 4.5, R 4.7), καθώς το προφίλ κατανάλωσης του μεθανίου και η ακρίβεια πρόλεξης των συνολικών επιπέδων C_2,είναι πολύ ικανοποιητικά, ιδιαίτερα σε υψηλότερες θερμοκρασίες. Αυτό συνεπάγεται ότι, μπορεί να υπάρχουν πρόσθετες διαδρομές παραγωγής υδρογόνου, όπως θερμικές αντιδράσεις πυρόλυσης, που περιλαμβάνουν ενδεχομένως υψηλότερα αλιφατικά, λ.χ. C_4, ή (πολυ-) αρωματικά χημικά είδη. Επίσης, το μοριακό υδρογόνο είναι "αριθμητικά" κλειδωμένο στα πολυαρωματικά χημικά είδη, δεδομένου ότι οι μηχανισμοί δεν περιλαμβάνουν αντιδράσεις αιθάλης.

Απεναντίας, τα επίπεδα υδρογόνου αναπαράγονται ικανοποιητικά στα πειράματα πυρόλυσης σε μικτό περιβάλλον αζώτου και διοξειδίου του άνθρακα. Αυτό οφείλεται στην παρουσία του CO_2, η οποία επάγει έναν οξειδωτικό χαρακτήρα στην πυρολυτική διαδικασία, καταλήγοντας έτσι σε μία πιο ισορροπημένη χημεία. Για παράδειγμα, στην περίπτωση T = 1200 °C εκτός από την αντίδραση (R 4.4) και τα μονοπάτια C_2 αλυσίδας που συζητήθηκαν παραπάνω, υπάρχει μία σημαντική συμβολή στο σχηματισμό H_2 από αντιδράσεις που περιλαμβάνουν οξυγονωμένα είδη, όπως φορμαλδεΰδη, κετένιο και προπιοναλδεΰδη. Η συνολική εικόνα δεν είναι εντελώς διαφορετική από

εκείνη που περιγράφεται ανωτέρω, ωστόσο οι ρίζες Η που επίσης αρχικά παράγονται από τη θερμική διάσπαση του μεθανίου (R 4.3), επιτίθενται αμέσως στα μόρια CO_2 και παράγεται CO και μια ρίζα υδροξυλίου, αντίδραση (R 4.10). Έτσι, υπό την παρουσία του CO_2, οι αντιδράσεις αφαίρεσης με ρίζες υδροξυλίου, αποτελούν ένα σημαντικό τμήμα του συνολικού ρυθμού καταστροφής του καυσίμου και οδηγούν στο σχηματισμό του νερού (*Σχήμα 4.6 – σελ.* 136), η οποία με την σειρά της ανταγωνίζεται την παραγωγή H_2. Ως αποτέλεσμα, η απόδοση σε υδρογόνο σε περιβάλλον διοξειδίου του άνθρακα και αζώτου, είναι σχεδόν η μισή σε σύγκριση με τα πειράματα σε αμιγές περιβάλλον αζώτου. Η παραπάνω ανάλυση δείχνει ότι το CO_2 λειτουργεί εν μέρει ως οξειδωτικό και όχι ως απλός διαλύτης, όπως το άζωτο.

Διεργασίες αύξησης μοριακού βάρους, προπομποί και σχηματισμός αιθάλης

Η διεργασία σχηματισμού αιθάλης είναι συνδεδεμένη με τη χημεία σχηματισμού ορισμένων ελαφρύτερων ενώσεων οι οποίες θεωρούνται προπομποί του τελικού σχηματισμού της αιθάλης. Για την πλήρη κατανόηση των ανωτέρω φαινομένων, η μελέτη εστίασε στα χημικά είδη με δύο και τρία άτομα άνθρακα καθώς και το βενζόλιο, που παρήχθησαν κατά τα προαναφερθείσες μελέτες περίπτωσης, όπου επετεύχθη σχετικά καλή συμφωνία μεταξύ πειραματικών αποτελεσμάτων και υπολογιστικών προλέξεων. Η C_2 αλυσίδα, ξεκινά από το σχηματισμό C_2H_6 (*Σχήμα 4.7 – σελ.* 137) και τελικά καταλήγει στον σχηματισμό ακετυλενίου (*Σχήμα 4.8 – σελ.* 138), όπως έχει περιγραφεί παραπάνω, έχοντας άμεση σχέση με τη χημεία καταστροφής του καυσίμου. Τα επίπεδα ακετυλενίου αναπαράγονται γενικά ικανοποιητικά, από το δεύτερο μηχανισμό που χρησιμοποιήθηκε, παρουσιάζοντας μέγιστα επίπεδα και για τις τρεις περιπτώσεις εντός της περιοχής θερμοκρασιών που μελετήθηκαν, τιμές 2000 ppm περίπου. Το ακετυλένιο που σχηματίζεται, ποσοτικά καταναλώνεται στα C_3H_4 (*Σχήμα 4.9 – σελ.* 138) ισομερή τα οποία, με τη σειρά τους, θα συμμετάσχουν σε περαιτέρω αντιδράσεις μοριακής ανάπτυξης. Ειδικότερα, η αλυσίδα C_3 εκκινείται με την προσθήκη μεθυλικής ρίζας σε ακετυλένιο, αντιδράσεις (R 4.13) και (R 4.14), οδηγώντας σε σχηματισμό προπαδιενίου και προπινίου αντίστοιχα.

Τα C_3H_4 είδη μετατρέπονται αποκλειστικά σε ρίζες προπαργυλίου, οι οποίες με τη σειρά τους ανασυνδυάζονται προς σχηματισμό βενζολίου. Το προπένιο σχηματίζεται επίσης από την προσθήκη CH_3 στο C_2H_4, ή άμεσα (R 4.15), είτε έμμεσα μέσω της κανονικής προπυλικής ρίζας, (R 4.16). Τα επίπεδα του C_3H_6 υπερ-εκτιμώνται κι από τα δύο υπολογιστικά μοντέλα. Από την στιγμή που ο σχηματισμός προπενίου οφείλεται αποκλειστικά στον ανασυνδυασμό ριζών βινυλίου και μεθυλίου, η ανωτέρω υπερ-εκτίμηση μπορεί να αποδοθεί στην συνολική υπερ-εκτίμηση του CH_3, όπως συζητήθηκε νωρίτερα. Αναφορικά με τα επίπεδα του βενζολίου ως συνάρτηση της θερμοκρασίας (*Σχήμα 4.10 – σελ.* 139), τα πειραματικά δεδομένα δεν επηρεάζονται σημαντικά από την θερμοκρασία, ενώ τα αριθμητικά αποτελέσματα υποδεικνύουν κάποια τοπικά μέγιστα. Οι διαφορές μεταξύ των πειραματικών και υπολογιστικών δεδομένων μπορούν να αποδοθούν στο γεγονός ότι ο σχηματισμός της αιθάλης δεν περιλαμβάνεται στο παρόν μοντέλο και αυτό υποδηλώνει την ανάγκη για περαιτέρω βελτίωση προκειμένου να αναπαράγει η σύνθετη συμπεριφορά της πυρόλυσης μιγμάτων μεθανίου.

Αναφορικά με τα επίπεδα αιθάλης που συλλέχτηκαν κατά μήκος του αντιδραστήρα συναρτήσει της θερμοκρασίας (*Σχήμα 4.11 – σελ.* 140), αναδεικνύουν με τη σειρά τους την αυξημένη δραστικότητα του μίγματος φυσικού αερίου έναντι του καθαρού μεθανίου. Το παραπάνω

οφείλεται στην παρουσία C₂ στη σύσταση του μίγματος φυσικού αερίου, και αντικατοπτρίζεται από το σχηματισμό αιθάλης στους T = 1050 °C, σε αντίθεση με τις υπόλοιπες μελέτες περίπτωσης, όπου ο σχηματισμός αιθάλης αρχίζει στους T = 1110 °C. Επίσης τα επίπεδα αιθάλης σε περιβάλλον διοξειδίου του άνθρακα και αζώτου, παρουσιάζουν τοπικό μέγιστο περίπου στους T = 1110 °C, ήτοι αρκετά νωρίτερα σε σύγκριση με τα πειράματα σε αμιγές περιβάλλον αζώτου. Τέλος, τα ευρήματα που αφορούν στα επίπεδα αιθάλης έρχονται σε απόλυτη συμφωνία με τα αντίστοιχα κατανομή των επιπέδων μετατροπής καυσίμου.

Μετρήσεις πολυκυκλικών αρωματικών υδρογονανθράκων.
Για την πληρέστερη κατανόηση των διεργασιών που διέπουν το σχηματισμό αιθάλης, επιλεκτικές μετρήσεις πολυκυκλικών αρωματικών υδρογονανθράκων, πραγματοποιήθηκαν για τις μελέτες περίπτωσης που συζητήθηκαν στα πλαίσια του κεφαλαίου. Οι πειραματική διαδικασία για τη συλλογή και ανάλυση των ανωτέρω μετρήσεων, έχει πρόσφατα δημοσιευτεί[266] για μίγματα ακετυλενίου-αιθυλενίου και πραγματώνεται με συνδυασμένη ανάλυση αέριας χρωματογραφίας και φασματοσκοπίας μάζας. Τα μετρούμενα επίπεδα αντιστοιχούν στις ενώσεις πολυκυκλικών αρωματικών υδρογονανθράκων που εναπόκεινται στον αντιδραστήρα, προσκολλώνται στην αιθάλη και συγκρατούνται σε ειδικό φίλτρο ρητίνης[265] στην έξοδο του αντιδραστήρα[267]. Γενικά, τα επίπεδα πολυκυκλικών αρωματικών υδρογονανθράκων είναι άμεση συνάρτηση του περιεχομένου στο καύσιμο άνθρακα, γεγονός που επαληθεύεται στις μετρήσεις για T = 1050 °C, όπου το μίγμα φυσικού αερίου παρουσιάζει κατά 30% υψηλότερα επίπεδα από αυτά του μεθανίου. Επίσης, τα συνολικά επίπεδα πολυκυκλικών αρωματικών υδρογονανθράκων στους T = 1110 °C είναι συστηματικά 20% μειωμένα σε σχέση με τα αντίστοιχα στους T = 1050 °C, όπως αντικατοπτρίζεται και από την ποσοτικοποίηση των επιμέρους κύριων χημικών ειδών (*Σχήμα* 4.12 – *σελ.* 140). Επιπροσθέτως, οι πολυκυκλικοί αρωματικοί υδρογονάνθρακες, εκτός του ότι μειώνουν την απόδοση των συστημάτων καύσης, είναι αποδεδειγμένα εξαιρετικά επιβλαβείς για την υγεία. Η δομή τους δε, καθορίζει σε μεγάλο βαθμό την επικινδυνότητα τους, ως προς το εάν είναι ή όχι καρκινογόνοι. Σε αυτό το πλαίσιο η ποσοτικοποίηση των δεκαέξι πιο επικίνδυνων ουσιών παρουσιάζεται στο τέλος του κεφαλαίου για της υπό μελέτη περιπτώσεις (*Σχήμα* 4.13 – *σελ.* 141).

Συμπερασματικά, το παρόν κεφάλαιο χρησιμοποιεί την τεχνική της αέριας χρωματογραφίας για την ανάλυση των ρύπων από μία βασική διάταξη αντιδραστήρα εμβολικής ροής. Οι συνθήκες που αναλύθηκαν, παρουσιάζουν μερική επικάλυψη με τη βιβλιογραφία δίνοντας την ευκαιρία αξιολόγησης της πειραματικής διαδικασίας, αλλά κυρίως δοκιμάζουν πρωτότυπα μίγματα με βάση το μεθάνιο, προσφέροντας καινοτόμα πειραματικά δεδομένα σε συνθήκες αναμόρφωσης καυσίμου από φυσικό αέριο και βιοαέριο. Επιπρόσθετα, μετρήθηκαν οι βασικοί παραγόμενοι πολυκυκλικοί αρωματικοί υδρογονάνθρακες και τα επίπεδα αιθάλης, βοηθώντας στη βαθύτερη κατανόηση των διεργασιών που διέπουν την πυρόλυση αλλά και τους μηχανισμούς παραγωγής ρύπων. Εν συντομία, οι μετρήσεις ανέδειξαν σημεία-κλειδιά, αναφορικά με τη χημεία μιγμάτων συνθετικού φυσικού αερίου και βιοαερίου σε σχέση με την πυρόλυση του καθαρού μεθανίου, όπως αυτά αντικατοπτρίζονται από το σχηματισμό αερίων ενώσεων-προπομπών αιθάλης, πολυκυκλικών ενώσεων και των επιπέδων αιθάλης καθαυτών. Τα πειραματικά δεδομένα αναπαρήχθησαν με τη χρήση δύο κατάλληλων υπολογιστικών εργαλείων αναλυτικής χημικής κινητικής με σχετικά ικανοποιητική συμφωνία. Η προσέγγιση που ακολουθήθηκε αναδεικνύει τη χρησιμότητα πειραματικών διερευνήσεων σε βασικές διατάξεις για τη βελτιστοποίηση υπολογιστικών

31

εργαλείων, όπως αναλύθηκε στην εισαγωγή της διατριβής και συνάμα προσέφερε επιπλέον πληροφορία για την ανάλυση των αποτελεσμάτων και την ανάδειξη φαινομένων συνέργειας.

Κεφάλαιο 5ο – Εφαρμογή και αξιολόγηση μη παρεμβατικών διαγνωστικών τεχνικών σε βασικές διατάξεις φαινομένων καύσης στα πλαίσια της διατριβής

Η αναγκαιότητα και το πεδίο εφαρμογής των διαγνωστικών εργαλείων συστημάτων καύσης αναλύθηκε διεξοδικά στα προηγούμενα κεφάλαια. Το τρίτο κεφάλαιο παρουσίασε τη βασική θεωρία και τα επιμέρους συστατικά τους συστήματος που πραγματώνει την τεχνική της φασματοσκοπίας φθορισμού επαγόμενης μέσω δέσμης λέιζερ. Πιο συγκεκριμένα, παρουσιάστηκε η πειραματική διαδικασία για τη δισδιάστατη απεικόνιση του μετώπου της φλόγας και των χαρακτηριστικών του, μέσω της παρακολούθησης της ρίζας του υδροξυλίου με τη χρήση της ανωτέρω τεχνικής. Κατά την ακολουθούμενη μεθοδολογική προσέγγιση, η τεχνική εφαρμόζεται αρχικά σε συστήματα μειωμένης λειτουργικής πολυπλοκότητας, που συνάμα προσφέρουν εύκολη οπτική πρόσβαση, πριν εφαρμοστούν σε σύνθετα συστήματα υψηλής πολυπλοκότητας. Στα πλαίσια του παρόντος κεφαλαίου, τα μη παρεμβατικά διαγνωστικά εργαλεία που περιγράφηκαν νωρίτερα, εφαρμόζονται αρχικά σε ένα καυστήρα τύπου Bunsen, παρουσιάζοντας τη δομή της γνώριμης φλόγας του, μέσω της τεχνικής του επαγόμενου από ακτινοβολία λέιζερ φθορισμού της ρίζας του υδροξυλίου. Εν συνεχεία, μία διάταξη φλόγας εγκάρσιας προανάμιξης μελετάται εισάγοντας παράλληλα την πολυπαραμετρική μεθοδολογία για τη μελέτη των χαρακτηριστικών της φλόγας που ακολουθείτε στην παράγραφο 7.2. Εν προκειμένω, η ψυχρή ροή μελετάται ιχνηλατώντας μόρια ακετόνης στη ροή του καυσίμου και τα χαρακτηριστικά του σχήματος της φλόγας αναλύονται μέσω της παρακολούθησης της ρίζας του υδροξυλίου στη ζώνη καύσης.

Θεμελιώδεις διατάξεις εφαρμογής και αξιολόγησης οπτικών τεχνικών – Ενδεικτική απεικόνιση φλόγας τύπου Bunsen.

Οι διατάξεις στις οποίες εφαρμόζονται κατεξοχήν καινοτόμες μεθοδολογίες με σκοπό την βελτίωση καθαυτών των διαγνωστικών εργαλείων, καθώς και των αντίστοιχων υπολογιστικών που τις μοντελοποιούν, παρουσιάζουν μεγάλη ποικιλομορφία. Ωστόσο, οι διατάξεις αυτές εμφανίζουν κοινά χαρακτηριστικά, τα οποία συνοψίζονται στο στατικό ή έστω ψευδοστατικό ροϊκό πεδίο (όταν αυτό δεν είναι αντικείμενο μελέτης), την οπτική προσβασιμότητα και την πολυεπίπεδη δομή, ώστε να προσφέρουν τη δυνατότητα αξιολόγησης δισδιάστατων οπτικών διαγνωστικών μεθόδων. Χαρακτηριστικές διατάξεις φλόγας διάχυσης για την εφαρμογή και αξιολόγηση οπτικών διαγνωστικών μεθόδων και δη διατάξεων φασματοσκοπίας φθορισμού, αποτελούν φλόγες ρευμάτων καυσίμου κι οξειδωτικού κατά ομορροή[251], φλόγες ανεστραμμένης διάχυσης καυσίμου κι οξειδωτικού[294] και φλόγες θυρίδας όπως αυτές του καυστήρα Wolfhard-Parker[104]. Ομοίως, φλόγες προανάμιξης που ενσωματώνουν τα προαναφερθέντα χαρακτηριστικά αποτελούν μεταξύ άλλων, διατάξεις τεχνηέντως σταθεροποιημένων φλόγων[214], φλόγες συστροφής[76], φλόγες ελευθέρας διάδοσης[317] και φλόγες τύπου Bunsen. Χαρακτηριστική περίπτωση συστήματος επίπεδης φλόγας προανάμιξης, στην οποία εφαρμόζονται κατά κόρον οπτικές διαγνωστικές μέθοδοι αποτελεί η φλόγα καυστήρα McKenna[215]. Ωστόσο, ο καυστήρας McKenna, αν και χαρακτηρίζεται από χαμηλά επίπεδα οξειδίων του αζώτου, σταθεροποιεί τη φλόγα στην επιφάνεια και όχι μέσα στη δομή ενός πορώδους στρώματος, προσφέροντας μειωμένη απόδοση.

Οι φλόγες τύπου Bunsen αποτελούν μία από τις πιο κλασσικές διατάξεις καύσης σε εργαστηριακό επίπεδο και έχουν εκτενώς μελετηθεί κατά το παρελθόν με μη παρεμβατικές διαγνωστικές μεθόδους[179]. Ενδεικτικά αναφέρεται ότι η τεχνική της φασματοσκοπίας φθορισμού έχει χρησιμοποιηθεί σε παρόμοιες διατάξεις για τη διερεύνηση της έντασης της τύρβης[199], των παραγόμενων ρύπων[227], του ρυθμού έκλυσης θερμότητας από τη φλόγα[236], επεκτείνοντας τα ευρήματα ακόμη και σε πρακτικές εφαρμογές, όπως μηχανές εσωτερικής καύσης[78]. Στα πλαίσια του κεφαλαίου, παρουσιάζεται η δισδιάστατη απεικόνιση της τυρβώδους δομής μίας τέτοιας φλόγας καθώς επίσης και του ψευδοστατικού ροϊκού πεδίου όπως αυτό περιγράφεται από την χρονική ολοκλήρωση διαδοχικών μετρήσεων (*Σχήμα* 5.1 – *σελ.* 150). Η στιγμιαίες μετρήσεις περιγράφουν ικανοποιητικά την ακανόνιστη, τυρβώδη εσωτερική δομή της φλόγας, όπου και το μίγμα καυσίμου-αέρα εισάγεται, ενώ η χρονικά ολοκληρωμένες μετρήσεις ορίζουν τα όρια της ομόκεντρης κατανομής του μετώπου της φλόγας. Η ενδεικτική απεικόνιση της φλόγας, με την αναπτυχθείσα τεχνική έρχεται σε απόλυτη συμφωνία με βιβλιογραφικά πειραματικά δεδομένα[119].

Πειραματική διερεύνηση της δομής φλόγας εγκάρσιας προανάμιξης

Στη συνέχεια του κεφαλαίου, μελετάται μία διάταξη φλόγας εγκάρσιας προανάμιξης[328] (*Σχήμα* 5.2 – *σελ.* 151), εισάγοντας παράλληλα την μεθοδολογία για τη μελέτη των χαρακτηριστικών της φλόγας που ακολουθείτε στην παράγραφο 7.2. Η διάταξη αυτή πλεονεκτεί τόσο στο γεγονός ότι προσφέρει άμεση οπτική πρόσβαση, εξίσου για τη διεγείρουσα ακτινοβολία και τη συλλογή του φθορισμού από τη διάταξη του ανιχνευτή, όσο και στο ότι πρόκειται για μία στρωτή φλόγα προανάμιξης μειωμένης εγγενούς περιπλοκότητας. Πλέον τούτων, η διάταξη αυτή αποτελεί ουσιώδες συστατικό ενός συνδυασμένου συστήματος προανάμιξης και φλογοπαγίδας[319] σε ένα βοηθητικό σύστημα παραγωγής θερμότητας μικρού μεγέθους[318], ιδανικό για εφαρμογές κυψελών καυσίμου ανταλλαγής πρωτονίων με καύσιμο υδρογόνο[116], προσδίδοντας κατά αυτόν τον τρόπο προοπτική στην παρούσα θεμελιώδη μελέτης σε πρακτικές εφαρμογές. Επιπροσθέτως, η επιλογή του υδρογόνου ως καύσιμο αφενός υπόσχεται υψηλά επίπεδα υδροξυλίου, τα οποία με τη σειρά τους διευκολύνουν τη μελέτη των χαρακτηριστικών και της μορφολογίας της φλόγας.

Η μορφολογία της φλόγας προσδιορίστηκε με τη χρήση του συστήματος που περιγράφεται στο τρίτο κεφάλαιο, συναρτήσει του επιβαλλόμενου ονομαστικού θερμικού φορτίου και της στοιχειομετρίας. Η πολυπαραμετρική μεθοδολογία αυτή για τη μελέτη των χαρακτηριστικών της φλόγας ακολουθείτε επίσης στην παράγραφο 7.2. Αρχικά η απεικόνιση της δισδιάστατης κατανομής της ρίζας του υδροξυλίου παρουσιάζεται για ονομαστικό φορτίο ίσο με 5 kW σε στοιχειομετρικές και πτωχές σε καύσιμο, ήτοι $\varphi = 0.5$, συνθήκες (*Σχήμα* 5.3 – *σελ.* 152). Τα αποτελέσματα αποκαλύπτουν ότι η στοιχειομετρική φλόγα, η οποία διατηρεί εμφανώς τη γνώριμη δομή της φλόγας προανάμιξης Bunsen, είναι διπλάσια σε πάχος, ενώ οι δύο παρουσιάζουν παρόμοια έκταση κατάντη για την ολοκλήρωση της ζώνης της φλόγας. Αναφορικά με την επίδραση του θερμικού φορτίου στη μορφολογία της φλόγας, οι περιπτώσεις που εξετάστηκαν αντιστοιχούν σε ονομαστικά θερμικά φορτία με 2 kW, 3 kW, 4 kW και 5 kW υπό στοιχειομετρία $\varphi = 0.5$ (*Σχήμα* 5.4 – *σελ.* 153). Τα αποτελέσματα εμφανίζουν σταδιακή αύξηση της ασυμμετρίας της φλόγας αυξανομένου του ονομαστικού θερμικού φορτίου, ιδιαιτέρως πλησίον του ακροφυσίου. Παράλληλα, είναι εμφανές ότι λόγω του αυξημένου ενεργειακού περιεχομένου της φλόγας, η έκταση της ζώνης αντιδράσεων αυξάνεται εξίσου χωρικά.

Φασματοσκοπία φθορισμού ιχνηλάτησης

Για την πληρέστερη απεικόνιση της μορφολογίας και του ροϊκού πεδίου της φλόγας, παρουσιάζονται τα αποτελέσματα της τρισδιάστατης σύνθεσης διαδοχικών μετρήσεων με χρήση της τεχνικής του φθορισμού της ρίζας του υδροξυλίου και της αντίστοιχης ψυχρής προαναμεμιγμένης ροής με χρήση φασματοσκοπίας ιχνηλάτησης ακετόνης[308]. Εν προκειμένω, η ψυχρή ροή μελετάται ιχνηλατώντας μόρια ακετόνης στη ροή του καυσίμου διατηρώντας τα χαρακτηριστικά της ροής, ενώ καθαυτά τα χαρακτηριστικά του σχήματος της φλόγας αναλύονται μέσω της παρακολούθησης της ρίζας του υδροξυλίου στη ζώνη καύσης (*Σχήμα* 5.5 – *σελ.* 155). Τα επιμέρους χαρακτηριστικά του συστήματος φθορισμού ιχνηλάτησης με χρήση λέιζερ παρουσιάζονται στο τρίτο κεφάλαιο, ενώ η μελέτη έχει δοκιμαστεί και στο παρελθόν σε παρόμοιο σύστημα[328]. Αν και η μελέτη της ανίχνευσης του φθορισμού αποτελεί ένα συμπληρωματικό κομμάτι της κυρίως ανάλυσης με τη φασματοσκοπία του φθορισμού της ρίζας του υδροξυλίου, παρέχει σαφή στοιχεία για την ορθότητα των ευρημάτων.

Συμπερασματικά, το κεφάλαιο παρουσιάζει τη δομή της φλόγας προανάμιξης τύπου Bunsen και εισάγει τη μεθοδολογία που ακολουθείται σε σύνθετες εφαρμογές, εφαρμόζοντάς τη σε μία διάταξη με άμεση οπτική πρόσβαση και υψηλά επίπεδα αναλογίας σήματος-θορύβου, αξιολογώντας κατά αυτόν τον τρόπο της τεχνική που παρουσιάστηκε στο τρίτο κεφάλαιο. Τέλος, το πεδίο εφαρμογής της υπό μελέτης με μη παρεμβατικές τεχνικές φλόγα, επεκτείνεται σε σύγχρονες πρακτικές εφαρμογές, όπως περιγράφεται στην εισαγωγή της διατριβής.

Κεφάλαιο 6ο – Αξιολόγηση καινοτόμων μιγμάτων καυσίμων με εφαρμογή των διαγνωστικών τεχνικών που αναπτύχθηκαν στα πλαίσια της διατριβής

Η ανάπτυξη εναλλακτικών καυσίμων, απολύτως συμβατών με τις υπάρχουσες υποδομές και συνάμα μειωμένο περιβαλλοντικό αποτύπωμα, καταλαμβάνει ολοένα αυξανόμενο μερίδιο στο πεδίο έρευνας συστημάτων καύσης[257]. Αντιστοίχως, τα διαγνωστικά εργαλεία συστημάτων καύσης, καλύπτουν την ανάλυση και τη δοκιμή τέτοιων καυσίμων, παρέχοντας την αναγκαία γνώση για την κατανόηση των θεμελιωδών διαφορών μεταξύ συμβατικών και εναλλακτικών καυσίμων. Μέσω της εκμετάλλευσης συμβατικών πηγών ενέργειας, όπως το φυσικό αέριο, δύνανται μέσω της διεργασίας Fischer-Tropsch να προκύψουν εναλλακτικά καύσιμα, συμβατά με τις υπαρκτές υποδομές[303]. Στα πλαίσια του παρόντος κεφαλαίου, παρόμοια συνθετικά καύσιμα εξετάζονται με τη χρήση ενός καυστήρα εργαστηριακής κλίμακας. Η χημική σύσταση των υπό μελέτη καυσίμων μιγμάτων, αποτελείται από σύνθετες αλυσίδες υδρογονανθράκων που προσομοιάζουν τη δομή της κηροζίνης αεροπορικών εφαρμογών[68]. Για αυτό το λόγο καλούνται να πληρούν απαιτητικές προδιαγραφές όσον αφορά στις φυσικοχημικές τους ιδιότητες[49]. Τα καύσιμα αυτά παρουσιάζουν σημαντική διαφοροποίηση ως προς τη σύσταση τους, κάτι που καθιστά δύσκολη την αντιστοίχιση της συμπεριφοράς τους σε συστήματα καύσης με το συστατικά που τα απαρτίζουν. Γι αυτό το λόγο το παρόν κεφάλαιο ακολουθεί μία αναλυτική μεθοδολογία υπολογισμού των θερμοχημικών ιδιοτήτων των καυσίμων βάσει των επιμέρους συστατικών τους, διευκολύνοντας την αντιστοίχιση μεταξύ χαρακτηριστικών της χημικής σύστασης και απόδοσης της καύσης, όπως αυτή αντικατοπτρίζεται μέσω θερμοκρασιακών μετρήσεων και ανάλυσης καυσαερίων με το σύστημα αέριας χρωματογραφίας που συζητείται στην παράγραφο 2.1.3.1.

Ανασκόπηση εναλλακτικών αεροπορικών καυσίμων.

Η χρήση εναλλακτικών αεροπορικών καυσίμων στα υπάρχοντα συστήματα αναμένεται να μετριάσει τις περιβαλλοντικές οχλήσεις και να ενισχύσει την ποικιλομορφία και βιωσιμότητα του ενεργειακού αποθέματος. Ειδικότερα στον τομέα των μεταφορών υπάρχει επιτακτική ανάγκη ενσωμάτωσης συνθετικής κηροζίνης, με τα μίγματα προέλευσης διεργασιών Fischer-Tropsch να είναι τα πιο υποσχόμενα[204]. Οι χρησιμοποιούμενες πρώτες ύλες για διεργασία Fischer-Tropsch ποικίλουν από ορυκτούς γαιάνθρακες και φυσικό αέριο έως διάφορα αποθέματα βιομάζας, προσδίδοντας την αντίστοιχη κατηγοριοποίηση στα παραγόμενα συνθετικά καύσιμα.

Οι περισσότερες πειραματικές μελέτες στη βιβλιογραφία ασχολούνται με την απόδοση αυτών των συνθετικών καυσίμων σε πρακτικά συστήματα όπως στροβιλομηχανές[309], μηχανές εσωτερικής καύσης[337] ή ακόμα και βοηθητικές μονάδες ηλεκτροπαραγωγής[258], συγκρίνοντας τις εκπομπές καυσαερίων και αιωρούμενων σωματιδίων σε σχέση με τα αντίστοιχα από τη χρήση συμβατικής κηροζίνης. Πλείστες μελέτες που πραγματεύονται την εφαρμογή συνθετικών καυσίμων Fischer-Tropsch σε πρακτικές μηχανές[4] συμπεραίνουν ότι τα ανωτέρω καύσιμα παρουσιάζουν γενικώς μειωμένα επίπεδα μονοξειδίου του άνθρακα, οξειδίων του αζώτου και άκαυστων υδρογονανθράκων[5], καταλήγοντας εν ολίγοις στο γεγονός ότι αποτελούν ιδεατή εναλλακτική λύση[221]. Ωστόσο, η ακριβής πειραματική και υπολογιστική ποσοτικοποίηση της χημείας της διεργασίας της καύσης, οφείλει να πραγματοποιείται σε διατάξεις με αυστηρώς ελεγχόμενες συνθήκες, αποφεύγοντας αλληλεπιδράσεις λ.χ. τύρβης-χημείας, δίνοντας θεμελιώδη πληροφορία για τη συμπεριφορά των εκάστοτε χρησιμοποιούμενων καυσίμων μιγμάτων. Τέτοιες μελέτες με συνθετικά καύσιμα έχουν πραγματοποιηθεί σε αφενός σε θαλάμους κρουστικού κύματος[153], διατάξεις 'οβίδας' καύσης[327] και μηχανές ταχείας συμπίεσης[176] για τη μελέτη της υστέρησης έναυσης, αφετέρου σε ισοχωρικούς θαλάμους[22] και φλόγες διάχυσης αντιπαράλληλης ροής[231] για υπολογισμό της στρωτής ταχύτητας καύσης και τέλος σε αντιδραστήρες τέλειας ανάμιξης[71], εμβολικής ροής[112] και φλόγες διάχυσης [263] για την αναλυτική ποσοτικοποίηση χημικών ειδών και επιπέδων αιθάλης. Σημειώνεται εδώ ότι η συντριπτική πλειονότητα των υπολογιστικών μελετών αναλώνεται στην εύρεση κατάλληλων υποκατάστατων[65], ήτοι εικονικών μιγμάτων[145], τα οποία αναπαριστούν τα χαρακτηριστικά των εναλλακτικών καυσίμων, χωρίς κατ' ανάγκη αντιστοιχία μεταξύ σύστασης πραγματικού-εικονικού καυσίμου[72].

Μεθοδολογία χαρακτηρισμού των μελετώμενων καυσίμων μιγμάτων

Το κεφάλαιο προτείνει μία αναλυτική μεθοδολογία υπολογισμού των θερμοχημικών ιδιοτήτων των καυσίμων, τα οποία διαφοροποιούνται συστηματικά σε παραφινικούς, ναφθενικούς και αρωματικούς υδρογονάνθρακες (*Πίνακας* 6.1 – *σελ.* 163), κατά τον ίδιο τρόπο που διαφοροποιείται η συμβατική κηροζίνη από τα αμιγώς παραφινικά καύσιμα Fischer-Tropsch[39] (*Σχήμα* 6.1 – *σελ.* 162). Με την ακολουθούμενη μεθοδολογία, ο χαρακτηρισμός των θερμοχημικών ιδιοτήτων των εξεταζόμενων καυσίμων υπολογίζεται θεωρητικώς μέσω της αναλυτικής τους σύστασης, δίνοντας έτσι τη δυνατότητα επιλογής κοινών, για όλα τα καύσιμα συνθηκών, όπως η στοιχειομετρία και το ονομαστικό θερμικό φορτίου, υπό τις οποίες θα εξεταστούν στον πρότυπο καυστήρα προανάμιξης. Το μέσο μοριακό βάρος και ο μοριακός τύπος των εξεταζόμενων καυσίμων υπολογίστηκε μέσω της στοιχειομετρικής ανάλυσης των συστατικών του κάθε μίγματος (*Εξισώσεις* 6.1 έως 6.5 – *σελ.* 163). Ομοίως, μέσω της επιλογής κατάλληλων τιμών ενθαλπίας

35

σχηματισμού για το κάθε συστατικό του μίγματος, υπολογίζεται και η κατώτερη θερμογόνος ικανότητα του καύσιμου μίγματος (*Πίνακας* 6.2 – *σελ.* 164).

Η αντιστοίχιση ενθαλπίας σχηματισμού στα αντίστοιχα συστατικά που απαρτίζουν το κάθε μίγμα, προϋποθέτει γνώση των ισομερών ενώσεων που είναι παρόντα, χωρίς αυτή η πληροφορία να είναι πάντα διαθέσιμη, μέσω φερ' ειπείν μία χρωματογραφικής ανάλυσης της σύστασης του καυσίμου. Η μόνη εξαίρεση είναι η κανονικές παραφινικές ενώσεις για τις οποίες η αντιστοίχιση ενθαλπίας σχηματισμού είναι αμφιμονοσήμαντη. Όσον αφορά στις ισο-παραφινικές ενώσεις οι πιθανοί συνδυασμοί αυξάνονται δραματικά στους ανώτερους υδρογονάνθρακες, εισάγοντας περεταίρω αβεβαιότητα στον υπολογισμό (*Πίνακας* 6.3 – *σελ.* 166). Αντίστοιχα επίπεδα αβεβαιότητας εισάγονται από την επιλογή των ισομερών για τις ενώσεις ναφθενικών και αρωματικών υδρογονανθράκων, όπου η συστηματική προσέγγιση που ακολουθείται αποφεύγει την επιλογή εξωτικών, μη ρεαλιστικών ισομερών και χρησιμοποιεί κατά το δυνατόν γραμμική συσχέτιση μεταξύ ενθαλπίας σχηματισμού και κατάλληλου ισομερούς (*Σχήμα* 6.2 – *σελ.* 165). Η προτεινόμενη μεθοδολογία έρχεται σε ικανοποιητική συμφωνία με διαθέσιμα πειραματικά δεδομένα αναφορικά με τα επίπεδα κατώτερης θερμογόνου ικανότητας των μιγμάτων (*Σχήμα* 6.3 – *σελ.* 165), παρουσιάζοντας σταθερή απόκλιση της τάξης του 2%. Επίσης, το προαναφερθέν σφάλμα θεωρητικού υπολογισμού της θερμογόνου δύναμης των καυσίμων είναι συστηματικό για όλα τα μίγματα και δεν επηρεάζει τη σύγκριση υπό κοινό ονομαστικό θερμικό φορτίο και στοιχειομετρία.

Αξιολόγηση της απόδοσης καυσίμων Fischer-Tropsch σε πρότυπο καυστήρα προανάμιξης

Η πειραματική μελέτη των καυσίμων Fischer-Tropsch πραγματοποιήθηκε σε μία πρότυπη διάταξη καυστήρα προανάμιξης εργαστηριακής κλίμακας (*Σχήμα* 6.4 – *σελ.* 167). Το ολοκληρωμένο σύστημα παροχής και ατμοποίησης του καυσίμου και παροχής αέρα (*Σχήμα* 6.5 – *σελ.* 167), εξασφαλίζει τη σταθερή και χρονικά αμετάβλητη λειτουργία του καυστήρα. Παρόλα αυτά για τη διασφάλιση της αξιοπιστίας του καυστήρα ανεξαρτήτως χρησιμοποιούμενου καυσίμου, πραγματοποιήθηκε χαρτογράφηση της λειτουργίας του με όλα τα υπό μελέτη μίγματα (*Σχήμα* 6.6 – *σελ.* 168), η οποία ανέδειξε τη δυσκολία διατήρησης ευσταθούς φλόγας για υπο-στοιχειομετρικές συνθήκες, ενώ παράλληλα παρατηρήθηκε σχηματισμός φλόγας διάχυσης, και κατά περιπτώσεις αιθάλη, σε συνθήκες στοιχειομετρίας πλούσιας σε καύσιμο με μόλις $\varphi \geq 1.5$, πράγμα που ενδεχομένως οφείλεται στην ανεπάρκεια χρόνου προανάμιξης για τις αντίστοιχες παροχές.

Κατόπιν της χαρτογράφησης του καυστήρα για όλα τα καύσιμα, οι συνθήκες που μελετήθηκαν αντιστοιχούν σε ονομαστικά θερμικά φορτία της τάξης των 150 W και 200 W σε στοιχειομετρικές συνθήκες (*Σχήμα* 6.7 – *σελ.* 169) και συνθήκες ελαφρώς πλούσιες σε καύσιμο με $\varphi = 1.2$ (*Σχήμα* 6.8 – *σελ.* 170). Οι στοιχειομετρικές φλόγες των καυσίμων που εξετάστηκαν παρουσιάζουν τη μέγιστη θερμοκρασιακή τιμή τους κοντά στην έξοδο του ακροφυσίου, αρκετά νωρίτερα από τις αντίστοιχες σε συνθήκες με $\varphi = 1.2$, οι οποίες παρουσιάζουν μία αρκετά πιο επίπεδο θερμοκρασιακή κατανομή. Επίσης, η αύξηση του ονομαστικού φορτίου οδηγεί σε υψηλότερες τιμές χωρίς αλλοίωση των ποιοτικών χαρακτηριστικών της κατανομής που περιγράφηκε. Μέσω των λεπτομερών θερμοκρασιακών μετρήσεων καθίσταται εμφανές ότι τα όλα τα καύσιμα μίγματα Fischer-Tropsch παρουσιάζουν παρόμοια συμπεριφορά και συστηματικά υψηλότερες θερμοκρασίες σε σχέση με τη φλόγα κανονικού δεκανίου που χρησιμοποιήθηκε ως αναφορά. Ανάμεσα στα καύσιμα Fischer-Tropsch, το αμιγώς παραφινικό παρουσιάζει τις χαμηλότερες

36

θερμοκρασίες, ενώ τις υψηλότερες απόλυτες τιμές εμφανίζει το μίγμα παραφινικών-αρωματικών υδρογονανθράκων, διατηρώντας παράλληλα την αναλογία κανονικών- και ισο-παραφινικών υδρογονανθράκων, πράγμα προς συνηγορεί προς την αυξημένη δραστικότητα της αρωματικής ομάδας.

Το σύστημα της αέριας χρωματογραφίας που αναπτύχθηκε στην παράγραφο 2.1.3.1, χρησιμοποιείτε εν συνεχεία για τη διεξαγωγή μετρήσεων ανάλυσης των καυσαερίων από τα παραπάνω καύσιμα. Οι μετρήσεις πραγματοποιήθηκαν σε δύο σημεία κατάντη της ροής, τα οποία αντιστοιχούν σε αποστάσεις ίσες με την ισοδύναμη διάμετρο και το ένα τρίτο αυτής (*Σχήμα* 6.9 – *σελ.* 171), ορίζοντας ως ισοδύναμη διάμετρο εκείνη που διασφαλίζει την ίδια παροχή με τη διατομή του ακροφυσίου του καυστήρα. Οι μετρήσεις επιπέδων διοξειδίου του άνθρακα και η σύγκριση τους με τα αντίστοιχα στοιχειομετρικά επίπεδα υποδεικνύει ότι το αμιγώς παραφινικό και το αρωματικό μίγμα παρουσιάζουν πληρέστερη καύση σε αντίθεση με το ναφθενικό μίγμα που παρουσιάζει τη χαμηλότερη μετατροπή, γεγονός που συμφωνεί σχετικά με τα ευρήματα των θερμοκρασιακών μετρήσεων. Οι παραπάνω παρατηρήσεις ενισχύονται επίσης από τις μετρήσεις επιπέδων μονοξειδίου του άνθρακα, υδρογόνου και άκαυστων υδρογονανθράκων (*Σχήμα* 6.10 – *σελ.* 171), οι οποίες επιπροσθέτως συμφωνούν με μελέτες ίδιων καυσίμων σε φλόγες διάχυσης[264].

Συμπερασματικά, το κεφάλαιο, χρησιμοποιώντας τα διαγνωστικά εργαλεία που συζητήθηκαν νωρίτερα στη διατριβή, παρουσιάζει φλόγες τεσσάρων εναλλακτικών συνθετικών καυσίμων και μία φλόγα κανονικού δεκανίου για αναφορά, σταθεροποιημένες σε ένα πρότυπο καυστήρα προανάμιξης εργαστηριακής κλίμακας. Τα καύσιμα μίγματα παρουσιάζουν συστηματική διαφοροποίηση αναφορικά με τους περιεχόμενους παραφινικούς, ναφθενικούς και αρωματικούς υδρογονάνθρακες, διευκολύνοντας την αντιστοίχιση της συμπεριφοράς τους με τα επιμέρους συστατικά τους. Οι βασικές θερμοχημικές ιδιότητες των καυσίμων υπολογίζονται θεωρητικώς βάσει της αναλυτικής τους σύστασης, εξασφαλίζοντας κατά αυτόν τον τρόπο τη διενέργεια των πειραματικών μετρήσεων υπό τις ίδιες συνθήκες ονομαστικού θερμικού φορτίου και στοιχειομετρίας, ανεξαρτήτως καυσίμου. Επιπροσθέτως, πραγματοποιείται χαρτογράφηση του καυστήρα, ώστε η μελέτη να πραγματοποιηθεί μέσα στα όρια ευστάθειας της εκάστοτε σύζευξης καυσίμου-διάταξης καυστήρα. Τελικά, μέσω μετρήσεων θερμοκρασίας και επιπέδων CO, CO_2, O_2, H_2 και άκαυστων υδρογονανθράκων σε διαφορετικές περιοχές της φλόγας, το κεφάλαιο αναλύει την χαρακτηριστικά των πρότυπων καυσίμων Fischer-Tropsch και συζητά την επίδραση των επιμέρους συστατικών τους σε σχέση με τα απόδοση της καύσης τους. Εν κατακλείδι, το κεφάλαιο παρέχει πρωτογενή πειραματικά δεδομένα για το χαρακτηρισμό καυσίμων Fischer-Tropsch, τα οποία βρίσκονται στην αιχμή της έρευνας της τεχνολογίας καυσίμων.

Κεφάλαιο 7ο – Πολυπαραμετρικός χαρακτηρισμός πρότυπου καυστήρα πορώδους αδρανούς μέσου με χρήση παρεμβατικών και μη διαγνωστικών εργαλείων

Η διεύρυνση του πεδίου ευστάθειας της καύσης δύναται να επιτευχθεί με την τεχνικής της καύσης σε περίσσεια ενθαλπίας[330] μέσω της ανακυκλοφορίας θερμότητας, ήτοι το *δάνειο μέρους της* θερμότητας των καυσαερίων στα αντιδρώντα. Εν αντιθέσει με την ελεύθερη φλόγα, η καύση σε πορώδεις αδρανείς δομές, ενισχύει τα φαινόμενα μεταφοράς θερμότητας[23] και γι αυτό δύναται να συντηρήσει υψηλά θερμικά φορτία και επαυξημένα όρια αναφλεξιμότητας[335]. Τα παραπάνω συνδυαζόμενα με χαμηλές εκπομπές ρύπων, καθιστούν την καύση σε πορώδες μέσο ιδανική για

πληθώρα εφαρμογών[229]. Τα πλεονεκτήματα της καύσης σε πορώδεις δομές καθιστούν τον καυστήρα πορώδους αδρανούς μέσου μία ελκυστική τεχνολογία, για την καύση υψηλής απόδοσης και χαμηλών εκπομπών και συνεπώς επιλέγεται για πλήρη χαρακτηρισμό με παρεμβατικές και μη τεχνικές στα πλαίσια της διατριβής. Επίσης, ο πορώδης καυστήρας είναι ένα σύστημα υψηλής πολυπλοκότητας αναφορικά με την οπτική προσβασιμότητα και κατ' επέκταση την εφαρμογή μη παρεμβατικών διαγνωστικών εργαλείων, εισάγοντας επιπλέον απαιτήσεις κατά την εφαρμογή οπτικών τεχνικών με χρήση λέιζερ, όπως αυτά που παρουσιάζονται στο τρίτο κεφάλαιο.

<u>Ανασκόπηση της τεχνολογίας του καυστήρα πορώδους αδρανούς μέσου.</u>

Η αυξανόμενη ζήτηση για αποδοτικότερα συστήματα, με χαμηλή κατανάλωση καυσίμου και εκπομπές ρύπων που ταυτόχρονα υπακούν σε αυστηρές προδιαγραφές, οδηγεί σε τεχνολογίες καύσης μη ελεύθερης-εμφανούς φλόγας[339], οι οποίες λειτουργούν υπό καθεστώς ήπιας καύσης[55]. Μία ευέλικτη εναλλακτική λύση είναι η καύση σε περιβάλλον περίσσειας ενθαλπίας[122]. Η καύση σε πορώδεις δομές πραγματώνει τις προαναφερθείσες προϋποθέσεις οδηγώντας σε υπεραδιαβατική καύση[302]. Η αρχή λειτουργίας του πορώδη καυστήρα έγκειται στο ότι το προαναμεμιγμένο καύσιμο και οξειδωτικό καίγονται στις κοιλότητες ενός υπεραγώγιμου πορώδους υλικού, ανακυκλοφορώντας κατά αυτόν τον τρόπο τη θερμότητα στα αντιδρώντα. Η φλόγα σταθεροποιείται στη διεπιφάνεια μεταξύ σταδίου προανάμιξης και πορώδους ζώνης καύσης, διευρύνοντας την περιοχή ευσταθούς λειτουργίας και προσφέροντας ευελιξία σε συνάρτηση με τη στοιχειομετρία και το επιλεχθέν καύσιμο[217].

Τα κύρια σχεδιαστικά χαρακτηριστικά ενός καυστήρα πορώδους αδρανούς μέσου αφορούν τον αριθμό, το μήκος, τον προσανατολισμό το σχήμα, την πυκνότητα και το υλικό των διαφορετικών πορωδών δομών[311]. Η πυκνότητα του πορώδους πλέγματος καθορίζει σε μεγάλο βαθμό τα υπόλοιπα γεωμετρικά χαρακτηριστικά. Η υψηλή πυκνότητα πορώδους δομής επαυξάνει την μετάδοση θερμότητας με αγωγή και συναγωγή λόγω έντονης υδραυλικής μίξης[98], ενώ η υψηλή διαπερατότητα ελαττώνει την επαγόμενη πτώση πίεσης. Ωστόσο η επιλογή υλικού και το γεωμετρικό σχήμα της δομής είναι ο πιο κρίσιμος παράγοντας σχεδιασμού, καθώς καθορίζουν την αντοχή του υλικού σε θερμικές τάσεις, χημική αδράνεια και κόπωση. Για το λόγο αυτό τα κεραμικά υλικά είναι τα πιο ευρέως χρησιμοποιούμενα σε πορώδεις καυστήρες[44]. Τα πιο συνήθη κεραμικά υλικά είναι το οξείδιο του αλουμινίου, το καρβίδιο του πυριτίου και το οξείδιο του ζιρκονίου. Αντιστοίχως οι πιο διαδεδομένες δομές είναι τα δικτυωτά μακρο-πλέγματα, τα ελάσματα και οι πληρωμένες κλίνες[248]. Το οξείδιο του αλουμινίου χρησιμοποιείται ως επί το πλείστον σε ελασματικές δομές ενώ το καρβίδιο του πυριτίου σε αμιγώς πορώδεις δομές[249].

Τα σύνθετα φαινόμενα που λαμβάνουν χώρα σε έναν καυστήρα πορώδους αδρανούς μέσου, απαιτούν το χωρικό και χρονικό συνυπολογισμό μετάδοσης θερμότητας και χημικής κινητικής μέσα στο πλέγμα καθώς και την αλληλεπίδραση της αέριας φάσης και των χαρακτηριστικών της δομής καθεαυτής. Σε αυτήν την κατεύθυνση έχουν πραγματοποιηθεί πολυάριθμες θεωρητικές[163] και αναλυτικές[287] μελέτες με χρήση ποικίλων υπολογιστικών μοντέλων[350] και σκοπό την ανάλυση[120] και παραμετροποίηση[210] της πολυδιάστατης φύσης του προβλήματος. Αρκετές υπολογιστικές προσπάθειες έχουν επίσης εστιάσει στη σταθεροποίηση της φλόγας μέσα στην πορώδη δομή[54], των υπολογισμό των υπεραδιαβατικών θερμοκρασιών[245] και των ορίων αναφλεξιμότητας[80]. Τέλος, ο χαρακτηρισμός των παραγόμενων ρύπων[45] με έμφαση στα οξείδια

του αζώτου[6] και δη το μηχανισμό σχηματισμού τους[105] αποτελεί το αντικείμενο εξίσου πολυπληθών αναλυτικών μελετών, πράγμα που καθιστά επιτακτική την ανάγκη ενδελεχούς πειραματικού χαρακτηρισμού του καυστήρα, όπως επιχειρείται στα πλαίσια του παρόντος κεφαλαίου, με σκοπό την επιβεβαίωση και βαθμονόμηση των ανωτέρω παραμέτρων.

Στα πλαίσια της διατριβής μελετήθηκε εκτενώς ένας καυστήρας πορώδους αδρανούς μέσου, δύο σταδίων και ορθογωνικής διατομής (*Σχήμα* 7.1 – *σελ.* 180). Το πρώτο στάδιο, κατασκευασμένο από οξείδιο του αλουμινίου, αποτελείται από οπές ενός χιλιοστού κατανεμημένα ανά πέντε χιλιοστά. Το πρώτο στάδιο παρέχει ομοιόμορφα το προαναμεμιγμένο καύσιμο και οξειδωτικό, δρώντας επίσης ως φλογοπαγίδα σε περιπτώσεις όπου η ταχύτητα καύσης ανάντη της ροής είναι μικρότερη της ταχύτητας του εισερχόμενου μίγματος. Το δεύτερο στάδιο, κατασκευασμένο από καρβίδιο του πυριτίου, είναι μία αμιγώς πορώδης δομή κατανομή (10 ppi) στην οποία λαμβάνει χώρα η καύση.

Χαρακτηρισμός του καυστήρα πορώδους μέσου με χρήση μη παρεμβατικών τεχνικών

Η χρήση μη παρεμβατικών διαγνωστικών τεχνικών είναι αναγκαία για τη μελέτη των διεργασιών στη δομή του πορώδους μέσου με την ελάχιστη δυνατή διαταραχή. Ωστόσο, τέτοιες τεχνικές δεν έχουν εφαρμοστεί αφενός λόγω της δυσκολίας οπτικής πρόσβασης και αφετέρου λόγω της περιορισμένης χωρικής έκτασης της ζώνης καύσης στην πορώδη δομή σε εφαρμογές καυστήρα[162], εν αντιθέσει με εφαρμογές μερικής οξείδωσης[190]. Συνεπώς οι περισσότερες μελέτες για το χαρακτηρισμό της ζώνης καύσης του πορώδη καυστήρα, χρησιμοποιούν δειγματολήπτες καυσαερίων και θερμοστοιχεία[10]. Εξαίρεση αποτελεί η εφαρμογή της τεχνικής της συμφασικής αντί-Stokes ανελαστικής σκέδασης για μετρήσεις θερμοκρασίας και συγκέντρωσης υδρογόνου, κατά μήκος μίας οπής του πρώτου σταδίου της φλογοπαγίδας και τεχνηέντως δημιουργηθείσας οπτικής διαδρομής μέσω της πορώδους δομής[164], χωρίς όμως η διάταξη αυτή να είναι πλήρως αντιπροσωπευτική της τυχαιότητας της πορώδους δομής.

Στον αντίποδα, η οπτική πρόσβαση στην πορώδη δομή είναι αδύνατον να επιτευχθεί κατά τρόπο που δεν διαταράσσει έστω ελάχιστα τα φαινόμενα[295], συνεπώς, στα πλαίσια του κεφαλαίου πραγματοποιήθηκε παραμετρική ανάλυση των γεωμετρικών χαρακτηριστικών της διάνοιξης της οπτικής διαδρομής. Η οπτική πρόσβαση καθίσταται δυνατή διανοίγοντας ένα μονοπάτι για την ακτίνα διέγερσης και ένα για τη συλλογή του επαγόμενου φθορισμού (*Σχήμα* 7.2 – *σελ.* 183). Σημειώνεται εδώ ότι η έντονη εκπεμπόμενη απαγόμενη ακτινοβολία φθορισμού, μέσω της παρακολούθησης της ρίζας του υδροξυλίου σύμφωνα με την τεχνική που περιγράφηκε νωρίτερα, αποδεικνύεται συγκριτικό πλεονέκτημα της επιλεχθείσας τεχνικής, καθώς η γωνία λήψης του σήματος μέσω της οπτικής διαδρομής μειώνει δραματικά την αναλογία σήματος-θορύβου. Το χαρακτηριστικό μήκος της υπό μελέτης πορώδους δομής είναι 5 mm[239] και η επιλογή οπτικών διαδρομών μεγαλύτερου πλάτους οδηγεί σε μη ρεαλιστική απεικόνιση της ζώνης καύσης (*Σχήμα* 7.3 – *σελ.* 184). Η παραμετρική μελέτη για την τοποθέτηση της οπτικής διαδρομής κατέληξε στην εναπόθεση της διεγείρουσας ακτινοβολίας μεταξύ γειτονικών οπών της φλογοπαγίδας ώστε να μην απεικονίζουν μικροδομές φλόγας τύπου Bunsen, αλλά να αιχμαλωτίζουν την ομοιόμορφη κατανομή της ρίζας του υδροξυλίου μέσα στην πορώδη δομή (*Σχήμα* 7.4 – *σελ.* 185). Αναφορικά με το μέγεθος της οπτικής διαδρομής, η πλευρά της διεγείρουσας ακτινοβολίας έχει πλάτος 1 mm, ώστε να διατηρείται η ισοτροπική κατανομή της δέσμης, ενώ η πλευρά του αισθητήρα έχει πλάτος 2 mm, για τη διασφάλιση ικανοποιητικής αναλογίας σήματος-θορύβου (*Σχήμα* 7.5 – *σελ.* 186).

39

Απεικόνιση της ζώνης καύσης συναρτήσει ονομαστικού θερμικού φορτίου και στοιχειομετρίας

Ο χαρακτηρισμός της λειτουργίας του υπό μελέτη πορώδους καυστήρα και ακολούθως ο διαχωρισμός των καθεστώτων συναρτήσει των χαρακτηριστικών της φλόγας, πραγματοποιήθηκε μεταβάλλοντας το επιβαλλόμενο θερμικό φορτίο και τη στοιχειομετρία με μεθάνιο υψηλής καθαρότητας ως καύσιμο. Αρχικά, μελετήθηκε η επιρροή της μεταβολής του επιβαλλομένου θερμικού φορτίου μεταξύ 200 και 800 kW/m^2, υπό σταθερή στοιχειομετρία $\varphi = 0.7$. Για λόγους αναφοράς, πραγματοποιήθηκε παρόμοια παραμετρική μελέτη των χαρακτηριστικών της φλόγας χωρίς το πορώδες υπόστρωμα (*Σχήμα* 7.6 – *σελ.* 187), περιορίζοντας στα ίδια χωρικά όρια το εξερχόμενο, από της οπές της φλογοπαγίδας, μίγμα. Τα αποτελέσματα που παρουσιάζονται, αφορούν δισδιάστατες κανονικοποιημένες απεικονίσεις του επαγόμενου φθορισμού της ρίζας του υδροξυλίου, ούτως ώστε να περιγράφουν με σαφήνεια τα γεωμετρικά χαρακτηριστικά της φλόγας στο πορώδες και όχι την απόλυτη συγκέντρωση του υδροξυλίου. Επιπρόσθετα, οι δισδιάστατες απεικονίσεις ολοκληρώνονται κατά την έννοια της διείσδυσης της δέσμης με σκοπό την πληρέστερη περιγραφή της ζώνης καύσης κατάντη της ροής, με τα αποτελέσματα αυτά να παρουσιάζονται παράλληλα.

Παρατηρώντας τα χαρακτηριστικά της φλόγας μέσα στην πορώδη δομή συναρτήσει του ονομαστικού θερμικού φορτίου διακρίνονται τρεις περιοχές ευσταθούς λειτουργίας (*Σχήμα* 7.7 – *σελ.* 188). Αρχικά, για σχετικώς χαμηλά επίπεδα ισχύος, περί τα 200 με 300 kW/m^2, η φλόγα αναπτύσσεται αμέσως μετά τη φλογοπαγίδα κι εκτείνεται έως τα μέσα του δευτέρου σταδίου της πορώδους δομής. Εν συνεχεία, για επίπεδα ισχύος 300 με 700 kW/m^2, η ζώνη καύσης είναι ανυψωμένη παρουσιάζοντας σχετική ανεξαρτησία γεωμετρικών χαρακτηριστικών και ονομαστικού θερμικού φορτίου. Τέλος η Τρίτη περιοχή που διακρίνεται αφορά σε επίπεδα ισχύος μεγαλύτερα των 800 kW/m^2, στα οποία τη ζώνη καύσης αναπτύσσεται κατάντη της ροής, εμφανίζοντας τάση εκφυγής από το πορώδες. Οι ανωτέρω παρατηρήσεις έρχονται σε ικανοποιητική συμφωνία με πειραματικές παρατηρήσεις[329] και θεωρητικές προβλέψεις[235].

Η μελέτη της επίδρασης της στοιχειομετρίας πραγματοποιήθηκε σε τρεις διαφορετικές περιοχές θερμικής ισχύος, μεταβάλλοντας τις συνθήκες καυσίμου αέρα από μίγματα εξαιρετικά πλούσια σε αέρα έως σχεδόν στοιχειομετρικά. Για επίπεδα ισχύος ίσα με 200 kW/m^2, η φλόγα προσκολλάται στη φλογοπαγίδα ενώ με την αύξηση του παρεχόμενου αέρα και τη μετάβαση σε καθεστώς υπέρπτωχης σε καύσιμο καύσης τη φλόγα ανυψώνεται κατάντη της ροής (*Σχήμα* 7.8 – *σελ.* 189), χωρίς όμως να επηρεάζει χωρικά το σημείο όπου εμφανίζεται η εντονότερη συγκέντρωση. Παρόμοιες παρατηρήσεις γίνονται για την επίδραση της στοιχειομετρίας σε πιο υψηλά επίπεδα ισχύος, όπως λόγου χάριν στα 600 kW/m^2 (*Σχήμα* 7.9 – *σελ.* 190) και 800 kW/m^2 (*Σχήμα* 7.10 – *σελ.* 190). Η κύρια διαφοροποίηση έγκειται στο γεγονός ότι σε αυτά τα επίπεδα ονομαστικού θερμικού φορτίου, η φλόγα είναι εξαρχής ανυψωμένη ενώ η αύξηση του παρεχόμενου αέρα οδηγεί στη συρρίκνωση της ζώνης καύσης και ολοκλήρωσης των αντιδράσεων εντός του μήκους του πορώδους υποστρώματος. Η παραπάνω μελέτη δείχνει επίσης ότι η εν γένει περιοχή φλόγας καθώς και η απόσταση κατάντη του πρώτου σταδίου του καυστήρα πορώδους μέσου με την εντονότερη συγκέντρωση παραμένουν σχετικώς ανεπηρέαστα από τη στοιχειομετρία.

<u>Χαρακτηρισμός του καυστήρα πορώδους μέσου με παρεμβατικές τεχνικές.</u>

Ο προηγούμενος χαρακτηρισμός της λειτουργίας του καυστήρα επεκτείνεται με τη χρήση παρεμβατικών διαγνωστικών τεχνικών, όπως αυτά που παρουσιάζονται στο δεύτερο κεφάλαιο της διατριβής, χαρακτηρίζοντας κατά τον τρόπο αυτό τον εξεταζόμενο καυστήρα πορώδους αδρανούς μέσου με όρους εκπεμπόμενων ρύπων, θερμικής απόδοσης και εναλλαξιμότητας καυσίμου. Οι θερμοκρασιακές μετρήσεις που παρουσιάζονται αφορούν στην πραγματική θερμοκρασία των καυσαερίων, όπως αυτή υπολογίζεται μέσω μετρήσεων με θερμοστοιχεία και εν συνεχεία διόρθωση των απωλειών ακτινοβολίας[133], οι οποίες με τη σειρά τους μετρώνται με χρήσης υπέρυθρης θερμογραφίας της επιφάνειας του καυστήρα[349]. Για τη διεξαγωγή των μετρήσεων και τη διασύνδεση της διάταξης του καυστήρα με τα συστήματα διαγνωστικών χρησιμοποιείται χρησιμοποιήθηκε σύστημα μετακίνησης τριών βαθμών ελευθερίας (*Σχήμα* 7.11 – *σελ.* 193). Παρόμοιες πειραματικές μελέτες έχουν πραγματοποιηθεί κατά το παρελθόν για διάφορα παρεμφερή είδη καυστήρων[259], εστιάζοντας στα επίπεδα εκπεμπόμενων ρύπων[187], ή άλλων παραμέτρων λειτουργίας όπως λ.χ. τα επίπεδα προθέρμανσης[143], χωρίς να εστιάζουν στην επιφανειακή κατανομή θερμοκρασιών και ρύπων[291] και των παραμετρικό χαρακτηρισμό συναρτήσει θερμικού φορτίου και στοιχειομετρίας.

Σε πρώτο στάδιο η πειραματική διερεύνηση εξετάζει την ομοιογενή θερμοκρασιακή κατανομή στην επιφάνεια του καυστήρα με τη χρήση των θερμοστοιχείων (*Σχήμα* 7.12 – *σελ.* 194) και της θερμογραφίας υπέρυθρου φάσματος εκπομπής της επιφάνειας του καυστήρα (*Σχήμα* 7.13 – *σελ.* 195), συγκρίνοντας τα επιμέρους αποτελέσματα (*Σχήμα* 7.14 – *σελ.* 195), μεταβάλλοντας συστηματικά τη στοιχειομετρία και την θερμική ισχύ. Σημειώνεται εδώ, ότι λαμβάνοντας υπόψη την εξάρτηση του συντελεστή εκπομής της επιφάνειας του υλικού του καυστήρα[194] από τη θερμοκρασία, καθώς και την εισαγωγή του όρου της αισθητής επιφάνειας εκπομπής[225], ο καυστήρας παρουσιάζει συντελεστή εκπομής ακτινοβολίας $\varepsilon = 0.99$, περίπου ίσο με τον αντίστοιχο του μέλανος σώματος. Η εξαιρετικά ομοιογενής θερμοκρασιακή κατανομή σε ολόκληρη την επιφάνεια του καυστήρα αντικατοπτρίζεται αναλόγως στα εκπεμπόμενα επίπεδα μονοξειδίου του άνθρακα (*Σχήμα* 7.15 – *σελ.* 196) και οξειδίων του αζώτου (*Σχήμα* 7.16 – *σελ.* 197), αντίστοιχα.

Η μελέτη συνεχίζει με την πειραματική διερεύνηση εξετάζοντας τη δυνατότητα εναλλαξιμότητας καυσίμου του καυστήρα, θεωρώντας ως αντιπροσωπευτικό σημείο δειγματοληψίας το κέντρο του άξονα συμμετρίας του καυστήρα. Ο καυστήρας λειτουργείται με καθαρό μεθάνιο και υγραέριο σύστασης προπανίου-βουτανίου κατ' όγκο 60:40. Οι μετρήσεις της θερμοκρασίας των καυσαερίων στην έξοδο του καυστήρα (*Σχήμα* 7.17 – *σελ.* 197) καταδεικνύουν ότι αυτές επηρεάζονται από το εφαρμοζόμενο θερμικό φορτίο, καθώς η αύξηση του μειώνει τις ειδικές θερμικές απώλειες, ενώ η στοιχειομετρία επηρεάζει τη θερμοκρασία σημαντικότερα από το λειτουργών καύσιμο. Η μειωμένη επίδραση του καυσίμου αντικατοπτρίζεται ομοίως στα επίπεδα ρύπων στην έξοδο του καυστήρα, όπως αυτά παρουσιάζονται μέσω των οξειδίων του αζώτου (*Σχήμα* 7.18 – *σελ.* 198) και μονοξειδίου του άνθρακα (*Σχήμα* 7.19 – *σελ.* 198). συναρτήσει θερμικού φορτίου και στοιχειομετρίας. Συμπερασματικά, καθίσταται προφανές ότι τα επίπεδα ρύπων κυμαίνονται σε εξαιρετικά χαμηλά επίπεδα ενώ με την επιλογή κατάλληλων συνθηκών πληρούν τους πιο απαιτητικούς νομοθετικούς περιορισμούς[255]. Χαρακτηριστικά, σε συνθήκες στοιχειομετρίας $\lambda = 1.4$ και ισχύος 400 kW/m^2 τα εκπεμπόμενα επίπεδα NO$_x$ και CO αγγίζουν οριακά τα 30 mg/kWh έκαστα με καύσιμο μεθάνιο, ενώ αντίστοιχα κυμαίνονται περί τα 40 mg/kWh με καύσιμο υγραέριο.

Χαρακτηρισμός λειτουργίας του καυστήρα με εναλλακτικά καύσιμα. Η περίπτωση του βιοαερίου

Η τεχνολογία της καύσης σε πορώδη μέσα ενδείκνυται για καύσιμα χαμηλού ενεργειακού περιεχομένου[330]. Ωστόσο υπάρχει ένας πολύ περιορισμένος αριθμός πειραματικών μελετών που ασχολούνται με τον πορώδη καυστήρα και τη λειτουργία του με παρόμοια καύσιμα, όπως αέριο οπτανθρακοποιείου[63] και χώρους υγειονομικής ταφής αποβλήτων[9]. Επίσης, η μελέτη μιγμάτων με περιεχόμενο διοξείδιο του άνθρακα σε πορώδεις καυστήρες[103] είναι εξαιρετικού ενδιαφέροντος για την ενσωμάτωση τέτοιων τεχνολογιών σε πρακτικές εφαρμογές[340]. Η παρούσα παράγραφος εξετάζει τη λειτουργία του καυστήρα υπό ένα τυπικό μίγμα βιοαερίου κατ' όγκο αναλογίας 60:40, μεθανίου-διοξειδίου του άνθρακα, ακολουθώντας τη μεθοδολογική προσέγγιση που διέπει τη διατριβή. Συνοπτικά, πραγματοποιείται χαρτογράφηση του καυστήρα συναρτήσει θερμικού φορτίου και στοιχειομετρίας συνδέοντας τα ευρήματα με της περιοχές που ανέδειξε η διερεύνηση με χρήση μη παρεμβατικών τεχνικών (*Σχήμα 7.20 – σελ.* 201) και στη συνέχεια χαρακτηρίζεται ο καυστήρας με όρους θερμικής απόδοσης και παραγόμενων ρυπογόνων ουσιών. Τέλος, με βάση τα πειραματικά δεδομένα, αναλύεται η επίδραση του διοξειδίου του άνθρακα ως φυσικός ή χημικός παράγοντας στα επίπεδα μετρούμενων ρύπων και θερμοκρασιών.

Η λειτουργία με βιοαέριο αυξάνει την ογκομετρική παροχή υπό το ίδιο ονομαστικό θερμικό φορτίο, συστηματικά κατά 5% σε σχέση με το μεθάνιο, έχοντας ευθέως αντίστοιχη επίδραση στο χρόνο παραμονής του μίγματος στην πορώδη δομή. Η αυστηρή εφαρμογή του ορισμού υπολογισμού της στοιχειομετρίας δίνει νομοτελειακά πλούσια σε καύσιμο μίγματα. Στην πραγματικότητα, ειδικά στην περίπτωση όπου το διοξείδιο του άνθρακα δρα περισσότερο ως διαλύτης παρά ως ενεργός χημικός παράγοντας, ο παραπάνω ορισμός δε διευκολύνει τη σύγκριση μεταξύ λειτουργίας του καυστήρα με καθαρό μεθάνιο και βιοαέριο και των συνεπαγόμενων φαινομένων συνέργειας. Τα αποτελέσματα που παρουσιάζονται δεν λαμβάνουν υπόψη το περιεχόμενο διοξείδιο του άνθρακα στη ροή του καυστήρα, δίνοντας τη δυνατότητα άμεσης σύγκρισης με τις προηγούμενες μετρήσεις.

Οι μετρήσεις θερμοκρασίας των καυσαερίων (*Σχήμα 7.21 – σελ.* 202) παρουσιάζουν εξαιρετική συνάφεια με τις προηγούμενες παρατηρήσεις, η οποία είναι εξίσου εμφανής στα επίπεδα μονοξειδίου του άνθρακα υπό τις αντίστοιχες συνθήκες (*Σχήμα 7.22 – σελ.* 203). Επιπλέον, γίνεται εμφανές ότι το διοξείδιο του άνθρακα επηρεάζει το σχηματισμό ρύπων κυρίως ως φυσικός παράγοντας και αμελητέα ως χημικός, αν και παρουσιάζει κατά 50% αυξημένα ποσοστά μονοξειδίου του άνθρακα, υπό ίδιες παροχές μεθανίου και αέρα. Τα παραπάνω επίπεδα δικαιολογούνται από τις κατά 10% χαμηλότερες θερμοκρασίες στην έξοδο του καυστήρα σε συνδυασμό με το μικρότερο χρόνο παραμονής στην πορώδη δομή (*Σχήμα 7.23 – σελ.* 203). Ακόμη, τα επίπεδα μονοξειδίου (*Σχήμα 7.24 – σελ.* 204) και διοξειδίου (*Σχήμα 7.25 – σελ.* 204) του αζώτου είναι κατά 60% μειωμένα από τα αντίστοιχα επίπεδα με καύσιμο το καθαρό μεθάνιο και δεν ξεπερνούν αθροιστικά τα 20 ppm υπό οποιεσδήποτε συνθήκες ισχύος και στοιχειομετρίας. Τέλος, η παραπάνω συζήτηση για την επίδραση του διοξειδίου του άνθρακα επιβεβαιώνεται από τη σύγκριση των μετρούμενων επιπέδων οξυγόνου και διοξειδίου του άνθρακα με τα αντίστοιχα υπολογιστικά επίπεδα χημικής ισορροπίας (*Σχήμα 7.26 – σελ.* 205), όπως υπολογίζονται με χρήση μηχανισμού χημικής κινητικής[323].

Κεφάλαιο 8ο – Ανακεφαλαίωση και συμπεράσματα της διατριβής

Η επιστήμη της διαγνωστικής συστημάτων καύσης αποτελεί ένα ταχέως αναπτυσσόμενο κλάδο που ενσωματώνει νέες τεχνολογίες, προσφέροντας μέσο για την ανάπτυξη καινοτόμων, αλλά και την βελτιστοποίηση των ήδη υπαρχόντων συστημάτων και διεργασιών. Ο ανωτέρω στόχος επιτυγχάνεται στην παρούσα διατριβή, σε μεγάλο βαθμό, μέσω τριών κυρίων κατευθύνσεων έρευνας κι ανάπτυξης[12]. Σε πρώτο επίπεδο προηγμένες τεχνικές διαγνωστικής εφαρμόζονται σε θεμελιώδεις, εργαστηριακής κλίμακας διατάξεις με σκοπό την ανάπτυξη και βελτιστοποίηση καθαυτών των διαγνωστικών εργαλείων. Αυτό το στάδιο απαιτεί πολυδιάστατη και συνδυαστική εφαρμογή της γνώσης που διέπουν ποικίλα ερευνητικά πεδία, καλύπτοντας ένα ευρύ φάσμα από μοριακή ηλεκτροδυναμική έως αναλυτική χημεία, όπως επεξηγείται στα πρώτα κεφάλαια της διατριβής. Σε δεύτερο επίπεδο, εκτενείς πειραματικές μελέτες πραγματοποιούνται σε εξίσου βασικές διατάξεις, οι οποίες αποφεύγουν σύνθετες αλληλεπιδράσεις, όπως λόγου χάρη φαινόμενα συνέργειας χημικής κινητικής και τύρβης, με σκοπό τη παραγωγή πρωτογενούς πληροφορίας για τις διεργασίες που διέπουν τα φαινόμενα καύσης, προσφέροντας παράλληλα πολύτιμα δεδομένα για τη βαθμονόμηση υπολογιστικών εργαλείων, όπως επιχειρείται στο τέταρτο κεφάλαιο. Τέλος, τα διαγνωστικά εργαλεία χρησιμοποιούνται *in situ* σε πρακτικές εφαρμογές, χαρακτηρίζοντας τους μηχανισμούς σταθεροποίησης φλόγας, κατανάλωσης καυσίμου, σχηματισμού ρύπων και απόδοσης της καύσης, όπως παρουσιάζεται στο έβδομο κεφάλαιο για έναν καυστήρα πορώδους αδρανούς μέσου. Το τελευταίο κεφάλαιο της διατριβής ανακεφαλαιώνει τα κύρια ευρήματα της διατριβής, παρουσιάζει τις επιστημονικές δημοσιεύσεις που προέκυψαν και προτείνει άξονες επέκτασης της διατριβής.

Σύνοψη και τελικά συμπεράσματα της διατριβής

Στα πλαίσια της διατριβής, παρεμβατικές και μη διαγνωστικές μεθοδολογίες αναπτύσσονται και εφαρμόζονται σε συστήματα καύσης βαθμωτής πολυπλοκότητας. Στο πρώτο τμήμα της διατριβής, παρουσιάζονται η αναγκαιότητα, η μεθοδολογία, η θεμελιώδης θεωρία, τα βασικά επιμέρους συστατικά και συνεισφορά της διατριβής στα υπό μελέτη διαγνωστικά εργαλεία που χρησιμοποιήθηκαν. Σε αυτό το πλαίσιο αναπτύχθηκε μια μέθοδος χρωματογραφικής ανάλυσης για μετρήσεις αέριων ρύπων, ενώ μία ήδη πιστοποιημένη μεθοδολογία[91] χρησιμοποιήθηκε στο τέταρτο κεφάλαιο. Εν συνεχεία, παρουσιάστηκε η μη παρεμβατική μεθοδολογία για την ανίχνευση του επαγόμενου φθορισμού της ρίζας του υδροξυλίου κατόπιν διέγερσης από το έκτο περιστροφικό του αντίστοιχου πρώτου δονητικού ενεργειακού επιπέδου της $A^2\Sigma^+ - X^2\Pi_i$ μετάβασης. Τα συστήματα που ενσωματώνουν τις παραπάνω τεχνικές και η ακόλουθη ανάλυση αβεβαιότητας παρουσιάζονται στο δεύτερο και τρίτο κεφάλαιο αντίστοιχα.

Όσον αφορά στα μελετώμενα είδη καυσίμων, η διατριβή εξετάζει μίγματα που εκτείνονται από καθαρό μεθάνιο και συνήθη μίγματα που προσομοιάζουν το φυσικό αέριο και το υγραέριο, έως εναλλακτικά αέρια μίγματα βιοαερίου. Σε αυτή την κατεύθυνση, μίγματα μεθανίου χρησιμοποιούνται αρχικά σε έναν αντιδραστήρα εμβολικής ροής σε περιβάλλον καθαρού αζώτου, όπως επίσης σε περιβάλλον μικτής σύστασης αζώτου και διοξειδίου του άνθρακα. Από την παραπάνω μελέτη εξάγονται χρήσιμα συμπεράσματα για τη συμπεριφορά των καυσίμων μιγμάτων και τη διαφοροποίηση που παρουσιάζουν οι μηχανισμοί που διέπουν τη χημεία του φυσικού αερίου και του βιοαερίου. Η γνώση αυτή μεταφέρεται στο έβδομο κεφάλαιο, όπου κατόπιν του χαρακτηρισμού της λειτουργίας ενός πορώδους καυστήρα, γίνεται έλεγχος της

δυνατότητας εναλλαξιμότητας καυσίμου του συστήματος, με δοκιμή πλείστων αερίων μιγμάτων, του βιοαερίου συμπεριλαμβανομένου. Δεδομένου επίσης του γεγονότος ότι με πρώτη ύλη τα διαθέσιμα αποθέματα των παραπάνω καυσίμων, δύνανται μέσω της διεργασίας Fischer-Tropsch να προκύψουν εναλλακτικά καύσιμα, συμβατά με τις υπαρκτές υποδομές, στο έκτο κεφάλαιο της διατριβής, δοκιμάζονται σύγχρονα συνθετικά αεροπορικά καύσιμα. Συνεπώς, καθίσταται προφανές ότι παράλληλα με τη βαθμωτή πολυπλοκότητα των εξεταζόμενων, στα πλαίσια της διατριβής, συστημάτων καύσης, ομοίως συστηματικά αυξανόμενη πολυπλοκότητα διέπει τα εξεταζόμενα καύσιμα μίγματα.

Το τέταρτο κεφάλαιο χρησιμοποιεί την τεχνική της αέριας χρωματογραφίας για την ανάλυση των ρύπων από μία βασική διάταξη αντιδραστήρα εμβολικής ροής σε συνθήκες που παρουσιάζουν μερική επικάλυψη με τη βιβλιογραφία δίνοντας την ευκαιρία αξιολόγησης της πειραματικής διαδικασίας. Επίσης, οι επιλεγμένες μελέτες περίπτωσης δοκιμάζουν πρωτότυπα μίγματα μεθανίου προσφέροντας καινοτόμα πειραματικά δεδομένα σε συνθήκες αναμόρφωσης καυσίμου από φυσικό αέριο και βιοαέριο. Η ποσοτικοποίηση της μετατροπής καυσίμου, των επιπέδων του παραγόμενου υδρογόνου και των κύριων παραγώγων της πυρόλυσης μιγμάτων συνθετικού φυσικού αερίου και βιοαερίου σε σχέση με την πυρόλυση του καθαρού μεθανίου, συναρτήσει της θερμοκρασίας προσδίδει χρήσιμη πληροφορία για την κατανόηση της χημικής συμπεριφοράς των ανωτέρω μιγμάτων. Επιπρόσθετα, μετρήθηκαν οι βασικοί παραγόμενοι πολυκυκλικοί αρωματικοί υδρογονάνθρακες και τα επίπεδα αιθάλης, βοηθώντας στη βαθύτερη κατανόηση των διεργασιών που διέπουν την πυρόλυση αλλά και τους μηχανισμούς παραγωγής ρύπων. Η μελέτη στα πλαίσια του κεφαλαίου προσφέρει επίσης πρωτογενή πειραματικά δεδομένα για τη βαθμονόμηση αναλυτικών μηχανισμών χημικής κινητικής. Για αυτό το λόγο τα πειραματικά δεδομένα αναπαρήχθησαν με τη χρήση δύο κατάλληλων υπολογιστικών εργαλείων αναλυτικής χημικής κινητικής με σχετικά ικανοποιητική συμφωνία. Η προσέγγιση που ακολουθήθηκε αναδεικνύει τη χρησιμότητα πειραματικών διερευνήσεων σε απλές διατάξεις, όπως αναλύθηκε στην εισαγωγή της διατριβής ενώ παράλληλα η ανάλυση των αποτελεσμάτων αναδεικνύει φαινόμενα συνέργειας.

Το πέμπτο κεφάλαιο εφαρμόζει την περιγραφείσα μεθοδολογία οπτικών μετρήσεων φασματοσκοπίας φθορισμού σε σχετικώς απλές δομές φλόγας. Η μελέτη αρχικά παρουσιάζει τη δομή της φλόγας προανάμιξης τύπου Bunsen ούτως ώστε ο αναγνώστης να εξοικειωθεί με την τεχνική της ανίχνευσης της ρίζας του υδροξυλίου σε περιβάλλον φλόγας. Στη συνέχεια, η μελέτη εισάγει τη μεθοδολογία που ακολουθείται σε σύνθετες εφαρμογές (βλέπε έβδομο κεφάλαιο), εφαρμόζοντάς τη σε μία διάταξη φλόγας εγκάρσιας προανάμιξης. Η υπό μελέτη διάταξη παρουσιάζει εύκολη, άμεση οπτική πρόσβαση και υψηλά επίπεδα αναλογίας σήματος-θορύβου, αξιολογώντας κατά αυτόν τον τρόπο της τεχνική που παρουσιάστηκε στο τρίτο κεφάλαιο. Κατά αντιστοιχία με το τέταρτο κεφάλαιο οι συνθήκες για τις μελέτες περίπτωσης επεκτείνουν το πεδίο εφαρμογής της μελέτης σε σύγχρονες πρακτικές εφαρμογές[319], όπως περιγράφεται στην εισαγωγή της διατριβής[318]. Συνολικά, η μελέτη περιγράφει με σαφήνεια τα δομικά και χωρικά χαρακτηριστικά της φλόγας, όπως αυτό επίσης επαληθεύεται μέσω συμπληρωματικών μετρήσεων με την τεχνική της φασματοσκοπίας φθορισμού ιχνηλάτησης.

Η μελέτη που πραγματοποιείται στα πλαίσια του έκτου κεφαλαίου επεκτείνει της δυνατότητες των αναπτυχθέντων διαγνωστικών εργαλείων στον τομέα της έρευνας καινοτόμων εναλλακτικών

καυσίμων. Η μελέτη παρουσιάζει φλόγες τεσσάρων εναλλακτικών συνθετικών καυσίμων, σταθεροποιημένες σε ένα πρότυπο καυστήρα προανάμιξης εργαστηριακής κλίμακας. Τα καύσιμα μίγματα παρουσιάζουν συστηματική διαφοροποίηση αναφορικά με τους περιεχόμενους παραφινικούς, ναφθενικούς και αρωματικούς υδρογονάνθρακες, διευκολύνοντας την αντιστοίχιση των επιμέρους συστατικών με την εν γένει συμπεριφοράς τους καθώς και την ανάλυση φαινομένων συνέργειας. Εν συντομία, το αμιγώς παραφινικό μίγμα παρουσιάζει τις χαμηλότερες θερμοκρασίες, ενώ τις υψηλότερες απόλυτες τιμές εμφανίζει το μίγμα παραφινικών-αρωματικών υδρογονανθράκων, διατηρώντας παράλληλα την αναλογία κανονικών- και ισο-παραφινικών υδρογονανθράκων, πράγμα προς συνηγορεί προς την αυξημένη δραστικότητα της αρωματικής ομάδας. Οι μετρήσεις επιπέδων CO, CO_2, O_2, H_2 και άκαυστων υδρογονανθράκων σε διαφορετικές περιοχές της φλόγας και η σύγκριση τους με τα αντίστοιχα στοιχειομετρικά επίπεδα υποδεικνύει ότι το αμιγώς παραφινικό και το αρωματικό μίγμα παρουσιάζουν την υψηλότερη ολοκλήρωση του σε αντίθεση με το ναφθενικό μίγμα που παρουσιάζει τη χαμηλότερη, γεγονός που συμφωνεί σχετικά με τα ευρήματα των θερμοκρασιακών μετρήσεων, οι οποίες επιπροσθέτως συμφωνούν με μελέτες ίδιων καυσίμων σε φλόγες διάχυσης[264]. Εν κατακλείδι, το κεφάλαιο παρέχει πρωτογενή πειραματικά δεδομένα για το χαρακτηρισμό καυσίμων Fischer-Tropsch, τα οποία βρίσκονται στην αιχμή της έρευνας της τεχνολογίας καυσίμων.

Οι διαγνωστικές τεχνικές που αναλύονται και εφαρμόζονται σε βασικές διατάξεις κατά τα προηγούμενα κεφάλαια της διατριβής, συνδυάζονται στο έβδομο κεφάλαιο για το χαρακτηρισμό ενός συστήματος καυστήρα πορώδους αδρανούς μέσου. Στα πλαίσια του κεφαλαίου αναλύονται τα κύρια χαρακτηριστικά και πλεονεκτήματα της τεχνολογίας της καύσης σε πορώδεις κοιλότητες[335], τα οποία δικαιολογούν την επιλογή του συστήματος για τη συνδυασμένη εφαρμογή των αναπτυχθέντων διαγνωστικών εργαλείων. Εν προκειμένω, ο καυστήρα που τέθηκε υπό μελέτη αποτελείται από δύο στρώσεις διαφορετικής πυκνότητας πορώδους. Το πρώτο πορώδες τμήμα χρησιμεύει, συν της άλλοις, ως φλογοπαγίδα ενώ η καύση λαμβάνει χώρα αποκλειστικά στο δεύτερο πορώδες τμήμα. Η πειραματική μεθοδολογία πραγματώνεται ως εξής: Αφενός πραγματοποιείται ο παραμετρικός χαρακτηρισμός της λειτουργίας του καυστήρα με χρήση μη παρεμβατικών τεχνικών, υπερθεματίζοντας τη δυσκολία της οπτικής πρόσβασης και αφετέρου χαρακτηρίζεται η απόδοση και ο σχηματισμός ρύπων κατά τη λειτουργία του καυστήρα με μία πληθώρα συμβατικών και αερίων καυσίμων.

Για την εφαρμογή της τεχνικής της φασματοσκοπίας του φθορισμού με χρήση λέιζερ είναι αναγκαία η διάνοιξη οπτικής διαδρομής διαμέσου της πορώδους δομής. Αρχικά πραγματοποιείται παραμετρική μελέτη για την εύρεση της βέλτιστης διάταξης για τη δέσμη λέιζερ και τους οπτικούς δέκτες, η οποία διαταράσσει ελαχίστως τα φαινόμενα. Εν συνεχεία, η ρίζα του υδροξυλίου παρακολουθείται με την προαναφερθείσα τεχνική, αναγνωρίζοντας τα χαρακτηριστικά της φλόγας σε συνάρτηση με την επικρατούσα στοιχειομετρία και το επιβαλλόμενο θερμικό φορτίο. Η μελέτη αναδεικνύει το εύρος της ευσταθούς λειτουργίας του καυστήρα και τα επιμέρους καθεστώτα ευστάθειας, καλύπτοντας το φάσμα θερμικών φορτίων από $200\,\mathrm{kW/m^2}$ έως $800\,\mathrm{kW/m^2}$ κι από στοιχειομετρικές έως συνθήκες στοιχειομετρίας υπερπλούσιες σε αέρα.

Στη συνέχεια, εξετάζεται η ομοιογένεια κατανομής θερμοκρασίας και ρύπων στην επιφάνεια του καυστήρα με αφενός χρήση υπέρυθρης θερμογραφίας και θερμοστοιχείων και των παρεμβατικών

τεχνικών που αναλύονται στο δεύτερο κεφάλαιο αφετέρου. Η μελέτη αποκαλύπτει ότι τα επίπεδα CO και NO_x είναι της τάξης των 50 και 25 ppm αντίστοιχα, παρουσιάζοντας ικανοποιητικώς ομοιόμορφη κατανομή. Επίσης, καθίσταται εμφανές ότι με την επιλογή κατάλληλων συνθηκών στοιχειομετρίας, ο εξεταζόμενος καυστήρας δύναται να πληροί τα αυστηρότερα πρότυπα περιορισμών εκπομπών[255], για λειτουργία με καύσιμα μίγματα μεθανίου, φυσικού αερίου και υγραερίου. Τελικώς, ο ίδιος καυστήρας τίθεται σε λειτουργία με τυπικό μίγμα διοξειδίου του άνθρακα και μεθανίου που προσομοιάζει το βιοαέριο. Ακολουθώντας τα προηγούμενα ευρήματα, ο καυστήρας ελέγχεται στην περιοχή σταθερής λειτουργίας του, όπου και καθίσταται εμφανές ότι το περιεχόμενο στη ροή του καυσίμου διοξείδιο του άνθρακα επηρεάζει τη λειτουργία του καυστήρα και το σχηματισμό ρύπων κυρίως ως φυσικός παράγοντας και αμελητέα ως χημικός, παρουσιάζοντας 50% αυξημένα ποσοστά μονοξειδίου του άνθρακα, τα οποία όμως μπορούν να δικαιολογηθούν από το μειωμένο χρόνο παραμονής στη ζώνη καύσης και τη χαμηλότερη αδιαβατική θερμοκρασία. Στο παραπάνω συνηγορεί το γεγονός ότι υπό παρόμοιες συνθήκες παροχής μεθανίου και αέρα, το μίγμα του βιοαερίου παρουσιάζει 10% χαμηλότερες θερμοκρασίες, και κατά 50 έως 60% μειωμένα οξείδια του αζώτου.

<u>Προτάσεις μελλοντικής εργασίας</u>

Το περιεχόμενο της παρούσας διατριβής δύναται εν δυνάμει να επεκταθεί διατηρώντας τους άξονες που αναπτύχθηκαν, μέσα σε ρεαλιστικά πλαίσια, δίνοντας μια ακόμη πιο ολοκληρωμένη εικόνα των φαινομένων που μελετήθηκαν. Χαρακτηριστικό παράδειγμα επέκτασης του περιεχομένου της διατριβής αποτελεί η πάντα επίκαιρη μελέτη μιγμάτων μεθανίου σε πρότυπες διατάξεις, όπως ο αντιδραστήρας εμβολικής ροής του τετάρτου κεφαλαίου. Σε αυτή την κατεύθυνση τα ίδια ή/και περισσότερα μίγματα θα μπορούσαν να διερευνηθούν υπό συνθήκες οξείδωσης μελετώντας παράλληλα το σχηματισμό των πολυκυκλικών αρωματικών ενώσεων, προσφέροντας κατά αυτόν τον τρόπο πρωτογενή πειραματική δεδομένα για τη βαθμονόμηση υπολογιστικών εργαλείων και συνάμα βαθύτερη κατανόηση των υποβοσκουσών φαινομένων.

Επίσης, η μελέτη περισσότερων καυσίμων διεργασίας Fischer-Tropsch, προερχόμενα από πλείστες πηγές πρώτων υλών, μπορούν να εξεταστούν στη βάση της μεθοδολογίας που προτείνεται στο πέμπτο κεφάλαιο. Κατά αυτόν τον τρόπο, καύσιμα βιολογικής ή μη προέλευσης μπορούν να μελετηθούν σε εργαστηριακής κλίμακας ελεγχόμενες διατάξεις και μέσω της εν δυνάμει πληθώρας πειραματικών δεδομένων, μπορούν να προκύψουν τα κατάλληλα υπολογιστικά μοντέλα για το σχεδιασμό και βελτιστοποίηση, αφενός των διεργασιών παραγωγής των καυσίμων και αφετέρου του σαφέστερου ελέγχου και ρύθμισης των πρακτικών εφαρμογών που αυτά χρησιμοποιούνται.

Τέλος, περεταίρω διαγνωστικές τεχνικές μπορούν να εφαρμοστούν στα συστήματα που εξετάστηκαν και δη στον καυστήρα πορώδους αδρανούς μέσου. Για παράδειγμα, οι μετρήσεις της ρίζας του υδροξυλίου μπορούν να συνδυαστούν με μετρήσεις φορμαλδεΰδης, παρέχοντας έτσι πληρέστερη εικόνα για την έκλυση θερμότητας στο περιβάλλον της φλόγας[97]. Η παραπάνω τεχνική μπορεί εν δυνάμει να πραγματοποιηθεί με τη χρήση της τρίτης αρμονικής γεννήτριας του Nd: YAG για τη διέγερση και εν συνεχεία ανίχνευση του φθορισμού στο ευρύ φάσμα εκπομπής της φορμαλδεΰδης περί τα 420 nm, σε μία διάταξη παρόμοια με εκείνη που περιγράφεται στα πλαίσια της διατριβής για την ανίχνευση της ακετόνης με τη χρήση της τέταρτης αρμονικής γεννήτριας. Επιπροσθέτως, η κατάλληλη τοποθέτηση της οπτικής διαδρομής μέσα στη δομή του πορώδους

καυστήρα, μπορεί να οδηγήσει σε μετρήσεις στρωτής ταχύτητας καύσης μέσω της παρακολούθησης της ρίζας του υδροξυλίου[343]. Τέλος μη παρεμβατικές και παρεμβατικές τεχνικές δύνανται να συνδυαστούν σε επικαλυπτόμενα αντικείμενα, όπως λόγου χάριν η μέτρηση του μονοξειδίου του αζώτου για τη βαθμονόμηση των οπτικών διαγνωστικών εργαλείων και τη διενέργεια ενδελεχών πειραματικών μελετών.

Chapter 1

Introduction

Combustion has accompanied mankind since humans became involved with the repetitive action of tool making, converting mechanical energy into heat and deposing it in their processing apparatus. Ever since, combustion has become the primary means of utilizing energy sources. Energy demand is steadily growing since the era of the industrial revolution and continuous to do so nowadays with an increasing rate. Prior to the present age of jet travel and space exploration, energy demands were relatively low and energy was comparatively cheap. Until recent events, including critical shortfalls in certain crucial fuel reserves and environmental consciousness, very little motivation existed to develop applied combustion engineering (Keating, 2007). Moreover, the world population growth itself, as well as the adoption of higher living standards by increasing people numbers, results in a dramatically escalating energy demand. Transport and energy are key components of the modern life and the foundation of economy. The majority of the produced energy originates from the combustion of fossil fuels and its share is not expected to substantially decrease despite the increased penetration of renewable energy sources. Despite its impressive age, combustion is still of crucial importance in many key human activities, such as heating, electrical power, waste handling and transportation, and will remain so for the foreseeable future. In technical combustion systems the chemical energy of fossil fuels such as coal, crude oil and

natural gas is converted into heat through oxidation with the oxygen present in air. However, fossil fuel resources are finite and this issue can, in principle, be overcome by two approaches; the incorporation of alternative fuels and the development of novel technologies such as fuel cells, which unfortunately are not yet matured. This dependence on fossil fuels is shown in Figure 1.1, where the global energy production in tons of oil-equivalent is depicted, along with the near future projections. Consequently, efficiency, maintainability and reliability of existing combustion devices must be further improved in order to enhance the sustainable use of fossil fuels. Achieving such improvements is unambiguously connected to an in-depth understanding of fundamental combustion chemistry, as well as in optimized engineering design (Kiefer and Ewart, 2011). Furthermore, improved understanding of combustion is a prerequisite in order to design devices with increased efficiency, which will in turn reduce the environmental footprint of fossil fuel combustion emissions; apart from greenhouse gases such as carbon dioxide, these emissions include nitric and sulfur oxides, polyaromatic hydrocarbons, soot and particulate matter, which are harmful to human health.
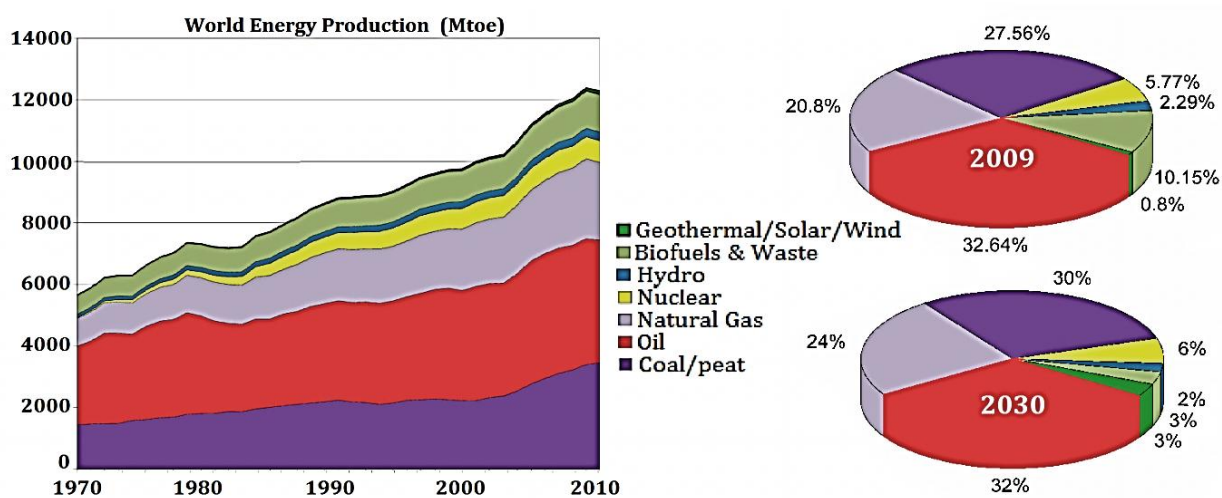
Figure 1.1 World energy production with respect to feedstock. Electricity trade excluded.
(International Energy Agency – *IEA*)

The thorough study of reacting flows is particularly important regarding the global dependence on fossil fuels and the detailed understanding of combustion-generated pollutants. Combustion is a result of dynamic, or time-dependent, events that occur on a molecular level among atoms, molecules, radicals and solid boundaries. The general performance of technical combustion systems in terms of efficiency, fuel consumption, pollutant formation, cost and reliability is determined through a multitude of interdependent parameters. Applied combustion engineering increasingly depends on computer simulation, which effectively models combustion processes in terms of cost and time. Computational fluid dynamics use the fundamental equations of conservation of mass, momentum, energy and individual species and generally require models in order to obtain closure and solution of these equations. Such computer models become increasingly reliable as a result of detailed measurements of velocity, temperature, species concentration, particle size and velocity, and number density as a function of both space and time. The quantification of these parameters necessitates the development and use of appropriate diagnostic tools. The new developments in

measurement techniques and the increased sophistication and quantity of these measurements are resulting in improved understanding of fundamental mechanisms as well as more accurate predictions (Chigier, 1991). However, while progress is currently being made in simulating the interaction of a turbulent flow field with the complex network of chemical reactions, a comprehensive description of practical combustion systems is far beyond the capability of computer models. In order to optimize and control combustion processes it is of crucial importance to have access to techniques which are able to measure critical parameters, such as temperature, species concentration, velocity profiles and particle characteristics. Combustion measurements can provide details of the chemical processes as they actually take place in a flame, highlighting the wide range of chemical reactions that occur even with simple fuels. This type of information can lead to the formulation of kinetic models, which coupled with fluid dynamic models, result in more accurate predictions and analyses. This thesis deals with the development and application of traditional and modern optical diagnostic techniques and their implementation in fundamental as well as complex combustion systems. The present chapter introduces the general framework for the development of the utilized diagnostic techniques, justifies their necessity and states the innovation and scope of the present study.

1.1.   Combustion technology and applications

Combustion encompasses diverse research areas, ranging from fundamental studies of the physics of flames and high temperature molecular chemistry to applied engineering programs, involved with producing clean burning coal plants and low emissions, high mileage combustion engines (Keating, 2007). In combustion, unlike for example in nuclear engineering in which understanding of the process had to precede its use, scientific understanding follows the technological advance. The resolution of various microscopic scales which compose combustion processes has been made possible by the joint application of advanced numerical and diagnostic tools, such as lasers and modern high speed computers. These innovations facilitated major progress in both scientific investigations and engineering applications of this most basic and universal phenomenon.

Currently, combustion technology has reached a certain level of development where further improvements require advanced, complementary methods. The classical trial-and-error approach based on experimental experience has been enhanced by numerical simulation with comprehensive models that describe all relevant aspects taking place. In practical devices such as internal combustion engines, furnaces and gas turbines, various submodels are used, based on conservation equations, elementary chemical reactions and closures such as physical models for transport processes and the equations of state. Due to the complexity of the underlying chemical and physical processes as well as their mutual interaction, simplifying assumptions are necessary (Tropea, 2007). As it is not granted *a priori* that these underlying assumptions are valid for a specific problem, experimental validation is imperative. A thorough experimental validation should examine each submodel as well all mutual interdependencies among the various physical and chemical processes and this enormous task can, in practice, only be fulfilled piecewise through the intelligent application of combustion diagnostic tools.

1.1.1. Conventional and alternative fuels

A fuel can be considered as a finite resource of chemical potential energy, or in other words, energy stored in the molecular structure of particular compounds that may be released via complex chemical reactions. Fuel choice is not a trivial issue, considering that the ideal chemical energy source, treating fuels as such, should comply with numerous conflicting requirements such as being nondepleting, nonpolluting, readily available, economically viable, politically neutral, technically accessible, legally valid, socially acceptable and aesthetically pleasing (Mahallawy and Habik, 2002). Ideally, combustion engineering demands high energy content and heat release, easiness of storage and vaporization and reduced environmental impact, hence respectively necessitating the fuel candidate to offer high energy density and high heat of combustion, good thermal stability and low vapor pressure, being at the same time nontoxic.

Combustion systems may be operated with gaseous, liquid and solid fuels. Examples of gaseous fuels include hydrogen, methane and natural or synthetic natural gas (SNG), as well as vapors such as propane, butane, and liquefied petroleum gas (LPG) which are condensable over normal temperatures and pressures. Most conventional liquid fuels such as gasoline, diesel and kerosene are distillate products of crude oil. Knowledge of the properties, structures, safety, reliability of these fuels, as well as the manner in which they affect the combustion system performance are important for design and control of combustion systems. From the stand point of pre-mixing and homogeneous delivery into the combustion chamber, gaseous fuels present the least difficulty, which under appropriate conditions may lead to reduced emissions and deposits. However, their field of operation is restricted from handling and storage demands, as is the case of the automotive industry. On the other hand, liquid fuels are being used to a larger extent, offering advantages like large energy contents per unit volume, and ease and safety of handling, storing, and transporting. Nevertheless, difficulties are met at distributing and vaporizing fuel droplets and mixing them with the primary combustion air in order to obtain complete combustion. Solid fuels include wood and other forms of biomass, lignite, anthracite and bituminous coal, with coal being the most prominent natural solid fuel resource. Solid fuels cannot compete with liquid and gaseous fuels following the modem trend for cleaner and efficient fuels operating on small sized furnaces. However, since solid fuels are cheap and easily available, they still supply approximately 30% of the total energy requirements of the world (see Figure 1.1). At the same time, solid fuels contain significant amounts of water, oxygen and ash, as well as nitrogen and sulfur compounds, which in turn increase pollutant formation and negatively affect system viability; for instance ash, the inorganic residue remaining after the fuel is completely burned, should be seriously considered in system design so as to minimize slagging, fouling, erosion, and corrosion (McAllister *et al.*, 2011).

Currently, conventional fuel prices and feedstock necessitate the investigation of alternative fuel blends which can resemble fossil fuel properties, in order to partially replace them without requiring tremendous modifications in existing applications. One may argue that the quest for alternative fuels originate as early as the 1920's, when Thomas Midgley working for the General Motors fuel selection, developed the tetraethyllead (TEL) additive to gasoline as well as some of the first chlorofluorocarbons, in order to prevent knocking in internal combustion engines. Currently, the fuel development is at the cutting edge of combustion research, motivated by the diverse

capabilities of alternative fuels, compared to traditional fuels, as far as their environmental impact is concerned. In order to be fully compatible with the running infrastructure, novel fuels should primarily resemble on the one hand the physical properties of conventional ones, such as density, boiling and flashing points, and on the other hand should satisfactory capture the chemical characteristics of conventional fuels such as ignition time delays. However, both alternative and conventional fuels involve mixtures of saturated and unsaturated hydrocarbons, oxygenated compounds as well as alcohols and esters. This suggests that the detailed chemistry of their constituents should be accurately determined, in order to design, develop and control combustors with enhanced efficiency and reduced emissions. In this sense, experimental campaigns are carried out in two main axes. Firstly, they verify that the new candidate fuels operate acceptably within the operational limits of a certain engine, such as a gas turbine, or secondly they focus in more fundamental issues, such as the kinetic behavior of these new fuels. The diversity of alternative fuels dictates the need for an analytical, systematic examination of their behavior in simple devices, avoiding for instance flow-induced uncertainties, in order to assign trends in each constituent species and further improve the understanding level of the reaction processes and eventually pollutant formation. The present thesis, dedicates a chapter in evaluating the behavior of novel aviation fuels addressing the above issues through a systematic experimental campaign.

1.1.2. Premixed flame burners

There is an increasing demand by air-quality regulations to reduce combustion-generated pollutant emissions to increasingly lower levels, while economic interests demand high efficiency equipment for a wide range of applications. Pollutant reducing procedures need to satisfy two competing trends, since it is crucial to achieve a fine trade-off between reducing nitric oxides as well as carbonaceous species formation. While low flame temperature favors NO_x reduction, it rapidly prevents the complete oxidation, hence increasing CO and unburned hydrocarbon levels. Practically, the objective is to cope with emission limits imposed by the legislation, by choosing the appropriate burner type and controlling its operating point.

There are two basic types of flames, namely premixed and diffusion flames. Specifically, combustion of gaseous fuels may occur as premixed flames, as diffusion flames, as radiation-dominated reactions of surfaces or porous media, or as detonation waves (Borman and Ragland, 1998). Premixed flames refer to the combustion mode that takes place when a fuel and oxidizer have been mixed prior to their burning. A premixed flame is a rapid, essentially constant-pressure, exothermic reaction of gaseous fuel and oxidizer. Due to the fact that a potentially ignitable mixture is created, premixed flame burners should be specifically designed in order to avoid ignition prior to the combustion chamber, also preventing flashback. This poses additional concerns when preheating is demanded, as for instance for operation in the low temperature, mild combustion regime. Nevertheless, premixed flame burners provide a homogenized fuel/air mixture distribution that allows good control over flame and noise characteristics. Since premixed flames are kinetically driven, exhibiting higher temperatures than diffusion flames in more confined space, premixed burners exhibit enhanced capabilities of producing significantly less emissions and nitric oxides. In this context the present thesis examines various premixed combustion systems and eventually

attempts a comprehensive characterization with the developed tools in a state-of-the-art premixed combustion system, as is the porous inert medium burner. Porous burner technology allows burner operation in lean and ultra-lean combustion regimes, further improving its emission reduction capabilities. Finally, since porous burners exhibit a remarkable flexibility with respect to stoichiometry, this type of burners may be operated with a wide variety of fuels, with a very satisfactory fuel interchangeability, as presented in sections 7.3.1and 7.3.3.

1.2. Combustion diagnostics

Modern world requirements make essential for combustion engineers to grasp both scientific and technological practices, in order to implement diverse activities, necessary to conceive, manufacture and maintain innovative products. This knowledge is classified in three distinct skill areas; theory, design, and operation (Keating, 2007). *Theory*, a predominantly academic-centered activity, focuses on precise formulation and development of basic principles, in order to predict specific characteristics of combustion systems. *Design* addresses the standardization and utilization of codes and practices, utilizing scientific achievements, in order to produce specific characteristics of systems and devices. *Operation* deals lastly with all necessary aspects and actions so as to protect and maintain specific characteristics of system components. Combustion diagnostic research requires the highest sophistication level from the aforementioned interrelated areas. Combustion diagnostics is the set of experimental operations that aims to measure important combustion parameters such as local velocities, temperatures and species concentrations. A diagnostic methodology engulfs both elements of theory and design in order to obtain trendsetting results. Combustion diagnostics cover a wide spectrum of applications including gas turbines and automotive industries to domestic products. Measurement techniques, developed in laboratories, are being used in high temperature, reacting, particle-laden flow systems. Information obtained on detailed temperature, velocity, particle size and gaseous species concentration distribution is leading to improved understanding of the chemical combustion processes and more sophisticated combustor design.

1.2.1. Necessity and applicability of combustion diagnostic

Combustion processes consist of a complex multi-scale interaction between fluid mechanics and chemical kinetics. Combustion diagnostic techniques must be based on the properties of the phenomena which are to be detected and the characteristics of the techniques which are to be employed (Zhao and Hiroyasu, 1993). Combustion diagnostic techniques serve as a means for establishing fundamental knowledge for the operation of a system, which is essential for comprehending the governing mechanisms for fuel consumption and pollutant formation. A comprehensive experimental analysis needs therefore measurements of flow and scalar fields, which have to be performed *in situ* with high temporal and spatial resolution, as well as high accuracy and precision. Additionally, combustion diagnostics supply measurements that critically assess an aspect predicted by simulations, as for example velocities, temperatures and species concentrations. As the experimental methods steadily improve, they provide extremely detailed

measurements that forward the fundamental understanding of the chemistry and physics involved in combustion environments. This fact leads to more sophisticated models which embody the latter findings. In this sense, it is not inappropriate to describe the future of combustion research as the future of combustion diagnostics. Apparently, diagnostic research not only validates the existing models but also focuses on fundamental aspects of combustion with regard to its environment, pushing towards the understanding of the flame at a local scale.

A detailed understanding of the combustion mechanisms is required for optimizing the complex relationship between fuel economy, combustion emissions and performance. The application of modern diagnostic methodologies aims at developing and testing solutions for a better and cleaner way to convert energy from fossil and alternative fuels and assess their performance in typical combustion systems as boilers, furnaces and combustors. In this sense, combustion diagnostics are essential for burner optimization, as well as novel combustion systems design. As a part of the design of a combustion process, one has to choose among various fuel characteristics, which in turn would lead to the appropriate engine choice. During this procedure, fuel characteristics such as chemical stability, energy content, flammability limits and flame speed should be appropriately coupled with engine characteristics. Various considerations concerning the engine choice include its use *i.e.* heat/power/thrust application and its combustion modes *i.e.* internal/external or continuous/intermittent. However, many crucial characteristics arise from the so called fuel-engine coupling (Keating, 2007). These include the fuel-engine compatibility, pollutants generated by burning particular fuels in certain engines, general energy input/output performance characteristics of individual engines operating on a given fuel and various interactions and efficiencies associated with those interfaces. The latter, up to a large extent, can be sufficiently examined only through the utilization of appropriate combustion diagnostic methods.

Additionally, measurements in combustion systems are required for purposes of analysis and control. Flow-rates, temperatures and concentration of fluids and materials introduced into the system or leaving it, need to be continuously monitored. This information is fed directly into the control system. Temperatures of the walls of a combustor and of gases flowing through the combustor also need to be monitored to prevent damage to inner walls and surfaces of the combustor. For example, the safe, clean and reliable operation of combustion devices depends to a large degree on the exact control of the fuel/air mixing process prior to ignition; hence the inlet gas mixture has to be accurately quantified. This suggests that combustion diagnostic tools hold and important role in the combustor's operation itself.

Finally, there is an increased interest in the application of control to combustion, in order to monitor the process and alleviate instabilities and their severe consequences. Combustion control may improve the system performance by reducing the levels of pollutant emissions, especially when exhaust after-treatment technologies are used, or even extend the stability domain by reducing the level of oscillation induced by coupling between resonance modes and combustion. Specifically, for premixed combustors operating near the lean stability limit, the flame is more susceptible to blowout, oscillation or flashback and research is carried out to reduce these dynamical problems with passive and active control methods (Docquier and Candel, 2002). The latter boost the research efforts for development for high-tech sensors for combustion control.

1.2.2.   Intrusive and nonintrusive diagnostic tools

Traditionally, the first diagnostic techniques required a physical probe to reach the specimen volume, in order to sample the investigated quantity and translate it into useful information. For example a hot-wire anemometer translates the thermal effect on the tip of the probe into velocity and a thermocouple correlates the Seebeck effect on its junction to a specific temperature. Techniques which require the introduction of a physical probe in the measuring volume are termed intrusive. For species measurements, a wide range of techniques have been employed as intrusive, utilizing various measuring principles, such as electron spin resonance, mass spectrometry, gas chromatography and Fourier transform infrared spectroscopy. In general, although a large variety of detectors can be combined after sapling, probe methods are cheap, inherently simple, easy to use and often still the most accurate. Moreover, in the case of concentrations measurements of large hydrocarbons with complex spectra, physical probing coupled with mass spectrometry may prove more successful than optical techniques such as absorption or fluorescence. However intrusive probing is a main concern as far as aerodynamic, thermic or chemical disturbances are concerned. Physical probes, due to their intrusion, can seriously perturb the fundamental flame behavior and in addition, are confronted with survival at high temperatures and pressure. Besides probe-flowfield interference, there are additional disturbances from its presence in a flame. For example, the flame can be disturbed by a thermocouple because its surface intrusion in an area of high radical concentrations may lead to catalytic processes, introducing additional uncertainties, which add up to radiation losses (Kohse-Höinghaus, 1994). Nevertheless, an important drawback of conventional, intrusive techniques is the lack of temporal resolution and hence the difficulty in interpretation the results. Since combustion takes place in quite narrow region and most of chemical reaction is fast, fine spatial as well as time resolutions are required for combustion diagnostics. These requirements disqualify intrusive techniques for studies of turbulent or unsteady flames. Finally, an important source of error is the recombination losses of radicals or even species in the sampling system, which can only be avoided via optical sampling.

In nonintrusive, optical techniques the laser light penetrates the specimen volume with minimum disturbance of the actual phenomena and the signal is either collected in the laser light direction or perpendicularly. The power in a laser beam permits the exploitation of very weak processes, formerly not practical for probing, or it reveals new, nonlinear phenomena not observed in low intensities. Laser-based diagnostic techniques, due to their advantages against conventional probes, have been finding an explosive application in the field of combustion research during the last decades (Penner *et al.*, 1984). Early studies provided phenomenological insight into the fundamental behavior of combustion systems. Laser combustion diagnostic tools have considerably matured during the last decade. Nowadays, lasers are routinely used in many practical applications where direct inspection of the combustion process is necessary. Specifically, laser spectroscopy is assuming an ever increasing role in combustion research due to the capability to provide remote, *in situ*, spatially and temporally resolved measurements of important parameters, avoiding any disturbances during the measurement. With the increasing availability of laser sources, laser spectroscopy is assuming an ever broadening role in the diagnostic probing of the hostile, yet easily perturbed, environments characteristic of combustion processes. Furthermore, the coherent nature of radiation, results in efficient delivery of the entire source power to the probing location, focusing

into very small volumes, hence obtaining high spatial resolution (Eckbreth, 1981). Currently, the main difficulties arise from the lack of optical access in practical devices.

Additionally, new measurement techniques based on planar imaging provide a powerful complement to single-point laser diagnostics. Although optical access may be a problem in some cases, imaging diagnostics may be expected to reveal previously unobserved phenomena in complex flow fields in practical devices. Progress in the development of flowfield imaging is tightly coupled to array detector technology and advances in laser sources, requiring higher power and repetition rates as well as broader wavelength tenability. Planar lased induced fluorescence approaches offer even higher sensitivity for species measurements and greater versatility for measuring multiple flowfield parameters (Hanson, 1986). Moreover, a number of fruitful combinations of methods allow the simultaneous measurement of different gas parameters with minimum flame disturbance. In such cases, temperature measurements *i.e.* with Rayleigh scattering provide additional information of molecular quenching effects (see paragraph 3.1.1.1), assisting in improving the accuracy of concentration measurements obtained with laser induced fluorescence. Finally, the utilization of such techniques may real-time visualize, the formation of radicals in the reaction zone, avoiding recombination losses, hence providing more reliable results.

1.2.2.1. Species and radical concentration measurements

Species concentration measurements are required in order to control, optimize and regulate the operation of a practical combustion system. Additionally, species measurements in fundamental configurations such as low pressure premixed flames with extended reaction zones, shock-tubes and well stirred and plug flow reactors (see section 4.1) provide useful information for the governing chemical processes concerning ignition, fuel consumption and pollutant formation. Moreover, there are important species that are considered to be intermediates in the formation of soot, such as acetylene and polycyclic aromatic compounds (Bockhorn *et al.*, 2012). However, the cutting-edge experiments that challenge the models today are largely based upon optical diagnostics dealing with radical concentration measurements.

Combustion proceeds through a multitude of elementary reaction steps, which involve small radicals. These intermediates play a dominant role in controlling the network of chemical processes and have attracted the interest of combustion researchers for a long time, since they are also quite readily detected with sensitive laser techniques. These species are predominantly involved in fuel consumption, oxidation and pyrolysis and are thus of eminent influence on ignition, heat release, flame propagation and flame quenching, as well as pollutant formation reactions (Kohse-Höinghaus, 1994). For example, the OH radical is probably the most commonly detected reactive intermediate in combustion, which is due to its prominent role in the reaction mechanism of hydrocarbon flames, its relatively high concentration and its well-known spectroscopy. Another important intermediate is the CH radical which is present in a thin layer of the reaction zone, hence also employed for flame front visualization. Moreover, CH radical, as well as CN and HCN radicals are strongly involved in the formation of nitric oxides through the prompt NO_x mechanism (Miller and Bowman, 1989). In addition, combined OH and HCHO radical measurements may be used in order to experimentally determine heat release rates (Fayoux *et al.*, 2005) or burning velocities (Yamamoto *et al.*, 2011). Finally, a typical example that underlines the usefulness of radical

examination against stable species formation studies, becomes obvious from comparison of formaldehyde (HCHO) and formyl radical (HCO) studies. Whereas formaldehyde may be formed and subsequently consumed in an early stage of the chemical conversion of hydrocarbons (Böckle *et al*., 2000), the formyl radical is generated in a reaction where a major part of chemical energy is released (Medwell, *et al*., 2007), hence capturing with more accuracy the actual flame front.

1.3. Structure of the thesis

The present paragraph describes the thesis structure and details the experimental investigations carried out. The importance, the classification and the field of applications of combustion diagnostics have been stated earlier in the present chapter. Within the context of the thesis, several and diverse intrusive and nonintrusive diagnostic techniques have been developed and utilized in order to investigate combustion phenomena of varying complexity. The scope of the next two chapters is to provide a comprehensive support to the experimental investigations carried out which assists in planning, executing and interpreting experiments. Chapter 2 presents the basic theory behind gas chromatographic separation techniques and describes the principle constituents of a chromatographic system. In this context, a novel gas chromatographic method was developed. A slightly different chromatographic configuration, used for the measurements presented in chapter 4, is also discussed. Additionally, chapter 2 presents the theory and instrumentation of a continuous gas analysis system, primarily based in non-dispersive infrared and ultraviolet spectrometry. Chapter 3 presents the fundamental principles of laser spectrometry, mainly as applied in a laser induced fluorescence system, and details the components of the utilized system. The detection scheme for hydroxyl radical as well as acetone-tracer LIF is also given.

The developed diagnostic tools are firstly implemented in configurations with generally moderate complexity. Gas chromatographic measurements are obtained in a simple flow reactor, where gaseous products up to toluene are quantified. The results are reproduced by two detailed chemical kinetic models, with satisfactory agreement. Additionally, soot and selected polycyclic aromatic hydrocarbons are monitored in order to obtain a complete picture of the process under study. The laser induced fluorescence system is firstly utilized for the study of a premixed laminar cross-flow flame, where its shape characteristics are discussed using hydroxyl radical and acetone-tracer LIF.

A premixed laboratory flame burner is utilized in an attempt to investigate the performance of virtually similar fuels of high complexity in chapter 6. The developed chromatographic method is utilized in order to assess the combustion performance of various Fischer-Tropsch aviation fuel blends. Aviation fuels have to meet strict criteria with respect to physico-chemical properties and this poses additional challenge to the work. Temperature and emission measurements are combined with an analytical methodology that aims at the systematic evaluation of the different fuels, facilitating the assignment of trends to constituent compounds.

In the chapter 7, both intrusive as well as nonintrusive diagnostic tools, for stable species and radical concentrations, are combined in order to fully characterize a complex combustor, namely a porous burner. For stable species, besides the continuous analyzers, the versatile technique of gas chromatography is employed. Furthermore, OH radical imaging measurements are utilized in order

to parametrically examine the burner operating regimes. The burner fuel interchangeability is thoroughly tested with respect to nominal thermal loads and stoichiometries.

Finally, the conclusions of the work are summarized in chapter 8 along with possible future work. A schematic diagram showing the structure of the thesis, graphically connecting the respective chapters, is presented in below.

1. Introduction		
Combustion Diagnostics	Fuels	Modern Systems

2. Intrusive Diagnostic Tools
Gas Chromatographic system
Continuous Gas Analysis systems

3. NonIntrusive Diagnostic Tools
Laser Induced Fluorescence system

3. Implementation of Intrusive Tools in Fundamental Applications
Plug Flow Reactor
Methane-Based mixtures Pyrolysis
Link to Practical Applications
Supplementary Investigation: PAH

5. Implementation of Nonintrusive Tools in Fundamental Applications
Bunsen-type flame OH-LIF
Cross-Jet flame OH-LIF
Link to Practical Applications
Supplementary Investigation: Acetone Tracer LIF

6. Alternative Fuels
Fischer Tropsch Aviation Fuels
Lab-Scale Premixed Burner
Fuel Analysis and Performance

8. Concluding Remarks
Future Work

7. Complex Systems: Porous Burner
Nonintrusive Investigation inside Porous Media
Burner Performance with Conventional Fuels
Porous Burner Operation with Biogas

Figure 1.2 Schematic depiction of the structure of the thesis

1.4. Innovation and prospects of the thesis

The overall scope of the thesis is to provide fundamental knowledge on the chemically reactive, combusting flows using advanced diagnostic methodologies, also focusing on the development of appropriate diagnostic tools for the studied phenomena. In this frame, both chromatographic and spectrometric techniques were utilized in numerous premixed flame configurations. Chapter 4 and 5 examine systems of moderate complexity, as it is essential to evaluate novel experimental methodologies in fundamental applications before their incorporation in complex systems. With regard to this, the choice of fuels and operating conditions were made so as exploit the produced results and link the fundamental investigations with practical systems and particularly fuel cells. Fuel cell development forms a promising, not yet matured energy production technology. Paragraphs 1.4.1and 1.4.2 describe the innovations of the conducted research in chapters 5 and 6, respectively, and discuss the prospects of the work to the field of application of fuel cell technology. The developed diagnostic methodologies are subsequently utilized in combustion applications with increased sophistication. In chapter 6, complex jet fuel mixtures are examined in a laboratory scale premixed burner, in order to investigate their combustion performance and assess trends to their constituent species. In chapter 7, the developed intrusive and nonintrusive diagnostic tools are combined for a multi-parametric characterization of a complex combustor, namely a porous medium burner. Paragraphs 1.4.3 and 1.4.4 summarize the innovative aspects of the conducted studies that respectively concern the experimental characterization of complex fuels and combustors, namely chapters 6 and 7, respectively.

1.4.1. Innovation of the 4th chapter and link to practical applications

Solid-oxide fuel cells (SOFC) constitute a particularly attractive technology both as standalone systems for power generation as well as part of hybrid systems with combined heat and power capabilities, due to their relatively high operating temperatures (Holtappels and Stimming, 2003; Singhal and Kendall, 2003) Additionally, SOFC systems are potentially ideal candidates for de-centralized micro-co-generation systems (Vourliotakis, 2012), producing both heat and electricity in a certain ratio to each other, providing potential reductions in carbon emissions and costs by generating both heat and electricity locally with efficient fuel use and by offsetting the use of centrally-generated electricity from the grid (Zink *et al.*, 2007; Zhang *et al.*, 2010; Liso *et al.*, 2011). SOFC operation directly on hydrocarbon fuels is also possible (Gorte and Vohs, 2003) but practical systems rely entirely on fuel reforming processes in order to convert the fuel into hydrogen and/or syngas (Ghosh and De, 2003; Varbanov and Klemeš, 2008). Syngas, in particular, is ideally suited for use in SOFC systems, with pure CO also being a viable option (Kee *et al.*, 2005; 2008).

Currently, methane and natural gas is the fuel of choice in fuel cell applications mainly in view of its high hydrogen to carbon ratio. Alternatively, renewable methane sources, such as biomass or biogas from anaerobic digestion gas from municipal waste incinerators, can also be utilized as syngas sources to feed SOFC systems (Farhad 2009; 2010). Synthetic natural gas (SNG) produced from biomass is a promising, environmentally-friendly, alternative fuel for use in SOFC applications, particularly for small scale domestic applications. Efficient operation of the fuel cell system requires

not only optimization of the syngas yield, under a wide range of operating conditions, but also minimization of the potentially harmful carbonaceous species formation. Furthermore, there are still significant gaps in the understanding of synergistic effects in the gas-phase chemistry of hydrocarbon blends and of soot formation processes under partially oxidative conditions, even for small hydrocarbon fuels (Appleby, 1996). Accurate and complete predictions of fuel conversion, molecular growth and carbon formation processes can only be accomplished by employing a full detailed description of the primary fuel combustion chemistry (Rabenstein and Hacker, 2008).

There are numerous studies on practical reformers and SOFC systems, operating with methane or natural gas mixtures available in the literature (Joensen and Rostrup-Nielsen, 2005). Nevertheless, the accurate quantification of the combustion chemistry needs to be performed in well-controlled fundamental experimental configurations as the flow reactors, which resemble the operating conditions of practical devices avoiding complexities. It is well established that exhaust gases from a plug flow reactor, satisfactory resemble the potential of a reforming process, as numerous studies suggest (Walters *et al.*, 2003; Sheng and Dean, 2004). It can be anticipated that detailed studies of methane mixtures chemistry under fuel-rich conditions are essential in order to explore the syngas production potential, which, in a way, is expected to be maximized under pyrolytic conditions and high temperatures, since they are required in order to achieve efficient operation in the absence of a catalyst. However, high temperatures and pyrolytic conditions provide ideal conditions for soot formation and coke deposition which in turn can seriously affect reformer and system performance.

In chapter 4, the pyrolysis of methane mixtures is investigated using gas chromatographic means, in an atmospheric, isothermal flow reactor, at the temperature range of 1000-1200 ^{o}C. The results concern the gaseous products from the pyrolysis of different methane mixtures, representative of natural gas and biogas, as their operation is resembled through pure nitrogen and mixed N_2/CO_2 atmospheres. Additionally, soot and selected polycyclic aromatic hydrocarbon levels from the respective investigations are experimentally determined in order to assess carbonaceous pollutants formation mechanisms. Subsequently, it is anticipated that the present study explores the potential of syngas production and soot formation tendency from non-catalytic reforming processes through the investigation of atmospheric pressure methane mixtures pyrolysis. Furthermore, the results presented in chapter 4 are valuable in calibrating and formulating numerical model schemes and in this context two literature detailed kinetic mechanisms are used to reproduce the experimental results. In addition, despite the fact that methane pyrolysis has been extensively studied in the past, chapter 4 presents novel polycyclic aromatic compounds speciation data from varying methane-based mixtures. Overall, the chapter examines synergistic effects among methane, natural gas and biogas mixtures serving as a reference case for chapter 7, where the fuel interchangeability is discussed in complex flames.

1.4.2.   Innovation of the 5th chapter and link to practical applications

As also stated in paragraph 1.4.1, the perspective of incorporating fuel cells as part of hybrid modern systems, both for heat and power production is a particularly attractive option. High temperature SOFC systems can operate directly on hydrocarbon fuels, syngas or hydrogen.

However, this is not the case for mobile applications (lower temperatures), where the dominant fuel cell type is the Proton Exchange Membrane (PEM) fuel cell, only functioning with pure hydrogen. Moreover, the powertrain costs of fuel cell vehicles are still far from being cost-competitive, unless the fuel cell costs are drastically reduced. Fuel cell cars may become a viable alternative to nowadays conventional cars equipped with a diesel or gasoline combustion engine. Most of the large car manufacturers have already presented demonstration models of fuel cell cars, which are mostly equipped with pure hydrogen storage systems or methanol reforming units, with conventional fuels also being an option, taking advantage of the existing infrastructure (Fischer *et al.*, 2005). However, life cycle analyses suggest that the economic efficiency and environmental impact of hybrid vehicles, substantially depends on the feedstock for hydrogen production *i.e.* fossil fuels or renewable sources (Granovskii *et al.*, 2006).

The use of hydrogen as an energy vector or the vision of hydrogen energy is not new. Until the 1960's, hydrogen was used in many countries in the form of town gas for street lighting as well as for home energy supply and the idea of a hydrogen-based energy system was already formulated in the aftermath of the oil crises in the 1970's. The breakthrough in fuel cell technology in the late 1990's is the main reason behind the revival of interest in hydrogen. The main product of hydrogen combustion is water, yielding obviously reduced carbonaceous emissions in comparison to fossil fuels and improved environmental impact. While hydrogen can be utilized in different applications, the transport sector is going to play the crucial role for the possible introduction of hydrogen. This is also where fuel cells can make the most of their high conversion efficiencies compared to the internal combustion engine (Ball and Wietschel, 2009).

One of the most challenging issues for automotive fuel cell applications is the freeze start ability for cold weather operation (Schießwohl *et al.*, 2009). In order to meet the requirements for automotive powertrain industry, an additional auxiliary power unit should be incorporated, also for covering the heating demand of the passenger compartment. One of the most promising solutions proposed in the literature is the incorporation of a porous inert medium burner (see section 7.1) for hydrogen combustion in the integrated fuel cell system (Voß *et al.*, 2011). The latter group proposed and innovative mixing stage consisting of multiple cross-jets, incorporated in the burner's flame trap and utilized the technique of laser induced fluorescence to visualize the resulting mixing efficiency (Voß and Trimis, 2009). The flame stabilization, the burner operation and, in general, all combustion related issues have been explicitly analyzed in the aforementioned studies. The innovation of the proposed mixing stage is of crucial importance for the size of the system, but it is expected to affect the mixing efficiency and eventually burner operation. Based on the latter concept, the geometry of a single cross flow premixed jet is isolated and studied in chapter 5 by means of laser induced fluorescence.

A cross flow premixed flame exhibits a non-uniform flame shape due to the T-connection mixing stage, hence affecting the fuel and air streams mixing. The work presented in chapter 5 concerns a parametric study of the flame characteristics of a single cross flow premixed flame, with respect to thermal load and stoichiometry variation. The studied cases cover the typical operating conditions of an auxiliary power unit for automotive fuel cell applications (Voß *et al.*, 2011). The exposed flame characteristics, although different in comparison with the flame structure inside the porous

medium, provide useful insight over the actual processes regarding the mixing efficiency, which is of high importance on the previously discussed configuration. Additionally, chapter 5 presents a fuel-tracer examination, in order to further support the findings from the flame structure study. Moreover, the investigation of such a cross-flow premixed flame constitutes, to the author's opinion, an ideal candidate for evaluating the methodology for capturing the flame front characteristics described in chapter 3 and since the very same methodology is followed in chapter 7, the work additionally serves reference purposes.

1.4.3.   Innovation and prospects of the 6th chapter

A fuel could be classified as alternative, either by originating from renewable sources or as a synthetic blend resembling the performance of conventional fossil fuels. As there is an increased research interest for alternative fuels, the developed combustion diagnostic tools are employed in a plain premixed flame burner, so as to assign fuel characteristics to their combustion performance, avoiding setup induced complexities. Aviation fuels are probable the most demanding from the viewpoint of physical as well as thermochemical properties, raising the challenge to the present work. The work presented in chapter 6 addresses the combustion behaviour of complex fuel blends of systematically varying compositions. In order to assess the effect of each constituent class on performance and emissions, experimental characterization of different fuels combustion behavior must be carried out in fundamental configurations, retaining the same global operating parameters *i.e.* thermal load and fuel/air ratio. An accurate determination of the above parameters requires a correct estimation of fuel heating value and molecular weight which, in turn, requires knowledge of their detailed composition. In this respect, a methodological approach is here formulated, for calculating fuel heating value and molecular weight based on detailed mixture composition.

The contribution of the present work is that it provides a detailed experimental investigation of combustion characteristics of selected FT blends, with systematically varying paraffinic, naphthenic and aromatic content. Flames of the above fuels were stabilized in a laboratory-scale premixed burner and flame stability maps, temperature profiles and species concentration were obtained for a range of operating conditions, so as to facilitate the evaluation of each constituent species contribution to the overall fuel performance. Additionally, n-decane was also used for benchmarking purposes. The work also demonstrates how a simple laboratory-scale premixed burner, coupled with the proper diagnostic tools, can be utilized in order to extract valuable information on fuel characterization.

1.4.4.   Innovation of the 7th chapter

As stated earlier, in this chapter, both intrusive and nonintrusive diagnostic tools are combined in order to fully characterize a complex combustor, as is the porous inert medium burner. The premixed flame in a porous burner propagates in three-dimensionally arranged cavities of an inert super-conductive porous medium. Apparently, combustion in a porous matrix is significantly different compared to homogeneous flames, since the highly developed inner matrix enhances the

heat transfer phenomena, increasing effective diffusion and heat transfer in the gaseous phase. The porous burner technology is a state of the art solution that fulfills the requirements for low pollutant formation and wide fuel interchangeability, as well as with significant prospects for the mitigation of anthropogenic methane emissions (Wood *et al*, 2009). Combustion in inert porous media has many important advantages including high combustion stability and the potential to operate even in ultra-lean combustion regimes. As a result, it continuously improves its place in numerous combustion applications utilizing these advantages. Although the advantages of porous burners have started to be systematically examined over the last 15 years, the actual processes taking place within the porous inert structure could not be investigated experimentally.

The study presented in the seventh chapter constitutes an innovative, comprehensive experimental burner characterization. The experimental campaign carried out in the frame of this chapter, utilizes the developed methodology for the hydroxyl radical in order to visualize the flame front. This is the first time that nonintrusive laser diagnostic techniques are employed, in order to visualize the flame inside a porous burner. This study parametrically correlates nominal thermal load and stoichiometry to the burner operating regimes. Accordingly, the work continues with the burner characterization with respect to methane and propane-based fuels and it concludes with the investigation of the burner's capability to operate with biogas-like mixtures.

Chapter References

Appleby AJ. Fuel cell technology: Status and future prospects. Energy 1996;21:521–653

Ball M and Wietchel M. The future of hydrogen – opportunities and challenges. Int. J. Hydrogen Energy 2009;34:615–627

Bockhorn H, D'Anna A, Sarofim AF and Wang H (Eds.). 2012. Combustion generated fine carbonaceous particles. Karlsruher Institut für Technologie-KIT Scientific Publishing

Böckle S, Kazenwadel J, Kunzelmann T, Shin D-I, Schulz C. Single-shot laser-induced fluorescence imaging of formaldehyde with XeF excimer excitation. Applied Physics B 2000;70:733–735.

Borman GL and Ragland KW. Combustion engineering. McGraw Hill (1998)

Chigier N (Ed.). 1991. Combustion Measurements. Hemishpere Publishing Corporation, USA

Docquier N and Candel S. Combustion control and sensors: a review. Prog. Energy Combust. Sci. 2002;28:107–150

Eckbreth AC. Recent advances in laser diagnostics for temperature and species concentration in combustion. Symposium (Int) Combust. 1981;18:1471–1488.

Farhad S, Yoo Y and Hamdullahpur F. Developing fuel map to predict the effect of fuel composition on the maximum efficiency of solid oxide fuel cells. J. Power Sources 2009;193:632–638.

Farhad S, Yoo Y and Hamdullahpur F. Effects of fuel processing methods on industrial scale biogas-fuelled solid oxide fuel cell system for operating in wastewater treatment plants. J Power Sources 2010;195:1446–1453.

Fayoux A, Zähringer K, Gicquel O and Rolon JC. Experimental and numerical determination of heat release in counterflow premixed laminar flames. Proc. Combust. Inst. 2005;30:251–257.

Fischer K, Rzepka M, Stimming U, Biermann JW, Johannaber M and Wallentowitz H. Performance of gasoline fuel cell cars–a simulation study. Proc. IMechE Part D: J. Automob. Eng. 2005;219:889–896

Ghosh S, De S. Energy analysis of a cogeneration plant using coal gasification and solid oxide fuel cell. Energy 2003;31:345–363.

Gorte RJ, Vohs JM. Novel SOFC anodes for the direct electrochemical oxidation of hydrocarbons. J. Catal. 2003;23:477–486.

Granovskii M, Dincer I and Rosen MA. Economic and environmental comparison of conventional, hybrid, electric and hydrogen fuel cell vehicles. J Power Sources 2006;159:1186–1193

Hanson RK. Combustion diagnostics: Planar imaging techniques. Symposium (int) combust. 1986;21:1677–1691.

Holtappels P, Stimming U. Solid Oxide Fuel Cells – SOFC. In Handbook of Fuel Cells - Fundamentals, Technology and Applications, edited by W. Vielstich, A. Lamm and H.A. Gasteiger. Wiley (2003).

Joensen F, Rostrup-Nielsen JR. Conversion of hydrocarbon and alcohols for fuel cells. J. Power Sources 2005;105:195–201.

Keating EL. 2007. Applied Combustion 2nd Ed. Taylor & Francis Group

Kee RJ, Zhu H, Goodwin DG. Solid-oxide fuel cells with hydrocarbon fuels. Proc. Combust. Inst. 2005; 30: 2379–2404.

Kee RJ, Zhu H, Sukeshini AM, Jackson GS. Solid oxide fuel cells: operating principles, current challenges, and the role of syngas. Combust. Sci. Technol. 2008; 180: 1207–1244.

Kiefer J and Ewart P. Laser diagnostics and minor species detection in combustion using resonant four-wave mixing. Prog Energy Combust Sci 2011;37:525–564

Kohse-Höinghaus K., Laser techniques for the quantitative detection of reactive intermediates in combustion systems, Prog. Energy Combust. Sci. 1994;20:203–279.

Mahallawy FE and Habik SED 2002. Fundamentals and technology of combustion. Elsevier Science Amsterdam

McAllister S, Jyh-Yuan C and Fernandez-Pello AC. 2011. Fundamentals of combustion processes. Springer New York

Medwell PR, Kalt PAM and Dally BB. Simultaneous imaging of OH, formaldehyde, and temperature of turbulent nonpremixed jet flames in a heated and diluted coflow. Combust. Flame 2007;148:48–61.

Miller JA and Bowman CT. Mechanism and modeling of nitrogen chemistry in combustion. Prog. Energy Combust. Sci. 1989;15:287–338.

Penner SS, Wang CP and Bahadori MY. Laser diagnostics applied to combustion systems. Symposium (Int) Combust. 1984;20:1149–1176.

Rabenstein G, Hacker V. Hydrogen for fuel cells from ethanol by steam-reforming, partial-oxidation and combined auto-thermal reforming: A thermodynamic analysis. J. Power Sources 2008;185:1293–1304.

Schießwohl E, von Unwerth T, Seyfried, F, Brüggemann D. Experimental investigation of parameters influencing the freeze start ability of a fuel cell system. J Power Sources 2009;193:107–115.

Sheng CY and Dean AM. Importance of gas-phase kinetics within the anode channel of a solid-oxide fuel cell. J. Phys. Chem. A. 2004;108:3772–3783.

Singhal SC and Kendall K. 2004. High-Temperature Solid Oxide Fuel Cells: Fundamentals, Design and Applications. Elsevier Science, Amsterdam.

Tropea C, Yarin AL and Foss JF. (Eds.). 2007. Springer Handbook of Experimental Fluid Mechanics. Springer-Verlag Berlin Heidelberg.

Varbanov P and Klemeš J. Analysis and integration of fuel cell combined cycles for development of low-carbon energy technologies. Energy. 2008;33:1508–1517

Voß S, Steinbrück R, Kautz M, Schießwohl E, Arendt M, Tom Felde J, Volkert J and Trimis D. Premixed hydrogen-air combustion system for fuel cell systems. Int J Hydrogen Energy 2011;36:3697–3703.

Voß S and Trimis D. Investigation of a combined flame trap- and mixing- system as surface burner support for lean hydrogen air combustion. In: De Azevedo T, Weber R, Tognotti L, (Eds.). Proc. of the 10th Conference on Energy for a Clean Environment; 2009 July 07-09; Lisbon, Portugal.

Vourliotakis G. Development and implementation of detailed chemical kinetics tools for performance and emissions assessment of domestic SOFC systems. PhD thesis, Athens 2012

Walters KM, Dean AM, Zhu H and Kee RJ. Homogeneous kinetics and equilibrium predictions of coking propensity in the anode channels of direct oxidation solid-oxide fuel cells using dry natural gas. J. Power Sources. 2003;123:182–189

Wood S, Fletcher DF, Stephen DJ, Dawson A and Harris AT. Design and evaluation of a porous burner for the mitigation of anthropogenic methane emissions. Environ. Sci Technol 2009;43:9329–9334.

Yamamoto K, Isii S and Ohnishi M. Local flame structure and turbulent burning velocity by joint PLIF imaging. Proc. Combust. Inst. 2011;33:1285–1292.

Zhao FQ and Hiroyasu H. The application of laser Rayleigh scattering to combustion diagnostics. Prog. Energy Combust. Sci. 1993;19:447–485.

Chapter 2

Intrusive combustion diagnostic techniques

Research, design and development of thermochemical processes increasingly depend on sophisticated experimental campaigns, which produce fundamental knowledge and assist in understanding the involved phenomena. In order to optimize and control combustion processes it is of crucial importance to have techniques which are able to measure critical parameters, such as temperature, species concentration, velocity, and particle characteristics. Experimental results can on the one hand help introduce unknown process parameters or, on the other hand, reduce the computational cost in computer simulations, in terms of achieving approximate solutions *i.e.* satisfactory agreement between predictions and observations in reasonable time, or even lead to numerical models of higher level of sophistication (Warnatz *et al.*, 2006). Early diagnostic tools required the sample to reach the detector through a sampling probe. This induced a disturbance of the local flow and much effort was placed in order to minimize those probe-induced effects. However, those techniques, namely intrusive diagnostic techniques are extremely accurate and achieve a high degree of selectivity, being at the same time, at most cases, highly cost effective.

The term *intrusive* refers to a physical probe carrying the sample from the specimen volume to the detector, meaning in other words that the sampling method locally disturbs the actual processes. Depending on the detector's principle of operation, an experimental technique can be characterized as *destructive* or not, which is not to be mistaken to the term *intrusive*. An intrusive diagnostic tool can be either destructive or not, with a typical example the use of a flame ionization detector which has to burn the sample in order to collect the ions formed, so as to quantify the species of interest. On the other hand, a sample can reach, for instance, a paramagnetic detector with the use of a physical sampling probe, characterizing the method as intrusive but non-destructive. It becomes obvious that in order to fully characterize an experimental procedure, the integrated diagnostic tool has to be assessed, hence sampling probe effects, detector operation and specimen volume coupling with the instrumentation, have to be taken into account. Additionally, experimental diagnostic tools can be further subdivided depending on whether continuous or not sampling is realized from the specimen volume, in online or batch sampling/analysis techniques.

Intrusive tools are widely used in temperature and velocity measurements with thermocouples and hotwire anemometers being, respectively, extremely popular. As far as species concentration measurements are concerned, a number of techniques have been utilized. Depending on the degree of sophistication for the measurement of interest and the necessity for real time monitoring of a process, the utilized tools can vary from simple continuous analyzers to a combination of complex analytical techniques. Numerous analytical tools, coupled with physical sampling probes have been employed in the field of combustion diagnostics over the past decades, with continuous gas analyzers and gas chromatographers being the most popular among them. The versatility of the chromatographic technique and its potential for coupling with other diagnostic tools is mainly responsible for the technique's popularity in various combustion subfields. In more detail, as far as fuel characterization (see paragraph 6.1 for typical two-dimensional gas chromatographic fuel analysis) is concerned, gas chromatography coupled with mass spectrometry, has been employed covering a range of fuels from simple higher hydrocarbons (Balès-Guéret *et al.*, 1992) to diesel (Mati *et al.*, 2007) and kerosene (Dagaut, 2007) mixtures. Moreover, premixed flame structures and their exhaust emission characterization, as attempted in paragraph 7.3 of the present thesis, have been studied utilizing chromatographic methods (Mishra *et al.*, 2005; 2006), frequently coupled with molecular beam mass spectrometry and continuous gas analysis systems (Turbiez *et al.*, 2004). Additionally, the applicability of chromatographic techniques extends to the field of higher hydrocarbons (see paragraph 4.4.2.1), sufficiently covering polycyclic aromatic compounds detection and analysis (Poddar *et al.*, 2012). Finally, chromatographic diagnostic tools are the main provider of comprehensive speciation data for detailed kinetic model validation (Dagaut and Nicolle, 2005), as also presented in paragraph 4.3 of the present thesis.

It becomes obvious that gas chromatographic instrumentation along with an online continuous gas analysis system, are essential to achieve the scope of the present thesis. This chapter provides the basic knowledge for the intrusive diagnostic techniques utilized in this framework. This includes methodological approach description and development, detectors' operation and instrumentation overview for all analytical and spectroscopic tools used in intrusive diagnostic means.

2.1.   Gas chromatographic basic theory and system overview

Gas chromatography–GC is a unique and revolutionary technique, which over the years has evolved in the versatile analytical chemistry separation tool, covering nowadays a large field of applications from drugs, pharmaceuticals, pesticides and food industries, to environmental and petroleum industries (Freitag and Allington, 2002). Gas chromatography, as an analytical technique, may be used for both qualitative and quantitative sample identification, and as it is also a physical research technique, can be utilized to investigate various system parameters, such as partition coefficients, thermodynamic functions and adsorption isotherms (Grob and Barry, 2004). Moreover, a gas chromatographer coupled with an automatic sampler, can be locked into a process line so as to monitor online the process and continuously perform routine analyses. The principle advantages that make gas chromatography a particularly attractive technique, and consequently the separation tool of choice, are enumerated below.

Gas chromatography is easily adapted for analysis of permanent gases samples, as well as high boiling point liquids or volatile solids. Moreover, since the mobile phase has a low degree of viscosity, very long columns can be employed, offering extremely high separation efficiency. Gas chromatography offers high resolution in systems containing components of similar boiling points where, by choosing an appropriate adsorbent, the separation of chemically and physically similar molecules can be accomplished. In addition, gas chromatography offers high sensitivity, with most of the utilized detectors allowing detectability ranges of a few parts per million up to even a few parts per billion (see section 2.1.2.3). The latter chromatographic properties largely account for the extensive GC use. In addition, the operation of a gas chromatographer is a relatively straight forward procedure, with detectors characterized by simplicity of design and operation, and requires little operating time, while the chromatographic analyses typically vary, for most cases, from a few minutes up to a maximum of one hour, being at the same time extremely cost effective. Finally, automation of the gas chromatographic processes and post-processing of the acquired data, have reached a high degree of maturity the recent years, through coupling the chromatographic systems with recording devices and computers facilitating enhanced reliability and repeatability ranges (Guiochon and Guillemin, 1990).

Gas chromatographic techniques have been utilized in the frame of the present thesis, in order to quantify gaseous emissions from the several combustion systems. The present section reviews the basic theory of chromatographic separation, states the main chromatographer components, presents the utilized system and investigates method development techniques in the context of various alternative configurations.

2.1.1.   Gas chromatographic fundamental theory

The term chromatography was introduced in the early 1900's by Mikhail Semyonovich Twsett who is considered to be the father of chromatography, mainly because he introduced the term and scientifically described the process, when he separated chloroplast pigment on $CaCO_3$ solid phase and petroleum ether liquid phase (Twsett, 1906). The term chromatography covers those

separation techniques in which the separation of compounds is based upon the partition or distribution, of the analytes between two phases in a dynamic system. In a classical manner, chromatography has been defined as a separation process that is achieved by the distribution of the substances to be separated between two phases, a stationary and a mobile phase. Those solutes, distributed preferentially in the mobile phase, will move more rapidly through the system than those distributed preferentially in the stationary phase. Thus, the solutes will elute in order of their increasing distribution coefficients with respect to the stationary phase (Cazes and Scott, 2002). It follows that during the development of a chromatographic separation, two processes will occur simultaneously and to large extent, independently. Firstly, the individual solutes in the sample are moved apart in the distribution system as a result of their different affinities for the stationary phase. Secondly, as the bands are moved apart, their tendency to spread or disperse is constrained to ensure that the separation that has been achieved is maintained. Thus, the phase system must be chosen to provide the necessary relative retention of the solutes, and the distribution system must be appropriately designed to minimize this dispersion and permit the components of the mixture to be eluted discretely. It is here noted, that the reader is strongly encouraged to refer to bibliographic references given along the text, for more detailed description of the respective aspects of gas chromatographic theory (*e.g.* Jönsson, 1987). The present chapter provides the information in order to adequately define chromatographic separation methodology and nomenclature.

The result of the interaction between the mixture under separation/analysis and the column material is the differing distribution of the sample components between the two phases. Fundamentally, the chromatographic separation may be achieved by one of the three techniques, namely frontal analysis, displacement development, or evolution development. In both frontal analysis and displacement development techniques, the components are not separated by a region of pure mobile phase, due to the strong dependence on -when present- mobile phase. The outstanding disadvantage of the aforementioned techniques is that the column still contains sample or displacer at the conclusion of the separation. The present thesis is dealing only with gas chromatography, hence separation with elution development technique. In gas chromatography there is a gaseous mobile and a liquid or solid stationary phase, whereas when the mobile phase is a liquid, the referred term is liquid chromatography.

The relative retention of two substances in a chromatographic system *i.e.* the time interval between their elution, will determine how well they are separated. The greater the retention difference between any pair of solutes, the better will be the resolution and the farther apart they will appear on the chromatogram. Consequently, an algebraic expression for the retention volume of a solute will display those factors that control retention, how the retention can be increased, and how the separation can be improved. The chromatogram that depicts the elution of a solute from a column is actually a graph relating the concentration of the solute in the mobile phase leaving the column to elapsed time. As the flow rate is constant, the chromatogram will also be a curve relating the concentration of solute in the exiting mobile phase to the volume of mobile phase passed through the column. Thus, an equation is required that will relate the concentration of the solute in the mobile phase leaving the column to the volume of mobile phase that has passed through it.

In order to obtain an expression for the retention volume of a solute, the equation for the elution curve of the substance must be derived. The process of chromatographic separation can be defined by two conditions, either from the linear/nonlinear interaction of adsorbent and sorbate at a specific temperature (isotherm), or depending on the ideal or non-ideal chromatographic system. Ideal, contrary to non-ideal, chromatography infers that the exchange between the two phases is thermodynamically reversible and in addition, the equilibrium between the solid granular particles or liquid-coated particles and the gas phase is immediate; that is, the mass transfer is very high and longitudinal and other diffusion processes can be ignored (Grob and Barry, 2004). Gas partition chromatography, which is here studied, is best described as linear, non-ideal and mostly viewed in two ways; the plate theory or the rate theory. Generally speaking, plate theory envisages the chromatographic system as a discontinuous process functioning as a distillation or an extraction system, that is, consisting of a large number of equivalent plates. On the other hand, rate theory considers the chromatographic system as a continuous medium where one accounts for mass transfer and diffusion phenomena.

In more detail, the plate theory assumes that the solute, during its passage through the column, is always in equilibrium with the mobile and stationary phases. However, as the solute is continuously passing from one phase to the other, equilibrium between the phases never actually occurs. To accommodate this non-equilibrium condition, a technique originally introduced in distillation theory is adopted (Martin and Synge, 1941), where the column is considered to be divided into a number of cells or plates. Each cell is allowed a specific length and, as a consequence, the solute will spend a finite time in each cell. The cell is chosen to be of such size as to give the solute sufficient residence time to establish equilibrium with the two phases. Consequently, the smaller the plate is found to be, the faster will equilibrium be achieved and the more plates will be in the column. It follows that the number of theoretical plates contained by a column will be directly related to equilibrium rate and, for this reason, has been termed the column efficiency. The elution curve equation is obtained from the plate theory, which assumes the column consists of a number of theoretical plates which are of such a size that equilibrium can be assumed to occur between the solute and the two phases in each plate. A mass balance is applied to a plate and, from this, the differential equation for the change of concentration of the solute in the plate, with the flow of mobile phase through it, is obtained. The integration of this differential equation provides the elution curve equation. Differentiating the elution equation and equating to zero discloses the expression for the retention volume of a solute, which is shown to depend on the distribution coefficient of the solute between the two phases and the volumes of stationary and mobile phase in the column. Having obtained the retention volume of a pair of solutes, their separation will depend on the relative magnitudes of their distribution coefficients with respect to the stationary phase and the relative amount of stationary phase available to the two solutes. Finally, plate theory states that the peak width (the dispersion or peak spreading) is inversely proportional to the square root of the efficiency and, thus, the higher the efficiency, the more narrow the peak (Cazes and Scott, 2002).

Although "plate theory" is a useful concept, it is an empirical approach. Since plate theory does not explain the mechanism that determines these factors, a more sophisticated approach bust be used, as is the rate theory to explain chromatographic behavior. The theory that results from the investigation of the dynamics of solute distribution between the two phases of a chromatographic

system and which allows the different dispersion processes to be qualitatively and quantitatively specified has been designated the *rate theory*, although has not been, historically, developed as such. Rate theory is based on such parameters as rate of mass transfer between stationary and mobile phases, diffusion rate of solute along the column, carrier gas flow-rate, and the hydrodynamics of the mobile phase. In conclusion, both "plate" and "rate" model may be used to describe the theory of chromatography, arriving at the same basic conclusion, that zone broadening is proportional to the square root of the column length and that the zone shape follows the normal distribution law (Grob and Barry, 2004).

2.1.2.   Gas Chromatographic system overview

Although instrumentation in gas chromatography has continually evolved since the introduction of the first commercial systems, the basic components of a typical, modern gas chromatographer have remained up to a large extent the same. The basic units of a chromatographer, which are essential for all types of chromatography, include carrier gas, flow control, sample inlet and sampling devices, columns, controlled temperature zones (ovens), detectors, and data acquisition systems, connected as schematically depicted in Figure 2.1.

A brief description of the function of a gas chromatographer is given below. The inert carrier gas is fed to the system through carefully monitored flow control systems and it continuously passes through the injection ports, the columns and the detectors. The flow rate control of the carrier gas is essential to ensure reproducible retention times and to minimize detector drift and noise. The liquid samples are injected and vaporized through a micro-syringe into the heated injection port, whereas gaseous samples are trapped in gas sampling valves, also kept in thermally controlled boxes.
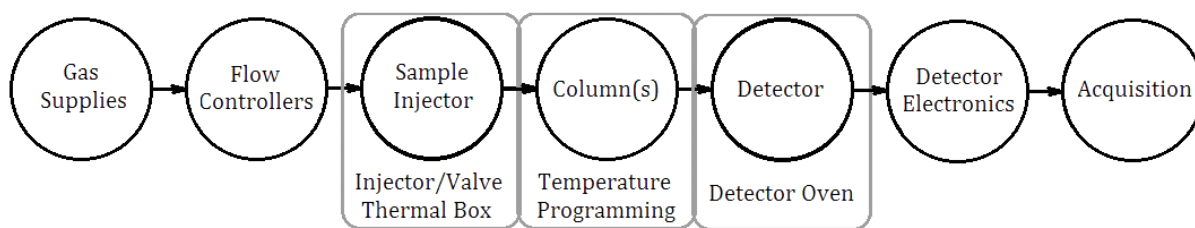
Figure 2.1 Flowchart of a gas chromatographer

As the sample leaves the system inlet, it is sent to the chromatographic columns, which are placed inside the GC main temperature controlled oven, so as to facilitate the chromatographic separation. The sample partitions between the mobile and stationary phases, and it is separated into individual components based on relative solubility in the stationary phase and relative vapor pressures. After the column, the carrier gas and sample, pass through a detector, which measures the quantity of the sample, and it generates an electrical signal. This signal goes to a data acquisition system that generates a chromatogram. In most cases the data-handling system automatically integrates the peak area, performs calculations, and prints out a report with quantitative results and retention times (McNair and Miller, 1998). It is clear that the carrier gas purity is of major importance to the

overall performance of a chromatographer, directly affecting chromatographic efficiency, method repeatability, column performance and system's lifetime. In fact, although an increase of an order of magnitude in carrier gas purity doubles the gas supply cost, in the long run it is proved that is more cost effective to use premium grades (e.g. 99.999% purity) carrier gases (Jennings *et al.*, 1997). Additionally, all fittings, O-rings, and pipes used for the carrier gas connection to the GC system, should be preferably made of stainless steel and generally fixed so as to avoid particle or oxygen contamination. The main parts of a gas chromatographer are discussed in more detail in the next sections.

2.1.2.1. Inlet system

The sample inlet should handle a wide variety of samples including gases and liquids and permit them to be rapidly and quantitatively introduced into the carrier gas stream. Besides *on-column* injection, different column types require different types of sample inlets. Specifically, inlet systems for packed columns include flash vaporizers, whereas inlet systems for capillary columns may be introduced with *split* or *splitless* modes, as explained later in the present chapter. Ideally, the sample is injected instantaneously onto the column, but in practice this is impossible and a more realistic goal is to introduce it as a sharp symmetrical band. The difficulty of keeping the sample sharp and narrow is related to the amount of gaseous sample introduced in the column. A large amount of sample will require more time to carry it into the column and this would result in poor column performance. Clearly, sampling is a very important part of the chromatographic process and the size of the sample is critical. For the best peak shape and maximum resolution, the smallest possible sample size should always be used. However, the more components present in the sample, the larger the sample size may need to be (McNair and Miller, 1998). The most universal method for liquid samples injection is the use of micro-syringes. However, since liquids expand considerably when they vaporize, small sample sizes, typically microliters are desirable. In those situations where the liquid samples are heated to allow rapid vaporization before passage into the column, as in all types of vaporizing injectors, care must be taken to avoid overheating that could result in thermal decomposition.
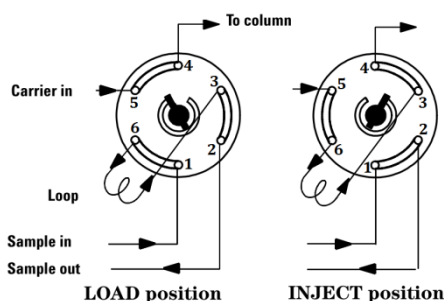
Figure 2.2 Gas sampling valve schematic of operation

The syringe is more flexible, less expensive and the most frequently used device. A gas sampling valve, on the other hand, gives better repeatability, requires less skill and can be more easily automated. Moreover, gas sampling valves are convenient in the case of sampling from fundamental combustion devices, such as flow reactors (see section 4.2), combustion bombs, shock tubes and jet

stirred reactors, where the gaseous products are directly sampled from the reactor outlet and subsequently quantified in the chromatographer. Gas samples are generally placed on a GC column using an external loop sampling valve connected directly to the column. A typical external loop sample system, employing six ports, is depicted in Figure 2.2. The external loop sample valve has three slots cut in the rotor so that any adjacent pair of ports can be connected. In the loading position, shown on the left, the mobile phase supply is connected by the rotor slot between port (4) and port (5) directly through to the column. In this position, the sample loop is connected across ports (3) and (6). Sample passes either from a syringe or other sample device into port (1) through the rotor slot to the sample loop at port (6) and the third slot in the rotor connects the exit of the sample loop to waste at port (2). The sampling position is shown by the diagram on the right. On rotating the valve, the sample loop is interposed between the column and the mobile phase supply by connecting port (3) and (4) and ports (5) and (6). After sampling, the rotor can be returned to the loading position, the system washed with solvent and the sample loop loaded in readiness for the next injection (Scott, 2003). Alternative configurations of sampling valves may include more ports, facilitating more complex operations, such as flushing out of the system undesired compounds, such as heavy components or water. A typical inlet valve with back-flush capability has 10 ports, which instead of simply passing the trapped sample to the main GC column; they introduce the sample to a first column where desired compounds are firstly separated. When the compounds under study are eluted form the primary to the main column, valve switching reverses the carrier gas flow and undesired compounds are flushed out from the system. Modern gas chromatographs that are used for routine analysis usually include an automatic sampling device. Samples can be injected automatically with mechanical devices that are often placed on top of gas chromatographs. These auto-samplers mimic the human injection process just described using syringes. After flushing with solvent, they draw up the required sample several times from a sealed vial and then inject a fixed volume into the standard GC inlet. Auto-samplers consist of a tray which holds a large number of samples, standards, and wash solvents, all of which are rotated into position under the syringe as needed. They can run unattended and thus allow many samples to be run overnight (Jennings *et al.*, 1997).

2.1.2.2.   Chromatographic columns

The column is the heart of any chromatographic system. It is in the column that the individual components contained in the mixture are moved away from each other as they pass through, emerging as individual sample bands that can be detected and measured. Column temperature controls the rate at which the solutes migrate through the column and thus the temperature must be carefully controlled and monitored. This is achieved by situating the column in a thermostatically controlled oven. There are two basic types of gas chromatography column, the packed column, and the open tubular or capillary column. They differ in that the carrier gas must percolate though a porous bed in a packed column but in the capillary column the gas flows through a central aperture that is unimpeded throughout the entire length of the column. This is true even for the Porous Layer Open Tubes (PLOT) columns as well as the Wall Coated Open Tubes (WCOT) columns, although PLOT columns contain adsorbents or loaded supports adhering to the walls, the solid material never extends across the tube to form a permeable bed. It follows that the flow impedance of the packed column is much greater than that of the capillary column when operated

76

at the same gas velocity. For this reason capillary columns can be made much longer and thus produce many more theoretical plates than the packed column, which implies that band dispersion is relatively much less in a long capillary column and the peaks will be much narrower and thus a higher resolution will be realized. However, the comparison between the two types of column is not as simple as that. The packed column contains much more stationary phase and solute retention is directly related to the amount of stationary phase in the column. Consequently, the packed column will move the peaks further apart than the capillary column which carries much less stationary phase (Scott, 1998). The separation is achieved by moving the peaks apart and keeping them sufficiently narrow so they are eluted discretely. In a packed column the separation is predominantly achieved by moving the solutes widely apart and thus, although the dispersion is relatively large compared with that from a long capillary column, the solutes are still separated. In the capillary column, the converse applies. Because the amount of stationary phase on the walls of the column is limited, the peaks are eluted relatively close together. However, due to the higher efficiency of the longer column, the solutes are still resolved as the peaks are relatively much narrower. The two processes for improving a separation are not the same. If the stationary phase loading on a packed column is doubled then the peak separation will also be doubled. However, the contribution to variance from the stationary phase is only one factor effecting band variance and thus the variance, initially, will only be increased slightly by the increase in column loading. Consequently the resolution will be improved. The stationary phase load can be increased as long as the increase in peak dispersion is not greater than the increase in separation. Thus for any particular separation there is an optimum stationary phase loading that will produce the best resolution. Conversely, if the column length is doubled, which can be easily achieved with capillary columns because their flow impedance is relatively small, then both the peak separation and the peak variance is doubled. As the peak width is proportional to the square root of the variance the resolution must be improved as the ratio of the peak separation to peak width will also be doubled (Scott, 1998). It follows that the resolution of a mixture can always be improved by increasing the column length. However, increasing the resolution by increasing either the stationary phase loading on a packed column or the length of a capillary column will always result in a proportional increase in retention time.

A successful setup of a chromatographic analysis depends to a large extent, on the choice of column and column temperature. Selecting the column temperature is less critical than selecting the appropriate stationary phase, because the temperature can be easily programmed through a range of values in order to obtain the optimum value. With packed columns, the choice of the stationary phase is critical, but it is less so for open tubular columns because of their higher efficiency. The stationary phase can be either liquid or solid. Liquids are more common and give rise to the sub-classification known as gas-liquid chromatography (GLC). On the other hand, solids are met in gas-solid chromatography (GSC). There are two types of packing employed in GC; the first is used as an adsorbent stationary phase, largely in GSC for the analysis of gases or low boiling materials; the second is merely a support on which the stationary phase is coated and is used for all types of GLC analyses. In order to use a liquid as the stationary phase in GC, some means must be found to hold the liquid in the column. For packed columns, the liquid is coated on a solid support, chosen for its high surface area and inertness. The coated support is dry-packed into the column as tightly as possible. For open tubular or capillary columns, the liquid is coated on the inside of the capillary. To

make it adhere better, the liquid phase is often extensively cross-linked and sometimes chemically bonded to the fused silica surface. The types of stationary phases, their classification, their applications and the criteria used in selecting an appropriate stationary phase are briefly discussed below.

<u>Packed columns</u>

A packed column consists of three basic components; the tubing in which packing material is placed, the packing retainers, such as glass wool plugs, inserted into the ends of the tubing to keep the packing in place and thirdly the packing material itself (Barry and Grob, 2007). The purpose and role of the solid support is the accommodation of a uniform deposition of stationary phase on the surface of the support. The most commonly used support materials are primarily diatomite earth supports and graphitized carbon (which is also an adsorbent for GSC) and to a lesser extent, Teflon, inorganic salts and glass beads. A support should have sufficient surface area so that the chosen amount of stationary phase can be deposited uniformly and not leave an exposure of active sites on its surface. Conversely, if excessive phase is deposited on the support, the phase may have the tendency to "puddle or pool" on a support particle and can even spread over to an adjacent particle, resulting in a decrease in column efficiency due to unfavorable mass transfer.

Diatomite supports are basically either derived from firebrick or from filter aid. The firebrick-derived supports offer high specific surface area and can accommodate up to 30% loading of liquid phase, which make them suitable for non-polar species such as hydrocarbons. However, although they offer less specific surface area, filter aid supports are more suitable for the analysis of polar compounds such as alcohols and amines. When the analysis of highly corrosive or very polar substances is required, teflon supports may be used as well (Supina, 1974). It has been well established that the surface of the diatomites are covered with silanol (Si–OH) and siloxane (Si–O–Si) groups. Both types of diatomites have two sites for adsorption; van der Waals sites and hydrogen-bonding sites. Hydrogen-bonding sites are more important, and there are two different types for hydrogen bonding; silanol groups, which act as a proton donor, and the siloxane group, where the group acts as a proton acceptor. Thus, samples containing hydrogen bonds (e.g. water, alcohol, and amines) may show considerable tailing, whereas those compounds that hydrogen-bond to a lesser degree (e.g., ketones, esters) do not tail as much. A support should ideally be inert and not interact with sample components in any way, otherwise a component may decompose on the column resulting in peak tailing or even disappearance of the peak in a chromatogram. The presence of active silanol groups (Si–OH functionalities) and metal ions constitute two types of active adsorptive sites on support materials. Polar analytes, acting as Lewis bases, can participate in hydrogen bonding with silanol sites and display peak tailing as well (Grob and Barry, 2004).

Contrary to gas-liquid chromatography (GLC), in gas–solid chromatography (GSC), surface adsorption is the prevailing separation mechanism. Adsorbents for GSC are basically made of porous polymers such as alumna and silica gel, molecular sieves and carbonaceous materials. Porous polymers are the adsorbents of choice for most applications focusing on the analysis of gases, organics of low carbon number, acids, amines, and water (Hollis, 1966; Hollis and Hayes 1966).Molecular sieves, also referred to as zeolites, are synthetic alkali or alkaline-earth metal aluminum silicates and are utilized for the separation of hydrogen, oxygen, nitrogen, methane, and

carbon monoxide. These substances are separated on molecular sieves because the pore size of the sieve matches their molecular diameter. There are two popular types of molecular sieves used in GSC; molecular sieve 5A with a pore size of 5 Å and calcium as primary cation and molecular sieve 13X with a pore size of 13 Å and sodium as primary cation. Finally, adsorbents containing carbon are commercially available in two forms, namely carbon molecular sieves and graphitized carbon blacks. Carbonaceous molecular sieves behave similarly to molecular sieves because their pore network is also in the angstrom range and are mostly used for permanent gases and C_1-C_3 hydrocarbons (Grob and Barry, 2004).

Capillary columns

Today, the open tubular or capillary columns are viewed as state of the art and are thus employed in probably over 80% of all GC analyses. The term capillary column, more properly refer to open tubular columns that are not filled with packing material. Instead, a thin film of liquid phase coats the inside wall and since the tube is open, its resistance to flow is very low and long lengths are possible. The tube can be made of fused silica, glass, or stainless steel, however almost all commercial capillary columns are now made of fused silica. Wall-coated capillary columns provide the highest resolution of all gas chromatographic columns. Tubing internal diameters from 0.10, to 0.53 mm are commercially available. Typical lengths vary from 10 to 50 m or even 100 m. Long column lengths, however, do require long analysis times. Film coating thickness varies from 0.1 to 5.0 µm. Thin films provide high resolution and fast analysis, but they have limited sample capacity. Thicker films have higher sample capacity, but show lower resolution and are typically used for only very volatile compounds. Two other types of capillary columns are the Support-Coated Open Tubular or SCOT column and the Porous Layer Open Tubular or PLOT column. SCOT columns contain an adsorbed layer of very small solid support coated with a liquid phase. SCOT columns can hold more liquid phase and have a higher sample capacity than the thin films common to the early WCOT columns. However, with the introduction of cross-linking techniques, stable thick films are possible for WCOT columns, and the need for SCOT columns has disappeared. A few SCOT columns are still commercially available but only in stainless steel tubing (McNair and Miller, 1998).

Many types of column tubing including glass, copper, nylon, and stainless steel have been used; however, fused silica is by far the most popular. Fused silica is the most inert tubing material and readily produces high resolution columns. The surface energy of fused silica matches well with the surface tension of silicon liquid phases. The silicon phases adhere the tubing very well, resulting in very uniform thin films and very efficient columns. Fused silica contains about 0.1% hydroxyl or silanol groups on the surface and less than 1 ppm of impurities e.g. Na, K, Ca. The high purity of fused silica is responsible for its inert chemical nature. Fused silica has a high tensile strength and most chromatographic columns have a very thin wall, about 25 µm, which makes them flexible and easy to handle. The thin wall, however, is subject to rapid corrosion and breakage, even on exposure to normal laboratory atmospheres (McNair and Miller, 1998). Therefore, a thin protective sheath of polyimide is applied to the outside of the tubing, which protects the fused silica from atmospheric moisture. It is this polyimide coating that limits most fused silica columns to a maximum operating temperature of approximately 360 °C. Nevertheless, for higher column temperatures, aluminum-clad fused silica columns or fused-silica-lined stainless-steel capillary columns can be used (Barry and Grob, 2007).

Oven Temperature Programming

Increasing the column temperature increases the speed of solute migration through the column. Thus in order to shorten the analysis time for mixtures that contain solutes that extend over a wide range of molecular weight or polarity, the temperature of the column must be continuously increased during chromatographic development in a carefully controlled manner. Increasing the column temperature will cause the slower moving peaks to be eluted more rapidly. The necessary temperature-over-time profile is established by a temperature programmer. This device can increase the temperature of the oven at a chosen rate and holds the oven at a specified temperature for a defined time before returning to a preset starting temperature. GC ovens usually require an operating range from about 5 ^{o}C to about 400 ^{o}C although the majority of GC analyses are carried out between temperatures of 75 ^{o}C and 200 ^{o}C (Scott, 2003). Temperature programming is an essential feature of all GC column ovens and is necessary to handle a sufficiently wide molecular and polarity range of samples. Linear programming is the most common although other functions of time are often available. The thermostatting medium used in GC ovens is almost exclusively forced air as the heat capacity of the GC mobile phase is relative small. Consequently, air has sufficient heat capacity to change the column temperature rapidly without significant cooling from the carrier gas. The temperature program can be controlled by a microprocessor incorporated in the programmer or can be controlled from a central computer that governs the operation of the whole instrument.

2.1.2.3.   Chromatographic detectors

A device that monitors the presence of a solute as it leaves the chromatographic system is an essential adjunct to all chromatography instruments. In fact, without it, chromatography would have a very limited performance and a very restricted field of application. The monitoring device has been given the general term detector, which encompasses all types of mobile phase monitoring instruments ranging from relatively simple detectors to very sophisticated spectrometric equipment such as the mass spectrometers. A brief categorization of GC detectors has as follows. Gas chromatographic detectors may be classified with respect to whether they detect a bulk physical property of the mobile phase, or a property of the solute that the mobile phase does not possess or has to a reduced extent, to either bulk or solute property detectors respectively. Bulk property detectors function by measuring some bulk physical property of the mobile phase, e.g. thermal conductivity, whereas an example of a solute property detector would be the phosphorus-nitrogen detector (PND), which responds only to nitrogen or phosphorus. In addition, some detectors respond to changes in solute concentration while others respond to the change in mass passing through the sensor per unit time, giving rise to the definition of concentration and mass selective detectors, respectively. Finally, detectors have also been classified on the basis of the nature of their response, *i.e.* whether they respond to a particular type of compound or a particular chemical group, as specific or non-specific detectors.

The design and performance of any detector depends heavily on the column and chromatographic system which it is associated with. Since it is necessary to relate the detector design to the properties of the column and chromatography apparatus, a simple chromatogram of a mixture, appropriately labeled, is shown in Figure 2.3. The elution point of an unretained substance occurs

at the dead time and the volume of mobile phase that has passed through the column between the injection point and the dead point is the dead volume. The dead volume is given by the flow rate of mobile phase through the column. The volume of mobile phase that passes through the column between the injection point and the peak maximum is called the retention volume. The difference between the retention volume and the dead is called the corrected retention volume. The distance between the baseline produced beneath the peak and the peak maximum is called the peak height (H). The width of the peak at 0.607 H, the position of the points of inflection of the Gaussian curve, is called the peak width and is equivalent to 2 standard deviations of the Gaussian curve. The peak width measured at 0.5 H is the peak width at half height. The distance between the points of intersection of the tangents drawn to the points of inflection, and the base line produced beneath the peak, is the base width and is equivalent to 4 standard deviations of the Gaussian curve. In fact, elution curves from GC columns are often not perfectly Gaussian but tend to be slightly asymmetric.
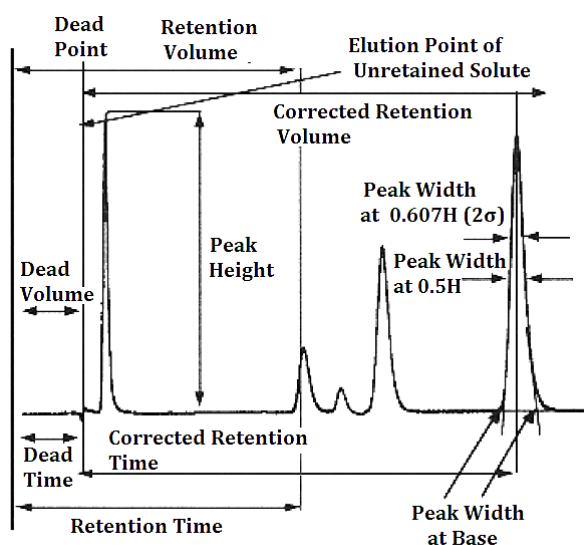
Figure 2.3 The Characteristics of a Chromatogram (Scott, 1996)

Accurate performance criteria or specifications must be available to determine the suitability of a detector for a specific application. This is necessary, not only to compare its performance with alternatives supplied by other instrument manufactures, but also to determine the optimum chromatography system with which it must be used to achieve the maximum efficiency. The specifications should be presented in a standard form and in standard units, so that detectors that function on widely different principles can be compared. The major detector characteristics that fulfill these requirements together with the units in which they are measured are summarized below in brief. The dynamic range of a detector is that concentration range over which a concentration dependent output is produced. Apparently, the linear dynamic range is defined as the range, where the latter correlation is linear. In practice, no detector has a truly linear response and a response index is usually applied, where its deviation from unity serves as a measure of its non-linearity. The detector response is defined either as detector output per unit change in solute concentration or as the detector output per unit change in the units of the detector measurement property (e.g. thermal conductivity). Detector sensitivity or minimum detectable concentration is

defined as the minimum concentration of solute passing through the detector that can be unambiguously discriminated from noise. The size of the signal that will make it distinctly apparent from the noise (the signal–to–noise ratio) is a somewhat arbitrary choice. Detector noise is the term given to any perturbation on the detector output that is not related to an eluted solute and it is a fundamental property of the detecting system that determines the ultimate sensitivity or the minimum detectable concentration possible. A critical issue met in all kinds of detectors is the peak dispersion that takes place in the mobile phase conduits and sensor volumes of the detector. However, due to the much higher diffusion rates in gas chromatography, dispersion is minimal and does not significantly affect chromatographic performance. Finally, when designing or comparing gas chromatographers, there are some detector specifications which need to be taken into account, such as the sensor dimensions, the detector time constant, the pressure and flow sensitivity and the operating temperature range. In the frame of the present thesis, two different chromatographic detectors were utilized, namely a Flame Ionization Detector (FID) and a Thermal Conductivity Detector (TCD), which are discussed in more detail in the next paragraphs. The latter detectors cover a wide range of applications offering catholic detection capabilities and excellent performance and each or both of them are used in the extreme majority of chromatographic systems in combustion research.

Flame Ionization Detector

The Flame Ionization Detector (FID) has been a commercial analyzer for about 50 years (McWilliam and Dewar, 1958). Since its introduction has become the most widely used detector in GC due to its reliability, low detection limits, wide dynamic range which offers a linear range that extends to about 10^7 orders of magnitude, and its general utility for a variety of problems in trace organic analysis. Additionally, under normal operation the detector response is not affected by modest changes in flow, pressure or temperature, also not responding to impurities such as CO_2 and water. The FID is a typical example of a mass sensitive GC detector which detects nearly all carbon containing solutes, with the exception of a limited number of small molecular compounds such as carbon disulfide, carbon monoxide, etc. In fact, due to its diverse and comprehensive response, it could be classified as a universal detector, at least for organic materials. Due to the nature of the detecting system, the FID can operate at very high temperatures and still maintain its high sensitivity and wide linear dynamic range.

The FID consists of a small hydrogen-air diffusion flame burning at the end of a jet, to which the eluted components from the column are directed with carrier and makeup gas flows as depicted in Figure 2.4a. As the organic components reach the flame, electrically charged species are formed and collected at an electrode set at a few volts above the flame, producing an increase in current proportional to the amount of carbon in the flame. The resulting current is amplified by an electrometer. The background current from the flame (ions and electrons formed by the combustion of hydrogen alone) is normally extremely small (1.2×10^{-12} amperes) and consequently, the noise level is commensurably minuscule *i.e.* about 10^{-14} amperes. The ionization process is relatively inefficient, only about 0.0018% of the solute molecules produce ions, that is about two ions or electrons per 10^5 molecules. However, due to the very low noise level, the minimum detectable mass of n-heptane is still as little as 2×10^{-12} g/sec. At a column flow rate of 20 ml/min. this would be equivalent to a minimum detectable concentration of about 3×10^{-12} g/ml. (Scott,

1998). The processes involved in the ionization mechanism in the FID begin at the tip of the jet and occur in discrete regions of the flame (see Figure 2.4b). The mixture of carrier gas, makeup gas and hydrogen flows out of the jet and expands outward, while air flows around the outside of the jet. The heat energy produced at the flame reaction zone preheats the flow of gases from the jet by back-diffusion. The organic materials eluting from the column undergo degradation reactions in this hydrogen-rich region, forming a group of single carbon species. As the two gas flows mix at the reaction methyl radical reacts with oxygen atoms forming formyl radical (CHO), which in turn reacts rapidly with water produced in the flame to generate hydronium ions. These positively charged ions are the primary positive charge carrying species. The process occurs approximately once every 100,000 carbon atoms introduced in the flame and it is almost a quantitative counter of carbon atoms being burned. In essence, therefore, the FID response is proportional to the number of carbon atoms, instead of the compound weight or moles (Grob and Barry, 2004). Moreover, there are studies evaluating the effective carbon atom number of various species with respect to their homologous series (Kállai et al., 2001), molecular structures (Kállai and Balla, 2002) and different experimental conditions (Kállai et al., 2003). The flame ionization detector is mass sensitive hence it responds to the mass of solute passing through it per unity time. The advantage of the mass sensitive detector is that the column eluent can be diluted without affecting the detector response. This characteristic is particularly useful when using a capillary column as the mobile phase can pass directly into the hydrogen flow of the FID and although the column eluent is extensively diluted, the response of the detector is unaffected due to the fact that the FID is mass sensitive.

Figure 2.4 (a) Schematic of an FID and (b) flame process in an FID (Grob and Barry, 2004)
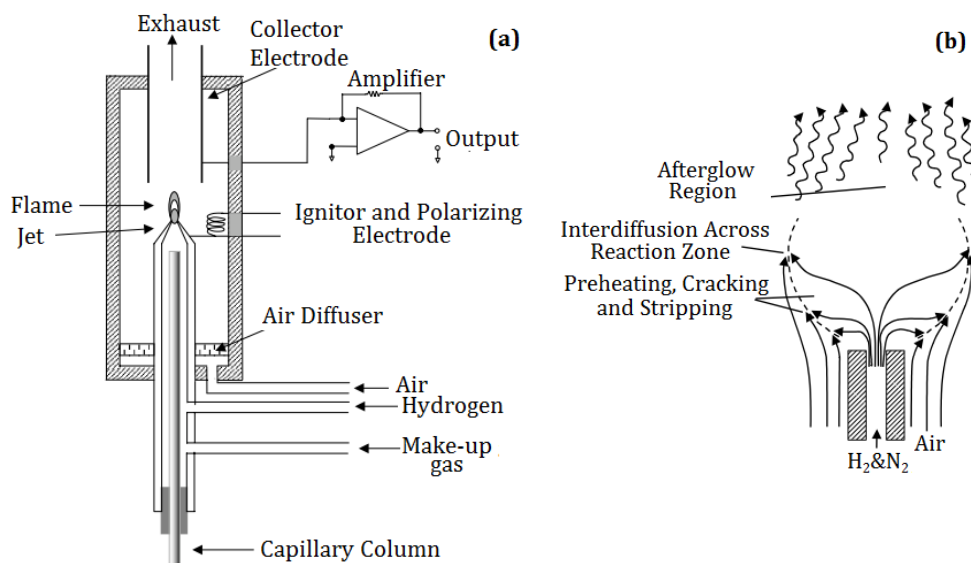
However, the mechanism that fully describes the flame ionization processes and the respective response of the detector is not totally understood. Nevertheless, an increasing effort is placed towards a better understanding of the actual phenomena (Schofield, 2008). In this respect the mechanism of the flame ionization detector has been reviewed (Holm, 1999) also accounting isotope and heteroatom effects (Holm, 1997). However, the detector's performance is such, that

facilitates numerous hydrocarbons measurements (Wierzchowski and Zatorski, 2000; Slemr *et al.*, 2004), offering also the ability of predicting their response factor from their molecular structures (Jorgensen *et al.*, 1990) constituting the FID the most frequently used detector in analytical combustion diagnostics.

Thermal Conductivity Detector

The thermal conductivity detector (TCD) is a universal, nondestructive detection sensor. and responds to the mass of the solute per unit volume of mobile phase passing through it, as all concentration sensitive detectors. Since thermal conductivity is a bulk physical property, it is also identified as a bulk property detector, because it responds to some difference in the thermal conductivity of the carrier gas caused by the presence of the eluted components. The TCD consists of four tungsten-rhenium filaments in a Wheatstone bridge configuration. Electric current flows through the four filaments causing them to heat up. A carrier gas of high thermal conductivity, typically helium, flows across the filaments removing heat with a constant rate. When a sample molecule with lower thermal conductivity exits the column and flows across the two sample filaments, the temperature of the filaments increase unbalancing the Wheatstone bridge and generating a peak as the sample molecules transit through the detector. The TCD detector is useful because it detects all molecules, not just hydrocarbons, so it is commonly used for fixed gas analysis (e.g. O_2, N_2, CO, CO_2, H_2S, NO, NO_2 etc.) where the target analytes do not respond well on other more sensitive detectors. A well-designed, maintained and operated TCD is capable of noise levels as low as 2 µV. The TCD has detectability in the range of 10^{-6} to 10^{-8} g/mL in carrier gas and its linear response is about four to five orders of magnitude. In other words, the TCD is able to detect concentrations from 100% down to about 100 ppm, but not lower. (Scott, 1998).
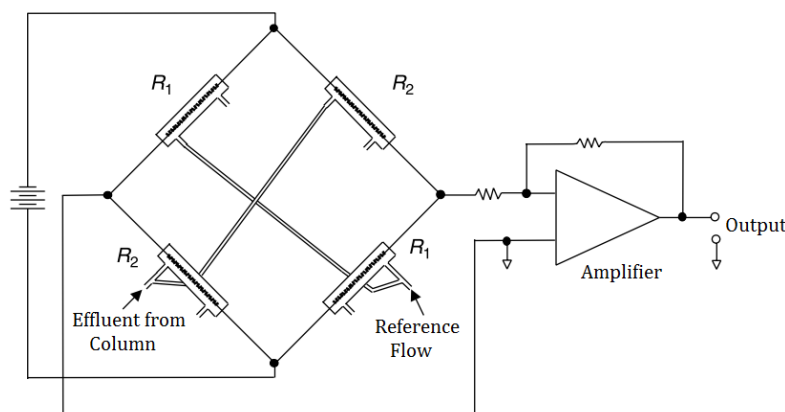
Figure 2.5 Typical bridge circuit used in a four-cell Thermal Conductivity Detector (Grob and Barry, 2004).

Temperature fluctuations or the adoption of temperature programming could affect the TCD performance. In order to overcome the effect of temperature on the conventional resistors of the TCD, one can control the temperature of the resistors or use resistors at very low temperatures. Alternatively, the four-filament configuration shown in Figure 2.5 replaces fixed resistors with a filament cell for improved stability. The flow from the analytical column enters two matched resistors of resistance R2, while the reference flow of the reference enters two matched reference

cells of resistance R1 (Grob and Barry, 2004). For such a design, the response factor is increased by a factor of 2 since the two filaments are contributing to the change in signal.

A trivial issue often met in thermal conductivity detectors is the appearance of negative peaks. There are several causes for negative peaks in bulk property detectors when actual sample peaks are eluted, including noise of contamination of the column. Negative peak is a relative term and is best defined as a signal from the detector that is opposite in sign to the signal from an eluting peak. The monitoring system is usually set up so that eluted peaks move upward on a recorder or computer chart and so negative peaks will be those that move downward and, hence, their name (Scott, 1998). In a gas-solid column separating the permanent gasses by adsorption using the thermal conductivity detector, negative sample peaks can often be obtained depending on the carrier gas employed and the sample gases that are being separated. If nitrogen is being used as the carrier gas to separate hydrogen, methane and carbon dioxide and the system is arranged to give positive peaks for hydrogen and methane then carbon dioxide, which will be eluted last will, under most circumstances give a negative peak. This is because the combined effects of the specific heat and thermal conductivity of hydrogen and methane relative to nitrogen will be opposite to the combined effects of specific heat and thermal conductivity of carbon dioxide.

2.1.2.4. Essential auxiliary systems for gas chromatography

Along with proper operation and careful use of the basic parts of a gas chromatographer described previously, it is essential to maintain constant operating conditions of a chromatographic method, so as to ensure measurement reliability and repeatability of results. Modern chromatographers incorporate numerous auxiliary systems to accomplish the latter target. Although details can be found in literature references given along this chapter, there are two groups of auxiliary systems worth mentioning. The first essential auxiliary system refer to the pneumatic modules that control the flow inside the column and the second correspond to a subcategory of the hot vaporizing injectors that facilitate sample analyses without overloading capillary columns, namely the split/splitless injection modules.

Capillary inlets: Split/Splitless mode
The development of capillary columns led to a fundamental problem, arising from the fact that these columns carry much less sample than packed ones. In other words, column overloading had to be avoided by the introduction of a special inlet system. There are four inlets, common use in capillary gas chromatography today, namely split, split-less, on-column and programmed-temperature vaporization. Split and splitless injection are both performed at the same inlet, often termed a split/splitless inlet. A split inlet is the simplest technique for concentrated samples that allows the introduction of a fraction of the injected sample into the capillary column by adjusting the relative flows of carrier gas into the column or to waste through a purge valve. Split inlets are heated to ensure that the entire injected sample evaporates quickly and mixes homogeneously with the carrier gas. Split inlet provides the rapid injection which leads to the narrowest initial bandwidth on the column and is the technique of choice for small-diameter columns and rapid separations. Splitless injection is performed using the same instrumentation as split, except that the purge valve is closed at the moment of injection leading the sample vapor into the capillary column.

When the purge valve is opened, any sample vapor remaining in the inlet is rapidly swept out of the purge valve and reaches the capillary column, avoiding sample overload and peak broadening (Grob and Barry, 2004). Injection using the splitless inlet is the most common means for improving detection limits and is currently the most commonly used technique for trace analysis, although complex sample preparation is often required.

Electronic pneumatic modules

Carrier gas supplies are provided either from synthetic air, oxygen or nitrogen generators, or, as in most cases, from storage vessels in line with pressure regulators which ensure the desirable set point values. The cylinders are usually situated outside and away from the chromatograph for safety purposes and the gases are passed to the chromatograph through copper or stainless steel conduits. It is apparent that the proper function of a chromatographic detector lies upon the reference or make up gases flow as well. The first control on any gas line is afforded by simple pressure controllers, with however, a number of pressure controllers, reducing valves and flow controllers, used for detector and column flow control. The latter are termed in many chromatographic systems as electronic pneumatic modules.

2.1.3. Development of a chromatographic method

The incorporation of columns, detectors and other chromatographic devises along with the appropriate configuration of temperature and flow settings is usually described under the term chromatographic method development. In the present paragraph two different chromatographic methods are presented, both implementing all techniques discussed in previous paragraphs. The first method was developed in the frame of the present thesis and the second, which has been used for the measurements in the fourth chapter and was developed in the University of Zaragoza, Spain. The described configurations, incorporated in an Agilent 7890A chromatographer, share the same detectors and stationary phases, with however, important differences in temperature programming and method capabilities, such as back-flushing of heavy compounds, as presented below.

2.1.3.1. Prime chromatographic configuration

The presented method targets on detecting light hydrocarbons and major combustion products in two separate channels that lead to a TCD and an FID detector respectively. The hydrocarbon quantities are quantified in the FID channel and all other major combustion products are identified on the TCD. In order to achieve this, the FID channel is equipped with a capillary column with dimethyl-polysiloxane stationary phase, whereas the TCD channel is equipped with packed columns with 80/100 and 60/80 supports, respectively. Table 2-1 describes in detail the chosen columns along with their commercial name, dimensions and gases that are eventually analyzed.

In the development of a separation, temperature programming is often not necessary and many samples can be quite satisfactorily separated by operating the column isothermally. Mixtures can be separated isothermally when the net combination of both polar and dispersive interactions are relatively similar. For example, a solute retained predominantly by dispersive forces can be retained to the same extent as a molecule retained predominantly by polar forces, providing the net

interactive forces between the different molecules and the stationary phase are of the same order of magnitude (Jennings *et al.*, 1997). Consequently, as long as the net forces on each molecule are similar, then the mixture can be separated by isothermal development. However, it might be necessary to reduce the oven temperature in order to avoid co-elution of the first compounds. In the given configuration the oven temperature was set at 30 ^{o}C, where methane is separated with good resolution from the ethane with a carrier gas flow of 0.5 ml/min in the capillary column.

Table 2-1 Column selection for the chromatographic method developed.

Column	Stationary phase	Commercial name	Dimensions	Detector	Gases Identified
A1	100% Dimethyl-polysiloxane	HP PONA	50 m x 0.2 mm 0.5 µm	FID	CH_4, C_2H_4, C_2H_6, C_3H_6, C_3H_8, C_4H_{10}, C_4H_8
A2	Porous Polymer Adsorbent Nickel mesh 80/100	Supelco Hayesep Q Support 80/100	3 ft x 1/8 in 2.1mm	TCD	Back-flush column
A3	Porous Polymer Adsorbent SS mesh 80/100	Supelco Hayesep Q Support 80/100	6 ft x 1/8 in 2.1mm	TCD	CH_4, H_2, O_2, N_2, CO, CO_2
A4	Synthetic zeolites based on SiO_4 and AlO_4 polyhedra Molecular sieve 5Å	Supelco MolSieve Support 60/80	6 ft x 1/8 in	TCD	H_2, O_2, N_2, CO, CH_4

On the first channel, species are eluted through the capillary column connected to the flame ionization detector, with nitrogen as carrier gas. The run-time events of this channel are quite straight forward, with the sample reaching the flame ionization detector, after leaving the sampling valve and passing through the 50:1 split mode. This configuration, which is primarily designed for liquid sample injection, can be utilized for gaseous samples as well, providing better resolution of the first solutes of the chromatogram with lowering, however, the detectability limit. In order to avoid sample condensation, split/splitless injection module, as well as gas sampling valve, is kept at 190 ^{o}C. The described setup identifies C_1 to C_4 alkanes and alkenes as described in Table 2-1.
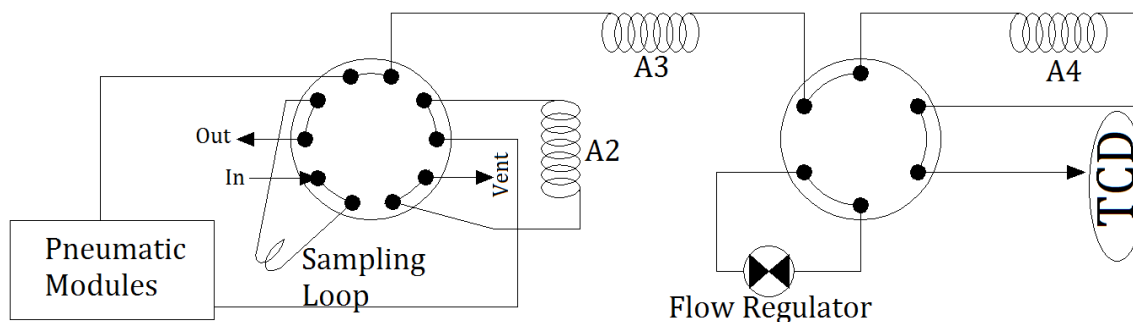
Figure 2.6 TCD channel configuration (valves set in OFF position)

The second channel leads to a thermal conductivity detector, utilizing two packed columns and a 5 Å molecular sieve column, as shown in Figure 2.6. The first two packed columns are both connected to a ten-port valve which links the sample inlet with the sampling loop and can additionally back-flush on demand any compounds trapped in the first column. In more detail, while the sample fills the sampling loop of the two-way, ten-port valve, the first packed column is fed individually with carrier gas, through the electronic pneumatic modules. When the chromatographic method starts, or in other words the valve switches to ON position, the carrier gas stream moves the sample from the loop onto the first column, which is already filled with carrier gas. From this time on the separation process starts and the eluents move from the first column to the next ones, reaching eventually the detector. However, the ten-port valve configuration can be set to its original set point on demand. This would result in reversing the flow in the first column, venting out of the system the eluents still trapped there, while the carrier gas flow in the columns will continue. This procedure is determined by trial-and-error runs and often termed back-flush. This technique can protect the installed columns or assist in avoiding species overlapping when more columns are utilized. In the given setup, the system is set so as water and species "heavier" than ethane are flushed out and do not reach the second column. The overall process at the two packed columns separates carbon dioxide, carbon monoxide, hydrogen and air. Additionally, in order to separately identify oxygen and nitrogen, a third molecular sieve column is installed. Unfortunately, carbon dioxide can damage the molecular sieve column, so extra care must be taken. In order to achieve O_2/N_2 separation on the third column and at the same time protect it from CO_2 contamination, a switching valve is installed. The developed chromatographic method is set up so as when the first eluents exit the second column, namely hydrogen, methane, air and carbon monoxide with that order, are trapped in the molecular sieve column and placed on hold in a stop-flow mode. This means that the switching valve bypasses the carrier gas through a flow regulator and leads the carbon dioxide to the detector directly after exiting the packed columns. The flow regulator balances the bypass flow in order to acquire the same levels of detector noise with the molecular sieve column on- and offline. One drawback of the latter method is that changes in the switching valve can cause small noise traces in the chromatogram. Finally, after carbon dioxide is eluted from the second column, the species that were in a stop flow reconnect to the carrier gas and eventually reach the detector, with O_2/N_2 separation achieved. In conclusion, immediately after the last solute of interest is eluted, the temperature of the column can be rapidly raised to the maximum temperature the stationary phase can satisfactorily tolerate. This procedure elutes the remaining peaks in the minimum time.

2.1.3.2. Alternative configuration

Along with the chromatographic configuration described in the previous paragraph, a second alternative set up was utilized in the framework of the present thesis, so as to facilitate the experimental campaign presented in the fourth chapter. This method has been described in numerous studies over the last years (Abián *et al.*, 2008; Esarte *et al.*, 2012) and only a comparative description is given in the present section. The configuration utilizes the same two detectors as in the previously described methodology, namely a thermal conductivity and a flame ionization detector. The lighter hydrocarbon species are identified on the TCD without back-flushing them out of the detector's channel, as in the previous set up, whereas the FID channel is utilized for

identifying heavier compounds such as benzene and toluene species. The latter choice necessitates the incorporation of temperature programming techniques in the chromatographic method, since an isothermal operation of the column would result a number of drawbacks. In particular, if the column temperature is too low, as in the first method, the early-eluting peaks will be closely spaced, while the more strongly retained components will be broad and low-lying. As discussed earlier, these strongly retained components can be more quickly eluted by selecting a higher isothermal temperature, also improving their detectability. Nevertheless, more rapid co-elution of components, results in an overall loss of resolution at the beginning of a chromatogram. This situation, which prevails in all practiced versions of elution chromatography, is often called the "general elution problem"; it is solved in GC by temperature programming, where the column oven temperature is gradually increased at a linear rate during an analysis.

Table 2-2 Column selection for the alternative chromatographic method utilized.

Column	Stationary phase	Commercial name	Dimensions	Detector	Gases Identified
B1	100% Dimethyl-polysiloxane	HP PONA	50 m x 0.2 mm 0.5 μm	FID	Benzene, ethylbenzene, toluene and xylene
B2	Bonded, polystyrene divinylbenzene	HP PLOT Q	30 m x 0.53 mm 40 μm	TCD	C_2H_6, C_2H_4, C_2H_2, C_3H_4, C_3H_6, C_3H_8, i-C_4H_{10}, n-C_4H_{10}, 1,3-butadiene
B3	Molecular Sieve 5Å Zeolite	HP-PLOT MoleSieve	15 m x 0.53 mm 25 μm	TCD	H_2, O_2, N_2, CO, CH_4

Temperature programming offers several attractive features such as reduced time of analysis and improved overall detectability of components or in other words, peaks are sharper and have nearly equal bandwidths throughout the chromatogram (Harris and Habgood, 1966). The alternative configuration starts from the same temperature as the prime method and follows a temperature ramp reaching a value as high as 210°C with a ramp of 20°C/min. The TCD channel is equipped with HP Plot Q columns coupled with a MoleSieve column and the FID channel is equipped with an HP PONA column, as described in Table 2-2. In this way the CO, CO_2, N_2, H_2, methane, ethane, ethylene, acetylene, propane, propylene, propadiene, 1,3-butadiene, isobutane, ethanol are quantified at the TCD and benzene, ethyl-benzene, toluene and xylene at the FID. In tis here noted that both sampling lines pass through a split injection module with a ratio of 10:1, using the same temperature, pressure and carrier gasses as the ones described in the previous section.

2.1.4. System calibration and error analysis

Gas chromatography can be used for two types of analysis; qualitative analysis which identifies a solute present in a mixture and quantitative analysis which determines how much of this substance is present in a mixture. Quantitative analysis is probably the major application of chromatography techniques. Given the fact that column length, stationary phase and its loading, oven temperature

and carrier gas flow are kept constant, the retention time can serve as a means to identify a given solute. While qualitative data is obtained from retention measurements, quantitative analysis involves the measurement of either peak heights or peak areas. Peak heights can be used as a relative measurement of the quantity of material present, providing the separation is highly reproducible. Alternatively peak areas are used for quantitative assessment and this approach is claimed to be more precise. Measurement of peak area accommodates peak asymmetry or peak tailing, without compromising the correlation between peak area and quantity. Consequently, peak area measurements give more accurate results under conditions where the peak shape is not perfect or appears in a non-Gaussian shaped profile. Quantitative analysis makes certain demands on the chromatographic apparatus, particularly the injection system and the detector. In the first instance, a truly representative sample must be placed on the column by the injection system and secondly, the detector must have a linear response that is known and defined by its response index. All contemporary GC detectors that are commercially available are designed to give a linear output over a defined concentration range. Consequently, providing the calibration standard is chosen to be appropriate for the linear dynamic range of the detector, quantitative accuracy can be achieved.

Quantitative measurements are obtained using either an internal or an external standard, which is chosen so as it elutes discretely and well-separated from all other mixture components. In the procedure termed internal standard method, a weighed amount of the standard can be added directly to the sample and the peak area of interest is compared with that of the standard. In the second procedure termed external standard method, a weighed amount of the standard can be made up in a known volume of solvent, and chromatographed under exactly the same conditions as the unknown sample, but as a separate chromatographic run. In this case the peak area of the standard solute in the reference chromatogram is compared to the peak areas of the solutes of interest in the sample chromatogram. For the purposes of the present thesis, the quantification of the obtained results was achieved using external standardization. Different standard vials, each one containing various species of interest in reference amounts, were utilized. The calibration method was realized, as described above, through repeating identical calibration runs. The calibration procedure and the respective error analysis presented hereon, concern the in house developed method, with the approach also applying for the alternative configuration previously described. Table 2-3 presents the reference amounts used, along with the respective response area and its standard deviation for each species. Apparently, the reference amounts are given in pA·s when the analysis was made using the flame ionization detector and in 25 µV·s, when the thermal conductivity detector was utilized.

As noted in Table 2-3, most species appear to have a calibration uncertainty of the order of 1-2 %, which suggests that the method operates reliably producing high measurement repeatability. The only inconsistency on the aforementioned uncertainty levels concerns hydrogen and methane, when the latter is identified on the TCD channel. Hydrogen presents higher calibration uncertainty, due to the fact that the reference amount of hydrogen used was only 5%. Such a small amount will not significantly disturb the overall Wheatstone bridge equilibrium on the TCD, due to the fact that that thermal conductivity of hydrogen and helium, which is used as carrier gas, does not vary appreciably. However, this level of reference amount ensures that the detector response is within its dynamic range and close to the expected measured levels. On the other hand, the higher

uncertainty levels for methane on the TCD, can be attributed to the fact that methane was eluted directly after column A4 was placed online following its stop-flow function (see paragraph above), hence the baseline was disturbed from valve noise, resulting in larger integration errors. Nevertheless, methane is also detected in the FID channel with very low levels of uncertainty and those measurements were preferred. It is here noted that the FID response was calculated to be within 2%, with respect to the effective carbon number of the analyzed hydrocarbons.

Table 2-3 Calibration table and overall uncertainty for the main method

Species	Reference Amount (%)	Calibration Area Average Response (pA·s or μV·s[*])	Calibration Standard Deviation (pA·s or μV·s)	Detector Channel	Normalized Calibration Uncertainty (%)	Overall Method error (%)
CO_2	10	5256.4	8.16	TCD	0.16	3.35
O_2	4.9	984.9	8.18	TCD	0.83	4.95
H_2	5.7	26.62	1.16	TCD	4.35	20.35
N_2 [†]	85.1	38695.2	118.35	TCD	0.31	2.99
N_2 [‡]	88.2	38521.7	377.10	TCD	0.98	5.15
CH_4	1.1	479.99	49.66	TCD	10.35	46.37
CO	5	2110.57	38.32	TCD	1.82	8.56
CH_4	1.1	128.38	1.33	FID	1.04	5.65
C_2H_6	1.24	290.09	3.72	FID	1.28	6.55
C_3H_8	0.91	311.59	3.37	FID	1.08	5.78
$i\text{-}C_4H_{10}$	1.08	493.49	3.15	FID	0.64	4.27
$n\text{-}C_4H_{10}$	1.1	490.13	5.35	FID	1.09	5.82
C_2H_4	0.99	890.27	6.19	FID	0.70	4.49
C_3H_6	0.98	1294.72	8.99	FID	0.69	4.42
C_4H_8	1.94	3294.88	56.095	FID	1.70	8.25

Additionally, in order to appreciate the produced results, it is important to comprehend the overall measurement uncertainty along with the 0th-order uncertainty that arises from the instrument itself (Taylor, 1997). As far as the overall measurements uncertainty a number of factors have to be assessed besides the calibration error. Such factors include the linearity response of the detector with respect to the calibrated range, the integration errors associated with the measurements and the instrument accuracy. In more detail, in order to facilitate such an analysis, it is assumed that the detector accuracy is of the order of 1% and its linear response within 1% for the FID and 2% for the

[*] Units correspond to pA·s for the FID and to μV·s for the TCD
[†] First out of two point calibration used for nitrogen
[‡] Second out of two point calibration used for nitrogen

TCD detector. The first order uncertainty associated with the scatter of the results of repeated trials is assumed to be twice as the 0th-order uncertainty accompanied with a 2% sampling uncertainty. Obviously, as described earlier the integration errors for methane, on the TCD channel, and the signal-to-noise generated error for hydrogen is higher than the ones for the rest aforementioned, with similar corrections applying on other species as proposed in the literature (Moffat, 1988). The calculated values accounting for multiple-sample uncertainty analysis are presented in Table 2-3.

2.2. Continuous gas analysis system

Gas chromatography is an extremely versatile technique which can provide extensive speciation data, as described earlier. However, although sampling procedures may be online and fully automated, they do not provide the ability of real-time monitoring of a process, since the analysis is made offline. On the other hand, there are various gas analysis systems that facilitate online monitoring of exhaust emissions, based on state of the art, nondestructive instrumentation. Continuous gas analyzers have a modular design that offers tailor-made, long-term, reliable operation and the ability to upgrade with new features. Moreover, the implementation of such diagnostic tools along with a sophisticated technique, as is gas chromatography, is also beneficial in terms of providing supplementary data, avoiding further complexities; for instance continuous nitric oxides monitoring with a continuous system can be easily combined with batched detailed species measurements, rather than setup a chromatographic method incorporating all the latter. These advantages of continuous gas analysis systems constitute them particularly attractive for process control. Additionally, they are often used for industrial performance optimization, since in such applications they can cover the majority of variables that need to be monitored. In the frame of the present thesis, different continuous analyzers have been utilized, with however similar principles of operation. This paragraph presents the employed instrumentation and discusses detector operating principles and characteristics, providing the essential background for the understanding of the experimental campaign which follows in the next chapters.

2.2.1. Continuous gas analysis detectors

Continuous gas analysis integrated systems may incorporate numerous detection schemes for the analysis of major combustion products, as well as for the quantification of important pollutant emissions. The choice of the appropriate detector is unambiguously connected to the process to be monitored. Studies of rapidly changing phenomena, for instance, would require the use of a detector with short time response, as is the incorporation of a chemiluminescence detector for nitric oxides monitoring in diesel engines transient operation studies (Giakoumis *et al.*, 2012). On the other hand, an integrated emission monitoring system should cover the diagnostic needs for all species of interest, as for example sulfur oxides monitoring in studies of fuels with sulfur content (Fryda *et al.*, 2012). In other words, the utilized diagnostic tool should incorporate detectors that cover all the species of interest and satisfy the detection specifications as well. In this regard, the present section presents the detectors used within the framework of the present thesis, which include infrared (ABB Uras26) and ultraviolet (ABB Limas11) photometers configured for the

detection of carbon, nitric and sulfur oxides, as well as a magneto-mechanical sensor (ABB Magnos206) for oxygen detection. The various detector modules where integrated in one central unit with common control and interface. Their characteristics, accuracy and calibration procedures are discussed in detail below.

2.2.1.1. Non-dispersive spectroscopic detectors

Before analyzing the principle of operation of non-dispersive detectors, it is essential to understand the fundamentals of the absorption of light in matter, as described by Beer Lambert's law. The intensity of absorption by a sample varies with the length of the sample according to equation 2.1.

$$\log (I/I_o) = - \varepsilon \cdot c \cdot l \tag{2.1}$$

Where I_o is the incident intensity at a particular wavelength, I is the intensity after passage through a sample of length l and c is the molar concentration of the absorbing species. The quantity ε is called the molar absorption coefficient, also widely termed extinction coefficient. The molar absorption coefficient depends on the frequency of the incident radiation and is greatest where absorption is more intense. The dimensionless product $A = \varepsilon \cdot c \cdot l$ is called the absorbance or optical density of the sample and the ratio I/I_o is the transmittance T (Ingle and Crouch, 1988). It becomes obvious that as a gas flow passes through a sampling cuvette with known dimensions, its concentration in the absorbing species of interest can be derived by measuring its transmittance. The term non-dispersive refers to the fact that all the light passes through the gas sample and is only filtered immediately before the detector. Dispersive infrared detectors use a grating or prism to pre-select the desired wavelength of light and pass only this through the gas sample to the detector. Dispersive infrared detectors are usually used in bench-top analytic instruments for their ability to scan a broad wavelength range.

Non-dispersive infrared sensors

Infrared gas analysis is one of the most basic techniques of gas detection (Luft, 1975). All gases absorb infrared light energy of various wavelengths. Multiple gases and gases with very complicated absorption spectra may be accurately quantified using this technique (Lammel *et al.*, 2001). Non-dispersive infrared absorption spectroscopy (NDIR) is currently the methodology of choice for the accurate and reliable measurement of gas concentrations. A sensor is used to monitor a specific range of the infrared spectrum corresponding to the signature wavelength of the target gas. When the target gas passes between an infrared source and the detectors, the absorption spectrum changes and instrument electronics are used to process this information and determine gas concentration. In more detail, these techniques rely on the energy absorption characteristics of a particular gas in the infrared region. Their key components are the infrared source, the sample chamber or light tube, the wavelength filter, and the infrared detector. The gas is pumped into the sample chamber and gas concentration is measured electro-optically by its absorption of a specific wavelength in the infrared. In most NDIR instruments, infrared light passes through two identical cuvettes and reach a detector. The first cuvette is filled with a non-absorbing gas such as nitrogen and it serves as a reference cell, while the second cuvette is the measurement cell from which the continuous gas flow of sample to be analyzed passes through. The detector has an optical filter in front of it that eliminates all light except the wavelength that the selected gas molecules can absorb.

Other gas molecules do not absorb light at this wavelength, and do not affect the amount of light reaching the detector. Energy in the region of interest is absorbed by the gas in the measurement cell, attenuating the energy passing through the cell and falling on the detector. This attenuated energy is compared to the unattenuated signal from the reference cell and the difference is proportional to the amount of absorbing gas in the measurement cell.

In particular, the utilized continuous non-dispersive infrared photometer can selectively measure concentrations of up to four sample components simultaneously. For the needs of the present thesis, the detector was configured to selectively measure the concentration of CO at the infrared spectrum around 4.7 μm and CO_2 at the infrared spectrum close to 4.2 μm. The utilised gas analysis incorporated a built-in calibration cell and was calibrated for detecting CO at a range of 0 to 10000 ppm and CO_2 at a range of 0 to 25% (vol.) with 1% span accuracy per volume. As far its overall uncertainty is concerned, the linearity deviation varied by 1% and its repeatability by 0.5% of the span measurement, whereas zero drift and sensitivity ranged by 1% and 3% respectively, resulting in an overall measurement error of nearly 4%.

Non-dispersive ultraviolet spectroscopy detectors

Despite the fact that numerous techniques have been employed for nitric oxides detection in the infrared (Wang *et al.*, 1998), ultraviolet light is often used for the analysis of nitric and sulfur oxides as well. Ultraviolet detection is moreover, advantageous against chemiluminescence detectors due to the fact that is generally not as cross sensitive towards major gaseous combustion products. CO_2 and H_2O do not absorb well the ultraviolet light and have no ability to interfere with the UV measurement of nitric oxides. Often, when the UV measuring principle is used it is actually termed non dispersive ultraviolet principle (NDUV). The measurement is made by leading a gas flow through a cuvette where the ultraviolet light source and the optical filter have been placed at one end of the cuvette and a detector at the other. The light source sends out a scattered ultraviolet light at a wavelength determined by the optical filter installed between the light source and the cuvette. The absorption of the light that is sent into the cuvette is an expression of the concentration of the gas to be analyzed, as described earlier. The amount of light passing through the gas is measured by the detector at the other end of the cuvette.

In particular, that utilized detector (ABB Limas11) is a process photometer which is easily configured to meet individual process measurement requirements. The measuring principle is particularly reliable because of its high stability which is based on the four-beam signal processing principle. As a result, it is unaffected by contamination in the cells. A high degree of selectivity is provided by using interference and gas filters as well as optimum selection of measured wavelength and reference wavelength. This allows electronic cross sensitivity correction. The utilised gas analysis incorporated a built-in calibration cell and was calibrated for detecting NO (close to 226nm) at a range of 0 to 1000 ppm and NO_2 at a range of 0 to 100 ppm with 1% span accuracy per volume. As far its overall uncertainty is concerned, the linearity deviation varied by 0.5% and its repeatability by 0.5% of the span measurement, whereas zero drift and sensitivity ranged by 1% and 0.1% respectively, resulting in an overall measurement error of nearly 2%.

2.2.1.2.   Paramagnetic detector for oxygen detection

Oxygen concentration measurements are of high importance in combustion diagnostics, since especially in fuel-lean flames, they constitute a major combustion product. Moreover, oxygen concentration levels can be used to experimentally determine the equivalence ratio and by this means reveal either system malfunctions or experimental flows (e.g. flow controller offsets). This section presents the oxygen detectors utilized in the frame of the present thesis.

Paramagnetic sensor

Some gasses such as oxygen have paramagnetic characteristics due to non-paired electrons. This feature can be used by letting the gas pass through a magnetic field in a gas analyzer. There are numerous designs for paramagnetic sensors (Schmid *et al.*, 2006) but mainly of two different types. The first, often called thermo magnetic, consists of a heated wire placed in a magnetic field, which serves as the measuring cell. Oxygen molecules are dragged towards the magnetic field and as they pass through the measuring cell, they cool the heated wire and thus change its resistance. The change of resistance in the heated wire is proportional with the O_2 concentration. Alternatively, a focused magnetic field is created and oxygen molecules that are present in the sample stream are attracted into the strongest part of the magnetic field. Two nitrogen filled glass spheres are mounted on a rotating suspension within a magnetic field. A mirror is mounted centrally on the suspension and light is shone onto the mirror. The reflected light is directed onto a pair of photocells. The attracted into the magnetic field oxygen molecules displace the nitrogen filled spheres, causing the suspension to rotate and the photocells detect the movement generating a signal. The signal generated by the photocells is passed to a feedback system, which pass a current around a wire mounted on the suspension. This causes a motor effect, which keep the suspension in its original position. The current measured flowing around the wire is directly proportional to the concentration of oxygen within the gas mixture.

2.3.   Concluding remarks

Combustion diagnostics using several different tools is commonly applied to obtain simultaneous measurements of a wide variety of combustion parameters, in order to develop sound understanding of process efficiency, flame stabilization, reaction kinetics, emissions generation and many other combustion related aspects. Accordingly, there are diagnostic tools presenting large diversity, such as batch or real-time monitoring of emissions, analytical chemistry or spectrometric detecting principles and so on. The present chapter examines two separate intrusive diagnostic techniques, which are utilized in the present thesis in chapters 4, 6 and 7. The first concerns a gas chromatographic and the second a continuous gas analysis system. The basic parts of the GC system and the developed methodology, along with an alternative configuration, were described. The operating principles and the respective uncertainty analysis for both systems were also discussed. This chapter presents the methodology and provides a solid background for understanding the results presented in the following chapters, which utilize the aforementioned techniques, namely chapters 4, 6 and 7.

Chapter references

Abián M, Esarte C, Millera A, Bilbao R and Alzueta MU. Oxidation of acetylene-ethanol mixtures and their interaction with NO. Energy Fuel 2008;22:3814–3823.

Balès-Guéret C, Cathonnet M, Boettner JC and Gaillard F. Experimental study and kinetic modeling of higher hydrocarbons oxidation in a jet-stirred flow reactor. Energy Fuel 1992;6:189–194.

Barry EF and Grob RL. 2007. Columns for gas chromatography, Performance and selection. Hoboken, New Jersey. John Wiley & Sons, Inc.

Cazes J and Scott RPW. 2002. Chromatography theory. Marcel Dekker, INC. New York Basel

Dagaut P. Kinetics of jet fuel combustion over extended conditions: Experimental and modeling. Transactions of ASME 2007;129:394–403.

Dagaut P and Nicolle A. Experimental study and detailed kinetic modeling of the effect of exhaust gas on fuel combustion: mutual sensitization of the oxidation of nitric oxide and methane over extended temperature and pressure ranges. Combust Flame 2005;140:161–171.

Esarte C, Abián M, Millera A, Bilbao R and Alzueta MU. Gas and soot products formed in the pyrolysis of acetylene mixed with methanol, ethanol, isopropanol or n-butanol. Energy 2012;43:37–46.

Freitag R and Allington RW (Eds). 2002. Modern Advances in Chromatography. Springer Verlag Berlin Heidelberg

Fryda L, Panopoulos K, Vourliotis P, Pavlidou E and Kakaras E. Experimental investigation of fluidised bed co-combustion of meat and bone meal with coals and olive bagasse. Fuel 2006;85:1685–1699.

Giakoumis EG, Rakopoulos CD, Dimaratos AM, Rakopoulos DC. Exhaust emissions of diesel engines operating under transient conditions with biodiesel fuel blends. Prog. Energy Combust Sci 2012;38:691–715.

Grob RL and Barry EF (Eds.). 2004. Modern practice of gas chromatography (4th Ed.) Hoboken, New Jersey. John Wiley & Sons, Inc.

Guiochon G and Guillemin CL. Gas chromatography. Rev. Sci. Instrum. 1990:61;3317–3339.

Harris WE and Habgood HW. 1966Programmed Temperature Gas Chromatography (2nd Ed.) New York. John Wiley & Sons, Inc

Hollis OL. Separation of gaseous mixtures using porous polyaromatic polymer beads. Anal. Chem. 1966;38:309–316.

Hollis OL and Hayes WV. Water analysis by gas chromatography using porous polymer columns. J Gas Chromatogr 1966;4:235–239.

Holm T. Mechanism of the flame ionization detector II. Isotope effects and heteroatom effects. J Chromatograph A 1997;782:81–86.

Holm T. Mechanism of the flame ionization detector. J Chromatograph A 1999;842:221–227.

Ingle JDJ and Crouch SR. 1988. Spectrochemical Analysis, Prentice Hall, New Jersey

Jennings W, Mittlefehldt E and Stremple P. 1997. Analytical gas chromatography (2nd Ed.) Academic Press Ltd. San Diego California.

Jönsson JA (Ed). 1987. Chromatographic Theory and Basic Principles. Dekker.

Kállai M, Veres Z and Balla, J. Response of flame ionization detectors to different homologous series. Chromatographia. 2001;54;511–517.

Kállai M and Balla, J. The effect of molecular structure upon the response of the flame ionization detector. Chromatographia. 2002;56;357–360.

Kállai M, Máté, V and Balla, J. Effects of experimental conditions on the determination of the effective carbon number. Chromatographia. 2003;57;639–644.

Lammel G, Schweizer S and Renaud P. MEMS infrared gas spectrometer based on a porous silicon tunable filter. The 14th IEEE International Conference on Micro Electro Mechanical Systems, 2001:578–581.

Luft KF. Infrared techniques for the measurement of carbon monoxide. Ann. Occup. Hyg. 1975;18:45–51.

Tswett M. Adsorptionanalyse und chromatographische Methode. Anwendung auf die Chemie des Chlorophylls (Adsorption analysis and chromatographic method. Application to the chemistry of chlorophyll.), Berichte der Deutschen botanischen Gesellschaft, 1906:24;384–393.

Turbiez A, Bakali El, Pauwels JF, Rida A and Meunier P. Experimental study of low pressure stoichiometric premixed methane, methane/ethane, methane/ethane/propane and synthetic natural gas flames. Fuel 2004;83:933–941

Mati K, Ristori A, Gail S, Pengoloan G and Daguat P. The oxidation of a diesel fuel at 1-10 atm experimental study in a JSR and detailed chemical kinetic modeling. Proc. Combust. Inst. 2007;31:2939–2946.

Martin AJP and Synge RLM. A new form of chromatogram employing two liquid phases. Biochem J. 1941;35:1358–1368 .

McNair HM and Miller JM. 1998. Basic gas chromatography. New York. John Willey & Sons, Inc.

McWilliam IG and Dewar RA, Nature 1958;181:760.

Mishra TK, Datta A and Mukhopadhyay A. Comparison of the structures of methane-air and propane-air premixed flames. Fuel 2006;85:1254–1263.

Mishra TK, Datta A and Mukhopadhyay A. Concentration measurements of selected hydrocarbons in methane/air partially premixed flames using gas chromatography. Int. J. Therm. Sci. 2005;44:1078–1089

Moffat RJ. Describing the uncertainties in experimental results. Exp Therm Fluid Sci 1988;1:3–17

Poddar NB, Thomas S and Wornat MJ. Polycyclic aromatic hydrocarbons from the co-pyrolysis of 1,3-butadiene and propyne. Proc. Comb. Inst. (2012) doi:10.1016/j.proci.2012.05.013

Schmid U, Seidel H, Mueller G and Becker Th. Theoretical considerations on the design of a miniaturized paramagnetic oxygen sensor. Sensors Actuators B 2006;116:213–220.

Schofield K. The enigmatic mechanism of the flame ionization detector: Its overlooked implications for fossil fuel combustion modeling. Prog Energ Combust Sci. 2008;34:330–350.

Scott RPW. 1996. Chromatographic detectors; Design, function and operation. Marcel Dekker, INC. New York Basel

Scott RPW. 1998. Introduction to Analytical Gas Chromatography (2nd Ed.) Marcel Dekker, INC. New York Basel

Scott RPW. 2003. Principles and practice of chromatography. Chrom-Ed Book Series, Libraryforscience, LLC.

Scott RPW. 2003. Gas chromatography Detectors. Chrom-Ed Book Series, Libraryforscience, LLC.

Slemr J, Slemr F, D'Souza H and Partiridge R. Study of relative response factors of various gas chromatograph-flame ionization detector systems for measurements of C2-C9 hydrocarbons in air. J Chromatograph A 2004;1061:75–84

Supina WR. 1974. The packed column in gas chromatography, Supelco, Inc., Bellefonte, PA

Taylor JR. 1997. Introduction to error analysis (2nd Ed.) University Science Books. Sausalito California

Warnatz J, Ulrich Maas U and Dibble RW. 2006. Combustion: Physical and Chemical Fundamentals, Modeling and Simulation, Experiments, Pollutant Formation (4th Ed.). Springer-Verlag Berlin Heidelberg

Wang CH, Crowder JG, Mannheim V, Ashley T, Dutton DT, Johnson AD, Pryce G. and Smith SD. Detection of nitrogen dioxide using a room temperature operation mid-infrared lnSb light emitting diode. Electronics Letters 1998;35:300–301.

Wierzchowski PT and Wieslaw Zatorski L. Determination of Cyclo C_6 and C_7 peroxides and hydroperoxides by gas chromatography. Chromatographia 2000;51;83–86.

Chapter 3

Nonintrusive combustion diagnostic techniques

One may argue that the first nonintrusive combustion research are the early experiments of emission spectra of heated elements by Robert Bunsen and Gustav Kirchhoff, roughly 150 years ago (Kirchhoff and Bunsen, 1861). However, it was the incorporation of laser-based techniques that revolutionized nonintrusive combustion research, with the first major review article appearing almost one century later (Schwar and Weinberg, 1969). Before the introduction of laser-based diagnostic tools, measurements in flames were made by inserting probes such as Pitot tubes and hot-wires for velocity, thermocouples for temperature, and suction probes for gas concentration measurements, while particle measurements required them to be collected on filters inside suction probes for subsequent removal and size analysis. Over the last decades, there has been an incredible development and application of laser-based tools that accompanied the respective increase in the amount of combustion research carried out, resulting in a better understanding of fundamental processes in high-temperature, reacting flow systems. Currently, there is a large number of linear and nonlinear laser-based techniques for nonintrusive measurements of species concentrations, temperatures, and gas velocities in a wide pressure and temperature range.

Instead of relying on global measurements, instruments have been developed so as to probe into flames and combustion environments, allowing spatially and temporally resolved measurements of temperature, flow and species concentration. An important factor that has contributed to the increased level of understanding of combustion phenomena is that laser diagnostics enabled to a large extent the real-time monitoring of important combustion intermediate species. This facilitated indirect measurements of heat release, mixture fractions, flame front visualization and many other aspects of combustion processes, with high temporal and spatial resolution. Data obtained from such experiments form the basis for comparison with detailed mathematical models of laminar and turbulent reactive flows in order to obtain optimal conditions to lower pollutant formation and fuel consumption. Beside the nonintrusive diagnostics of technical combustion devices, the kinetics and microscopic dynamics of elementary chemical combustion reactions can be further investigated in great detail by laser spectroscopy. These investigations show, that a small number of relatively simple elementary steps control a large variety of combustion phenomena and pollutant formation processes (Wolfrum, 2002). In addition, laminar flames have proved ideal for laser spectroscopic method developing for testing and improving gas-phase reaction mechanisms in models for practical combustion systems, which in turn are of basic importance in the validation and further development of turbulent combustion models (Kuo and Parr, 1994).

In general, laser combustion diagnostics can be classified into flow field measurements, scalar field measurements and combined flow-scalar diagnostics (Tropea *et al.*, 2007). Primarily, point flow field measurements rely on Doppler shift and are obtained using Laser Doppler Anemometry or Velocimetry (Schneider *et al.*, 2003), which are met in the literature with the acronyms LDA or LDV, respectively. Additionally, plannar or even global flow field measurements are obtained by tracking molecular traces or particles using Particle Imaging Velocimetry–PIV (Upatnieks *et al.*, 2004).

Temperature profiles, are mainly measured using either elastic/Rayleigh scattering, by measuring gas phase density and hence temperature (Knaus *et al.*, 2005), or by inelastic/Raman scattering (Pitz *et al.*, 1990; Cheng *et al.*, 2010), or even combining both (Masri *et al.*, 1996). In addition, new techniques like laser-induced breakdown thermometry (Kiefer *et al.*, 2012), or two-line atomic fluorescence (Burns *et al.*, 2011) thermometry are increasingly appearing in the literature.

On the other hand, concentration measurements for major and intermediate combustion products, including soot, are obtained using various optical and spectroscopic techniques, such as chemiluminescence (Nau *et al.*, 2012; Hardalupas and Orain, 2004), Intra-Cavity Laser Absorption Spectroscopy–ICLAS (Goldman and Cheskis, 2008) or Cavity Ring-Down Spectroscopy–CDRS (Mercier *et al.*, 2001). Furthermore, temperature and species measurements are obtained using nonlinear techniques, such as Coherent anti-Stokes Raman Scattering–CARS (Kiefer and Ewart, 2011; Dreier and Rakestraw, 1990), Degenerate Four-Wave Mixing–DFWM (Seeger and Leipertz, 1996; Hancock *et al.*, 1997; Marrocco, 2012) and polarization spectroscopy (Suvernev et al., 1995). Moreover, electron ionization and Resonance-Enhanced Multi-Photon Ionization–REMPI techniques are also used in order to explore formation pathways of aromatic compounds (Hansen *et al.*, 2012). Finally, particle sizes and concentrations are observed by laser-heating the particles and detection of the subsequent incandescence in a process called Laser-Induced Incandescence–LII (Axelsson *et al.*, 2000; Shaddix and Smyth, 1996).

Evidently, Laser Induced fluorescence–LIF is a powerful diagnostic tool and holds a distinguishing place among the aforementioned optical and spectroscopic techniques, which justifies the reason for being the most frequently utilized nonintrusive technique in combustion research. Its major advantages which constitute its application straightforward rely on the comparatively simple optical adjustments which provide a low level of experimental setup complexity, and on the fact that the short-nanosecond exposure time scales give clear two or three dimensional images. Additionally, the LIF technique is advantageous, as it is an extremely sensitive probe for minor species detection, providing the experimental basis for understanding flame chemistry (Wolfrum, 1998). However, in order to perform LIF measurements, an accurate determination of excitation and detection wavelengths has to be made, also accounting the difficulties in operating tunable lasers. In addition, the quantification of such measurements is quite demanding and even more essential when the species of interest appear in low concentrations. Due to the high selectivity and wide flexibility with respect to species detection of the method, laser induced fluorescence spectrometry has been applied to a large number of experimental investigations, covering different aspects of combustion systems.

The most frequently, as well as the first species to be systematically by means of laser induced fluorescence spectroscopy is the hydroxyl radical (Dryer and Crosley, 1982) and as a result its spectrum along with the associate molecular transitions are nowadays clearly defined (Brockhinke *et al.*, 2005). Accordingly, nitric oxides formation in flames has been also studied extensively, although their detection posses several difficulties (Bessler *et al.*, 2002; 2003). The accurate knowledge of the molecular transitions for the hydroxyl radical and the nitric monoxide, facilitates the utilization of laser induced fluorescence technique for temperature measurements as well (Hartlieb *et al.*, 2000; Bessler and Schulz, 2004), with two-line excitation also possible, in order to simplify the quantification of the results (Stelzner *et al.*, 2012). Among other major combustion products (Aldén *et al.*, 1984), species that have been systematically investigated by means of laser induced fluorescence include CH (Gibaud *et al.*, 2005), NCN (Sutton *et al.*, 2008) and formaldehyde (Gordon *et al.*, 2008). These, so called minor species, are of significant importance in the combustion research, as for instance, OH^* and CH^* are important flame front markers and combined with CH_2O can yield valuable information about the flame heat release (Kohse-Höinghaus and Brockhinke, 2009). In addition, there are studies utilizing the LIF technique for poly-aromatic hydrocarbon species detection in flames (Mercier *et al.*, 2008; Bakali *et al.*, 2012). Apparently, LIF is met in various applications as diverge as toxic metals detection from flames (Zhang *et al.*, 1998), to burning velocity measurements (Yamamoto *et al.*, 2009) and mixing visualization in engines (Zhao and Ladommatos, 1998), also using tracers (see section 5.2.1.1).

It becomes obvious that laser induced fluorescence is the tool of choice, that covers the diagnostic demands which are essential to achieve the scope of the present thesis. This chapter provides the basic knowledge for the nonintrusive diagnostic techniques utilized in this framework. This includes the description of the methodology followed for the hydroxyl radical detection, for flame front visualization. Accordingly, the essential parts of the utilized instrumentation are overviewed, for all optical and spectroscopic tools used in nonintrusive diagnostic means.

3.1.   Laser combustion diagnostic tools – Laser induced fluorescence

Laser diagnostics are widely used in fundamental combustion science, research and development to investigate transient phenomena without influencing the system under study by inserting probes and surfaces. Fluorescence-based diagnostic tools are advantageous against common optical measurement techniques based on planar imaging of scattered light, due to the increased strength of the process itself. In addition, fluorescing techniques are beneficial against traditional ones, especially in the case of measuring radicals, which unlike stable combustion gases, do not survive a sampling line leading, for example, to a gas chromatographer. It is thus important that the methods used for detecting radicals are noninvasive as well as nonintrusive, contrary to, for example, molecular beam mass spectrometer (Hanson *et al.*, 1990). Laser-induced fluorescence is frequently used for remote detection of concentration and temperature. Within the duration of a single laser pulse, typically a few nanoseconds, volume elements in the sub-millimeter range can be observed. Two-dimensional cross-sections can be illuminated with light sheets and the resulting signal light can be imaged on charge-coupled device cameras (Schulz and Sick, 2005). Laser induced fluorescence is the versatile technique which is employed in the frame of the present thesis to serve as a means of detecting OH* radical for flame front structure, position and propagation visualization. This technique yields valuable information about cross sections in turbulent combustion media and therefore distinguishes between isolated areas and flame structures. This section presents the fundamental theory behind spectrometric techniques, along with the basic instrumentation for laser induced fluorescence measurement realization.

3.1.1.   Fundamentals of laser spectrometry

Classically, light-matter interactions are a result of an oscillating electromagnetic field resonantly interacting with charged particles. Quantum mechanically on the other hand, light fields will act to couple quantum states of the matter. As a simple definition, laser induced fluorescence is the spontaneous emission from atoms or molecules that have been previously excited by laser radiation. In order to explain the phenomena involved in fluorescence, as also in all inelastic processes, closer attention to the states of energy of the atom or molecule has to be given. The motion of the nuclei and electrons that make up atoms and molecules is described by the well-known Schrödinger wave equation, which correlates the wave function with the mass of the atom or molecule, and the potential field in which the nuclei and electrons move. According to the quantum-mechanic theory, only discrete energy states, associated with the respective wave-functions, are allowed, which are called quantum states. The allowed quantum states depend on the total energy and angular momentum of the system, and the angular momentum of each particle in it. In order to define the structure of a real system, approximate or numerical solutions must be used. For diatomic molecules the energy is determined by three important motions; orbiting and spin of electrons, and vibration and rotation of the nuclei with respect to each other. For the purpose of the analysis, according to the Born-Oppenheimer approximation, the motion of the electrons may be separated from the slower motion of the nuclei, due to their small mass. In

essence, the nuclei move within a potential field created by the motion of the electrons and the total energy of the molecule is obtained by the summing the electronic, the vibrational and the rotational energy (Daily, 1997).
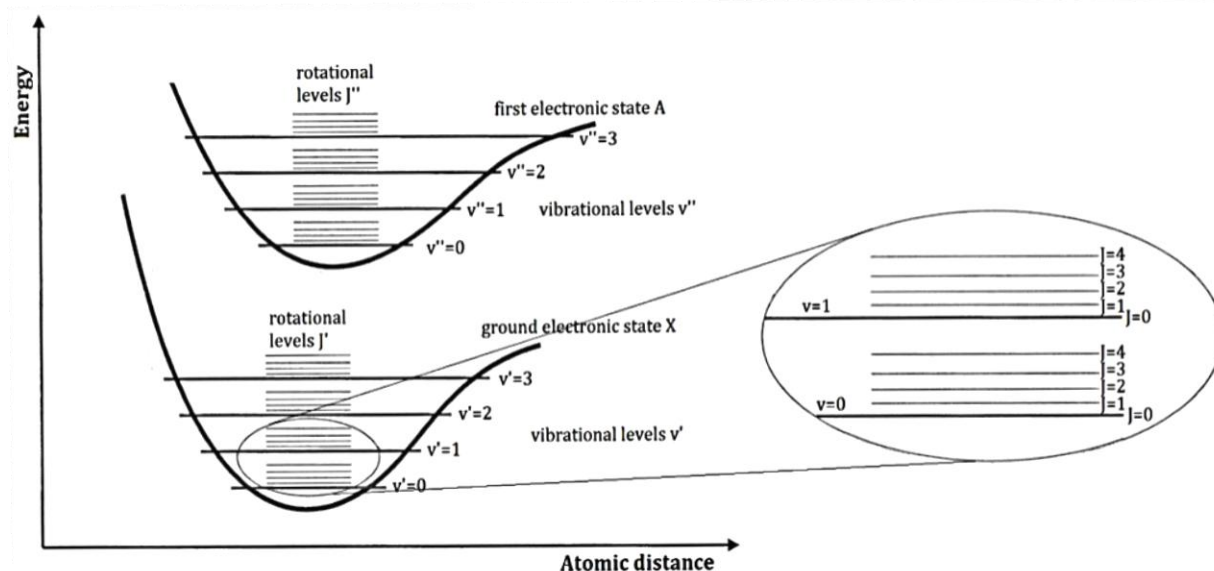
Figure 3.1 Energetic states of a diatomic molecule (Mayunger and Feldmann, 2001). The three characteristic parameters; rotational state J, vibrational state v and electronic state X, A, B etc. Primarily in laser spectroscopy the ground and first electronic state are involved, hence the terms are simply denoted by one (lower term) or two (higher term) primes.

The detailed structure of atoms and molecules have been extensively described over the past (Feynman, 2005) and reach beyond the scope of the present thesis. Here, the fundamental transitions between energy states associated with laser diagnostics are briefly described, using the simple diatomic molecule as described earlier. The electronic transitions in an atom can even be described using the well-known Bohr model, which, although not exactly valid, states that the electrons move in certain radial pathways around the nuclei and the atom contains higher energy with increasing electron motion radius. As a result, an electron can change its path of motion in discrete steps which accordingly correspond to discrete changes of energy. Because the molecule exists in definite states, only definite amounts of energy can be transferred. The configuration of the electrons with the lowest energy content is called electronic ground state and all others are termed excited states. In the diatomic molecule considered, there are two more possibilities for energy storage beside electronic excitation of each atom; vibration and rotation. The atoms in the molecule can vibrate against their center of the mass, due to the forces between the bonded electrons of the atoms. The third mode of energy storage is the rotation of the molecule around its center of mass. Like the electrons in atoms, only discrete states are allowed both for rotation and vibration (Mayunger and Feldmann, 2001). The difference between adjacent rotational energy levels is much lower than that between adjacent vibrational states, which in turn is much lower than the energy difference between a molecule in an excited and its ground state. It is usual to represent this three stage molecular energy states diagram graphically, as in Figure 3.1. There are quantum numbers that identify the discrete energy levels, which correspond to the values of J for rotational, v for

103

vibrational and *X*, *A*, *B* capital letters for electronic quantum numbers. Note that not all electronic configurations result in stable potential as the ones drawn in the figure above, and these states are called predissociative.
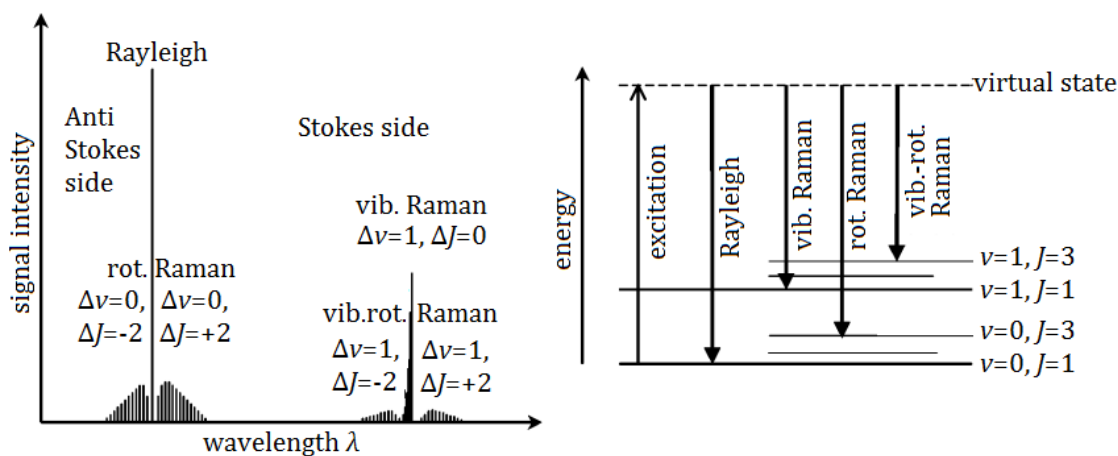
Figure 3.2 Raman and Rayleigh scattering (Hassel and Linov, 2000)

The spectral absorption and emission of radiation results in the transition of the atom or molecule between the energetic states described earlier. As initially proposed by Einstein, the radiative processes include absorption and induced and spontaneous emission. Induced emission arises when the presence of a radiation field forces the molecule to a lower energy state, whereas spontaneous emission occurs as the result of the natural instability of excited states. When intense monochromatic radiation of a laser passes through a gas, elastic or Rayleigh scattering at the laser wavelength, as well as inelastic or Raman scattering with shifted wavelengths is observed. Since Rayleigh scattering is an elastic process the signal is subject to interference from the intense scattered light produced by particles and nearby surfaces. However, if the total Rayleigh scattering cross-section of the sample volume composition is known, this method alone can produce extremely accurate temperature measurements. Rayleigh scattering is a relatively weak effect, but from intense laser beams it is nonetheless visible to the eye. Raman scattering is an inelastic process in which the oscillating polarizability of the molecule modulates the scattered radiation, thereby leading to the appearance of two side-band frequencies (Zhao and Hiroyasu, 1993). Inelastic scattering is approximately three orders of magnitude weaker, but there appear many extra signals at lower as well as higher wavelengths of the exciting laser. All these bands are part of the Raman signal. Figure 3.2 illustrates the basic process, in which the scattering photon either gains energy from the molecule *i.e.* the anti-Stokes side, or loses energy to the molecule *i.e.* the Stokes side of the Raman spectrum.

The various Raman transitions of a species characterize its spectrum, which follows a distinct pattern; near the Rayleigh line there are relatively strong rotational Raman lines, which are, usual in combustion experiments, totally blended with Rayleigh scattering due to the low resolution of the used apparatus. At a molecule-specific position, strong purely vibrational transitions are packed closely together, surrounded by very weak vibrational-rotational transitions. This part of the spectrum on the Stokes side is usually employed for concentration measurements (Hassel and

Linov, 2000). In summary, the electronic spectrum is composed of bands which arise from transitions between specific vibrational and electronic states. Each pair of vibrational states may give rise to a band, which is composed of transitions between different rotational levels. The selection rules for electronic and vibrational transitions depend in detail on the molecular structure (Daily, 1997). For a diatomic molecule possessing zero angular momentum around the internuclear axis (Σ state), the selection rules for Raman scattering are given by $\Delta v = 0, \pm 1$ and $\Delta v = 0, \pm 2$. Hence, the pure rotational Raman spectrum ($\Delta v = 0$) is characterized predominantly by a series of Stokes and anti-Stokes rotational lines. The vibrational Raman spectrum also consists of a Stokes ($\Delta v = \pm 1$) and an anti-Stokes ($\Delta v = -1$) component, each with three branches: S ($\Delta J = +2$), Q ($\Delta J = 0$), and O ($\Delta J = -2$). Since the rotational lines in the Q-branch are stronger and not normally resolved, this branch is usually two orders of magnitude more intense than the S- and O-branches, and is thus the most characteristic feature of the Stokes and anti-Stokes components of the vibrational Raman spectrum (Laurendeau, 1988).

3.1.1.1. Theoretical considerations on laser induced fluorescence

Fluorescence is the emission of light from an atom or molecule following promotion to an excited state by means of electron bombardment, heating, chemical reaction or photon absorption, appearing in lifetimes between 10^{-10} and 10^{-5} seconds (Eckbreth *et al.*, 1979). Laser induced fluorescence is absorption, followed after a finite time period by spontaneous emission from the excited manifold. The energy of the emitted photon(s) is, according to Planck's law, directly proportional to the frequency of the emitted light. Since natural fluorescence occurs in transitions from weakly populated excited energy electronic levels, the signal is as weak as the population density. The role of laser induced fluorescence is to promote a considerable number of atoms or molecules, from the densely populated lower energy levels to the excited ones, so as to enhance the subsequent fluorescence. The detected fluorescence in not necessarily from the directly pumped state, which in other words means that the fluorescing light may appear in a different frequency than the excitation light, so the latter can be filtered out, avoiding potential interferences from particle (Mie) or spurious laser scattering. Moreover, since fluorescence involves the cross sections between two different electronic states, it generally results many orders of magnitude stronger signal than the light scattering methods, described earlier. The latter, poses several difficulties in quantitative measurements since depopulation via collisionally induced energy transfer must be determined. Since fluorescence is only one of the aforementioned concurrent effects, it becomes obvious that absorption lines and the emission pattern are highly specific for particular species, so LIF is very sensitive not only to concentration levels but also to species present at the probed volume, as well as to operating conditions.

Although LIF measurements are realized based on the same principle, which is to observe the resulting spontaneous emission that follows the excitation of a molecule, different detection strategies are distinguished. Different methods are distinguished according to the characteristics of the actual transition processes involved and the configuration of the probe. In order to characterize those detection schemes, it is essential to comprehend the subsequent processes that follow the one-photon excitation of a molecule in a higher electronic level. Those processes are schematically depicted in Figure 3.3 and briefly summarized (Mayunger and Feldmann, 2001) as follows.
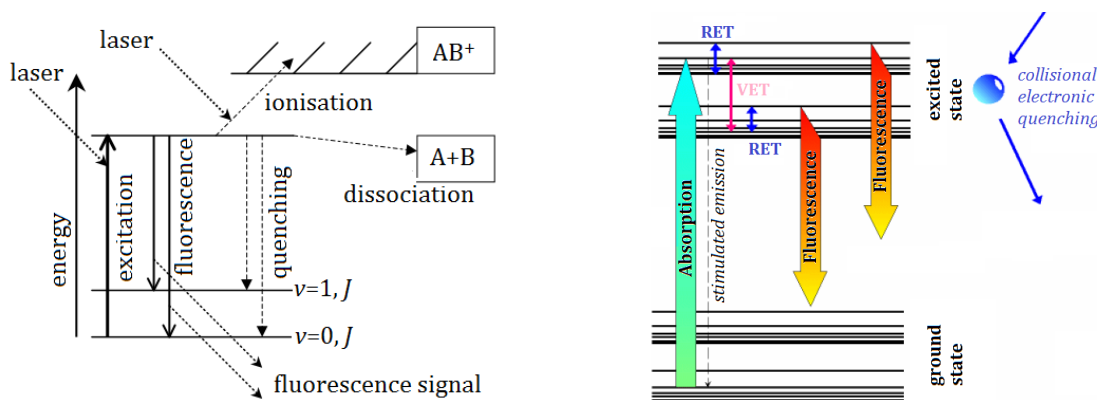
Figure 3.3 Graphical depiction of the processes occurring after excitation of a molecule AB (Hassel and Linov, 2000). Fluorescence and quenching are getting the molecule back to back into its ground state, whereas ionization and dissociation change the molecule into AB+ or into fragments A and B.

Firstly, the excited molecule can undergo a laser stimulated transition back to its original quantum state with subsequent emission of a photon at the laser beam frequency and direction, or fluoresces back to its ground electronic state, also involving light emission. Secondly, the molecule can absorb an additional photon from the incident light and go to an even higher energy level or even reach ionization. Thirdly, the internal energy of the system can be altered in inelastic collisions with other molecules, which may cause a transition to a lower electronic state without emission of light; an effect commonly referred as collisional quenching and depends on pressure, temperature and intermolecular characteristics of individual colliders. As a rule of thumb for flame applications, only one out of a thousand excited species fluorescence, due to large cross sections produced as a result of the high reactivity of species under investigation. Nonetheless, collisions with other molecules may cause vibrational and rotational transitions within the excited state with subsequent fluorescence. Finally, interactions between the separate atoms of the molecule produce internal energy transfer and dissociation of the molecule; if the dissociation caused by a shift from a stable configuration to an unstable electronic configuration, showing a repulsive energy potential curve without specific energy minimum, the process is called pre-dissociation (Hanson *et al.*, 1990). Accordingly, three main domains of excitation can be distinguished. In the case of weak excitation, the ground state is not disturbed and the signal depends linearly on the laser power, hence this approach is termed linear-LIF. On the other hand, if an intense excitation is achieved, saturation connects the upper and lower levels; this approach is termed Laser Induced Saturated Fluorescence–LISF. The signal from LISF is independent of collisional effects and the laser power, but saturation over the whole space and time of a measurement is not easy to achieve (Hassel and Linov, 2000). Finally, an approach to avoid the dependence of the measurement on momentary environment uses the effect of pre-dissociation. In this technique strongly dissociating states are pumped, which depend only on the molecule itself hence this approach is termed Laser Induced Pre-dissociation Fluorescence–LIPF (Cooper *et al.*, 1998).

A major problem for specific diagnostic techniques is the competition of collisions with the radiation process that leads to the observable signal. In order to perform accurate measurements, the structure and distribution of the energy levels of the species of interest, along with the possible transitions and transition probabilities or transition saturation levels must be known. This involves

the calculation of cross section of individual lines, which in turn necessitates the knowledge of the relative intensities of all the transitions from the excited rovibronic level. For molecules with complex spectra this is rather difficult or sometimes even impossible. The problem is that the measured radiation time corresponds to the transitions from the excited electronic rovibrational level to all the vibrational levels of the lower electronic state. Therefore, the radiation time corresponds to the total absorption from all these levels. This demands detailed knowledge of the spectrum, including, for example, Franck–Condon factors. Moreover, in some molecules the relationship between the absorption cross section and emission Einstein coefficient can be distorted because of the different types of intermolecular interactions, such as the ones between rovibronic levels of the excited and the ground electronic states, *i.e.* the so called Douglas effect (Cheskis, 1999). Explicit details on the calculation of Einstein coeffiecients and cross sections (Hilborn, 1981) and in general, the approaches followed to treat those issues are available in the literature (Kohse-Höinghaus *et al.*, 2005).

In order to clarify the previous discussion, the governing equations for fluorescence signal calculation are briefly summarized below. As the fluorescence depends on the population of the upper state, the state-dependent population dynamics must be solved. In order to avoid the complexity of a quantum mechanical solution based on density-matrix interaction descriptions, a simpler semi-empirical rate analysis is presented. The rate equations are conceptually and mathematically more treatable than the quantum approach and are generally valid for combustion measurements, where the laser pulses rise slowly compared to the characteristic collision time (Hanson *et al.*, 1990). In order to illustrate the essential properties of laser induced fluorescence and practically understand the difference between the various applied approaches, a two-level molecular system, based on the two levels coupled by the laser radiation, is assumed. In order to further simplify the equations, steady state is assumed, as justified for most combustion environments, since laser pulses are long compared to the process time constant. Moreover, collisional excitation from lower to upper level is omitted, since the two states are typically separated by a few electron-volts. Finally, as conservation constrain, it is assumed that the higher level was negligibly populated prior to laser pulse and that no chemical reactions occur during the measurement. Given the latter, the population of the second energy level N_2, as a subset of the previous one N_1, as well as for the N_1, is described by equation 3.1 (Eckbreth, 1996).

$$\frac{dN_1}{dt} = -N_1 b_{12} + N_2 \left(b_{21} + A_{21} + Q_{21} \right)$$

Equation (3.1a)

$$\frac{dN_2}{dt} = N_1 b_{12} - N_2 \left(b_{21} + A_{21} + Q_{21} + P + W_{2i} \right)$$

Equation (3.1b)

Here, A_{21} is the Einstein coefficient for spontaneous emission, b_{12} is the absorption rate coefficient and b_{21} is the stimulated emission rate coefficient. Quantities b_{21} and b_{12} are related to Einstein coefficient for stimulated emission B from $b = B \cdot I_v / c$, where c is the speed of light and I_v the incident laser intensity per unit frequency interval (spectral irradiance). Symbols Q, P, W_{2i} denote the rate constants for quenching, predissociation and photoionization respectively.

By formulating the solution of the two-level model into the integrated optical configuration, the fluorescence signal power is related to the state population densities via equation 3.2.

$$F = h\nu N_2 A_{21} \frac{\Omega}{4\pi} lA = h\nu \frac{\Omega}{4\pi} lAN_1^0 \frac{B_{12}}{B_{12}+B_{21}} \frac{A_{21}}{1+\frac{I_{sat}^v}{I_v}}$$

Equation (3.2a)

In the above described relation, h is the Planck constant, v is the frequency of emitted radiation, A is the focal area of the laser beam, l is the axial extent along the beam from which the fluorescence is observed and Ω is the detection solid angle. The term I^v_{sat} is the saturation spectral irradiance and ginen by equation 3.2b.

$$I_{sat}^v = \frac{(A_{21}+Q_{21})c}{B_{12}+B_{21}}$$

Equation (3.2b)

At low laser excitation irradiances, *i.e.* $I^v \ll I_{sat}^v$ and neglecting the P, W_{2i} terms, which is very usual unless they are intensely introduced, equation 3.2b is simplified to equation 3.3.

$$F = \frac{h\nu}{c} \frac{\Omega}{4\pi} lAN_1^0 B_{12} I_v \frac{A_{21}}{A_{21}+Q_{21}}$$

Equation (3.3)

The latter equation describes the linear regime where fluorescence is namely linearly proportional to the input laser irradiance. Ont the other hand, when $I^v \gg I_{sat}^v$ the correlation between fluorescence and ground state population is formed into equation 3.4 and as noted previously, the quenching corrections could be avoided; this regime corresponds to the LISF approach.

$$F = \frac{h\nu}{c} \frac{\Omega}{4\pi} lAN_1^0 I_v \frac{B_{12}}{B_{12}+B_{21}} A_{21}$$

Equation (3.4)

Finally, when the transition is excited to a predissociative state, which implies that the the LIPF approach is utilized, the resulting fluorescence is given by equation3.5, given the fact that $P \gg Q$.

$$F = \frac{h\nu}{c} \frac{\Omega}{4\pi} lAN_1^0 B_{12} I_v \frac{A_{21}}{P}$$

Equation (3.5)

It becomes obvious from the last equation that in LIPF approach, the effect of collisions in the electronically excited state is completely eliminated, contrary to e.g. LISF approach, which is based on sufficiently fast redistribution. However, in both techniques, care must be taken to avoid depletion of the ground state, otherwise collisions within the electronic ground state repopulate the level and make the signal sensitive to gas composition. Detailed description of the assumptions made for the two-level model, as well as for three- and four-levels systems reach beyond the scope of this thesis, but can be found in the literature references provided along this section (*e.g.* Mayunger and Feldmann, 2001; Daily, 1997).

3.1.2. Basic components of the laser induced fluorescence detection system

The rather complex (inter-) molecular interactions described earlier, caused by laser intrusion on the species under study, raise notable demands for the diagnostic instrumentation. These equally

concern the achievement of desired excitation, as well as the obtainment of proper detection bands. As far as the excitation of a specific species is concerned, a narrowband monochromatic light, with sufficient energy output, corresponding to the chosen wavelength, has to be achieved. This is not trivial, since in order to obtain the targeted wavelength, a compromise for the systems' output power is usually made, which in many cases results in a highly "inefficient" configuration; a typical diagnostic setup may originally produce a few joules per pulse, which are reduced, in favor of the desired wavelength, to only a few millijoules per pulse. As far as the detection instrumentation is concerned on the other hand, it is crucial to identify which bands of the emitted fluorescence will be monitored, which would be the spatial and temporal resolution and more importantly, how is the signal post processing going to be realized, in order to obtain accurate results. The present section demonstrates the utilized instrumentation for the realization of the experimental campaigns carried out in the frame of the thesis by nonintrusive means, namely in chapter 5 and section 7.2.
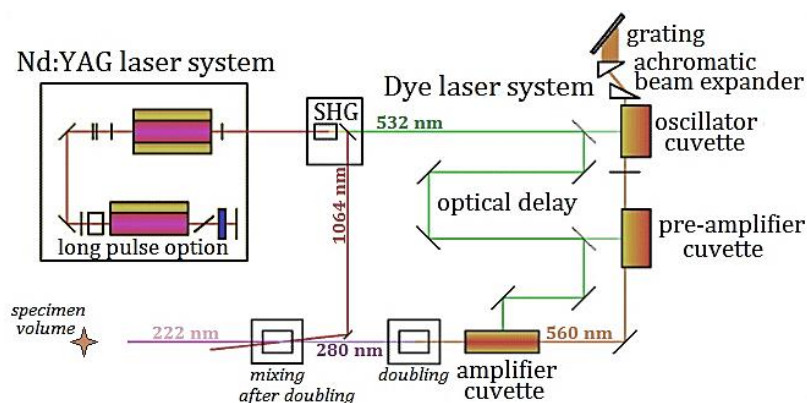
Figure 3.4 Experimental configuration for laser beam and wavelength manipulation

A schematic representation of the experimental configuration is given in Figure 3.4. In the depicted scheme, the laser beam undergoes changes in its energy and wavelength, namely from 1064 nm and 1 J/pulse to either 280 or 220 nm with approximately 10 or 2 mJ/pulse, in order to obtain the desirable wavelengths for hydroxyl radical and nitrogen monoxide detection, respectively. Although the description of the setup along with the operating principles of its components, are described in more detail in the following sections, a brief summary of the instrumentation at the T.U.-Bergakademie Freiberg, where this experimental campaign was realized has as follows. The utilized laser system consists of a Q-switched Nd: YAG (Brilliant B) laser which produces laser emission at a fixed wavelength of 1064 nm, coupled with a tunable dye laser (Quantel-TDL90). The dye laser system consists of the oscillator and the dye cells. The addition of a second harmonic generator (SHG) to the Nd:YAG doubles the frequency, resulting in a wavelength of 532 nm. This beam is divided via a beam splitter into the fundamental beam which goes inside the oscillator (~10%) and the pumping beam which is used for the amplifiers (~90%). The wavelength tuning inside the oscillator is accomplished by a fixed grating mirror. The fundamental beam is intensified by a pre-amplifier and a capillary amplifier. After this stage, it is possible to double the laser beam which again halves the wavelength. Furthermore, it is possible to mix the pumped beam with the 1064 nm, or even use mixing after doubling. Due to the fact that the energy of the Nd:YAG laser changes from pulse to pulse, it is necessary to measure this in order to achieve quantitative

evaluation of the fluorescence. The last stage is a light sheet generator which builds up the two-dimensional measurement domain. The fluorescence is eventually captured from the specimen volume by the collection optics with a charge-coupled device camera with a specialized filter mounted, according to the detection needs.

3.1.2.1. Nd: YAG laser and harmonic generators

Light sources used for LIF measurements vary in their spectral, temporal and spatial characteristics (Rothe and Andersen, 1997). Practically, temporal characteristics are distinguished by either the continuous wave or pulsed laser output. Spectral characteristics on the other hand are primarily classified into single frequency or tunable wavelength systems. In any case, the produced laser light ought to have a uniform radial spectral irradiance distribution. The adopted technique followed in the frame of the present thesis, was to utilize a dye laser, pumped with a frequency-doubled Nd: YAG pulsed laser. The Nd: YAG stands for Neodymium-doped Yttrium Aluminum Garnet or Nd: $Y_3Al_5O_{12}$. The Nd: YAG is a solid state laser system in which the active gain medium is the YAG, or in more detail, the triply ionized neodymium which replaces a small fraction of the YAG crystal structure. The active gain medium, also referred as lasing medium, is the source of optical gain within a laser, resulted by the stimulated emission of electronic or molecular transitions from a previously populated higher energy state to a lower one, after population inversion is achieved. The Nd: YAG can be described as a four level solid state laser (Träger, 2007) and provides the capability to run it in continuous wave mode, with however, pulsed operation producing higher peak power levels. Solid-state lasers are optically pumped, mostly with pump sources such as flashlamps (which is the case here), or as increasingly done nowadays, with semiconductor diode lasers, which operate with much higher efficiency and reduced heat load in solid-state laser materials (Schulz *et al*., 2008). The laser material interacts with the radiation field of its own or another resonator and is pumped by one or more excitation sources (flashlamps). The pump light may be incident on the laser material from any direction relative to the laser radiation. Nd: YAG lasers typically emit light with a wavelength of 1064 nm in the infrared region.
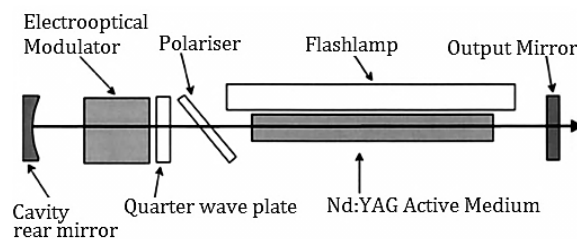
Figure 3.5 Layout of the used Nd: YAG laser (Quantel Brilliant B)

Q-Switch

Flashlamp pumped solid state lasers such as the Nd: YAG ones, generally produce laser emission with an undefined energy structure; a behavior commonly called spiking. These generated spikes, which occur due to different population environments, are fully random in amplitude, duration and spike-to-spike time distance. In order to avoid this behavior and increase the generated laser emission energy as well, an electro-optical cell is used. This is usually called Q-switch, due to the fact that it alters the quality factor of the configuration's optical resonator. The optical switch is

inserted in the laser cavity waiting for a maximum population inversion in the neodymium ions before it opens. After the electric energy which stored in the capacitors is discharged into the flashlamps, the emitted optical energy is subsequently stored in the laser crystal. When the maximum of population inversion is reached the optical cavity opens by means of this electro-optical cell. Then the light wave can run through the cavity, depopulating the excited laser medium at maximum population inversion. In this Q-switched mode, output powers in the megawatt region and pulse durations of a few nanoseconds may be achieved. In general a Q-switch is an opaque shutter inside the laser cavity which can be opened or closed; an often used shutter is the Pockels cell along with a polarizer (Figure 3.5). If the Q-switch is closed no radiation takes place due to high resonator losses and thus the number of excited atoms can reach a very high level. If the shutter is opened after a certain time period, where the inversion has reached a high level, the resonator losses reduce drastically and laser emission occur in a single short pulse with very high energy. The pulse time is determined by the runtime of the laser light in the laser cavity. The Q-switch delay, for all experiments carried out in the frame of the present thesis, was set at 215 µs.

Harmonic generators

Frequency conversion based on a neodymium doped solid state laser to generate harmonic waves is an effective way to obtain visible and ultraviolet lasers. The high-intensity produced infrared emission of the Nd: YAG laser may be efficiently frequency doubled to generate laser light at 532 nm, utilizing the so-called Second Harmonic Generator (SHG). The nonlinear crystals with high nonlinear coefficient and good quality are key factors for harmonic generation. Specifically, this green light is widely used in combustion diagnostics for dye laser pumping, as well as for Raman scattering measurements. The latter procceses are realized via optical frequency multipliers. An optical frequency multiplier is a nonlinear optical device, such as potassium dihydrogen phosphate or KTP crystals, in which photons interacting with the nonlinear material are froming photons with greater energy and thus higher frequency or, in other words, shorter wavelength. The physical mechanism behind frequency doubling or, in other words, second-harmonic generation, can be understood as follows. Crystal materials lacking inversion symmetry can exhibit a so-called $\chi^{(2)}$ nonlinearity. Due to this nonlinearity, the fundamental (pump) wave generates a nonlinear polarization wave which oscillates in the medium with twice the fundamental frequency, which in turn radiates an electromagnetic field with this doubled frequency. In most cases, the pump wave is delivered in the form of a laser beam, and the frequency-doubled (second-harmonic) wave is generated in the form of a beam propagating in a similar direction (Paschotta, 2008). By additional optically non-linear frequency conversion, wavelengths of 355 nm and 266 nm are also attainable, which are respectively referred as the third (THG) and fourth (FHG) harmonic generators. The infrared 1064 nm beam may be used for additive frequency mixing with the output of a dye laser.

3.1.2.2.   Dye laser

Contrary to most laser systems where the active medium dictates the fixed-wavelength generated laser emission, dye lasers offer a tuning ability in a wide frequency range, from the near infrared to the ultraviolet region. The active media in this type of lasers are solutions of certain complex organic dye compounds in liquid solvents, such as ethyl or methyl alcohols and can be pumped with either flashlamps or lasers. It is essential for a dye to have minimum overlapping between

absorption and emission spectra, short fluorescence lifetimes and high quantum yield and photochemical stability. Generally, these complex molecules contain a number of ring structures, leading to complex absorption and emission spectra. Dyes are able to emit in a small wavelength range, and due to their narrow range, different dyes are necessary to cover the entire spectral range. The laser dyes can be categorized into different classes by virtue of their structures that are chemically similar, such as coumarins, xanthenes and pyrromethenes. Typical solvents for laser dyes are ethanol, p-dioxane and dimethylsulfoxid, with common dye concentrations normally well below a gram per liter, although the exact levels normally depend on the used pumping power. Figure 3.6 presents the emission spectra of the most common dyes after Nd: YAG pumping. In addition to tunability, an intrinsic feature of dye lasers is their inherent ability to yield high pulse energies and high-average powers in the visible spectrum region.
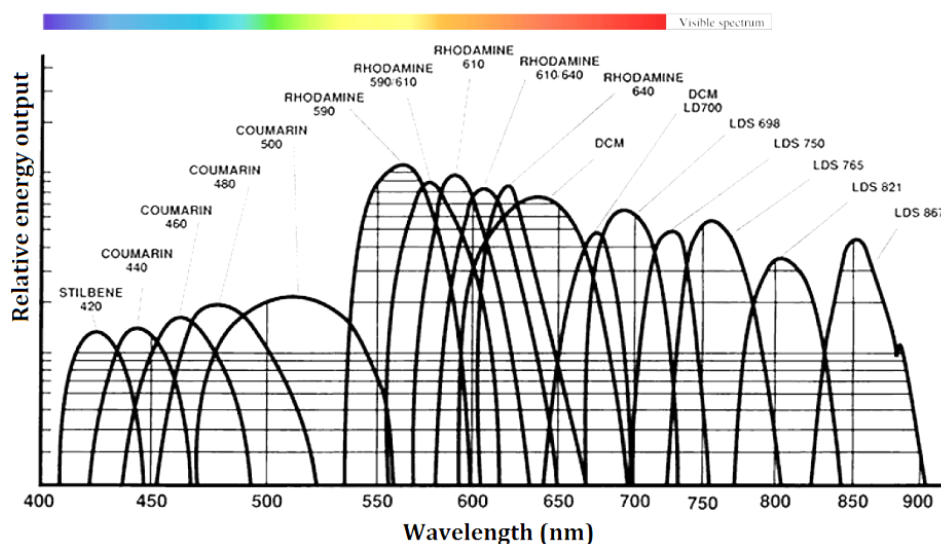
Figure 3.6 The approximate working ranges of various Nd: YAG-pumped laser dyes (Stuke, 1992).
(Relative energy in logarithmic scale)

Dye lasers are normally pumped at relatively short wavelengths. Intense dye laser pulses can be obtained with pulsed pumping, using a Q-switched pump laser, with power conversion efficiency typically up to 30%. Pulsed pumping allows the excitation of large volumes and thus the generation of pulses with high energies. A common strategy is to pump a green laser such as a frequency-doubled solid state laser, as the one described earlier. As indicated also from Figure 3.6, a 532 nm pumping beam may result in laser emission in the green, yellow, orange, red or near infrared spectral region, depending on the utilized dye. Laser dyes for shorter emission wavelengths, such as coumarin, have to be pumped at shorter wavelengths, typically with ultraviolet light. In order to achieve excitation of the latter, the third or fourth harmonic generators of an Nd: YAG laser, are commonly utilized. In the frame of the present thesis, a xanthene family dye, Rhodamine 590 also known as Rhodamine 6G ($C_{27}H_{29}ClN_2O_7$) has been used, solved in ethanol. Most of the xanthene laser dyes show efficient laser action in the 560 to 800 nm region, which may produce target wavelengths around 280 to 400 after frequency doubling. Rhodamine 6G shows efficient laser action in the 590 nm region and efficiently lases in most flashlamps pumped dye lasers. Rhodamine 6G exhibits good photostabilty and is one of the most often used and studied, or even used as

112

reference to measure the efficiencies of other dyes. Since Dyes are circulated on the system and pumped through thin transparent cuvettes, which obviously are of high optical quality and are resistant to the laser and pump light. Although dye solutions have to be periodically exchanged in order to avoid chemical degradation, they constitute a reliable laser tuning solution. Due to the low dye concentration, the solvent plays an additional, important role. For example, the ethanol-solved Rhodamine 6G presents a maximum main absorption at 530 nm, whereas the same dye solved in either hexa-fluoro-isopropanol or dimethyl-sulfoxide presents absorption maximum values at 514 nm or 540 nm, respectively.
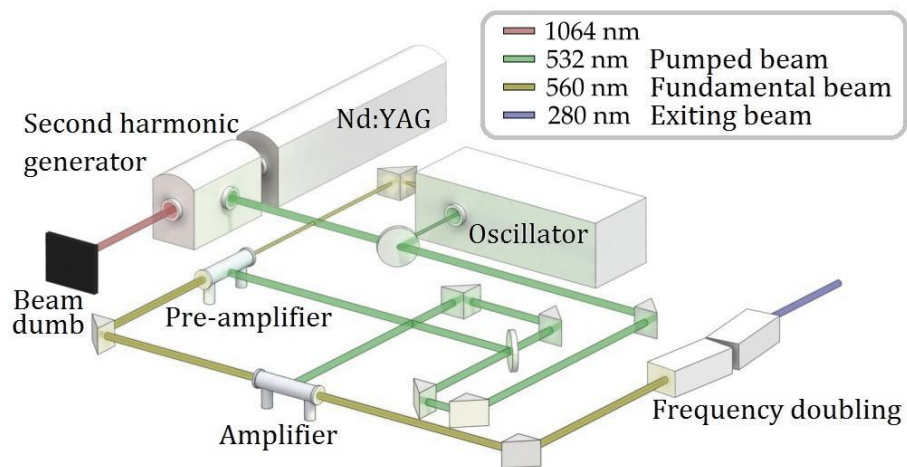
Figure 3.7 The integrated dye laser system overview

Dye laser system overview; Oscillator and Amplifiers for fine tuning

In order to achieve a narrowband, fine tuning with dye lasers, an optical parametrical oscillator– OPO, is often utilized. An optical parametric oscillator is a light source similar to a laser, but based on optical gain from parametric amplification in a nonlinear crystal rather than from stimulated emission. A main attraction of optical parametric oscillators is that the signal and idler wavelengths can be varied in wide ranges, which are determined by a phase-matching condition. Most oscillators are pumped with nanosecond pulses from a Q-switched laser, as is the case here, which assists to overcome the pumping power threshold (Paschotta, 2008). The output pulses are often slightly shorter than the pump pulses, since parametric oscillation sets in with some delay. The parametric amplification process requires efficient phase matching, which primarily determines the oscillation wavelength. Wavelength tuning is in most cases achieved by influencing the phase-matching conditions, such as changing the angular orientation of the crystal. Here, wavelength tuning is simply achieved by grating rotation, based on a diffraction grating in the so-called Littrow configuration (Träger, 2007). This is achieved by rotating a tuning mirror which in turn rotates the grating mirror with an accuracy of 2400 lines per mm, resulting in respectively tuning the produced laser beam in the range of 420 to 750 nm. This laser beam is referred as the fundamental beam and after leaving the oscillator is inte0nsified by a preamplifier and a capillary amplifier. The amplification is enhanced by a 532 nm light-pumped Rhodamine 6G dye, as described earlier. The overall process of described the wavelength tuning is graphically depicted in Figure 3.7. Respectively, the energy levels are correspondingly dropping from almost 1 J per pulse on the

Nd: YAG, to approximately 400 mJ/pulse after the second harmonic generator, reaching eventually approximately 80 mJ/pulse for the fundamental beam and almost 10 mJ/pulse at 283 nm.

<u>Alternative configurations: Mixing, doubling and mixing after doubling techniques</u>
The final stage of laser tuning includes doubling, mixing or if necessary mixing after doubling techniques. Nonlinear crystal materials, lacking inversion symmetry, are utilized to manipulate two pumped beams and generate another with the sum or difference of the optical frequencies of the pumped beams. In a sum frequency mixer, both pump waves experience pump depletion when the signal becomes intense. For efficient conversion, the photon fluxes of both input pump waves should be similar. In a differential frequency mixer, the lower-frequency wave is amplified rather than depleted. This is because photons of the beam with highest photon energy are effectively split into two lower-frequency photons, thus adding optical power to both lower-frequency waves (Paschotta, 2008). For example, a frequency doubled fundamental beam, results in a laser light around 280 nm, which is close to the OH-LIF target wavelength (see next section). A sum frequency mixer is often called a Frequency Addition Source of Optical Radiation or simply FASOR. The resulting beam after frequency mixing reveals a wavelength of $\lambda_{mix} = \lambda_1\lambda_2/(\lambda_1 + \lambda_2)$, where λ_1 and λ_2 are the initially mixed beam wavelengths. For instance, mixing the Nd: YAG initial infrared (1064 nm) with the frequency doubled fundamental beam results in a wavelength around 222 nm, as depicted in Figure 3.4, which , along with the respective adjustments on the collection optics, is of great importance in NO-LIF measurements

3.1.2.3.   Receiving optics, detectors and filters

The combination of the Nd: YAG laser along with the associated harmonic generators and the tunable dye laser system, provide the basis for acquiring laser light at the desirable wavelength, for achieving the excitation of the species under investigation. The light is passed through a cylindrical lense to acquire a planar sheet shape, in order to perform two dimensional measurements. A portion of the emitted fluorescence is collected from the appropriate optics and led to the detector. The detection system includes the collection optics, such as lenses and filters, as well as detectors, amplifiers, digitizers and control electronics. Although the most severe error source is primarily introduced by the laser light itself, the choice of an appropriate detector is of great importance, as far as a reliable measurement signal is concerned.

The variety of optical signal devices exploit several physical principles, such as photoemissive, photothermal, photoconductive, photovoltaic or charge coupling phenomena. Practically, detectors may vary from simple photodiodes, used for point measurements, to charge-coupled device – CCD image sensors, used for two dimensional analyses, as is the case here. The CCD image sensor is a low noise, high sensitivity and high resolution device, well suited for combination into arrays. On the other hand, it exhibits relatively slow rise times, hence they are often combined with photoemissive intensifiers in array configurations. The utilized camera (Dantec Dynamics - HiSense MkII) uses a high performance progressive scan interline CCD chip, with 1280 x 1024 light sensitive storage cells, reaching a quantum efficiency of up to 70% near the green light region. The selection of a lens is a major tradeoff between spatial response and light gathering ability, hence the attached Nikon lens (Micro-Nikkor) had focal length of f = 60 mm and an f-ratio of 2.8. However, the

detector's quantum efficiency drops in the blue and ultraviolet region, necessitating the use of an intensifier. Image intensifiers allow capturing of instantaneous images of fast processes, by intensifying the signal at high gain and high speed gating. The so-called gated mode operation serves as a powerful means of reducing background radiation, which, along with the proper filtering, can eliminate noise signals. The utilized intensifier (Hamamatsu C9546-03L) had a refreshing rate of 12 Hz in order to follow the 10 Hz repetition rate of the laser system.

(a) Filter for detection of hydroxyl radical.
Transmission peak at 313 nm, FWHM* = 25 nm

(b) Acetone fluorescence spectrum and detection filter.
Transmission peak at 439 nm, FWHM = 154 nm
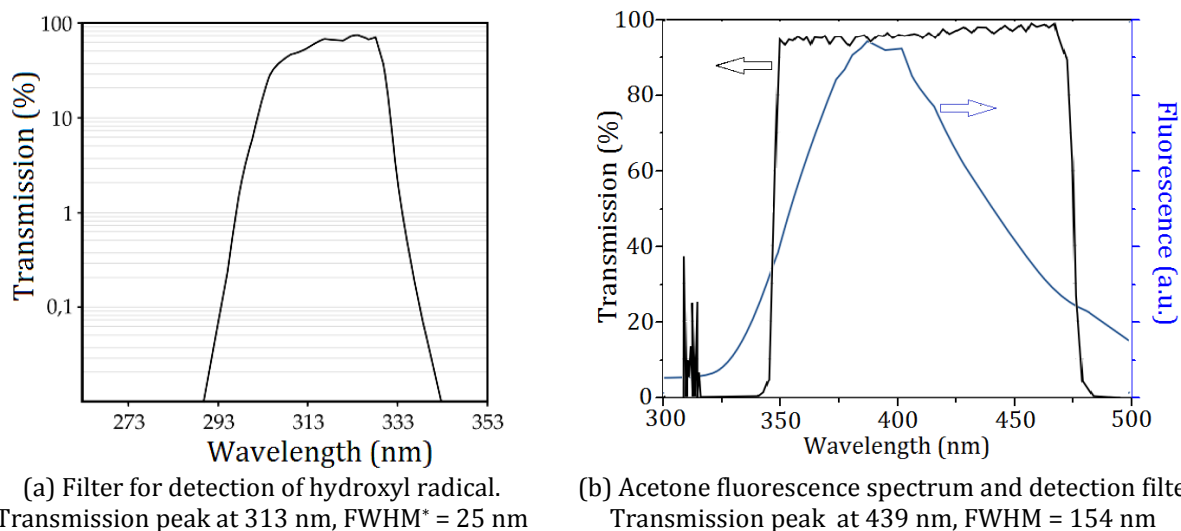
Figure 3.8 Specifications of utilized filters in the frame of the thesis.

An important component of the detection system is the filter that determines which part of the spectral radiation will reach the detector. During the experimental campaign of the present thesis, laser induced fluorescence measurements were carried out for hydroxyl radical and acetone detection. The choice of excitation and detection band for the hydroxyl radical poses several concerns, which are analyzed in detail in the next section. However, for continuity purposes, it is here noted that fluorescence at the OH (0,0,) band was observed, which is satisfactorily captured by a filter with spectral characteristics presented in Figure 3.8a. As far as acetone detection is concerned, the followed methodology suggested an excitation wavelength at 266 nm using the fourth harmonic of the Nd: YAG laser, which resulted in peak energy levels close to 90 mJ per pulse. The highest absorption in the acetone spectrum is observed near 280 nm, but, as shown in Equation 3.2a, it is diagnostically more beneficial to exploit the high laser beam energy obtained from the FHG, rather than to tune to the absorption peak, with significantly weaker laser beam at the latter wavelength (approximately 15mJ/pulse). This strategy can be applied since acetone has a broad fluorescence spectrum, which, as shown in Figure 3.8b, is widely captured from the employed filter. Finally, the post processing of the signal was realized using an in-house developed code, though which the instantaneous measurements were integrated, in order to provide a statistically independed description of the flame size and position in the respective studies (see section 7.2.1.2).

---

* Full width at half maximum (FWHM) is an expression of the extent of a function corresponding approximately to *FWHM* ≅ *2.3548·σ*, where *σ* is the standard deviation of the Gaussian distribution function.

3.2. Hydroxyl radical imaging with laser induced fluorescence

The hydroxyl radicals are primarily formed from oxygen atom attack on hydrocarbon molecules and are subsequently combined with hydrogen atoms to form water. This sequence makes the hydroxyl radical of great importance for understanding combustion chemistry, as well as for comprehending flame characteristics and validating kinetic models. All the latter have contributed in turning the hydroxyl radical into the most widely investigated radical with nonintrusive laser diagnostic techniques. Consequently, there are extensive theoretical studies describing the OH molecule's energetic states (Brockhinke and Köhse-Hoinghaus, 2001), which assess the modeling of the energy transfer phenomena within the hydroxyl molecule, also assisting the experimental campaigns and vice versa.

When performing LIF measurements, during the lifetime of the excited level, collisional processes lead to a redistribution of energy and population, depending on the chemical composition, temperature and pressure of the combustion environment. The accurate determination of the latter facilitates the performance of high precision absolute concentration measurements. However, this feature is not always essential. In certain situations, the mere detection of a particular species in a specific combustion environment may provide a wealth of unique information, as well as some insight into the chemistry of the process. In this context, it may often be sufficient to measure the relative concentration and relative spatial distribution of the molecule under investigation. A typical example is the reaction zone imaging of a combustion process, which can be visualized by detecting the laser-induced fluorescence of the hydroxyl radical (Kohse-Höinghaus, 1990). As in absolute measurements, the uncertainty in relative OH measurements arises from variations in the quenching rate coefficient across the flame structure and from changes in the Boltzmann population fraction with variations in temperature. The Boltzmann fraction for the ground level of a particular excitation transition can be chosen to be fairly independent of temperature over a range of operating conditions; however, the quenching rate coefficient often cannot be sufficiently modeled, and assumptions must be made to interpret the planar LIF images correctly. Additional issues that arise in linear LIF measurements concern the intensity of the laser. In order to avoid the saturation threshold, the laser light must not be too intense. Nevertheless, if the light is too weak the image may be distorted due to absorption of the light as the beam passes through the flame. Nonetheless, a strong absorption is required, so as to result in strong fluorescence, hence a satisfying signal. This section presents the followed diagnostic strategy for the hydroxyl radical measurements, presented in chapters 5 and 7.

3.2.1. Detection scheme for OH radical measurements

Determining the absorption cross section in spectra of stable molecules is usually not a very difficult problem, because of the ability to directly calibrate. A similar procedure is much more complicated for atoms and radicals or molecules with complex spectra (Cheskis, 1999). For the excitation of the OH radical, the transition between the ground and the first energy state, which is symbolized as $A^2\Sigma^+ - X^2\Pi_i$, was chosen due to the high transition probability (high Frank-Condon factor), the relatively similar nuclear distance and the relatively low energy needed for excitation.

Additionally, the excitation transition was chosen in order to avoid predissociation; a molecule can undergo predissociation if the excited state lies higher than the dissociation limit and there exists a state that can couple excited and predissociation states – Some $A^2\Sigma^+ – X^2\Pi_i$ (3,0) transitions are predissociative (Hassel and Linov, 2000). As explained earlier, the excitation and detection bands were intentionally different, in order to avoid scatter from laser light. Specifically, fluorescence was observed in the OH (0,0) band, whereas excitation to $v' = 1$ vibrational level was achieved. In addition, the excitation of the weaker OH (1,0) band helps avoiding problems of optical thickness in the flame. Overall, this transition has been extensively studied over the last decades. In more detail, the $A^2\Sigma^+$ state vibrational and rotational energy transfer along with the respective factors against various combustion-related colliders have been described in detail in the literature. As far as the involved bands are concerned, the $A^2\Sigma^+$ $v'=0$ (Jörg et $al.$, 1992) and the $A^2\Sigma^+$ $v'=1$ (Kienle et $al.$, 1993) have been thoroughly investigated leading to a rate-equation model of multiple quantum vibrational energy transfers (Kienle et $al.$, 1999), which is of great importance for quantitative LIF measurements, since the influence of collisions is the most troublesome aspect of making accurate profile measurements of minor species with LIF. Nevertheless, for qualitative measurements, it is not necessary to determine the aforementioned energy transfer phenomena, as long as the appropriate bands are excited and monitored. Such a detection scheme is depicted in Figure 3.9 and described in more detail below.
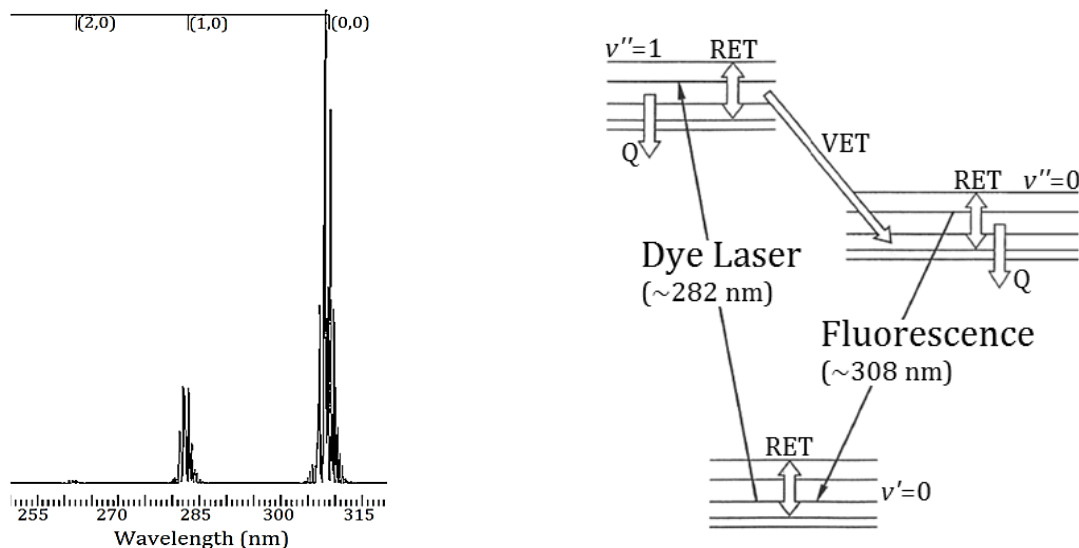
Vibrational transitions (0,0), (1,0) and (2,0) of OH molecule. Simulation performed with LIFBASE (Luque and Crosley, 1999)

Schematic diagram of collisional effects, when exciting $v' = 1$ in the upper state and observing the (0,0) band in fluorescence to the ground state (Kohse & Jeffries, 2002)

Figure 3.9 Hydroxyl bands involved in the followed excitation strategy

Figure 3.9 (left) presents a part of the OH molecule's $A^2\Sigma^+ – X^2\Pi_i$ state spectrum, as a function of wavelength, which captures the (0,0), (1,0) and (2,0) vibrational transitions, as calculated by the LIFBASE software (Luque and Crosley, 1999). Although absorption intensity is presented in arbitrary units, it is clear that the choice of (1,0) band can assist in providing image distortion due to optical saturation, since it exhibits significantly lower potential. In order to obtain a clearer picture of the followed methodology, Figure 3.9 (right) illustrates the subsequent collisions that

follow the excitation of the OH (1,0) vibrational band. The initially excited $v' = 1$ level with a laser light around 282 nm, besides the obvious fluorescence back to $v'' = 1$, also emits fluorescence to the $v'' = 0$ via vibrational energy transfer (VET). This facilitates the detection of the (0,0) band which appears approximately around 308 nm, avoiding scattering from the laser sheet. The depicted lines arise from a single vibronic transition, namely with vibrational quantum number $v'' = 0$ and end at the vibrational quantum number $v' = 0$. Vibrational energy transfer is a very complex process which cannot be generally treated by a simple physical model and such an analysis reach beyond the scope of the present thesis, hence are not further discussed. The ramification of this so called (0,0) vibrational band arises from the manifold of rotational levels. The quantum number of rotation is named J. Simultaneously, the OH molecule undergoes various collisions which in turn populate the respective rotational levels. In more detail, rotational energy transfer distributes the population from the initially excited rotational level (J') among other J' levels of $v' = 1$, and these can have different radiative and collisional characteristics. Vibrational energy transfer moves population downward into $v' = 0$, resulting in a possible non-thermal J' population in that level (Kohse-Höinghaus and Jeffries, 2002). Rotational energy transfer affects the J' population distribution in $v' = 0$ as well, causing compilations similar to those in $v' = 1$. In order to obtain a clear population depiction from the measurements, a temperature independent rotational level should be chosen, as discussed in the next paragraph. Finally, all excited states are depopulated by quenching (Q) without emission of light during the experiment. Quenching removes the electronically excited hydroxyl radical molecule altogether, transferring population to v'' levels within $X^2\Pi_i$ ground electronic state (Kohse-Höinghaus, 1994). Quenching is commonly understood as collisional deactivation to a lower electronic state, whereas VET and RET denote collisional transfer to different vibrational or rotational levels in the same electronic state.

3.2.1.1. OH-LIF imaging measurements – Choosing a temperature independent rotational line

Different types of collision processes influence the fluorescence signal and quantum yield. The excited level in the electronic state can be depopulated by electronic quenching, vibrational and rotational energy transfer. Given the energy transfer processes described in the previous section, a detection scheme for accurate OH population imaging has as follows. The aforementioned processes are temperature depended, so if population measurements are targeted, it is of crucial importance to choose a temperature-independent rotational level for excitation. Rotational levels from excitation of the (1,0) vibrational band of the OH molecule, proposed by numerous publications, vary from the $Q_1(1)$ near 282 nm and the $Q_1(8)$ near 283 nm. Instead of measuring all necessary coefficients as a function of quantum state, collision partner and temperature, it may therefore be preferable to simulate the collisional energy transfer with an appropriate formalism in order to describe the entire matrix of energy transfer coefficients on the basis of the previously measured ones. Here, a simulation-based solution for the temperature-dependance of the excited rotational level is examined.

Using the LASKIN software (Bülter *et al.*, 2004), different rotational lines from the (1,0) vibrational band were investigated. This software incorporates a rate equation model which includes VET, RET and quenching collisional effects that arise from the described excitation. It can be clearly seen that

the $Q_1(6)$, the $Q_1(7)$ and the $Q_1(8)$ rotational levels, which are presented in the left part of Figure 3.10 with solid lines, have the least dependence on temperature as far as their level population is concerned. The apparent result in the respective fluorescence is demonstrated in the right part of Figure 3.10, where the fluorescence in the (0,0) vibrational band is shown after exciting the $Q_1(1)$ and the $Q_1(6)$ levels, respectively. It can be concluded from the figure below, that although the excitation of both rotational states results in similar fluorescence signal levels in the (0,0) band, it is clear that $Q_1(6)$ appears a relatively temperature independent behavior, especially in the temperature region up to 1500 °K, providing a good depiction of the population. The necessary laser light wavelength to excite the $Q_1(6)$ line of the OH (1,0) band near 283 nm, was achieved as described earlier with doubling the fundamental beam, which in turn led to a mean laser beam energy of approximately 8-10 mJ/pulse. Accordingly, the signal of the OH (0,0) transition was selectively filtered (Figure 3.8) to record the two dimensional LIF images.

Temperature dependence of different OH (0,1) band rotational levels.

Indicative fluorescence signal at (0,0) band after excitation of $Q_1(1)$ (up) and $Q_1(6)$ (bottom) rotational levels, for different temperatures
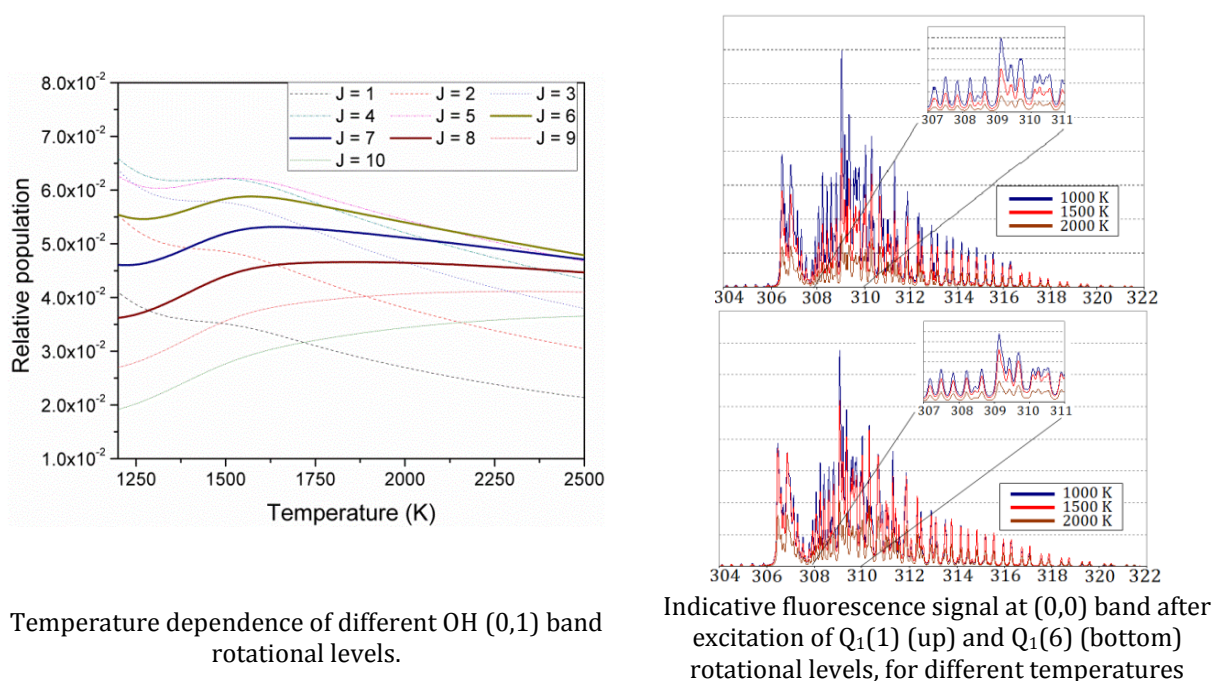
Figure 3.10 Temperature dependence of LIF signal, for different rotational level excitation. Simulation performed with LASKIN (Bülter *et al.*, 2004)

3.3.   LIF system calibration and error analysis

The most common cause for measurement uncertainty in laser induced fluorescence is the variation in collisional quenching. The collision-based processes, whereby excited state molecules become de-excited without light emission, are competing with fluorescence. The rate for collisional de-excitation determines the fluorescence yield, which is the fraction of fluorescing molecules of the total excited ones. For concentration measurements, the accuracy is a measure of how close the measured value of excited state population is to the actual one. The purpose of calibration is to define the precision of the measurement and evaluate systematic errors. For short-lived free radicals or atoms such as OH, absolute measurements pose a problem, because there is no way of

introducing known amounts of these radicals in the flame, so as to calibrate the signal intensity, hence the confidence interval has to be estimated by evaluating systematic and random errors. If random errors are limiting the accuracy or a measurement, the averaging of a series of repetitive measurements may increase the confidence of the result (Daily, 1997). However, if accuracy is limited by systematic sources of error, only calibration may improve the measurement confidence level. The OH radical can be calibrated in two ways; direct absorption and numerical calculation. Nevertheless, if the scope of the investigation is the visualization of the flame front through monitoring the OH concentration, those errors could be limited.

Hydroxyl radical LIF measurements realized in the frame of the present thesis, focused, mainly, on capturing flame positioning and shape characteristics. In this respect, no absolute OH concentration measurements are presented. Moreover, averaging of a series of repetitive measurements was systematically performed in order to subtract random errors sourcing from laser intensity fluctuations and periodical flow disturbances. As equation 3.2 suggests, the fluorescence signal is directly correlated with the laser excitation intensity, hence it is essential for planar imaging to maintain a uniform energy profile along the specimen volume. In all measurements a flat excitation laser intensity profile was constantly maintained within 5% of its maximum energy, resulting in the respective uncertainty for the OH population. In addition, in order to further reduce the spatial uncertainty concerning the flame front positioning, which is not limited by resolution, all two-dimensional data were normalized with its minimum signal, leading to a clear description of the reaction zone.

Another issue is that as the laser beam and fluorescence signal respectively travel through the flame, the possibility exists that they will be attenuated due to absorption by gaseous species. This effect will manifest itself as a reduction in the excitation rate in the case of the laser beam attenuation and attenuation of the fluorescence signal as it reaches the detector. However, since the weaker (compared to the fluorescence signal) OH (1,0) absorption spectra were choosen for excitation, such issues were not met. Other sources of error may originate from signal interference due to emission from other species, or due to scattering. In particular, laser beam scattering avoidance is a highly demanding procedure for measurements inside porous media, as the ones presented in chapter 7. There are several possible scattering interferences that must be taken into account and which may limit detectability or even harm the detector. Scattering from windows and other surfaces can harm the detection system, because such directly scattered laser light will be many orders of magnitude greater in amplitude than LIF signal, so extra caution should be placed as far as the optical layout is concerned.

3.4. Concluding remarks

Progressing, development and application of laser-based diagnostics to combustion problems is proceeding rapidly. The combustion research community aggressively applies emerging measuring techniques including laser sources, cameras and computational tools, which could further revolutionize the development of combustion diagnostics depending on the character of the technological advance. Laser induced fluorescence remains the most sensitive and straight forward

method for concentration measurements, since it is relatively easy to implement, with the least restrictive constraints on optical alignment. The present section describes the LIF technique for performing detailed species measurements in combustion environments. The fundamental background in molecular structure and spectroscopic concepts is given, followed by a discussion concerning LIF measurement strategies and the principal rate equations that govern them. The utilized system is afterwards presented, including laser excitation and tuning sources along with optical signal collection and uncertainty analysis. Finally, the followed strategy for measuring hydroxyl radical concentration in order to monitor the flame front characteristics is given.

Chapter references

Aldén M, Wallin S and Wendt W. Applications of two-photon absorption for detection of CO in combustion gases, Appl. Phys. B 1984;33:205–208.

Axelsson B, Collin R and Bengtsson PE. Laser-induced incandescence for soot particle size measurements in premixed flat flames Appl Opt 2000;39:3683–3690.

Bakali AEl, Mercier X, Wartel M, Acevedo F, Burns I, Gasnot L, Pauwels JF and Desgroux P. Modeling of PAHs in low pressure sooting premixed methane flame. Energy 2012;43:73–84.

Bülter A, Lenhard U, Rahmann U, Kohse-Höinghaus K, Brockhinke A. LASKIN: Efficient simulation of spectra affected by energy transfer. In: Proceedings of LACEA 2004 (Laser Applications to Chemical and Environmentel Analysis). 2004.

Bessler WG and Schulz C. Quantitative multi-line NO-LIF temperature Imaging, Appl. Phys. B 2004;78:519–533.

Bessler WG, Schulz C, Lee t, Jeffries JB and Hanson RK. Strategies for laser-induced fluorescence detection of nitric oxide in high-pressure flames. I. A–X (0,0) excitation. Appl. Opt. 2002;41:3547–3557.

Bessler WG, Schulz C, Lee t, Jeffries JB and Hanson RK. Strategies for laser-induced fluorescence detection of nitric oxide in high-pressure flames. I. A–X (0,0) excitation. Appl. Opt. 2003;42:2031–2042.

Bessler WG, Schulz C, Lee t, Jeffries JB and Hanson RK. Strategies for laser-induced fluorescence detection of nitric oxide in high-pressure flames. III. Comparison of A–X excitation schemes. Appl. Opt. 2002;42:4922–4936.

Brockhinke A, Lenhard U, Bulter A and Kohse-Hoinghaus K, Energy transfer in the OH $A^2\Sigma^+$ state: The role of polarization and of multi-quantum energy transfer, Phys. Chem. Chem. Phys 2005;7:874–881.

Brockhinke A and Kohse-Hoinghaus K, Energy transfer in combustion diagnostics: Experiment and modelling. Faraday Discuss. 2001;119:275–286.

Burns IS, MercierX, Wartel M, Chrystie RSM, Hult J and Kaminski CF. A method for performing high accuracy temperature measurements in low-pressure sooting flames using two-line atomic fluorescence Proc. Combust. Inst. 2011;33:799–806.

Cheng TS. Yuan T, Lu CC and Chao YC. The application of spontaneous vibrational raman scattering for temperature measurements in high pressure laminar flames. Combust. Sci. Technol. 2002;174:111–128.

Cheskis S. Quantitative measurements of absolute concentrations of intermediate species in flames. Prog. Energy Combust. Sci. 1999;25:233–252.

Cooper CS, Ravikrishna RV and Laurendeau NM. Comparisons of laser-saturated, laser-induced, and planar laser-induced fluorescence measurements of nitric oxide in a lean direct-injection spray flame. Appl. Opt. 1998;37:4823–4833.

Daily JW. Laser Induced Fluorescence Spectroscopy in Flames, Prog. Energy Combust. Sci., 1997;23: 133-199.

Dreier T and Rakestraw DJ. Degenerate Four-Wave Mixing Diagnostics on OH and NH Radicals in Flames. Appl. Phys. B 1990;50:479–485.

Dryer AJ and Crosley DR. Two-dimensional imaging OH laser-induced fluorescence in a flame.Opt. Letter 1982;7:382–384.

Eckbreth AC, Bonczyk PA and Verdieck JF. Combustion diagnostics by laser Raman and fluorescence techniques. Prog. Energy Combust. Sci. 1979;5:253–322.

Eckbreth A. 1996. Laser Diagnostics for Combustion Temperature and Species, 2nd Edition, Gordon & Breach, Amsterdam.

Feynman RP, Leighton RB and Sands M. 2005. The Feynman Lectures on Physics including Feynman's Tips on Physics: The Definitive and Extended Edition (2nd Ed.) Addison-Wesley, Boston

Gibaud C, Snyder JA, Sick V and Lindstedt R.P. Laser-induced fluorescence measurements and modeling of absolute CH concentrations in strained laminar methane/air diffusion flames. Proc. Combust. Institute 2005;30:455–463.

Goldman A and Cheskis S. Intracavity laser absorption spectroscopy of sooting acetylene/air flames. Appl. Phys. B 2008;92:281–286.

Gordon RL, Masri AR and Mastorakos E. Simultaneous Rayleigh temperature, OH- and CH_2O-LIF imaging of methane jets in a vitiated coflow. Combust Flame 2008;155:181–195.

Hancock RD, Bertagnolli KE and Lucht RP. Nitrogen and Hydrogen CARS Temperature Measurements in a Hydrogen/Air Flame Using a Near-Adiabatic Flat-Flame Burner. Combust. Flame 1997;109:323–331.

Hansen N, Miller JA, Klippenstein SJ, Westmoreland PR. and Kohse-Höinghaus K. Exploring Formation Pathways of Aromatic Compounds in Laboratory-Based Model Flames of Aliphatic Fuels. Combust.Expl. Shock Wave 2012;48:508–515.

Hanson RK, Seitzman JM and Paul PH. Planar laser-induced fluorescence imaging of combustion gases. Appl. Phys. B 1990;50:441–454.

Hardalupas Y and Orain M. Local measurements of the time-dependent heat release rate and equivalence ratio using chemiluminescent emission from a flame. Combust Flame 2004;139:188–207.

Hartlieb AT, Atakan B and Kohse-Höinghaus K, Temperature measurement in fuel-rich non-sooting low-pressure hydrocarbon flames, Appl. Phys. B 2000;70:435–445.

Hassel EP and Linov S. Laser diagnostics for studies of turbulent combustion. Meas. Sci. Technol. 2000;11:37–57.

Hilborn RC. Einstein coefficients, cros sections, f values, dipole moments, and all that. Am.J. Phys. 1982;50:982–986

Jörg A, Meier U, Kienle R and Kohse-Höinghaus K. State-specific rotational energy transfer in OH ($A_2\Sigma+$, $v'=0$) by some combustion relevant Collision partners. Appl. Phys. B 1992;55:305–310.

Kirchhoff and Bunsen. On chemical analysis by spectrum-observations. (Quarterly Journal of the Chemical Society of London) Q. J. Chem. Soc. 1861;13:270–289.

Kiefer J, Tröger JW, Li Z, Seeger T, Alden M and Leipertz A. Laser-induced breakdown flame thermometry. Combust Flame (2012) dx.doi.org/10.1016/j.combustflame.2012.08.005

Kiefer J and Ewart P. Laser diagnostics and minor species detection in combustion using resonant four-wave mixing. Prog Energy Combust Sci 2011;37:525-564

Kienle R, Jörg A and Kohse-Höinghaus K. State to state rotational energy transfer in OH ($A_2\Sigma+$, $v'=1$) Appl. Phys. B 1993;56:249-258.

Kohse-Höinghaus K and Brockhinke A, Experimental and numerical methods for studying the flame structure Combust Expl. Shock Wave 2009;45:349–364.

Kohse-Höinghaus K. and Jeffries JB. 2002. (Eds.), Applied Combustion Diagnostics, Taylor Francis, New York.

Kohse-Höinghaus K., Laser techniques for the quantitative detection of reactive intermediates in combustion systems, Prog. Energy Combust. Sci. 1994;20:203–279.

Kohse Höinghaus K. Quantitative Laser-Induced Fluorescence: Some recent developments in combustion diagnostics. Appl. Phys. B 1990;50:455–461.

Kohse Höinghaus K, Barlow RS, Alden M and, Wolfrum J, Combustion at the focus: Laser Diagnostics and Control, Proc. Comb. Inst. 2005;30:89–123.

Kuo KK and Parr TP. 1994. Non-Intrusive Combustion Diagnostics. Begell House

Knaus DA, Sattler SS and Gouldin FC. Three-dimensional temperature gradients in premixed turbulent flamelets via crossed-plane Rayleigh imaging. CombustFlame 2005;141:253–270.

Laurendeau NM. Temperature measurements by light-scattering methods. Prog. Energy Combust. Sci. 1988;14:147–170.

Luque J and Crosley DR. LIFBASE: Database and spectral simulation (version 1.5), SRI International Report MP 99-009 (1999).

Masri AR, Dibble RW and Barlow RS. The structure of turbulent nonpremixed flames revealed by Raman-Rayleigh-LIF measurements. Prog. Energy Combust. Sci. 1996;22:307–362.

Marrocco M. Vibration–rotation interaction in time-resolved coherent anti-Stokes Raman scattering for gas-phase thermometry. J. Raman Spectrosc. 2012;43:621–626.

Mayunger F and Feldmann O (Eds.). 2001. Optical Measurements: Techniques and Applications, 2nd Edition, Springer- Verlag Berlin Heidelberg.

Mercier X, Therssen E, Pauwels F and Desgroux P. Quantitative Features and Sensitivity of Cavity Ring-Down. Combust. Flame 2001;125:656 – 667.

Mercier X, Wartel M, Pauwels JF and Desgroux P. Implementation of a new spectroscopic method to quantify aromatic species involved in the formation of soot particles in flames. Appl. Phys. B 2008;91:387–395.

Nau P, Krüger J. Lackner A, Letzgus M and Brockhinke A. On the quantification of OH*, CH*, and C_2* chemiluminescence in flames. Appl Phys B 2012;107:551–559.

Paschotta R. 2008. Encyclopedia of Laser Physics and Technology. John Willey & Sons. New York.

Pitz RW, Wehrmeyer JA, BowlingJM and Cheng TS. Single pulse vibrational Raman scattering by a broadband KrF excimer laser in a hydrogen/air flame. Appl. Opt. 1990;29:2325–2332.

Rothe EW and Andersen P. Application of tunable excimer lasers to combustion diagnostics: a review. Appl. Opt. 1997;36:3971–4033.

Seeger T and Leipertz A. Experimental comparison of single-shot broadband vibrational and dual-broadband pure rotational coherent anti-Stokes Raman scattering in hot air. Appl Optics 1996;35:2665–2671.

Schulz W, Weber H and Poprawe R. 2008. Laser Physics and Applications–B: Laser Systems. Springer-Verlag, Berlin, Heidelberg, New York.

Schneider Ch, Dreizler A, Janicka J and Hassel EP. Flow field measurements of stable and locally extinguishing hydrocarbon-fuelled jet flames. Combust Flame 2003;135:185–190.

Schwar MJR and Weinberg FJ. Laser techniques in combustion research. Combust. Flame. 1969;13:335–374.

Shaddix CR and Smyth KC. Laser-induced incandescence measurements of soot production in steady and flickering methane, propane, and ethylene diffusion flames. Combust. Flame 1996; 107:418–452.

Sutton JA Williams BA and Fleming JW. Laser-induced fluorescence measurements of NCN in low-pressure $CH_4/O_2/N_2$ flames and its role in prompt NO formation. Combust. Flame 2008;153:465-478.

Suvernev AA, Dreizler A, Dreier T and WolfrumJ. Polarization-spectroscopic measurement and spectral simulation of OH ($A_2\Sigma$-$X_2\Pi$) and NH($A_3\Sigma$-$X_3\Pi$) transitions, Appl. Phys. B 1995;61:421–427

Stelzner B, Hunger F, Voss S, Keller J, Hasse C and Trimis D. Experimental and numerical study of rich inverse diffusion flame structure. Proc. Combust. Institute 2012 dx.doi.org/10.1016/j.proci.2012.06.153

Stuke M. (ed.), 1992. Dye lasers: 25 Years. Springer Verlag Berlin Heidelberg.

Träger F (Ed.). 2007. Springer handbook of laser and optics. Springer Science & Business Media, LLC New York.

Tropea C, Yarin AL and Foss JF. (Eds.). 2007. Springer Handbook of Experimental Fluid Mechanics. Springer-Verlag Berlin Heidelberg

Upatnieks A, Driscoll JF, Rasmussen, CC and Ceccio SL. Liftoff of turbulent jet flames–assessment of edge flame and other concepts using cinema-PIV. Combust Flame 2004;138: 259–272

Wolfrum J. Lasers in combustion: From basic theory to practical devices. Proc. Combust. Institute 1998;27:1-41.

Wolfrum J. Advanced laser spectroscopy in combustion chemistry: From elementary steps to practical devices. Faraday Discuss. 2002;119:1–26.

Yamamoto K, Ozeki M, Hayashi N and Yamashita H. Burning velocity and OH concentration in premixed combustion. Proc. Combust. Institute 2009;32:1227–1235.

Zhang Y, Yoon Y, Kelly P and Kennedy IM. LIF measurements of atomic arsenic in hydrogen and methane diffusion flames. Proc. Combust. Institute 1998;27:1777–1783

Zhao FQ and Hiroyasu H. The applications of laser Rayleigh scattering to combustion diagnostics Prog. Energy Combust. Sci. 1993;19:447–85.

Zhao H and Ladommatos N. Optical diagnostics for in-cylinder mixture formation measurements in IC engines. Prog. Energy Combust. Sci. 1998;24:297–336.

Chapter 4

Implementation of gas chromatographic system in fundamental combustion applications and performance evaluation

The configuration and the methodology developed for the realization of experimental investigations utilizing intrusive diagnostic techniques has been described in detail in chapter 2. This included a gas chromatographer and a system for continuous gaseous emission analyses. The continuous gas analyser is a built-ready instrument, as long as it is properly used within its calibration and operational capabilities; hence there is no necessity for validating its performance. However, this is not the case when a novel gas chromatographic method is developed, since its proper operation is a multi-parametric problem, linked with its various components *i.e.* columns, detector capabilities, method events etcetera. The present chapter attempts to access the GC methodological approach and evaluate its capabilities utilizing a simple fundamental configuration, as is the flow reactor, and validate the obtained results against numerical predictions. The flow reactor configuration is one of the most fundamental applications for species measurements for

detailed chemistry schemes validation and for this reason two different literature detail kinetic mechanisms were used, so as to investigate the measurements' validity. In order to evaluate the system's performance, a study of the pyrolysis of various methane mixtures has been carried out at atmospheric pressure in the 1000 ^oC to 1250 ^oC temperature range. The investigation explored the influence of the bath gas used (N_2 and CO_2) and the presence of small amounts of ethane to simulate natural gas. Exhaust gases, including methane, hydrogen, carbon monoxide and key pollutants, from the reactor were monitored and quantitatively analyzed online, using the gas chromatographic system, described in section 2.1.3.2 and total soot was determined by collecting and weighing soot samples from the reactor's exit as well as from deposits along the reactor for each case. In addition, Polycyclic Aromatic Hydrocarbons (PAH), also collected along the reactor and at the reactor exit, were measured using a coupled gas chromatographic and molecular spectrometric system (GC-MS), at selected temperatures.

The choice of fuel mixtures in the flow reactor additionally serves to establish a base case that links this investigation with modern practical applications. Such a study can be useful for understanding and optimizing the performance of modern engines, gas turbines and particular fuel cell systems, where the syngas feed is obtained from the partial oxidation of different mixtures with possible formation of soot and other undesired products. The choice of fuels covers a range of methane-based mixtures, from natural gas to biogas, aiming at the understanding of their behaviour in a fundamental reactor, before utilizing them in complex state-of-the-art applications, as is for example porous burners (see chapter 7). Moreover, these fuels can serve as the primary feedstock for Fischer–Tropsch synthesis, which eventually leads to fuels that are directly applicable and fully compatible with the existing infrastructure (see chapter 6). Additionally, the present work provides a basis for further development and optimization of existing detailed chemical kinetic schemes.

4.1.　Literature review of the pyrolysis methane-based mixtures

Methane pyrolysis has been extensively studied over the past, providing the solid background to evaluate the developed methodology as well as, partially, the obtained results. However, the choice of the investigated mixtures carries innovative research especially linking the conducted experimental campaign to modern applications. Detailed studies of methane mixtures chemistry are equally essential in order to understand and optimize the performance of modern engines, turbines and fuel cell (FC) systems operating with hydrogen rich mixtures. Currently, hydrogen is primarily produced from fossil fuels and in particular from natural gas, since several methane-related hydrogen production processes have reached maturity for commercial exploitation, such as Steam Methane Reforming (SMR), catalytic decomposition of natural gas, biomass gasification, and methane pyrolysis (Momirlan and Veziroglu, 2002). It is well known that hydrogen production is enhanced under fuel rich conditions and it is anticipated that it could be maximized under pyrolytic conditions. In the latter case, however, soot and non-gaseous carbonaceous products may be maximized as well. In this context, considering pyrolysis as an extreme of high fuel-rich regime, the obtained data define the maximum hydrogen production and soot deposition.

Methane pyrolysis in shock tubes (Hidaka *et al.*, 1999; Agafonov *et al.*, 2008), Jet Stirred Reactors (JSR) (Tan *et al.*, 1994; 1995) and flow reactors (Olsvik *et al.*, 1995; Arutyunov *et al.*, 1991) has been extensively studied over the past decades. However, most of the above studies focus on high temperatures and relatively high pressures. Methane pyrolysis at low temperatures (lower than 1000 ^{o}C) was reported in an early work by Chen and coworkers (Chen *et al.*, 1975; 1976) as well as in more recent studies incorporating modern techniques concerning temperature controlling (Sun *et al.*, 2000). The formation of soot from methane pyrolysis at 1100 ^{o}C in a similar flow reactor to the present work has been also reported (Mendiara *et al.*, 2006). As far as methane based mixtures are concerned, a number of studies have addressed the pyrolysis of methane/ethane mixtures (Bilbao *et al.*, 1997) under non-sooting conditions. However, although there are several experimental (Du *et al.*, 1991) and numerical (Liu *et al.*, 2001) studies of the effect of CO_2 addition on soot formation in flames, literature data relating to the effect of CO_2 dilution of methane mixtures on soot formation are scarce.

The effect of CO_2 addition on combustion performance and soot formation has been mainly studied in flames. The CO_2 addition to methane mixtures is of particular importance since it is related to the increasing interest of incorporating biogas mixtures in practical applications (Xuan *et al.*, 2009). Additionally, the results of such investigation can also be utilized for evaluating the performance and determining the carbonaceous emissions threshold in devices incorporating Exhaust Gas Recirculation (EGR) strategies [Bermúdez *et al.*, 2011; Natelson *et al.*,2010). Studies of the presence and effect of CO_2 on the conversion of CO and on the formation of soot have been reported in the same reactor installation as here (Abián *et al.*, 2011). In this context, the present work aims to study the pyrolysis of methane mixtures (namely CH_4/N_2, CH_4/CO_2, and $CH_4+C_2H_6/N_2$) in the 1000 ^{o}C to 1250 ^{o}C temperature range and atmospheric pressure.

4.2.   Flow reactor apparatus and coupling with GC system

The experimental facility consisted of the reactor configuration, the soot collection and gas analysis systems. The reactor main components, as shown in Figure 4.1, are the gas feeding system, which in turn is made from the reactor head and the mobile outlet module that allows retention time's parameterization. The gas feeding system consisted of two inlets allowing mixing of the reactants before entering the reaction zone. Mixture components were introduced at the desirable concentrations through mass flow controllers (Bronkhorst High-Tech B.V.). A digital optical flow meter was utilized to crosscheck flow rates. A total volumetric flow of 1000 Nml/min (STP) was maintained in each case by balancing with nitrogen flow. The reaction system consisted of a quartz tube of 45 mm inner diameter and 800 mm length placed in an electrically heated oven, allowing temperature control between 700 ^{o}C and 1200 ^{o}C, with an accuracy of ±10 ^{o}C. The reactor inlet and outlet were cooled by auxiliary air flows running through tubes concentric to the reactor, in order to keep temperature fluctuations along the reaction zone within ±10 ^{o}C of the specified temperature. During the experiments, soot deposition (and water formation when CO_2 was also introduced in the inlet mixture) resulted in a slight overpressure. In order to prevent leakages or air entrainment from the reactor connections, care was taken so that the overpressure was never above the value of 50 mbar. Gas products were identified and quantified at the reactor outlet by

using the Gas Chromatographic system described in section 2.1.3.2 and here is briefly summarized as follows; The GC system was equipped with FID and TCD detectors, capable of detecting CO, CO_2, N_2, H_2, methane, ethane, ethylene, acetylene, propane, propylene, propadiene, 1,3-butadiene, isobutane, ethanol, benzene and toluene, with less than 10 ppm uncertainty. The TCD channel was equipped with HP Plot Q columns coupled with a MoleSieve column and the FID channel was equipped with an HP PONA column. Soot formed at the exhaust of the reactor was collected in a quartz fiber thimble of 25 mm diameter and 60 mm length, with a pore size of the order of 1 µm. The soot formed at the reactor body was also collected after disassembling the reactor parts described previously at the end of each experiment. In order to collect a significant amount of soot, each experiment lasted three hours (3 h). Such duration is necessary in order to minimize systematic error from soot collection while avoiding system over-pressurization. After collecting the soot from each experiment, the samples were weighted in a high precision electronic balance. In order to ensure repeatability measurements were reproduced twice for most of the cases studied. Indicatively it is noted that measured soot mass varied less than 2%.

| Reactor main body | Mobile outlet module | Reactor head |
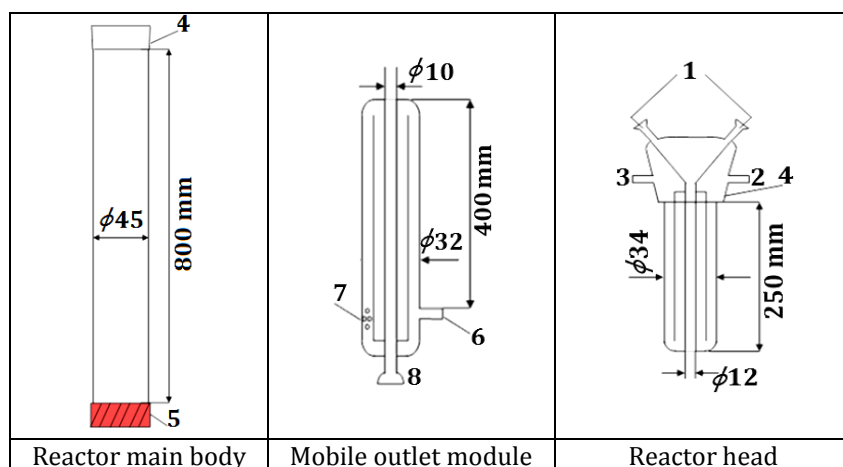
Figure 4.1 The flow reactor main features. Drawings not in scale.

4.2.1.   Case studies

The isothermal flow reactor described above, has been extensively used in the past in many studies at the research group of the Universidad de Zaragoza, for the pyrolysis studies of hydrocarbon fuels, such as acetylene (Ruiz *et al.*, 2007), ethanol (Esarte *et al.*, 2011a) and acetylene/ethanol mixtures (Esarte *et al.*, 2009; 2011b), where a detailed description of the experimental setup can be found.

Table 4-1 Initial species mole fractions for Cases A-C

Case	CH$_4$ (%)	C$_2$H$_6$ (%)	CO$_2$ (%)	N$_2$ (%)
A	10	-	-	90
B	10	-	33	57
C	9	1	-	90

The current experiments addressed the pyrolysis of pure methane and a typical natural gas in a nitrogen atmosphere, as well as the pyrolysis of methane in an N_2/CO_2 atmosphere, as a base case facilitating useful conclusions for CO_2 addition effect in the context of biogas mixtures chemistry. Initial mixture composition for all cases is provided in Table 4-1. In all cases the hydrocarbon concentration did not exceed the 10% threshold of the total mixture in order to ensure isothermal conditions in the reactor.

4.3. Computational model

Experimental campaigns in ideal flow reactors are of great importance for numerical model validation. The conditions of the flow reactor facilitate the numerical simulation via incorporating detailed kinetic schemes. In this respect, numerical simulations of the experimental results have been carried out using two detailed kinetic mechanisms. The first mechanism has been developed over the past years in the National Technical University of Athens and for this reason will be referred hereon as "NTUA mechanism". The second used mechanism has been used to evaluate experiments in the very same reactor configuration and was developed in the Universidad de Zaragoza, hence it will be referred from now on as "UZ mechanism". Calculations have been performed using commercial computational software (Kee *et al.*, 1991).
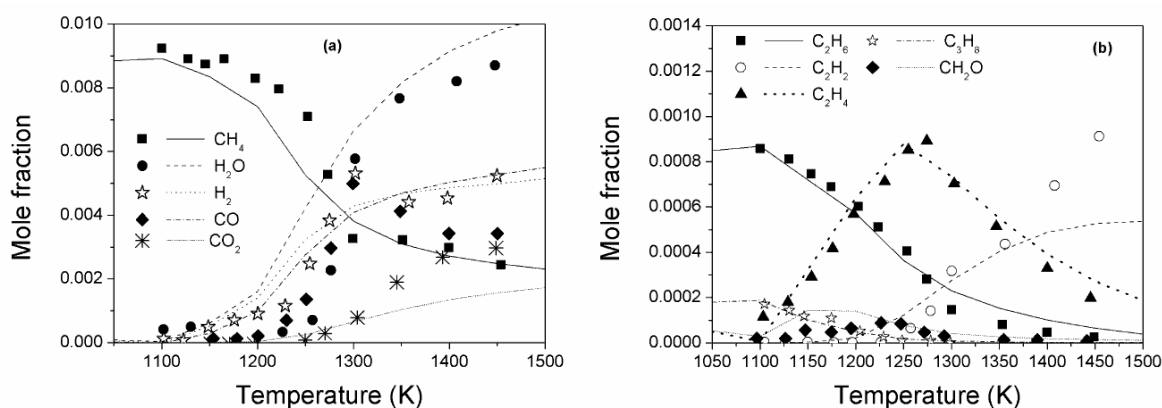
Figure 4.2 Comparison between computed and experimental data (Dagaut and Nicolle, 2005) for the oxidation of a rich (φ = 2.0) natural gas (CH_4: 8928 ppm, C_2H_6: 879 ppm, C_3H_8: 198 ppm) blend in an atmospheric pressure JSR at a residence time of 120ms.

The NTUA comprehensive mechanism has been extensively validated in the past against experimental speciation data from counter-flow and premixed flames, including laminar flame speeds, shock tubes, including ignition time delays, as well as from perfectly stirred and plug flow reactors, all under a wide range of temperatures, pressures and stoichiometries. In particular, the mechanism has been shown to successfully reproduce the chemistry of both conventional e.g. CH_4, C_2H_2, C_2H_4 and C_3H_4 (Lindstedt and Skevis, 1997, 2000; Gazi *et al.*, 2011), as well as alternative C_1-C_4 fuels e.g. CH_3OH and C_2H_5OH (Vourliotakis *et al*, 2012). Recently, the C_6 part of the mechanism has been updated against recent experimental data from a total six laminar premixed benzene flames, as well as data from shock tubes, stirred and flow benzene reactors, providing the opportunity for a

critical assessment of benzene oxidation and combustion chemistry under a broad range of operating conditions (Vourliotakis *et al*, 2011).

Previous validation studies with the NTUA mechanism did not consider PAH species and soot formation. In order to realistically simulate fuel chemistry in a pyrolytic environment, where the formation of gaseous PAH species and eventually soot, is expected to be particularly pronounced, a literature detailed PAH submechanism (Slavinskaya and Frank, 2009) has been coupled with the previously described C_1-C_6 detailed mechanism. This PAH model including 181 reactions among 42 species, up to benzo-a-pyrene (A4), has been previously validated and optimized for rich methane combustion and has been shown to very accurately reproduce a series of PAH data, from toluene to pyrene in atmospheric pressure rich methane and ethane premixed flames. The current version of the mechanism consists of 164 species and 1011 reactions.
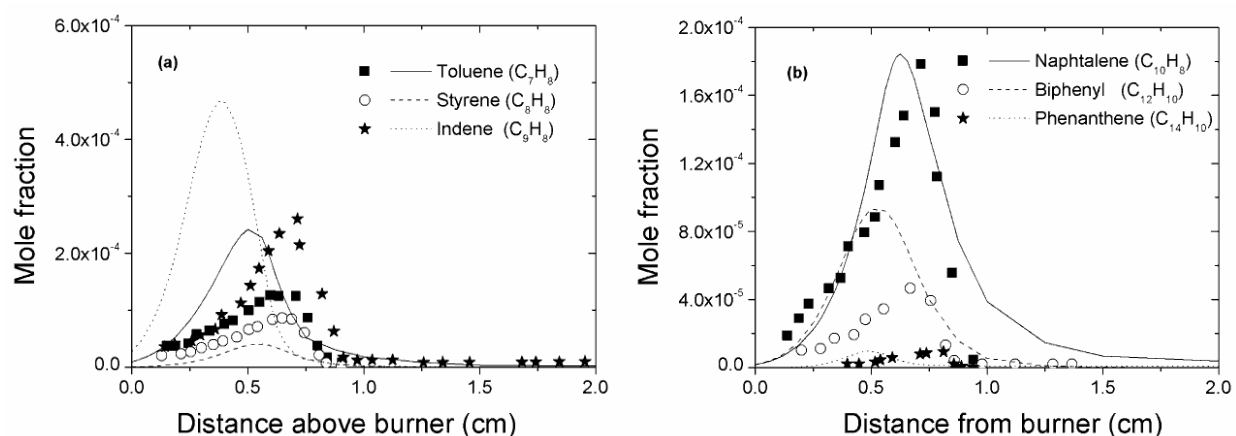
Figure 4.3 Comparison between computed and experimental (a) C_7-C_9 aromatic species and (b) A2 (naphthalene), P2 (biphenyl) and A3 (phenanthrene) profiles from the rich (φ = 1.8), low pressure (p = 50 mbar) benzene premixed flame (Yang *et al*., 2007).

In the framework of the present work, the mechanism has been further validated. Excellent agreement has been obtained between computed and experimental species profiles from the oxidation of a natural gas blend, with a similar typical composition with the present study (literature data also introduce 2% C_3H_8) in the atmospheric pressure rich natural gas jet stirred reactor (Dagaut and Nicolle, 2005) over the temperature range of 1100–1450 K, as shown in Figure 4.2. Moreover, further validation against measured PAH species profiles concerning low pressure rich premixed benzene flames (Yang *et al*., 2007) is presented in Figure 4.3.

The mechanism developed at the University of Zaragoza (UZ mechanism) takes as a starting point the GADM mechanism (Glarborg *et al*., 1998), including oxidation reactions for parabenzoquinone (Alzueta *et al*., 1998) and benzene (Alzueta *et al*., 2000). This mechanism was recently updated in a study of acetylene conversion (Alzueta *et al*., 2008), and has been completed with reactions for ethanol conversion (Alzueta *et al*., 2002) and the PAH reactions, up to pyrene, from the well-known ABF mechanism (Appel *et al*., 2000). The UZ mechanism consists of 156 species and 929 elementary reactions and has been successfully validated against combustion parameters directly relevant to this work, as mentioned in paragraph 4.2.1.

4.4. Results and discussion

In the present section, the results obtained for the pyrolysis of various methane based mixtures are presented. The results are presented along with the numerical predictions, so as to achieve a deep understanding of the actual processes taking place in the reactor and extract valuable information concerning the prospect of the work concerning practical applications such as SOFC systems (paragraph 1.4.1). The interpretation of the experimental data utilizing two different detail kinetics schemes is not only beneficial for the procedure validation, but facilitates the explanation of synergetic effects as well.

4.4.1. Fuel conversion and major species

Experimental results for the pyrolysis of the three methane mixtures listed in Table 4-1 are presented in the following sections. First, results for fuel conversion and major products are presented. Experimental data for key intermediate species participating into the molecular growth processes, and eventually, soot formation, are presented in the following section. Figure 4.4 presents fuel conversion and hydrogen production data at the reactor exit for the pyrolysis of pure methane, Case A (Figure 4.4a) and for the methane-ethane mixture, Case C (Figure 4.4b). Results for methane pyrolysis in the presence of CO_2, Case B, are shown in Figure 4.5. Numerical simulations using the two detailed kinetic mechanisms, described in section 4.3, are also presented for all cases.

Figure 4.4 Comparison between experimental data and numerical simulations for methane conversion and H_2 mole fraction in (a) pure methane pyrolysis (Case A) and (b) methane/ethane pyrolysis (Case C). Symbols correspond to experimental data, black lines correspond to the NTUA and grey lines to the UZ mechanism.

$C_2H_6(+M)=C_2H_5+H(+M)$ (R 4.1)

$CH_3+CH_3(+M)=C_2H_6(+M)$ (R 4.2)

$CH_3+H(+M)=CH_4(+M)$ (R 4.3)

$CH_4+H=CH_3+H_2$ (R 4.4)

Generally, the results confirm the enhanced reactivity of the methane-ethane mixture as compared to pure methane, which is also in agreement with earlier studies (Alzueta *et al.*, 1997). For example, methane conversion in Case A is of the order of 25% at a temperature of 1050 ^oC, while total initial carbon (CH_4 and C_2H_6) conversion reaches almost 50%, at the same temperature, in Case C. This is due to the fact that, at such temperatures, the relatively more unstable ethane molecule decomposes to the ethyl and hydrogen radicals, reaction R 4.1. The hydrogen radical subsequently feeds into reaction R 4.4 and accelerates methane conversion (Bilbao *et al.*, 1997). At higher temperatures, reaction R 4.1 becomes significantly slower than the ethane thermal decomposition (-R 4.2) and, as a result, hydrogen radical production diminishes.
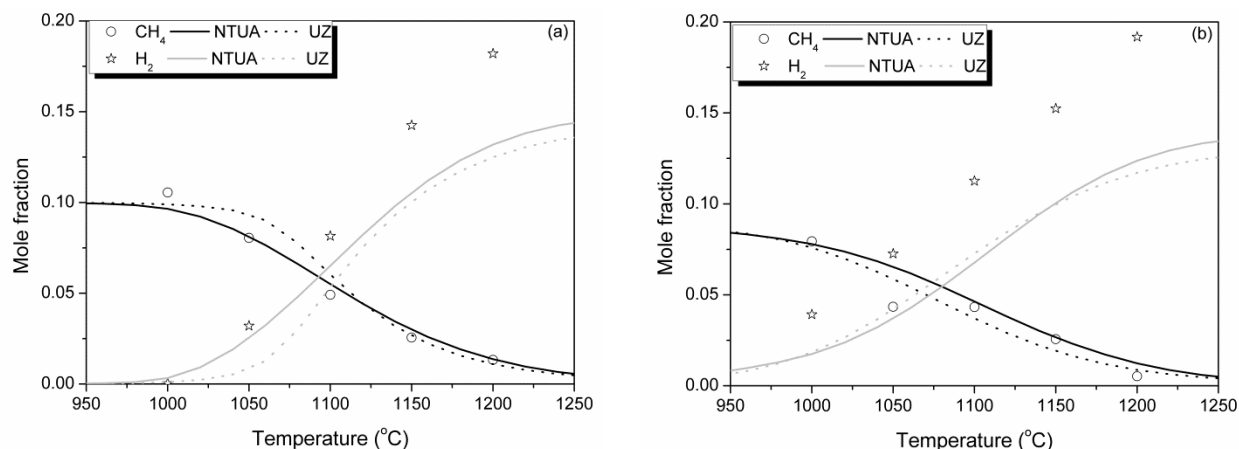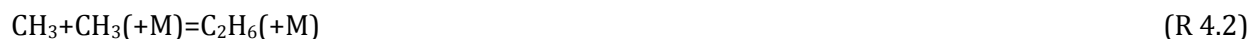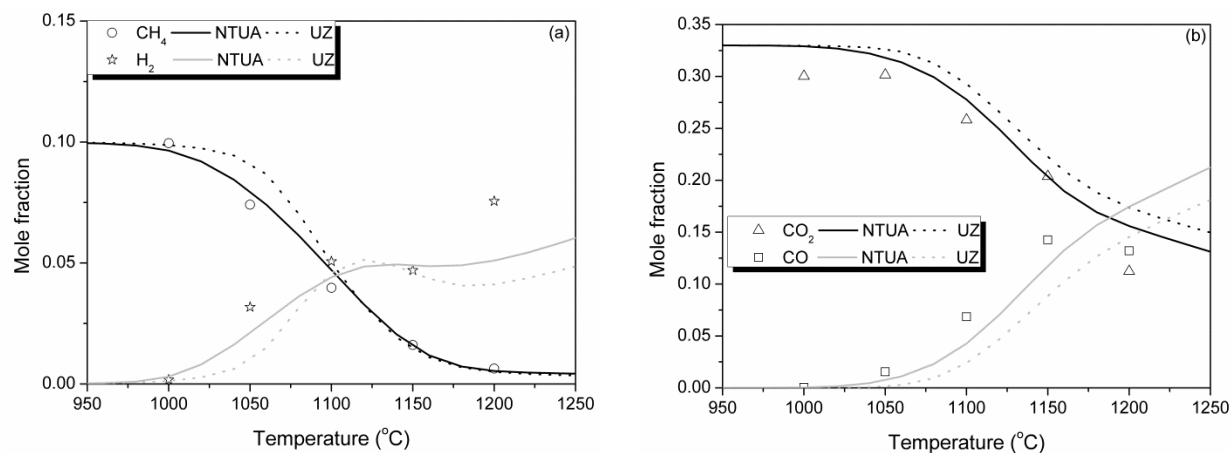

Figure 4.5 Comparison between experimental data and numerical simulation for (a) methane conversion and H_2 mole fraction and (b) CO and CO_2 levels in methane pyrolysis in the presence of CO_2 (Case B).

On the other hand, the addition of carbon dioxide has no discernible effect on methane conversion at low temperatures. As the temperature is increased, hydrogen radicals produced from methane pyrolysis (-R 4.3) favor the $CO_2+H=CO+OH$ reaction leading to enhanced OH radical formation rate. The latter initiates H radical abstraction reactions from methane, thus enhancing its conversion. Despite differences in the respective fuel consumption rates, hydrogen mole fractions are of the same level in both Cases A and C, as can be deduced from Figure 4.4. On the other hand, H_2 production is greatly diminished when CO_2 is added. Overall, numerical predictions for major species, using both mechanisms, come in reasonable agreement with the experimental data for all cases. Both mechanisms are shown to be able to reproduce methane conversion and H_2/CO production trends along the temperature range studied, with hydrogen levels being a notable exception, particularly under high temperatures (T > 1100 ^oC), mainly in Cases A and C. The reason for this discrepancy is discussed below.

$C_2H_6+H=C_2H_5+H_2$ (R 4.5)

$C_2H_5(+M)=C_2H_4+H(+M)$ (R 4.6)

$C_2H_4+H=C_2H_3+H_2$ (R 4.7)

$C_2H_3(+M)=C_2H_2+H(+M)$ (R 4.8)

Rate-of-production analysis has been performed in order to investigate the paths through which methane and the methane/ethane mixture evolve during pyrolysis. In all three cases studied, both mechanisms suggest that the overall reaction starts with methane thermal decomposition to produce methyl and hydrogen radicals, reaction -R 4.3. Subsequently, the H radical attacks methane generating more CH_3 (R 4.4). This sequence contributes over 50% of the total molecular hydrogen in Case A, for both mechanisms. Methyl radical is then exclusively converted to C_2H_6, via the self-recombination reaction R 4.2, initiating the C_2 chain. Hydrogen radicals act as chain carriers of a sequence of H abstraction reactions leading from ethane down to acetylene and shedding H_2 molecules along the way, as follows;

The above described paths (R 4.4, R 4.5, R 4.7) account for the H_2 production. However, both mechanisms tend to under-predict hydrogen mole fractions at higher temperatures (T > 1100 ^{o}C) and in particular in Cases A and C, with discrepancies of the order of 30%. Such discrepancies cannot easily be attributed to deficiencies of the two major H_2 production paths described above (R 4.5, R 4.7). The reason is that methane consumption profile and total C_2 levels, particularly in higher temperatures, are adequately captured. This implies that, there may be additional hydrogen production paths, such as thermal cracking reactions, possibly involving higher aliphatic, e.g. C_4, or (poly-) aromatic species. The UZ mechanism includes some molecular elimination reactions, such as reaction R 4.9, but they do not appreciably contribute to H_2 formation. Also note that molecular hydrogen is "numerically" locked in higher PAH species, since both mechanisms do not include any soot reactions.

$C_2H_4+M=C_2H_2+H_2+M$ (R 4.9)

On the other hand, hydrogen levels are satisfactorily reproduced in Case B, for both mechanisms. This is due to CO_2 presence which induces an oxidative character into the pyrolytic process, resulting into a more balanced chemistry. For instance, and at a the case of 1200 ^{o}C, in addition to R 4.4 and the C_2 chain paths discussed above, there is a substantial contribution to H_2 formation from reactions involving oxygenated species, such as formaldehyde, ketene and propionaldehyde. Note that the above discussion is applicable to both mechanisms. In the CO_2 atmosphere, H radicals interact efficiently with CO_2, reaction R 4.10, as documented in oxy-fuel combustion studies (Abián *et al.*, 2011), where the differences between the use of N_2 and CO_2 atmospheres were addressed.

$CO_2+H= CO+OH$ (R 4.10)

In the presence of CO_2, the abstraction reactions with OH radicals constitute a considerable fraction of the total fuel abstraction reactions and lead to water formation, competing with H_2 production. As a result, the yield of hydrogen in Case B is almost half as compared to Cases A and C, The above discussion suggests that CO_2 acts as an oxidizer and not as a mere diluent, like N_2. The issue is further numerically explored in the last section of the present paper.

In the present experiments, the production of a significant amount of water was found, which is in agreement with the findings of similar studies (Abián *et al.*, 2012). Figure 4.6 presents estimated water levels at the reactor exit. These estimated values were obtained through balancing the H atom content in the inlet mixture, with the total H atom content in the gaseous (C_1-C_7) species

quantified at the reactors exit. The difference is roughly proportional to the water levels, since contributions from hydrogen contained in PAH species can be assumed to be minor. Estimated water values presented in Figure 4.6 are thus an upper threshold and carry an uncertainty level of ±25%. Computations using both models are also presented in Figure 4.6. Both mechanisms qualitatively capture the trend in water formation, with also satisfactory agreement in peak values. A closer examination of the numerical and estimated H_2O results, reveals that there are essentially two distinct regions; a sharp increase in exhaust water levels followed by a plateau. The transition point occurs at around 1150 ºC. In order to explain such a behavior, rate-of-production analyses have been performed at 1050 ºC and 1200 ºC, the former being chosen as the starting point of the sharp increase while the latter is located well within the plateau. Under lower temperatures, water is still being formed by OH radical attack to the fuel, reaction R 4.11, with a minor (up to 20%) contribution from reaction R 4.12. At higher temperatures, water achieves steady state behavior; it is now formed through reaction R 4.12 and destroyed mainly via addition reactions with C_2 (mainly acetylene) and C_3 (mainly propargyl radical) hydrocarbons leading to the formation of C_2 and C_3 oxygenated species.

$$CH_4+OH=CH_3+H_2O \qquad\qquad\qquad (R\ 4.11)$$

$$OH+H_2=H_2O+H \qquad\qquad\qquad (R\ 4.12)$$
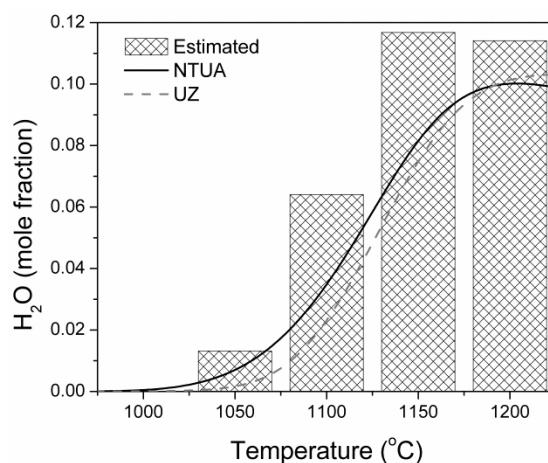
Figure 4.6 Comparison between estimated water levels against numerical predictions at the reactor.

It can be anticipated that changes in H_2O behavior are directly related to a more subtle alteration in the overall system behavior, from a purely kinetically controlled to a partially equilibrated regime, especially above 1200 ºC, when the water-gas-shift reaction quotient, is markedly distinct from the thermodynamic equilibrium (Keramiotis *et al.*, 2012).

4.4.2. Soot and soot precursors formation

Soot formation tendency is closely linked to the chemistry of several key soot precursors. Acetylene, ethylene and benzene, in particular, are closely linked both to PAH formation and soot mass growth processes. Accordingly, a quantification of the acetylene and benzene formation

dynamics is expected to provide valuable information on carbonaceous formation and deposition processes. Experimental and predicted data for C_2H_6, C_2H_4, C_2H_2, C_3H_6 and a-C_3H_4 (allene) are shown in Figure 4.4 to Figure 4.9, respectively. The initiation of the C_2 chain, starting form C_2H_6 formation and finally leading to acetylene formation, has been described above (R 4.5 to R 4.8), and found to be directly linked to fuel consumption chemistry. Overall the agreement is satisfactory, although there is room for improvement. While both mechanisms result in very similar predictions for the major species, they behave quite differently for most intermediates. By a careful inspection of both numerical and experimental results, two major deficiencies of the mechanisms appear. The NTUA mechanism over-estimates C_2H_6 levels under lower temperatures, for Cases A and B, by a factor of five (Figure 4.7). Since C_2H_6 comes exclusively from methyl radical recombination, and the latter in the low temperature regime is determined by the rate of reaction R 4.3, it is reasonable to argue that the rate constant of the latter reaction is inappropriate. Reaction R 4.3 is pressure dependent, with a temperature independent high pressure limit, and an enhanced collision efficiency for ethane of 5 for the low pressure limit (Baulch *et al.*, 2005). Thus, the above reaction is catalyzed under the studied conditions by the high C_2H_6 levels in the system, resulting in such an over-prediction. This further indicates that the rate is not appropriate for such pyrolytic conditions. At higher temperatures reaction -R 4.3 becomes irrelevant for CH_3 production, since abstraction reaction R 4.4 dominates, and the level of agreement between experimental and predicted data improves. Finally, for Case B the sudden drop in C_2H_6 profiles for temperatures above 1100 ºC, is corroborated by the lack of detection in the same range implying that ethane levels are below TCD detection limit under the present conditions. Further downstream the C_2 chain, ethylene levels are in general satisfactorily described.

Figure 4.7 Comparison between experimental data and numerical simulation for C_2H_6 (left) and C_2H_4 (right) exhaust levels in (a) Case A, (b) Case B and (c) Case C. Symbols correspond to experimental data, black lines correspond to the NTUA mechanism and grey lines to the UZ mechanism.

On the other hand, UZ mechanism over-predicts acetylene levels by almost an order of magnitude, particularly at higher temperatures (Figure 4.8). Reaction path analysis indicates that acetylene is formed through the molecular decomposition, reaction R 4.9, with an increasing contribution as temperature increases. This indicates that the above reaction features a fast rate. Peak acetylene levels for all three cases, and within the studied temperature range, are similar, with values of

around 2000 ppm. The acetylene formed, is quantitatively consumed to C_3H_4 species which in turn initiate further molecular growth reactions. In particular, the C_3 chain is initiated by CH_3 radical addition to acetylene, reactions R 4.13 and R 4.14, leading to allene and propyne respectively.

$$C_2H_2 + CH_3 = a\text{-}C_3H_4 + H \hspace{6cm} \text{(R 4.13)}$$

$$C_2H_2 + CH_3 = p\text{-}C_3H_4 + H \hspace{6cm} \text{(R 4.14)}$$

Figure 4.8 Comparison between experimental data and numerical simulation for C_2H_2 exhaust levels in (a) Case A, (b) Case B and (c) Case C.

C_3H_4 species are exclusively consumed to the propargyl radical, which in turns recombines to form benzene. Propene (Figure 4.9) is also formed by CH_3 addition to C_2H_4 either directly, reaction - R 4.15, or indirectly, through the n-propyl radical, reaction R 4.16, and subsequently goes down the C_3 chain, as described above.
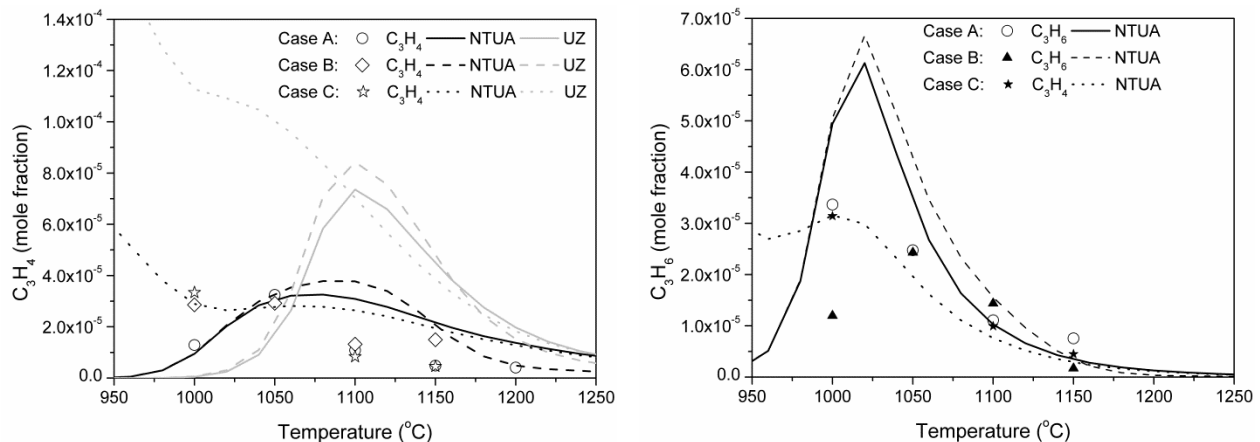
Figure 4.9 Comparison between experimental data and numerical simulation for Allene/a-C_3H_4 (left) and C_3H_6 (right) exhaust levels in (a) Case A, (b) Case B and (c) Case C. Symbols correspond to experimental data, black lines correspond to the NTUA mechanism and grey lines to the UZ mechanism

As a result of the above sequence, a-C_3H_4 levels in the UZ mechanism are over-predicted by a factor of 4 and are shifted to higher temperatures. Further upstream in the C_3 chain, C_3H_6 levels are over-

138

predicted by a factor of 2 by the NTUA mechanism (Figure 4.9). Since propene formation is solely due to the methyl vinyl radical recombination, the above over-prediction can be attributed to the overall CH_3 over-prediction, as discussed earlier.

$$C_3H_6+H=C_2H_4+CH_3 \qquad\qquad\qquad (R\ 4.15)$$

$$n\text{-}C_3H_7=C_2H_4+CH_3 \qquad\qquad\qquad (R\ 4.16)$$

Exhaust benzene levels as a function of temperature are shown in Figure 4.10. Experimental data appear to be insensitive to temperature, while numerical results show distinct peaks at intermediate temperatures. Generally, the simulated pyrolysis of the methane/ethane mixture (Case C) appears to result in significantly higher benzene levels, particularly at lower temperatures and as compared to the pure methane pyrolysis case (Case A). Since numerical results are generally higher than experimental data, the discrepancies found are attributed to the fact that the formation of soot is not included in the models and this suggests the need for further improvement in the current models in order to reproduce the complex behavior of soot formation.
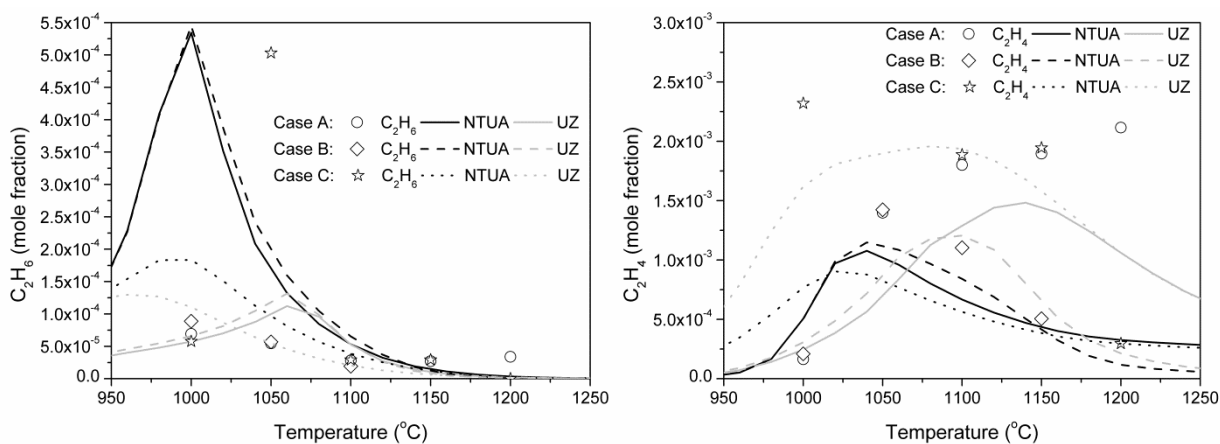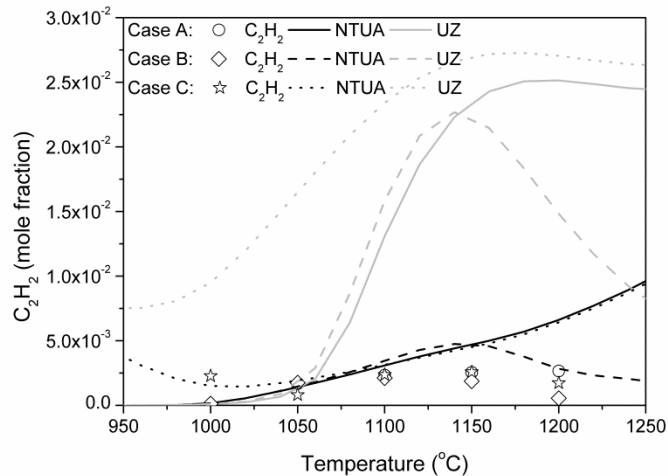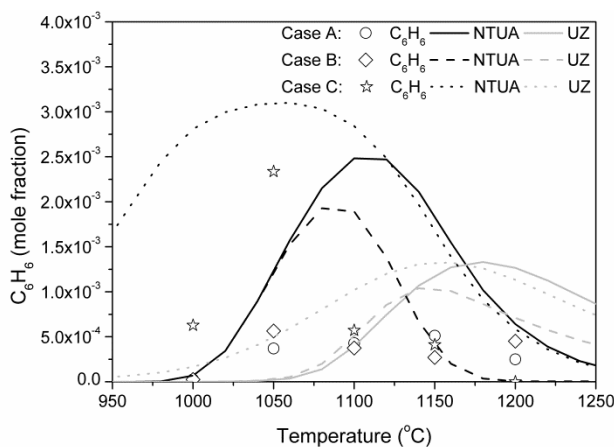

Figure 4.10 Comparison between experimental data and numerical simulation for C_6H_6 exhaust levels in (a) Case A, (b) Case B and (c) Case C.

Finally, Figure 4.11 presents total soot amounts collected for all studied cases. The values correspond to soot collected at the soot trap and to the amount deposed along the reactor body. As shown in Figure 4.11 the temperature threshold for soot formation appears to be higher (1050 oC) for the case of methane pyrolysis (case A) than for the methane/ethane mixture (case C) (1000 oC), which is explained in terms of the temperature at which the conversion of hydrocarbons is produced, *i.e.* the sequence $C_2H_2<C_2H_4<C_2H_6<CH_4/C_2H_6$ mixture$<CH_4$ (Bilbao *et al.*, 1997). A striking feature is that soot production appears to correlate with the computed rate of fuel conversion. Also, the amount of soot produced from the methane/ethane mixture pyrolysis, systematically exhibits higher values than the pure methane pyrolysis in nitrogen diluent. This comes in agreement with the higher carbon content of the former mixture, due to the C_2H_6 presence. However, for a temperature of 1100 oC, soot levels for case B, are substantially higher than Cases A and C. Indeed, at that temperature, fuel conversion for Case B is significantly faster than for the other two cases.

Further, soot levels for Case B do not appreciably increase above that temperature, something that also follows the similar trend in fuel conversion rate.
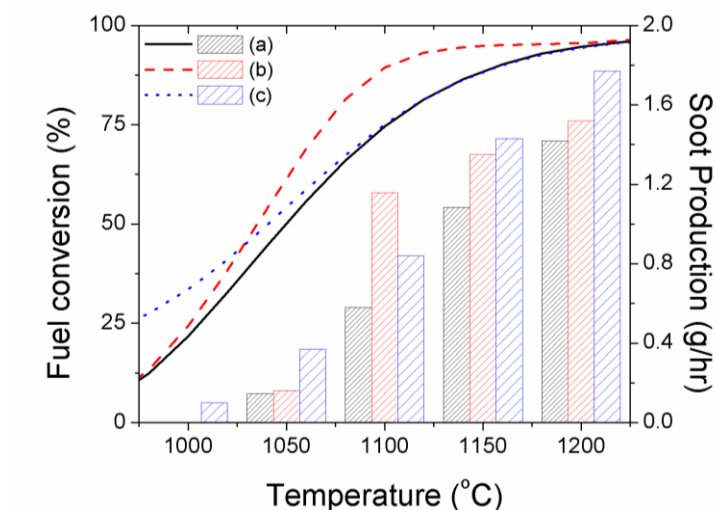
Figure 4.11 Total weight of soot (g/hr) collected at reactor surface and reactor exit, compared against calculated fuel consumption (%).

4.4.2.1.   Supplementary PAH measurements

In addition, separate experiments were conducted for the identification and quantification of Polycyclic Aromatic Hydrocarbons (PAH) compounds. These measurements are presented here to escort the respective soot measurements and aim towards a better understanding of the overall processes. The total PAHs correspond to the amount extracted from the soot formed in the reactor, from the amount adsorbed at a resin filter and from the amount attached along the reactor.
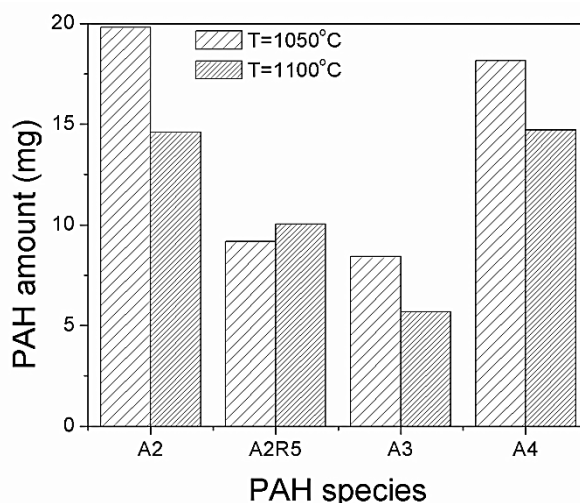
Figure 4.12 Comparison between temperatures T=1050°C and 1110°C PAH species levels for Case B for naphthalene (A2), acenaphthylene (A2R5), anthracene (A3) and pyrene (A4), during one hour experiment

Generally, PAHs are a function of the inlet mixture composition and hence the initial carbon content. For instance, at T=1050 °C, total PAH amounts for cases B and C were 30% higher than for Case A. A comparison of PAH levels at two selected temperatures (T=1050 °C and T=1100 °C) was carried out for Case B in order to preliminary investigate temperature effects on PAH formation. The results revealed that at T=1100 °C the total PAH amount was 20% less than for T=1050 °C. Speciation data presented in Figure 4.12 also reveals interesting features. Naphthalene, anthracene and pyrene decrease with temperature, following the trend of total PAHs. This can be explained as a result of either increased dissociation at higher temperatures or to conversion to soot particles. However, acenaphthylene levels appear to be unaffected and a possible explanation is that acenaphthylene levels are mainly controlled by acetylene levels which, as shown earlier, remain constant over the temperature window considered here.

Besides reducing performance efficieny, PAH species have been proven extremely hazardous. It is nowadays well established that PAH species are responsible for various effects on human health and depending on their composition can be extremely carcinogenic. PAHs toxicity is very structurally dependent, with isomers varying from being nontoxic to extremely toxic. In this respect, the United States Environmental Protection Agency (EPA) has classified those compounds as probable human carcinogens.
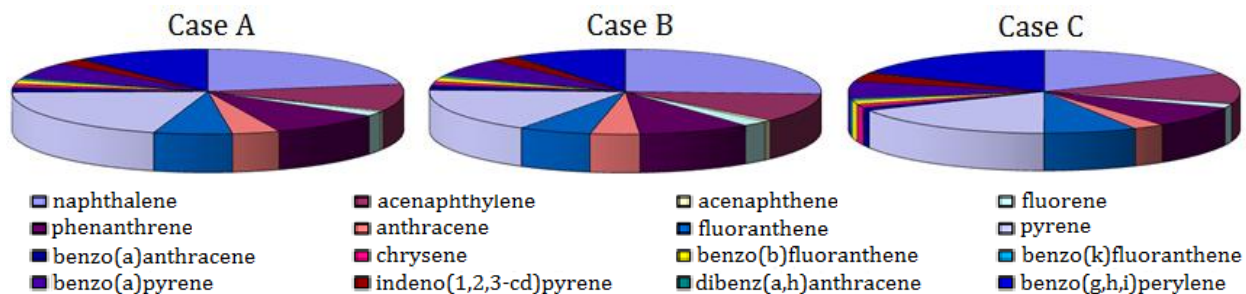
Figure 4.13 The 16 quantitatively analyzed PAHs for all studied cases at 1050°C

The sixteen most hazardous ones have been quantified and presented here for purely demonstrative reasons. Figure 4.13 indicatively presents these sixteen PAH species from the respective studied cases for reactor temperature of T = 1050 °C. It is clear that primarily naphthalene, pyrene and benzo-perylene and secondly acenaphthylene and phenanthrene, are primarily formed in all cases. The increased carbon content of Case C, when compared to the similar Case A, appears to result in lower naphthalene quantities in favor of higher PAH species formation; this observation points towards the higher mixture reactivity, as also noted earlier. The presence of CO_2 in Case B on the other hand, reveals similar PAH distribution, with respect to the different species as in case A, leading to similar conclusions for this case as the ones noted for soot formation processes.

The details for the experimental procedure are not described here, since PAH measurements constitute a wide field in combustion research outside of the scope of the present thesis. However details concerning the methodology followed in the same configuration can be found in recent studies (Sánchez *et al.*, 2010; 2012a; 2012b).

4.5.   Concluding remarks

Experimental methodologies such as novel gas chromatographic methods need to be evaluated in well-controlled, fundamental configurations. In this concept, the approach described in paragraph 2.1.3.2, was validated, utilizing an isothermal flow reactor configuration. Cases studied, also relevant also to fuel reforming process in SOFC systems, included methane pyrolysis in pure nitrogen and in N_2/CO_2 atmospheres, as well as the pyrolysis of a typical natural gas, with a composition of 90% methane and 10% ethane, in pure nitrogen atmosphere. Experimental results for fuel conversion, H_2 and CO and levels and concentrations of key species *i.e.* ethane, ethylene, acetylene, propene, allene and benzene as well as selected PAH species up to pyrene, were presented and critically analyzed. Trends in exhaust gaseous species levels as a function of temperature and initial mixture composition were identified. In particular the chemical effect of CO_2 was demonstrated. The higher carbon content and reactivity of the natural gas mixture were reflected in soot measurements and the temperature threshold for soot formation was measured for all cases studied. Furthermore, it was preliminary shown that soot levels follow fuel consumption variation for all cases. The results were also reproduced with two comprehensive detailed kinetic mechanisms, with the adoption PAH models.

As far as the major pyrolysis products are concerned, the numerical predictions came in very close agreement with experimental results. Methane and natural gas pyrolysis yielded hydrogen of the order of 20% in the temperature range of 1200 ᵒC, whereas the numerical results under predicted this potential. In the case of N_2/CO_2 atmosphere, hydrogen production was suppressed and CO was also present at the exhaust of the reactor. Key species for soot formation, such as ethylene, acetylene, allene and benzene were also measured and compared against numerical predictions. The numerical predictions captured the trends of the mixture behavior for all cases, but failed to accurately quantify benzene levels. The higher carbon content and reactivity of the natural gas mixture were reflected in soot measurements and the temperature threshold for soot formation was estimated or all cases studied. Furthermore, it was revealed that soot formed follows the fuel consumption trend at all cases. For assessing the synergetic effects appearing in soot formation processes of the different mixtures behavior a preliminary experimental study for PAH species was conducted.

Chapter references

Abián M, Giménez-López J, Bilbao R, Alzueta MU. Effect of different concentration levels of CO_2 and H_2O on the oxidation of CO: Experiments and modeling. Proc. Combust. Inst. 2011; 33: 317–323.

Abián M, Millera A, Bilbao R, Alzueta MU. Experimental study on the effect of different CO_2 concentrations on soot and gas products from ethylene thermal decomposition. Fuel 2012; 91: 307-312.

Agafonov GL, Borisov AA, Smirnov VN, Troshin KYa, Vlasov PA, Warnatz J. Soot formation during pyrolysis of methane and rich methane/oxygen mixtures behind reflected shock waves. Comb. Sci. Technol. 2008; 180: 1876–1899

Alzueta MU, Glarborg P, Dam-Johansen K. Low temperature interactions between hydrocarbons and nitric oxide: An experimental study. Combust. Flame 1997; 109: 25–36.

Alzueta MU, Oliva M, Glarborg P. Parabenzoquinone pyrolysis and oxidation in a flow reactor. International J. Chem. Kinet. 1998; 30: 683–697.

Alzueta MU, Glarborg P, Dam-Johansen K. Experimental and kinetic modeling study of the oxidation of benzene. International J. Chem. Kinet. 2000; 32: 498–522.

Alzueta MU, Hernández JM. Ethanol oxidation and its interaction with nitric oxide. Energy Fuels 2002; 16: 166–171.

Alzueta MU, Borruey M, Callejas A, Millera A, Bilbao R. An experimental and modeling study of the oxidation of acetylene in a flow reactor. Combust. Flame 2008; 152: 377–386.

Appel J, Bockhorn H, Frenklach M. Kinetic modeling of soot formation with detailed chemistry and physics: laminar premixed flames of C_2 hydrocarbons. Combust. Flame 2000; 121: 122–136.

Arutyunov VS, Vedeneev VI. Pyrolysis of the methane in the temperature range 1000-1700K. Uspekhi Khimii Russian Chemical Reviews 1991; 60: 2663-2684.

Baulch DL, Bowman CT, Cobos CJ, Cox RA, Just T, Kerr JA et al. J, Evaluated Kinetic Data for Combustion Modeling: Supplement II. J. Phys. Chem. Ref. Data 2005; 34: 757-1359.

Bilbao R, Millera A, Alzueta MU, Prada L. Evaluation of the use of different hydrocarbon fuels for gas reburning. Fuel 1997; 76: 1401–1407.

Bermúdez V, Lujan JM, Pla B, Linares WD. Effects of low pressure exhaust gas recirculation on regulated and unregulated gaseous emissions during NEDC in a light-duty diesel engine. Energy 2011; 36: 5655-5665.

Chen CJ, Back MH, Back RA. The Thermal Decomposition of Methane. I. kinetics of the Primary Decomposition to C2H6 + H2; Rate Constant for the Homogeneous Unimolecular Dissociation of Methane and its Pressure Dependence. Can J. Chem. 1975; 53: 3580–3590.

Chen CJ, Back MH, Back RA. The thermal decomposition of methane. II. Secondary reactions, autocatalysis and carbon formation; non-Arrhenius behavior in the reaction of CH_3 with ethane. Can. J. Chem. 1976; 54: 3175–3184.

Dagaut P and Nicolle A. Experimental and detailed kinetic modeling study of hydrogen-enriched natural gas blend oxidation over extended temperature and equivalence ratio ranges. Proc Combust Inst 2005;30:2631–2638.

Du DX, Axelbaum RL, Law CK. The influence of carbon dioxide and oxygen as additives on soot formation in diffusion flames. Symposium (International) on Combustion 1991;23:1501-1507.

Esarte C, Millera Á, Bilbao R, Alzueta MU, Gas and soot products formed in the pyrolysis of acetylene–ethanol blends under flow reactor conditions, Fuel Process. Technol. 2009;90:496–503.

Esarte C, Callejas A, Millera A, Bilbao R, Alzueta MU. Influence of the concentration of ethanol and the interaction of compounds in the pyrolysis of acetylene and ethanol mixtures, Fuel 2011;90: 844–849.

Esarte C, Peg M, Ruiz MP, Mellera Á, Bilbao R, Alzueta MU. Pyrolysis of ethanol: Gas and soot products formed. Ind Eng Chem Res 2011;50:4412-4419

Gazi A, Vourliotakis G, Skevis G, Founti MA. A modelling study of allene and propyne combustion in flames, in: Fifth European Combustion Meeting ECM2011, Cardiff, UK, 2011.

Glarborg P, Alzueta MU, Dam-Johansen K, Miller JA. Kinetic modeling of hydrocarbon/nitric oxide interactions in a flow reactor. Combust. Flame 1998;115:1–27.

Hidaka Y, Sato K, Henmi Y, Tanaka H, Inami K. Shock-Tube study of methane pyrolysis and oxidation. Combust. Flame 1999;118:340–358.

Kee RJ, Rupley FM, Miller JA. Chemkin-II: A fortran chemical kinetics package for the analysis of gas-phase chemical kinetics. Sandia National Laboratories Report SAND 1991;87-8215.

Keramiotis Ch, Vourliotakis G, Skevis G, Founti MA, Esarte C, Sánchez NE, Millera A, Bilbao R and Alzueta MU. Experimental and computational study of methane pyrolysis in a flow reactor under atmospheric pressure. Energy. 2012;43:103–110.

Liso V, Olesen AC, Nielsen MP, Kær SK. Performance comparison between partial oxidation and methane steam reforming processes for solid oxide fuel cell (SOFC) micro combined heat and power (CHP) system. Energy 2011; 36: 4216-4226

Liu F, Guo H, Smallwood GJ, Gulder O. The chemical effects of carbon dioxide as an additive in an ethylene diffusion flame: Implications for soot and NOx formation. Combust. Flame 2001; 125: 778–787.

Lindstedt RP, Skevis G. Chemistry of acetylene flames. Combust. Sci. Technol. 1997;125: 73–137.

Lindstedt RP, Skevis G. Molecular growth and oxygenated species formation in laminar ethylene flames. Proc. Combust. Inst. 2000; 28: 1801-1807.

Mendiara MT, Oxidación de hollín (soot) obtenido por pirólisis de hidrocarburos gaseosos y su interacción con NO, Doctoral Thesis, Zaragoza, Spain, 2006.

Momirlan M, Veziroglu TN. Current status of hydrogen energy. Renew. Sustain. Energy Rev. 2002; 6: 141–179.

Natelson RH, Johnson RO, Kurman MS, Cernansky NP, Miller DL. Comparison of reactivity in a flow reactor and a single cylinder engine. Exp. Therm. Fluid. Sci. 2010; 34: 928–932.

Olsvik O, Rokstad, Holmen A. Pyrolysis of methane in the presence of hydrogen. Chem. Eng. Technol. 1995; 18: 349–358.

Ruiz MP, Guzmán de Villoria R, Millera A, Alzueta MU, Bilbao R. Influence of different operation conditions on soot formation from C2H2 pyrolysis, Ind Eng Chem Res 2007;46:7550–7560.

Sánchez NE, Callejas A, Millera Á, Bilbao R and Alzueta MU. Determination of Polycyclic Aromatic Hydrocarbons (PAH) Absorbed on Soot Formed in Pyrolysis of Acatylene at Different Temperatures, Chemical Engineering Transactions 2010;22:131–136

Sánchez NE, Callejas A, Millera Á, Bilbao R and Alzueta MU. Formation of PAH and soot during acetylene pyrolysis at different gas residence times and reaction temperatures. Energy. 2012;43(1):30–36.

Sánchez NE, Callejas A, Millera Á, Bilbao R and Alzueta MU. Polycyclic Aromatic Hydrocarbon (PAH) and Soot Formation in the Pyrolysis of Acetylene and Ethylene: Effect of the Reaction Temperature. Energy Fuels 2012;26:4823-4829

Slavinskaya N, Frank P. A modelling study of aromatic soot precursors formation in laminar methane and ethene flames. Combust. Flame 2009; 156: 1705–1722.

Sun Qi, Tang Y, Gavalas GR. Methane pyrolysis in a hot filament reactor. Energy Fuels 2000; 14: 490– 494.

Tan Y, Dagaut P, Cathonnet M, Boettner JC. Pyrolysis, oxidation and ignition of C1 and C2 hydrocarbons - Experiments and modeling. J. Chim. Phys. PCB 1995; 92:726–746.

Tan Y, Dagaut P, Cathonnet M, Boettner JC. Oxidation and ignition of methane-propane and methane-ethane-propane mixtures: Experiments and modeling. Comb. Sci. Technol. 1994; 103:133–151.

Vourliotakis G, Skevis G, Founti MA. A detailed kinetic modelling study of benzene oxidation and combustion in premixed flames and ideal reactors. Energy Fuels 2011; 25: 1950–1963.

Vourliotakis G, Skevis G, Founti MA. Combustion chemistry aspects of alternative fuels reforming for high-temperature fuel cell applications. Int J Hydrogen Energy Int J Hydrogen Energy 2012;37:16649–16662

Yang B, Li Y, Wei L, Huang C, Wang J, Tian Z, Yang R, Sheng L, Zhang Y, Qi F. Proc Combust Inst 2007;31:555–563.

Zhang X, Chan SH, Li G, Ho HK, Li J, Feng Z. A review of integration strategies for solid oxide fuel cells. J. Power Sources 2010; 195: 685-702.

Zink F, Lu Y, Schaefer L. A solid oxide fuel cell system for buildings. Energy Convers. Manage. 2007; 48: 809–818.

Chapter 5

Implementation of laser induced fluorescence technique in fundamental premixed combustion systems.

Combustion diagnostics have been used in systems as diverse as Bunsen flames and full-scale power plants. The necessity of nonintrusive diagnostic methodologies has been explicitly justified in previous chapters. Chapter 3 described the technique of laser induced fluorescence (LIF) along with the experimental configuration utilized and the methodology developed for hydroxyl radical detection in flames. Following the proposed methodology the flame front can be characterized, serving as a useful indicative tool for flame stabilization and heat release. However, before incorporating this methodology in complex combustion systems (see chapter 7), it is essential to evaluate the system's performance in fundamental applications of moderate complexity. The present chapter is covering the gap between the system and method development and their implementation in state-of-the-art burners, so as to certify the validity of the approach. Simple fundamental applications for laser-based diagnostic tools can include a variety systems from

laminar to turbulent flames, with however some common denominators; the easy of optical access and the stationary (mean) flow field. However the variability of mean stream lines influences the flame characteristics, implying a nontrivial coupling between the flow field and the flame. Furthermore, for the purposes of such studies, the flame two-dimensionality is a prerequisite for the evaluation of planar optics strategies. In order to achieve the chapters' goals, two simple configurations have been utilized among the various configurations proposed in the literature; a Bunsen-type flame and a simple cross-flow mixing jet flame. The results demonstrate that the followed methodology captures satisfactory the flame front and can be further used for numerical simulations or system calibration.

5.1.   Fundamental flame configurations for optical measurements

Fundamental flames investigations are commonly used to validate and improve modern diagnostic tools performance and more specifically laser induced fluorescence configurations. These flames are characterized by simple geometries, convenient optical access and physically or artificially stationary flow fields (when not under study), allowing numerical reproduction of the results and eventually leading to the optimization of both numerical and experimental methodologies.

One dimensional flames are often used for the latter reasons, with the well-known McKenna burner being the most commonly used configuration for flat flame investigations (Migliorini *et al.*, 2008). McKenna burner configurations have been studied over the past, utilizing a variety of traditional spectroscopic methods (Etzkorn *et al.*, 1992), as well as for introducing and calibrating modern optical techniques (Sutton, *et al.*, 2006). The design simplicity and the wide stable operation regime, along with the burners' capability to resemble large scale flat flame configurations, constitute the McKenna burner an attractive technology among other premixed flame, NO_x reduction technologies. NO_x formation mechanism on a McKenna burner has been extensively studied, both numerically and experimentally by means of nonintrusive techniques, for methane flames (Juchmann *et al.*, 1998), hydrogen enriched methane flames (Sepman *et al.*, 2008) and natural gas blends (Mokhov and Levinsky, 1996). However, despite the fact that McKenna burners are producing low NO_x exhaust levels, the flame stabilizes at the burner surface rather than inside of a porous material, hence presenting reduced efficiency in comparison to porous radiant burners, which are examined in detailed in chapter 7.

Additionally, although the present thesis investigates premixed combustion systems, it is worth mentioning some outstanding fundamental diffusion flame configurations, frequently met in the literature for optical and more specifically LIF measurements. Methane based mixtures have been studied over the past decades in simple flames, such as co-flow burners (Plessing *et al.*, 1998) and inverse diffusion flame configurations (Stelzner *et al.*, 2012), or even Wolfhard-Parker slot burners (Garman and Dunn-Rankin, 1998). Specifically, LIF measurements have been performed for measuring stable species (Norton *et al.*, 1993), radicals, such as hydroxyl radical (Smyth *et al.*, 1985) as well as other important combustion products, as is NO (Smyth, 1995) and formaldehyde (Harrington and Smyth, 1993) profiles above Wolfhard-Parker slot burners.

Finally, for the case of turbulent premixed flames, the conceptually ideal configuration of a steady plane turbulent premixed flame with a constant normal velocity flow cannot be stabilized on a burner because the inherent non-uniformities of the turbulent flow will always destroy the planar configuration (Chen *et al.*, 1996). Therefore, one must choose among several other, at least two-dimensional, configurations for a laboratory study of premixed turbulent combustion such as, rod stabilized V-shaped flames, wall-stabilized stagnation flames, edge-stabilized flames (Micka and Driscoll, 2012), swirl-stabilized flames (Day *et al.*, 2012), bluff-body (recirculation bubble) stabilized flames or rim (pilot flame)-stabilized conical flames (Bunsen burner), with freely propagating flames being also an option allowing the avoidance of flame stabilizer effects (Videto and Santavicca, 1990). For all these flame configurations, the mean flow field is stationary, making the numerical predictions easier and facilitating the investigation of the interaction of flame propagation and turbulence structure.

5.1.1.   Indicative Bunsen-type flame front imaging using OH-LIF

The Bunsen type conical flame is a classic configuration for fundamental combustion research. However, Bunsen-type flames, if stabilized by the burner rim, are unstable and blow-off easily under fuel-lean and high flow rate conditions. Although the use of a pilot flame can extend the operating range, in many cases the emissions from the pilot alter the overall flame emissions and can hinder research on ultra-lean premixed combustion systems (Johnson *et al.*, 1998). Nevertheless, flames from Bunsen-type burners are by far the most studied turbulent flames in the literature. Bunsen-type flame configurations have been extensively studied in the past, with the usage of nonintrusive diagnostic techniques, investigating the flame stabilization mechanisms (Lacour *et al.*, 2008). Specifically, the OH-LIF technique has been used, for studies of turbulence intensity in premixed Bunsen flames (Mansour *et al.*, 1998), among other optical techniques also utilized over the last years (Pfadler *et al.*, 2004). There are also studies investigating the latter phenomena using LIF excitation of other important combustion intermediates, such as NO (Mokhov and Levinsky, 1999) or coupled CH and OH radicals LIF (Nogenmur *et al.*, 2010) or even exploiting their research with OH-LIF in practical applications, such as internal combustion engines (Deschamps *et al.*, 1996).

In the present section, the hydroxyl radical detection scheme presented in the paragraph 3.2 is applied for the study of a Bunsen-type flame. This part of the thesis mainly focuses on evaluating the methodology earlier described, with respect to the accuracy of capturing the flame front characteristics and does not discuss the turbulent flame structure since the latter is beyond the scope of the present thesis. The work presented here serves as an indicative study that assists the reader in the familiarization with the OH-LIF technique for the flame visualization. Additionally, it serves reference purposes, as it introduces a typical Bunsen-type flame shape which is of high importance in comprehending the discussion in chapter 7, concerning the optics positioning above the flame trap and inside a porous inert medium burner (see paragraph 7.2.1).

Figure 5.1 presents single shot (left) and averaged mean of two hundred single shot normalized OH-LIF images (right) for a typical Bunsen-type flame. The turbulent premixed conical flames

presented in the figure below were produced by an axisymmetric Bunsen-type burner with a nozzle diameter of approximately 20 mm. Premixed turbulent stoichiometric propane-air flames were stabilized by a propane pilot flame. The instantaneous flame fronts were visualized by planar laser-induced fluorescence of the OH radical. The irregular, random, turbulent structure of the flame is clearly captured in the single shot OH-LIF image, especially in the inner part of the flame where the fuel/air mixture is introduced. Moreover, the coaxial flame fronts, where the OH radicals greatly produced, are also satisfactory captured. However, this is even clearer with the averaged OH imaging where the inner irregular flame front is diminished, implying that the main heat release is produced in the coaxial direction. The latter is also useful for calculating the burning velocities through the cone angle, as proposed in the literature (Yamamoto *et al*., 2009). It is finally stated that the results concerning the mean OH profiles although not capturing the total flame height due to the laser sheet insufficient width, are in fine agreement with the OH radical profiles found in the literature for various equivalent/normalized distances above the burner (Gülder *et al*., 2000), as well as with literature studies using also, besides OH-LIF, other techniques, such as chemiluminescence for the OH radical detection (Hardalupas *et al.,* 2004). However, no further analysis is attempted here, since one the one hand, such flames have been systematically examined as explained earlier and on the other hand the scope of the paragraph, *i.e.* the LIF system validation, will be accomplished in simpler laminar cross-jet flame as shown in the next section, where the complex turbulent interactions are avoided.
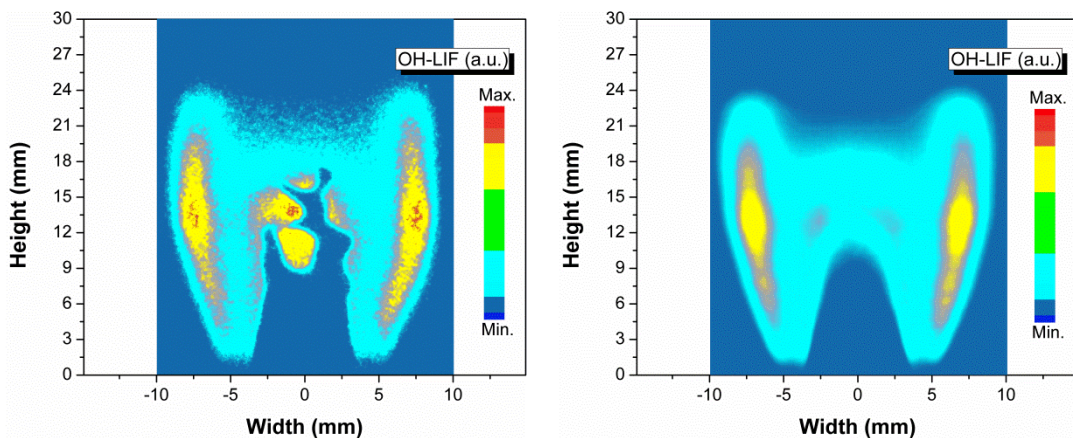
Figure 5.1 Single shot (left) and averaged mean normalized OH-LIF images (right) for a typical Bunsen flame

5.2. Premixed, cross-flow mixing hydrogen/air flame

As stated earlier, the development of a novel experimental procedure necessitates its evaluation in simple, fundamental applications. The presented Bunsen-type flame indicatively introduced the detection scheme followed for the flame front visualization, through monitoring the hydroxyl radical induced fluorescence. The present section extends the previous investigation and, at the same time, introduces the parametrical methodology for the study of flame shape characteristics with respect to stoichiometry and power variation as, followed in paragraph 7.2.1.2, also serving as a reference case study compared to the results resented there. Moreover, the present paragraph being in line with Chapter 4, not only validates the developed nonintrusive diagnostic tools, but

attempts to expand this basic piece of research in the context of modern practical applications as described in paragraph 1.4.2. In this framework, a premixed flame with a cross-flow mixing configuration is investigated by means of laser induced fluorescence and the flame shape and height is discussed, in the context of hydrogen/air combustion, at varying stoichiometry and nominal thermal load. A premixed cross-jet flame does not have the inherent limitations of the Bunsen-type flame and it is therefore, herewith investigated. The chosen configuration is beneficial for the scope of the chapter, since the cross-flow mixing stage is expected to introduce a non-uniform spatial flame distribution, challenging in this way the diagnostic methodology to capture the flame shape variations.

As far as the choice of fuel for this study is concerned, the H_2/O_2 reaction system is fundamental in combustion science and has historically received significant attention due to both its fundamental importance for chemical kinetics and to energy conversion in a variety of applications. Since H_2 and the intermediate oxidation species are also dominant intermediate species in the oxidation of all hydrocarbon and oxygenated fuels, the H_2/O_2 mechanism not only forms an essential subset of any hydrocarbon or oxygenate oxidation mechanism but also contains a number of reactions whose rate constants are among the most sensitive for combustion predictions for all hydrocarbon and oxygenate fuels (Burke *et al.*, 2012). Furthermore, it can be anticipated that hydrogen-air mixtures combustion are ideal for validating the present diagnostic methodology since the investigation is performed via monitoring the hydroxyl radical, thus avoiding complexities from the interaction with hydrocarbon fractions.
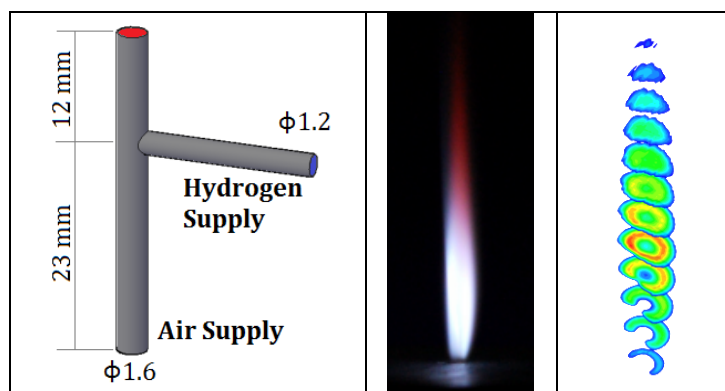
Figure 5.2 A schematic of the premixed jet flame configuration (left). Picture of the hydrogen flame from the jet-flame burner (middle) and OH-LIF scanning (right)

The burner itself, presented in Figure 5.2, is made of two crossed tubes, joined approximately seven equivalent diameters before the outlet, so as to maintain a laminar flow. All studied cases refer to flow conditions with maximum Reynolds number of the order of Re ≈ 1300, which by far ensure laminar flows. Additionally, the tubes were enclosed in a larger box, confining the vicinity of the burner tip, hence avoiding entrainment and disturbance of the flow from the surrounding air. Figure 5.2 also presents a picture of the hydrogen/air flame (middle) and 3D OH-LIF imaging (right), as firstly presented for the current setup (Werner, 2009). From this early study, it is clear that the fuel/oxidizer flows do not produce a three-dimensional, isotropic flame, due to the mixing configuration and this is analyzed in detail below.

5.2.1.   Qualitative OH-LIF results for cross-flow premixed flames

The present section presents qualitative hydroxyl radical concentration with the methodology described in section 3.2. It is here noted that contrary to the indicative OH-LIF profiles shown in paragraph 5.1.1, the height of the laser sheet was sufficient to totally enclose the flame. The primary result of this investigation concerns the depiction of the flame front and its altered characteristics with respect to thermal load and stoichiometry variation, serving as a means for evaluating the methodology as well as for introducing the parametric methodological approach, followed for complex systems in chapter 7. Furthermore, the configuration of the cross-jet induces an anisotropic flame shape, facilitating the study of its mixing efficiency.

All figures presented herein demonstrate the hydroxyl radical distribution for flames, above the burner's centerline or in other words with the laser sheet alignment placed so as to coincide with the flame inlet-hole diameter. A first parametric study concerns the flame characteristics as a function of the air supply *i.e.* the mixture's global stoichiometry. Both images in Figure 5.3 represent the OH distribution for a 5 kW thermal load hydrogen/air mixture, under (a) stoichiometric and (b) fuel-lean regime, namely fuel-air equivalence ratio of $\varphi = 0.5$ ($\lambda = 2$). It is here stated that since all flames were operating under laminar flow conditions, there is no necessity in presenting mean or averaged OH-LIF profiles as for the case of the Bunsen flame, which was briefly examined earlier in this chapter.
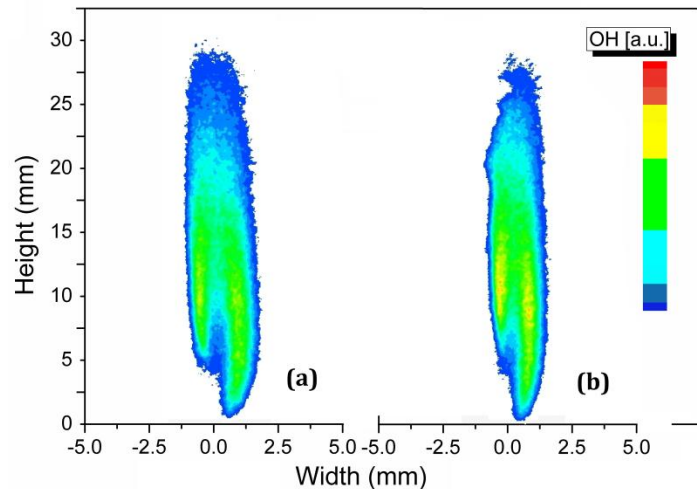
Figure 5.3 Normalized OH LIF for a thermal load of 5 kW and stoichiometry values of (a) $\varphi = 1$ and (b) $\varphi = 0.5$

The results reveal that the stoichiometric flame is nearly twice as thick compared to the one corresponding to an equivalence ratio of $\varphi = 0.5$, with the latter however requiring more height for the reaction completion. A more detailed observation reveals that the flame corresponding to an equivalence ratio of $\varphi = 0.5$, presents stronger signal intensity along the flame body with a signal peak area at a height of 5 to 10 mm. This behavior implies that the examined fuel-lean flame presents higher hydroxyl radical concentration, suggesting a more intense reaction zone. It can be anticipated that the latter behavior is mainly due to the increase of total mass flow rate, which is of the order of 60%. The additional mass flow rate directly correlates with the increase of the air

content in the mixture, hence stretching the flame, confining the reaction zone in a narrower window. Moreover, the described behavior is also noticeable at the mixing region side, where the stoichiometric flame is trying to maintain the Bunsen-like flame shape. On the other hand, the Bunsen-like flame shape is greatly diminished with the presence of higher air content, leading eventually the fuel-lean flame appearing as a lifted flame from the fuel supply side. Finally, it is here noted that the local peak hydroxyl radical concentration is of the same order for both flames, leaving the main difference lying on the OH distribution, as discussed earlier.

Continuing the cross-jet parametric investigation, the influence of thermal load variation is examined for flames under the same stoichiometry. Figure 5.4 presents qualitative hydroxyl radical profiles for four different flames under a constant global stoichiometry of $\varphi = 0.5$ ($\lambda = 2$) and thermal loads of (a) 2 kW, (b) 3 kW, (c) 4 kW and (d) 5 kW. This parametric investigation significantly differs from the previous mainly due to the fact that both fuel and air supplies change in order to maintain the desired conditions. As a matter of fact, the influence of the total air supply is highlighted in the first flame (Figure 5.4a) where the fuel is not confined by the air stream resulting the most axisymmetric flame among all studied cases. With increasing thermal load the flame symmetry is lost, with the fourth studied flame (Figure 5.4d) appearing the most distorted, especially in the region close to the burner inlet. Nevertheless, it is obvious that the flame front intensity, as monitored through the hydroxyl concentration, is enhanced with increasing the thermal load, as expected due to the enriched mixture enthalpy content. The reaction zone is also augmented in terms of flame height and width, due to the same reason, with an obvious tendency of reaching a threshold for complete conversion at approximately 20 mm. Finally, the phenomenal lifted flame from the fuel supply side is noticed here as well. Overall, this study showed that the system described in chapter 3 along with the proposed methodology, are able to capture flame characteristics with respect to various combustion parameters variation. The described, aforementioned approach is later used, in more complex systems $i.e.$ the porous inert medium burner in chapter 7, where also optical access and flame thermal radiation interaction issues arise.
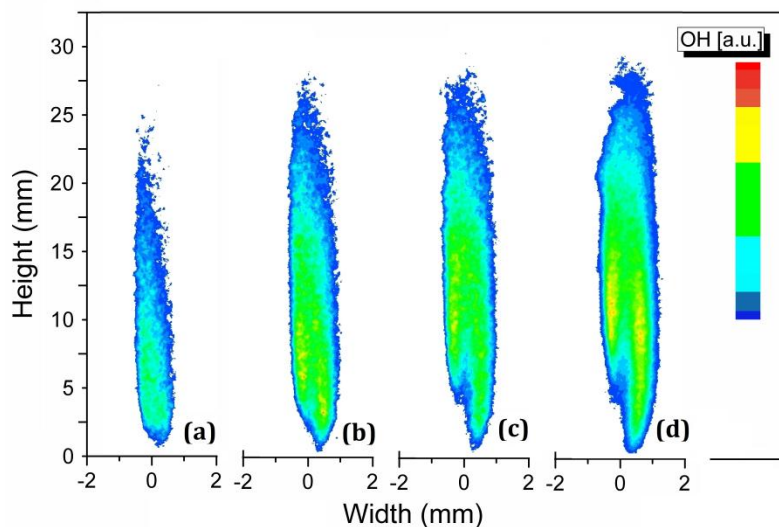

Figure 5.4 OH LIF imaging for constant stoichiometry of $\varphi = 0.5$ and varying thermal load of (a) 2 kW, (b) 3 kW, (c) 4 kW and (d) 5 kW

5.2.1.1. Supplemental investigation using acetone tracer-LIF

The present chapter concludes the cross-jet examination study, utilizing tracer laser diagnostics. Laser-induced fluorescence detection has been acknowledged as an ideal technique for tracer diagnostics. Tracer species molecules are electronically excited by absorbing a photon and spontaneous emission from the excited molecule is detected, typically representative of the local tracer concentration. There is, however, a strong influence of the bath gas on absorption, energy transfer in the excited state, and non-radiative relaxation from the excited state on signal intensities and spectral distribution. An interpretation of measured signal intensities therefore requires a detailed knowledge of the underlying photophysical processes, as long as significant changes of these processes are expected relative to the calibration system. The aforementioned issues however have been analyzed in detail in the literature (Shulz and Sick, 2005).

Ideally, the tracer should yield LIF signal intensities that are directly proportional to the desired quantity and should not be influenced by the ambient conditions. Unfortunately, signals from all fluorescent tracers show at least some dependence on local temperature, pressure, and bath gas variation. Therefore, in experiments where ambient conditions change in time or space, the underlying interdependencies with the tracer signal must be understood in order to obtain quantitative results. The pressure and compositions dependence of acetone laser induced fluorescence have been thoroughly reviewed in the literature (Thurber and Hanson, 1999), as well as its implications on temperature measurements (Thurber *et al.*, 1998).

The use of acetone feed as a tracer on combustion diagnostic studies have been introduced over the past decades (Lozano *et al.*, 1992). Acetone tracer LIF, gained attention for use in laser-induced fluorescence measurements of gas flows and especially for mixing efficiency validation (Lakshmanarao *et al.*, 2001). The absorption band of acetone is 225–320 nm, with a peak near 275 nm. Acetone can be excited by the fourth harmonic of the Nd:YAG laser at 266 nm and is noncorrosive, weakly toxic, and emits strong LIF. This enables flow images capturing with high temporal resolution, as well as to obtain enlarged images of the flow field with a high signal-to-noise ratio. Additionally, the stray light problem is avoided because of the large difference between laser and fluorescence wavelengths (Handa *et al.*, 2011). Here, the acetone molecule was excited using the forth harmonic of the Nd:YAG laser (section 3.1.2.1) at 266 nm with a maximum energy per pulse approximately 90 mJ. Although this wavelength does not correspond to the maximum acetone absorption region, the high energy achieved by the fourth harmonic, correspondingly results in high signal intensity. The detection was realized by adjusting a filter with transmission peak at 439 nm and FWHM 154 nm, hence taking advantage of the broad absorption/emission spectrum of acetone.

In the present section, the cold cross-flow mixing is investigated and the results are compared with a typical hydroxyl radical distribution from the flame. The latter investigation is essential for understanding the mixing efficiency of the described configuration, as well as for evaluating the previously obtained results. Acetone was introduced in the hydrogen flow so as for monitoring the fuel cold flow stream. It is here noted that since the experiments were conducted for cold flow conditions, the complexities described above *i.e.* pressure and temperature dependencies, are only limited in altering of the flow physical properties characteristics, when compared to the pure

hydrogen/air flow. In this concept it can be anticipated that the introduction of the acetone tracer in the air flow could be a better choice, but even the applied methodology is providing indicative results for the scope of the present paragraph. The desired acetone feed was achieved through controlling its evaporation when passing the hydrogen stream through an acetone vessel and simultaneously weighting its mass loss. The details for the experimental procedure have been described in detail in previous studies in the very same configuration (Werner, 2009).
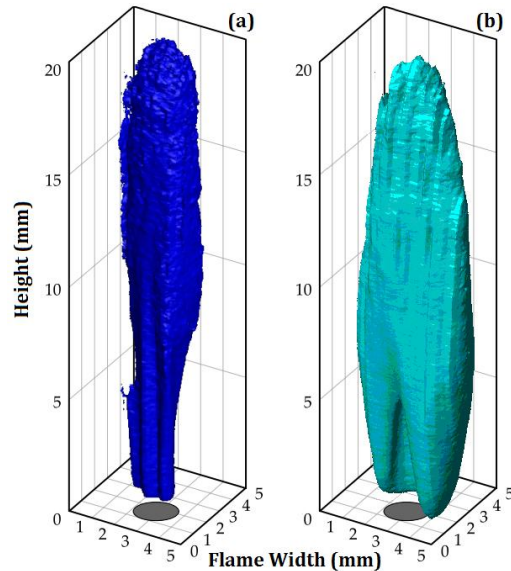
Figure 5.5 Iso-surface profiles for (a) acetone-tracer LIF and (b) OH-LIF above the burner

Figure 5.5 presents the three-dimensional obtained results for a (a) acetone tracer and (b) hydroxyl radical laser induced fluorescence. The three-dimensional structure was reproduced by integrating a series of planar images, obtained by moving the sampling probe parallel to the laser sheet. The conditions in the cold flow as well as the actual ones in the flame correspond to a flame of 5 kW thermal load operated in a stoichiometry of φ =0.5. The results shown in the figure above are indicative of the qualitative distribution, hence they are presented through the iso-surface of both acetone and hydroxyl obtained signals.

It is clear that mixing is not achieved in a three-dimensional isotropic way due to the cross-flow mixing configuration itself. As captured also in Figure 5.4d, hydroxyl radical concentration, opposite to the fuel side is absent, implying that the air stream acts as a barrier for the flame propagation at the specific volume. The acetone tracer LIF for the cold flow (Figure 5.5a), proves the validity of the latter statement, resembling the fuel stream distribution. In conclusion, it can be anticipated that, although a brief, indicative case study, the present paragraph comes in full agreement with previously obtained results, hence strengthening the validity of the proposed methodology.

5.3. Concluding remarks

The present chapter validated the performance of the previously described laser induced fluorescence detection system in simple fundamental applications. The hydroxyl radical laser

induced fluorescence methodology, described in section 3.2, and has been placed into practice in a simple cross-jet configuration. The setup was introduced earlier in the literature for similar studies (Werner, 2009) and was a part of an integrated innovative system (Voß and Trimis, 2009), similar to the one examined in chapter 7, with extension capabilities to the fuel cell research field. The results captured the OH radical distribution and revealed the inhomogeneous mixing induced from the cross-jet configuration. The latter, was also confirmed by supplementary examinations with acetone-tracer LIF by presenting three-dimensional, qualitative iso-surfaces for both hydroxyl and acetone LIF. Overall, the chapter familiarizes the reader with the hydroxyl radical profile in a premixed flame through an indicative Bunsen-like flame investigation, realized via monitoring the hydroxyl distribution along the flame. As far as the evaluation of the methodology is concerned, the hydroxyl radical distribution satisfactory captured the flame front, introducing also a parametric study for flame variation with respect to thermal loads and stoichiometry, which is followed also later in this thesis.

Chapter references

Burke MP, Chaos M, Ju Y, Dryer FL and Klippenstein SJ. Comprehensive H_2/O_2 kinetic model for high-pressure combustion. Int J Chem Kinet 2012;44:444-474

Chen YC, Petters N, Schneemann GA, Wruck N Renz U and Mansour MS. The detailed flame structure of highly stretched turbulent premixed methane-air flames. Combust Flame. 1996;107:223–224

Day M, Tachibana S, Bell J, Lijewski M, Beckner V and Cheng RK. A combined computational and experimental characterization of lean premixed turbulent low swirl laboratory flames I. Methane flames. Combust Flame 2012;159:275-290

Deschamps BM, Smallwood GJ, Prieur J, Snelling DR and Gülder ÖL. Surface density measurements of turbulent premixed flames in a spark-ignition engine and a Bunsen-type burner using planar laser-induced fluorescence. Symposium (Int) on Combustion 1996;26:427-435

Etzkorn T, Muris S, Wolfrum J, Dembny C, Bockhorn H, Nelson PF, Attia-Shahin A and Warnatz J. Destruction and formation of no in low pressure stoichiometric CH_4/O_2 flames. Symposium (Int) on Combustion 1992;24:925–932

Garman JD and Dunn-Rankin D. Spatial averaging effects in CARS thermometry of a nonpremixed flame. Combust Flame 1998;115:481-486

Gülder ÖL, Smallwood GJ Wong R Snelling DR, Smith R, Deschamps BM and Sautet JC. Flame Front Surface Characteristics in Turbulent Premixed Propane/Air Combustion. Combust Flame 2000;120:407-416

Hardaloupas Y, Orain M, Panoutsos CS, Taylor AMKP, Olofsson J, Seyfried H, Richter M, Hult J, Aldén M, Hermann F and Klignmann J. Chemiluminescence sensor for local equivalence ratio of reacting mixtures of fuel and air (FLAMESEEK). Appl Therm Eng 2004;241619–1632

Harrington JE and Smyth KC. Laser-induced fluorescence measurements of formaldehyde in a methane/air diffusion flame. Chem Phys Lett 1993;202:196-202

Handa T, Masuda M, Kashitani M and Yamaguchi Y. Measurement of number densities in supersonic flows using a method based on laser-induced acetone fluorescence. Exp Fluids 2011;50:1685–1694

Johnson MR, Kostiuk LW and Cheng RK. A Ring Stabilizer for Lean Premixed Turbulent Flames. Combust Flame 1998;114: 594–596

Juchmann W, Latzel H, Shin DI, Peiter G, Dreier T, Volpp HR, Wolfrum J, Lindstedt RP and Leung KM. Absolute radical concentration measurements and modeling of low-pressure $CH_4/O_2/NO$ flames. Symposium (Int) on Combustion 1998;27:469–476

Lacour C, Honore D, Boukhalfa A and Hauguel R. Stabilization mechanisms of laminar partially premixed from domestic like burner. Combust. Sci Tech. 2007;180-156-175

Lakshmanarao A, Renfro MW, King GB and Laurendeau NM. Acetone as a tracer for mixture fraction time-series measurements in turbulent non-reacting jets Exp Fluids 2001;30:595-596

Lozano A, Yip B and Hanson RK. Acetone: a tracer for concentration measurements in gaseous flows by planar laser-induced fluorescence Exp Fluids 1992;13:369-376

Mansour MS, Chen YC and Peters N. Highly Strained Turbulent Rich Methane Flames Stabilized by Hot Combustion Products. Combust Flame 1999;116:136-153

Micka DJ and Driscoll JF. Stratified jet flames in a heated (1390 K) air cross-flow with autoignition. Combust Flame 2012;159:1205-1214

Migliorini F, De Iuliis S, Cignoli F and Zizak G. How "flat" is the rich premixed flame produced by your McKenna burner?. Combust Flame 2008;153:384-393

Mokhov AV and Levinsky HB. A LIF and CARS study of the effects of upstream heat loss on NO formation from laminar premixed burner-stabilized natural-gas/air flames. Symposium (Int) on Combustion 1996;26:2147–2154

Mokhov AV and Levinsky HB. NO formation in a burnout region of a partially premixed methane-air flame with upstream heat loss. Combust Flame 1999;118:733-740

Nogenmyr KJ, Kiefer J Li ZS Bai XS and Aldén M. Numerical computations and optical diagnostics of unsteady partially premixed methane/air flames. Combust Flame 2010;157:915-924

Norton TS, Smyth KS , Miller JH and Smooke MD. Comparison of Experimental and Computed Species Concentration and Temperature Profiles in Laminar, Two-Dimensional Methane/Air Diffusion Flames Combust Sci Technol 1993;90:1-34

Pfadler S, Löffler M, Dinkelacker F and Leipertz A. Measurement of the conditioned turbulence and temperature field of a premixed Bunsen burner by planar laser Rayleigh scattering and stereo particle image velocimetry. Exp Fluids 2005;39: 375–384

Plessing T, Terhoeven P, Peters N and Mansour MS. An experimental and numerical study of a laminar triple flame. Combust Flame. 1998;115:335–353

Schulz C and Sick V. Tracer-LIF diagnostics: quantitative measurement of fuel concentration, temperature and fuel/air ratio in practical combustion systems. Prog Energ Combust Sci 2005;31:75–121

Sepman AV, van Essen VM, Mokhov AV and Levinsky HB. The effects of hydrogen addition on Fenimore NO formation in low-pressure, fuel-rich-premixed, burner-stabilized$CH_4/O_2/N_2$ flames Int J Hydrogen Energy 2008;331957–1964

Smyth KC, Miller JH, Dorfman RC, Mallard WG and Santoro RJ. Soot inception in a methane/air diffusion flame as characterized by detailed species profiles. Combust Flame 1985;62:157-181

Smyth KC. NO production and destruction in a methane/air diffusion flame. Combust Sci Tech 1996;115:151-176

Stelzner B, Hunger F, Voss S, Keller J, Hasse C and Trimis D. Experimental and Numerical Study of Rich Inverse Diffusion Flame Structure. Proc Comb Institute *10.1016/j.proci.2012.06.153*

Sutton G, Levick A, Edwards G and Greenhalgh D. A combustion temperature and species standard for the calibration of laser diagnostic techniques. Combust Flame 2006;147;39–48

Thurber MC, Grisch F, Kirby BJ, Votsmeier M and Hanson RK, Measurements and Modeling of Acetone Laser-Induced Fluorescence with Implications for Temperature-Imaging Diagnostics. Appl Opt 1998;37:4963-4978

Thurber MC and Hanson RK, Pressure and composition dependences of acetone laser-induced fluorescence with excitation at 248, 266, and 308 nm. Appl Phys B 1999;69:229–240

Videto BD and Santavicca DA. Flame-Turbulence Interactions in a Freely-Propagating, Premixed Flame. Comb Sci Tech. 1990;70:47-73.

Yamamoto K, Ozeki M, Hayashi N and Yamashita H. Burning velocity and OH concentration in premixed combustion, Proc Combust Inst 2009;32:1227–1235

Voß S and Trimis D. Investigation of a combined flame trap- and mixing- system as surface burner support for lean hydrogen air combustion. In: De Azevedo T, Weber R, Tognotti L, editors. Proceedings of the 10th Conference on Energy for a Clean Environment; 2009 July 07-09; Lisbon, Portugal.

Werner M. Experimentelle Untersuchungen zur teil-vorgemischten Verbrennung von Wasserstoff-Luftgemischen. Diplomarbeit Technische Universität Bergakademie Freiberg, Freiberg, Deutschland, 2009

Chapter 6

Investigation of innovative complex fuel mixtures using the validated diagnostic tools

Previous chapters described and analyzed the methodologies followed and validated their capabilities in fundamental applications, using common gaseous fuel mixtures. The present chapter attempts to extend the diagnostic capabilities of the aforementioned methodologies in complex fuel mixtures. A simplified approach is proposed in order to extract valuable information for such mixtures' combustion characteristics and performance.

The development of drop-in fuel mixtures is receiving increased attention by the engine fuel industry, providing also that alternative fuels produce a reduced environmental footprint (Rye *et al.*, 2010). However, the increasing use of synthetic fuels, such as Fischer-Tropsch (FT) products in various fields *i.e.* transportation and aviation, should be accompanied with an in-depth knowledge of their fundamental combustion characteristics, so as to demonstrate their advantages. This chapter deals with the characterization of innovative Fischer-Tropsch blends of varying

composition, in a simple laboratory scale burner. In order to perform the investigation of complex fuel mixtures, a variety of modern aviation Fischer-Tropsch blends were chosen. Appropriate aviation fuel choice is demanding as far as thermochemical and physical properties are concerned (Bruno and Smith, 2010a; 2010b) and this induces an additional challenge for the present work. Fischer-Tropsch process eased the production of fuels, lubricants and waxes facilitating alternative primary sources during the period prior and during the Second World War. Nowadays, Fischer-Tropsch synthetic fuels are becoming a major alternative energy carrier and have noticeable share in the global final energy mix regardless of the CO_2 policy (Takeshita and Yamaji, 2010), mainly due to their low transportation and refueling costs and their compatibility with infrastructure and end-use technologies for petroleum products. Aviation kerosene is a multi-component fuel with a carbon chain length of C_8–C_{16} (CRC, 2004). However, the chemical structure of the FT kerosene is significantly different from that of conventional kerosene consisting mainly of straight-chain alkanes with small quantities of non-alkane compounds and virtually no aromatic content. The effect of such chemical structure on combustion and emissions from gas turbine combustors is currently not accurately known. Fully paraffinic components of the FT kerosene do not meet the restrictions for density and thermal stability whereas naphthenic and aromatic compounds resolve those issues but act in favor of particulate matter emissions. The scope of the present section is not to access the fuel performance in modern gas turbines, but to demonstrate how a simple laboratory scale premixed burner coupled with the previously validated diagnostic tools, can be utilized in order to extract valuable information on the fuel characterization. This chapter compares several flames of Fischer-Tropsch (FT) fuels stabilized in a laboratory-scale premixed burner. A total of five fuels were assessed namely a neat, paraffinic FT blend, FT blends with varying aromatic and naphthenic content, along with a pure n-decane for reference purposes. All thermochemical properties where measured and calculated based on the detailed composition of each fuel and temperature profiles and emission measurements using the GC method described in section 2.1.3, were obtained.

6.1.   Alternative Fischer-Tropsch aviation fuels

The use of alternative, renewable fuels is expected to mitigate the effects of global warming, enhance environmental protection and increase diversity and security of energy supply (Gökalp and Lebas, 2004). The increasing demand for such fuels in the transport sector is linked to the availability of alternative fuels for gas turbines (Maurice *et al.*, 2001). Fischer-Tropsch (FT) kerosene offers substantial advantages as an alternative aviation fuel. It is physically similar to kerosene and thus compatible with current fuel storage and handling facilities. It is a sulfur-free fuel leading to complete elimination of SO_x emissions. Depending on the primary fuel source used in the FT process, FT kerosene can be classified as CTL (Coal-to-Liquid), GTL (Gas-to-Liquid) or BTL (Biomass-to-Liquid), which is also virtually CO_2 neutral.

As far as practical applications are concerned, there are several studies in the open literature dealing with the performance and emissions of FT fuels in gas turbine engines, such as Rolls-Royce T63 turboshaft (Timko *et al.*, 2010) and a Pratt and Whitney PW308 (Corporan *et al.*, 2007), suggesting that synthetic blends also demonstrate reduced particulate matter emissions in

comparison to commercial kerosene e.g. JP-8. Additionally, the usage of alternative synthetic fuels mixtures has been also demonstrated in auxiliary power units (Dewitt *et al.*, 2008), with equally satisfactory operational performance as with conventional fuels. Overall, it was shown that FT blends exhibited better atomization and mixing behavior when compared to conventional fuels and revealed improved ignitability (Rye and Wilson, 2012). Generally, there are even studies concluding that some fully synthetic paraffinic blends are the fit-for-purpose alternative aviation fuels (Moses and Roets, 2009). Furthermore, there are similar studies for diesel engines running on FT blends (Wu *et al.*, 2007). Generally, the use of FT blends has been shown to result in significantly reduced carbon monoxide, unburned hydrocarbons, nitrogen oxides and particulate matter emissions when compared to conventional diesel fuel (Abu Jrai *et al.*, 2006; 2009).

On the other hand, the potential use of FT fuels in engines requires a thorough understanding of their fundamental combustion properties. The accurate quantification, both experimental and numerical, of the combustion chemistry needs to be performed in well-controlled fundamental experimental configurations that resemble the operating conditions of practical combustion devices avoiding complexities from e.g. complex turbulence-chemistry interactions. Experimental investigations in such configurations include shock tubes (Kahandawala *et al.*, 2008), combustion bombs (Nguyen *et al.*, 2010; Wang, 2012) and rapid compression machines (Kumar and Sung, 2010) for ignition time delay measurements, constant volume champers (Azimov and Kim, 2008) and opposed-flow diffusion flames (Naik *et al.*, 2011) for laminar flame speed determinations (Kumar *et al.* 2011) and jet-stirred (Dagaut and Cathonnet, 2006) and flow reactors (Gokulakrishnan *et al.* 2003) and diffusion flames (Moss and Aksit, 2007) for species and soot (Saffaripour *et al.*, 2011, 2013) measurements.

Since FT is more a generic term than a specific fuel, it is expected that the physical properties and chemical composition of a particular blend will strongly affect combustion characteristics (Edwards and Maurice, 2001). Synthetic fuels are complex hydrocarbon mixtures albeit with a well-defined composition in contrast to distillate fuels, whose detailed composition may vary between batches. However, in order to meet the same specifications with conventional fuels, FT blends have a varying composition with respect to their paraffinic, naphthenic, aromatic and even oxygenated constituents. In order to assess this issue numerically, an enormous amount of effort is placed in simulating FT mixtures via coupling their chemistry with the appropriate surrogates (Humer *et al.*, 2007; Cooke *et al.*, 2005) hence, a number of model fuels have been proposed (Aksit and Moss, 2005; Dagaut *et al.*, 2006) in order to resemble their performance stability and emission behavior with the commercial kerosene.

In order to assess the effect of each constituent class on performance and emissions, experimental characterization of different fuels' combustion behaviour must be carried out in fundamental configurations, retaining the same global operating parameters *i.e.* thermal load and fuel/air ratio. An accurate determination of the above parameters requires a correct estimation of fuel heating value and molecular weight which, in turn, requires knowledge of their detailed composition. In this respect, a methodological approach is here formulated for calculating fuel heating value and molecular weight based on detailed mixture composition. The calculated heating values are used in the detailed experimental investigation of combustion characteristics of selected FT blends with

systematically varying paraffinic, naphthenic and aromatic content, which forms the core of the present work. Flame stability maps, temperature profiles and species concentration are obtained in a laboratory-scale premixed burner for a range of operating conditions, so as to facilitate the evaluation of each constituent species contribution to the overall fuel performance. Additionally, n-decane is used for benchmarking purposes.

6.2. Fuel analysis methodology and theoretical calculation of thermochemical properties

The FT blends studied, as well as commercial kerosene, are complex mixtures of C_7-C_{17} hydrocarbons, containing normal and iso-paraffins, naphthenic and aromatic compounds. In more detail, mono-, di- and tri-naphthenic (MN, DN, TN), mono- and di-aromatic (MoAr, DiAr), and napthenic- monoaromatic (NmoAr) compounds can be present. Figure 6.1 demonstrates a typical commercial kerosene mixture (Blakey *et al*., 2011) and neat paraffinic FT synthetic blend. All other blends studied in the present section, are mixtures with compositions among these two "extreme" blends *i.e.* from fully paraffinic blends with varying aromatic and naphthenic constituents.
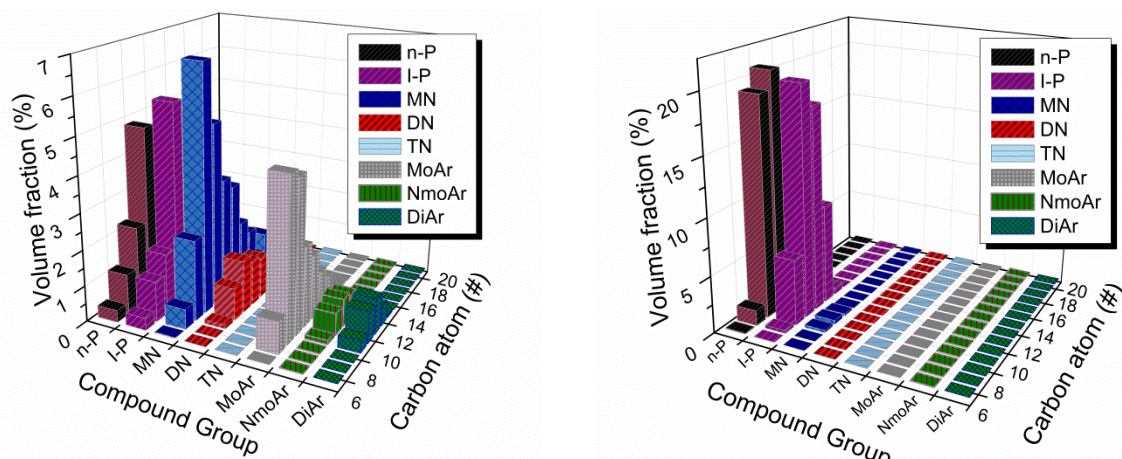
Typical composition of a Jet A-1 kerosene   Typical composition of a neat paraffinic FT fuel

Figure 6.1 Generic composition of the tested Jet A-1 (left) and the neat paraffinic FT synthetic fuel (right). (Jet A-1 approximate composition obtained from Blakey *et al*., 2011)

The high hydrogen to carbon ratio of paraffins gives a high heat to weight ratio whereas the naphthenic and aromatic compounds reduce the heat release per unit weight but also reduce the fuel freeze point which is a vital parameter for high altitude flight (Blakey *et al*., 2011). The generic composition of the FT blends examined here, is presented in Table 6-1. All blends were supplied by Shell Global Solutions (UK). The experimental determination of physical and chemical properties of the FT blends has been previously performed *and these data were available to the author. This included determination of fuel density, obtained with the IP365 †method, and heating values,

---

* ECATS – Environmentally Compatible Air Transport System. Project No. ANE-CT-2005-012284. Network of Excellence; Aeronautics (2010) [www.ecats-network.eu]
†The Institute of Petroleum (IP) IP 365 - Density & Relative Density of Liquids by Digital Density Meter, 2003.

obtained according to the ASTM D4809 *method, as well as the detailed composition data for all FT blends, obtained via two dimensional GC analyses. The mean mixture molecular formula and weight were calculated via the detailed composition data, following the following systematic methodology.

Table 6-1 Generic composition of blends under study

Fuel	Blend	Compound content
1	P	Paraffins (99%)
2	PAr	Paraffins (80%) + Aromatics (20%)
3	PN	Paraffins (60%) + Naphthenes (40%)
4	PNAr	Paraffins (50%) + Naphthenes (30%) + Aromatics (20%)

The mean mixture molecular weight and formula were calculated by formulating the equivalent stoichiometric reaction from the constituent species and the mixture (lower) heating value was calculated through the heat of formation of the equivalent stoichiometric reaction. The later allowed the usage of global parameters for controlling the experiments, as is the nominal thermal load and stoichiometry. Knowledge of the detailed composition is also beneficial in the assignment of an appropriate fuel surrogate for detailed chemical kinetic computations. In more detail, the required thermochemical properties can be calculated if the detailed composition in known, either in the form of mass or mole fraction, as follows. The mean mixture molecular weight is simply calculated by equation (6.1)

$$W = \left[\sum_{i=1}^{n} \frac{Y_i}{W_i} \right]^{-1}$$

Equation (6.1)

where, X_i, Y_i and W_i are the mole fraction, mass fraction and molecular weight of species i and W is the mean molecular weight of the mixture. The mole fraction of species i, accordingly calculated as

$$X_i = \frac{Y_i}{\frac{W_i}{W}}$$

Equation (6.2)

The equivalent molecular formula is obtained by formulating the stoichiometric reaction for each component, equation (6.3).

$$C_{x_i} H_{y_i} + v_{O_2}^i \left(O_2 + 3.76 N_2 \right) \longrightarrow v_{CO_2}^i CO_2 + v_{H_2O}^i H_2O + v_{N_2}^i N_2$$
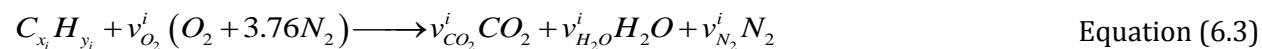
Equation (6.3)

The stoichiometric coefficients v^i for the equation (6.3) are obtained by the following expressions

$$v_{O_2}^i = \left(x_i + \frac{y_i}{4} \right), \ v_{CO_2}^i = x_i, \ v_{H_2O}^i = \frac{y_i}{2}, \ v_{N_2}^i = 3.76 \left(x_i + \frac{y_i}{4} \right)$$

Equation (6.4)

---

* American Society for Testing and Materials (ASTM). ASTM D4809 - Standard Test Method for Heat of Combustion of Liquid Hydrocarbon Fuels by Bomb Calorimeter, ASTM 2006

This leads to the equivalent mixture molecular formula C_xH_y, calculated by equation (6.5)

$$x = \sum_{i=1}^{n} X_i v_{CO_2}^i \qquad \& \qquad y = 2\sum_{i=1}^{n} X_i v_{H_2O}^i \qquad\qquad \text{Equation (6.5)}$$

Finally, the fuel blend (lower) heating value is then calculated using equation (6.6)

$$\Delta H^o{}_{f,mixture} = \sum_{n=1}^{i} X_i \left(v_{CO_2}^i \Delta H^o_{f,CO_2} + v_{H_2O}^i \Delta H^o_{f,H_2O} - \Delta H^o_{f,i} \right) \qquad \text{Equation (6.6)}$$

In total, Table 6-2 presents the calculated thermochemical properties for all tested fuels as they were obtained with the described methodology, based on the knowledge of their detailed composition and these values were used in all subsequent experiments

Table 6-2 Calculated thermochemical properties of tested fuel blends

Blend	MW [g]	Molecular Formula	ΔH_f [MJ/kg]
P	143.96	$C_{10.14}H_{22.25}$	44.64
PAr	141.51	$C_{10.08}H_{20.35}$	44.00
PN	171.44	$C_{12.18}H_{25.28}$	44.16
PNAr	160.10	$C_{11.48}H_{22.18}$	43.59

Determination of fuel heating value requires knowledge of the heat of formation of all constituent hydrocarbons. The CGxGC composition data reveals the species distribution with respect to carbon atom and constituent classes, *i.e.* paraffinic, naphthenic, aromatic etc., without determining the exact isomers present in the mixture (see Figure 6.1). In order to assign a heat of formation value to each constituent, its exact molecular structure must be known. The choice of the appropriate molecular structure poses some difficulties and is a potential source of error. The assumptions made in order to assign appropriate molecular structure are described below.

For n-paraffins a unique, unambiguous assignment is possible. Iso-paraffins were assumed to have a structure of 2-methylalkanes with a very good correlation of heat of formation values with carbon number, as shown in Figure 6.2. Additionally, the combustion chemistry of 2-methylalkanes has been extensively characterized recently in the literature (Sarathy et al., 2012). The mono-naphthenic isomers were assumed to have the structure of a straight, mono-substituted cyclohexane e.g. for the C_{10} naphthenic species, the butyl cyclohexane was chosen and so forth. The di-naphthenic isomers were assumed to have the structure of mono-substituted decahydro-naphthalene while the structure of 1,1-bicyclohexyl has been assumed for the C_{12} di-naphthenic species. A linear correlation between heats of formation and carbon numbers was also noted for the naphthenic compounds, as shown in Figure 6.2. Finally, the mono-aromatic compounds were assumed to have the structure of straight-chained, mono-substituted benzenes e.g. butyl benzene for C_{10}, and the di-aromatics the structure of straight-chained, mono-substituted naphthalenes.
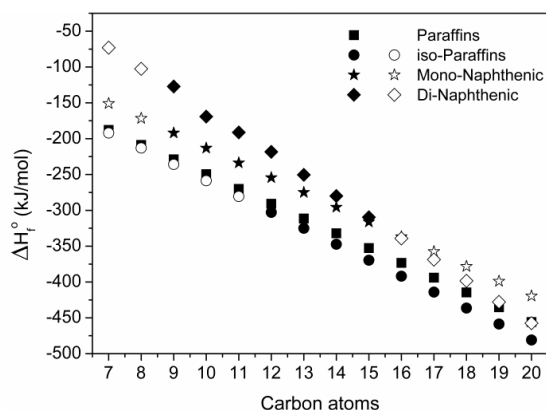
Figure 6.2 Normal and iso-paraffins, and mono and di-napthenes heat of formation values as a function of carbon atom number. Solid symbols represent values obtained from literature and blank symbols represent extrapolated values respectively..

After choosing the appropriate isomers, the heats of formation values of the constituent species were obtained using the literature database (Linstrom and Mallard, 2005), appropriate compilations (Poling *et al.*, 2005) or obtained using the group additivity method (Benson, 1976). In some cases, demonstrated in the present section, linear correlations between heating values of some constituent group compounds allowed extrapolation and these values are indicated separately. The paraffinic group constitutes a sticking example of a case where the linear correlation between the group species' heat of formation and their carbon atoms allows extrapolating values.
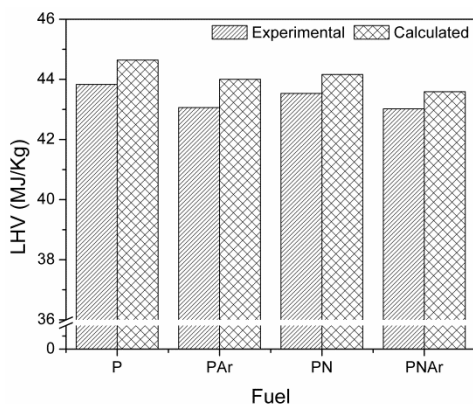
Figure 6.3 Measured and calculated (lower) heating values for the tested fuel blends

Calculated and measured heating values for all blends are presented in Figure 6.3. It is shown that the methodology satisfactory captures the measured trend in the heat of formation of all FT blends. However, the calculated values are systematically overestimated by approximately 2%. Further, the level of agreement deteriorates with increasing presence of paraffinic compounds in the blend (see Table 1). In order to explore the reason for this discrepancy, a sensitivity analysis on the choice of isomeric structure for each constituent group was performed. Indicative results for C_8H_{16} isoparaffins are presented in Table 6-3. It is apparent that the thermodynamic stability of a particular isomer increases as the size of the side chain(s) decreases and/or the topological

165

complexity increases. Thus, as shown in Table 6-3, the most stable isomer for C_8H_{16} is the tetramethyl-butane, which has a heat of formation approximately 5% lower than 2-methyl-heptane. One may argue that adopting the most thermodynamically stable isomer for each class, would result in a more accurate heating value calculation and may also be a more correct representation of the actual isomers mix. However, there are several reasons for not doing so. On the one hand, the choice of a complex side chain isomer induces difficulties in heat of formation determination, due to limited data availability in the literature and uncertainties in using the group additivity method. Moreover, there is no indication that the most stable isomer is the dominant one in each blend. Further, as the sensitivity analysis suggests, the adoption of the most stable isomer would result in severe under prediction of the mixture heating value.

Table 6-3 Heats of formation for selected C_8H_{16} iso-paraffin isomers (Linstrom and Mallard, 2005)

Species	Structure	ΔH_f^o [kJ/mol]	Uncertainty
Heptane, 2-methyl-		-215.5	±1.3
Heptane, 3-methyl-		-212.6	±1.1
Heptane, 4-methyl-		-212.1	±1.2
Hexane, 2,4-dimethyl-		-219.4	±1.1
Hexane, 3,4-dimethyl-		-213	±1.5
Hexane, 2,2-dimethyl-		-224.7	±1.1
Hexane, 3,3-dimethyl-		-220.1	±1.1
Butane, 2,2,3,3-tetramethyl-		-226.2	±1.9

The above discussion highlights that the adopted methodology can produce reliable and consistent heating values calculation for all blends. The reported 2% margin in blends heating value calculation is reasonable given all the aforementioned uncertainties. Moreover, since the constituent species assignment is the same for all blends, the resulting uncertainty is systematic and does not affect fuel comparison under the same conditions.

6.3. Sampling and coupling apparatus with a laboratory-scale premixed flame burner

Experimental investigations were performed in a laboratory-scale premixed burner (Figure 6.4). A simplified schematic diagram of the burner configuration for the fuel and air supply along with the fuel evaporation system is also shown in Figure 6.5. The burner consists of a glass base which leads

to the burner main body, the stem. The latter is connected to a prismatic flame holder, located at the tip of the stem and having a length of 20 mm and a width of 2 mm. The burner itself is approximately 42 cm tall with a base diameter of 13 cm and stem diameter of approximately 3 cm. The burner assembly sits on a lab-hotplate (Heater 1), maintained at an independently-set temperature, which heats up the base.

The flame holder (a), stem (b), base (c) & fuel/air nozzle (d).	Configuration for temperature and emission measurements.	Flame sampling setup. Probe above the flame holder.	Burner in operation, with base hotplate exposed.
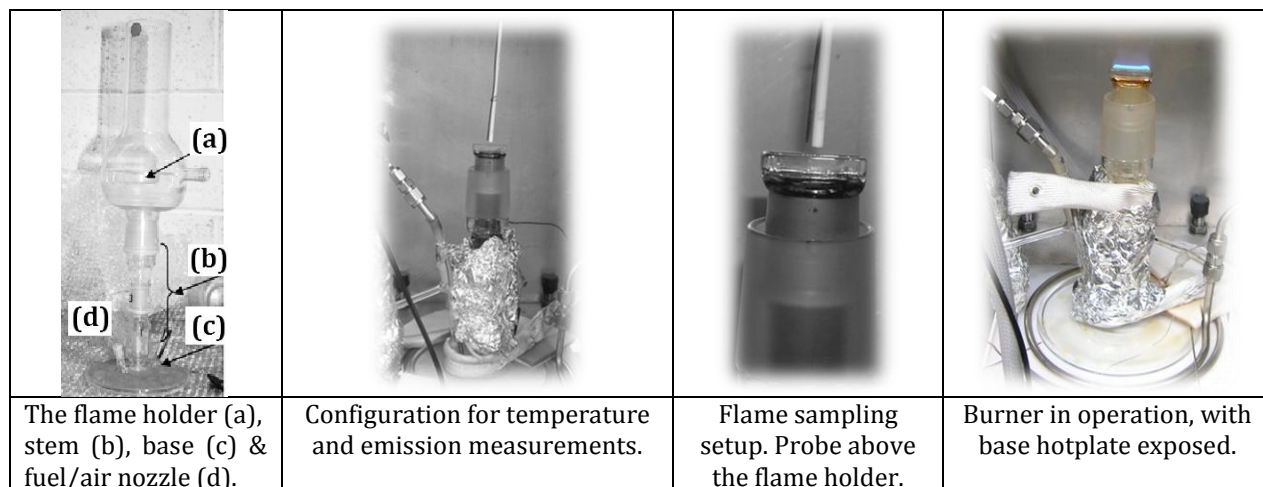
Figure 6.4 The burner assembly configuration

Air was preheated by passing through a spiral coil which also sat on top of the hotplate. The preheated air was then directed to the outer tube of a coaxial, capillary glass heat exchanger. Fuel was fed through an automated syringe pump (Graseby 3100 Syringe Driver) into the inner tube of the capillary heat exchanger. The nozzle of the capillary heat exchanger was located near the burner base.
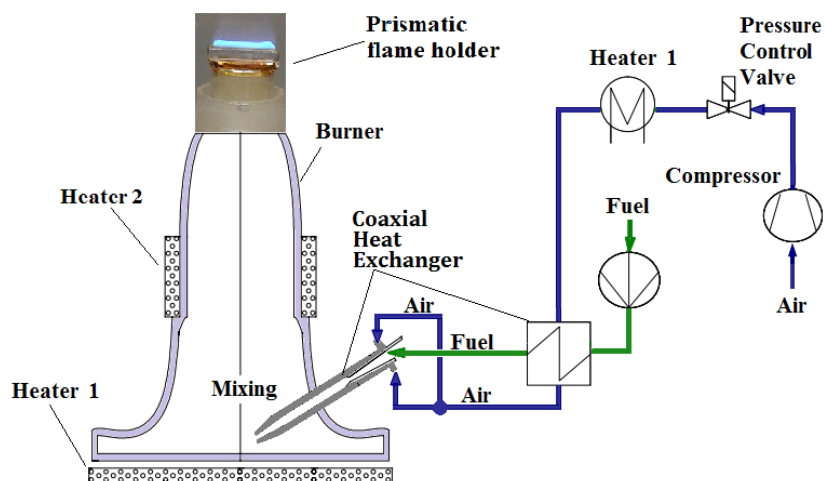
Figure 6.5 Schematic diagram of the burner configuration

Fuel vaporization is initiated inside the capillary heat exchanger and is completed as the fuel/air mixture enters the burner. In order to reduce the heat losses and achieve sufficient control over the evaporation process a second heater was utilized, consisting of a thermal resistor/controller

167

(Heater 2), covered with insulating material. The liquid fuel supply at the syringe was varied from 15 to 30 ml/h, depending on the particular case, while the air supply varied from 2 to 4 l/min. The fuel/air mixture was subsequently ignited by a pilot flame and stabilized on the burner flame holder. Complete fuel evaporation, coupled with constant fuel and air supply rates, are crucial factors for maintaining the same stoichiometry and thermal power for all experiments and avoiding periodic flame fluctuations due to droplet formation. In order to achieve complete fuel evaporation, the temperature at the nozzle vicinity must exceed the fuel boiling point. On the other hand, an extreme temperature at the above location is highly possible to cause fuel cracking and even autoignition. In order to accomplish complete fuel evaporation and at the same time avoid the above issues the temperature of Heater 1 was set at 670 K and at the Heater 2 at 500 K.

6.4.   Combustion performance evaluation of the FT blends

For the evaluation of the different fuel performances on the lab scale premixed burner described, temperature profiles and emission measurements were obtained. An Aluminum Oxide (Al_2O_3) ceramic sampling probe of 3 mm external diameter along with a thermocouple attached to monitor the temperature at the edge of the probe, were used. The sampling was realized through the probe by a peristaltic pump connected at the exit of the GC system. Temperatures were obtained along the main burner axis, using an S-type thermocouple with a ceramic insulated body, with a junction diameter of 350 μm, attached on a traversing system. Measurements were recorded over a distance of 25 mm above the burner, or in other words about 3.5 equivalent diameters. This corresponds to approximately 3.5 hydraulic diameters, defined as the diameter of a circle having the same area with the cross sectional area of the flame holder. Radiation losses were of the order of 250 °C, which is in agreement with the respective error from such thermocouple probes found in literature (Heitor and Moreira, 1993). Emission measurements were performed for selected cases with the gas chromatographic method developed (see section 2.1.3).

Figure 6.6 Indicative flame stability map for all fuels, on a simple premixed burner configuration

An extensive stability mapping was performed in order to define the flame extinction limits for all six fuels, as a function of the fuel and air supply. As an example, the f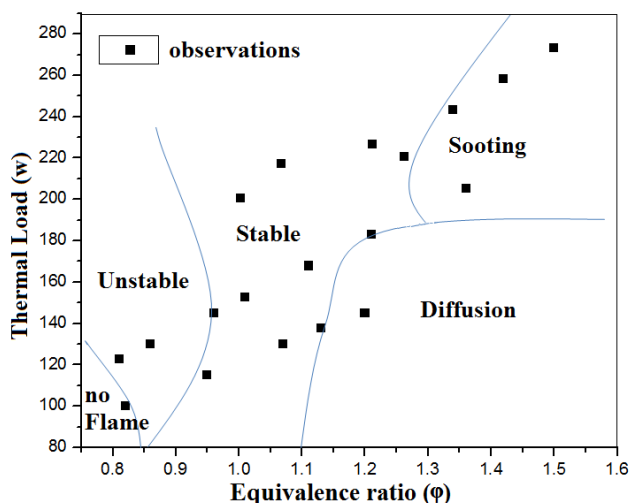lame stability map with blend P is presented in Figure 6.6. Overall, the flame stability mapping indicated that the burner was capable of operating near stoichiometric conditions, maintaining a short blue laminar flame on top of the flame holder. It was rather difficult to maintain a stable flame in under-stoichiometric regimes and impossible to ignite for equivalence ratios lower than $\phi \leq 0.8$. As fuel supply rates increased towards fuel-rich flames, fuel vaporization was found to be incomplete, resulting in the formation of a diffusion flame that rapidly became unstable and fluctuating, eventually leading to soot formation at stoichiometries much lower than those normally expected for paraffinic mixtures, namely with equivalence ratio of only $\phi \geq 1.4$. Consequently, the cases studied concerned equivalence ratios of $\phi = 1$ and $\phi = 1.2$ under 150 W and 200 W nominal thermal load. Although the limitations concerning burner operation resulted in a narrow burner stability window, the current setup provides consistent trends, facilitating the systematic analysis of the various tested blends.

Figure 6.7 Temperature distribution above the burner for $\phi = 1$ under 150 W (left) and 200 W (right) of nominal thermal load

Temperature and species profiles, presented here, originate from respective mean values obtained over ten time-averaged measurements, at each location. Error bars indicate the standard deviation of the instantaneous measurements from the mean values. The x-axis represents the dimensionless distance from the flame holder, normalized with the hydraulic diameter (D_{eq}) of the latter. The results presented here start from a height of 2 mm above the flame holder. It was impossible to obtain accurate temperature measurements closer to the flame holder, since the thermocouple tip blocked the thin slot of the flame holder, greatly distorting the flame local behavior. Temperature profiles along the burner main axis, for stoichiometric conditions and nominal thermal loads of 150 W (right) and 200 W (left), are shown in Figure 6.7 for all blends. The corresponding temperature profiles for $\phi = 1.2$ and the same thermal loads are shown in Figure 6.8. Under stoichiometric conditions temperature profiles exhibit a maximum in the vicinity of the flame holder and decay downstream of the burner, for all FT blends. For $\phi = 1.2$ the temperature profiles for the FT blends, reach a maximum value downstream of the flame holder, followed by a flat region and a smooth decay. Increasing the operating power from 150 W to 200 W at $\phi = 1$, results in higher maximum temperatures (of ca. 100 K) for both stoichiometries.

169

The above observations are valid for all FT fuel mixtures. Several further observations can be made from simple inspection of the above figures. These relate both to burner operation and fuel behaviour. For both thermal loads, maximum temperature values at ϕ = 1.2 are about 150 °C lower than those measured at stoichiometric conditions. A wider flame zone is observed at ϕ = 1.2, where the flame loses its thin prismatic shape and tends to behave as a diffusion flame (see stability map) with also higher temperature fluctuations recorded.
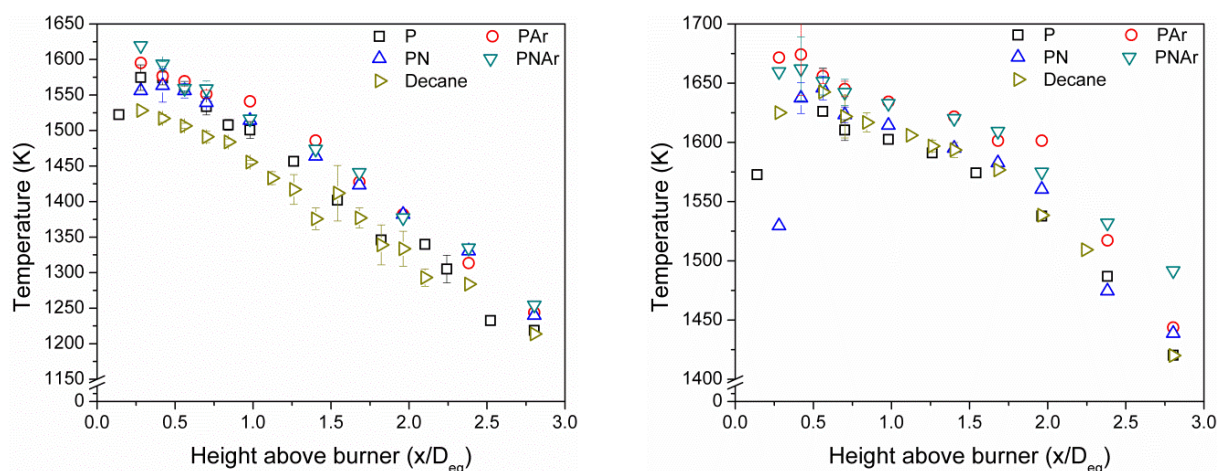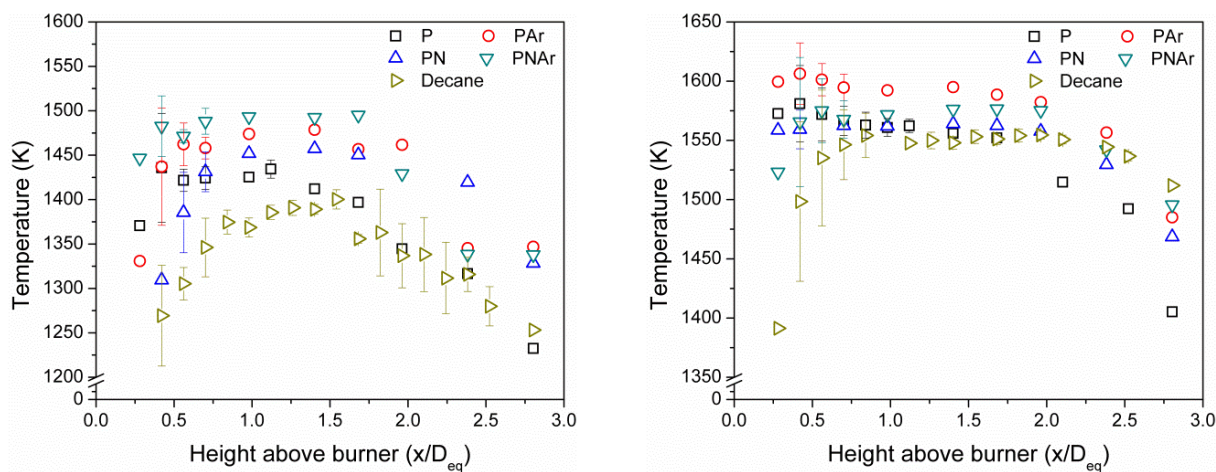

Figure 6.8 Temperature distribution above the burner for ϕ = 1.2 under 150 W (left) and 200 W (right) of nominal thermal load

Regarding the combustion performance of the fuels, all FT blends exhibit similar trends with significant quantitative differences. Overall, n-decane appears in all cases to yield the lowest temperatures, while the highest recorded temperatures are associated with aromatic-enriched FT blends. Among the FT blends, the lowest temperatures are associated with the neat paraffinic mixture (P) – with similar levels of normal- and iso- alkanes in its composition -, which also has similar temperatures to n-decane. The highest temperatures are recorded for the PAr mixture, which retains the relative normal- to iso- alkanes ratio. This suggests that the higher temperatures could be attributed to the increase of the aromatic content. Moreover, the temperatures of the naphthenic (PN) mixture are lower than those of the PAr although the naphthenic content of the former is twice the aromatic content of the latter, and the normal- to iso- alkanes ratio is unchanged. This may imply that the naphthenic components are less reactive than the aromatic ones. However, it cannot be inferred whether the temperature trends are just a reflection of differences in reactivity or whether synergistic effects are dominant. The above discussion is also valid for the naphthenic-aromatic blend (PNAr).

Emission measurements were performed for all blends under stoichiometric conditions and nominal thermal load of 200 W, at two locations above the flame holder. The first measurement point, chosen so as to 1/3 ofindicate the edge of the flame prism, was set at a distance of 1/3 D_{eq}. The measurements obtained at this location are referred as *flame emissions*. The second point was set at a distance equal to D_{eq} above the flame edge and the measurements obtained there are referred as *exhaust emissions*.

(a) **(b)**
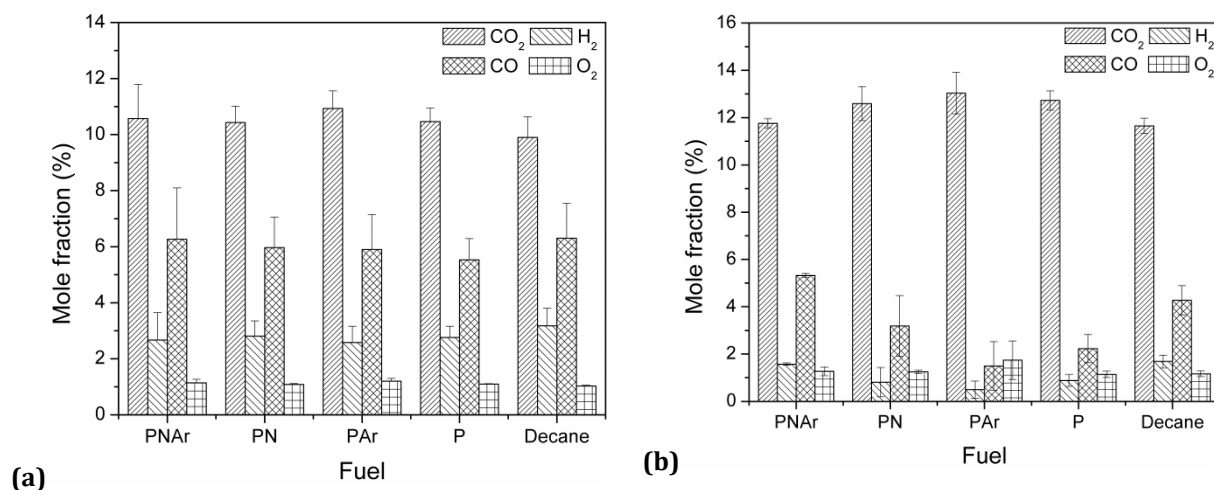
Figure 6.9 Flame emission measurements for $\phi = 1$ under 200 W of thermal load at a distance of $1/3d_{eq}$.

Figure 6.9a presents CO_2, H_2, CO and O_2 *flame emission* measurements. Oxygen levels are approximately 1% for all blends, suggesting low air entrainment and hence good sampling. All FT fuels and n-decane, are characterized by similar major species levels. A comparison of the measured *flame emission* CO_2 levels with the theoretical CO_2 levels obtained from the stoichiometric reaction for each fuel, can provide a measure of conversion efficiency. The P and PAr blends demonstrate the higher conversion rates as compared to the other fuels. Additionally, the naphthenic content appears to reduce mixture reactivity. These trends roughly scale with the ones obtained from temperature measurements. The same trends are more pronounced in the case of *exhaust emission* measurements (Figure 6.9b) mainly due to the fact that the reaction is more complete downstream the burner. The accurate quantification of exhaust emission results carries high risk, mainly associated with the fact that by moving downstream of the flow, the uncertainty of sampling from the same flame space or at the same flame timescale is greater. However, in agreement with the previous discussion, Figure 6.9 underlines that blends with naphthenic content exhibit higher CO and H_2 levels, and respectively higher CO_2 levels, than P and PAr blends. However, an important difference between the two set of measurements, is that for *flame emissions* significant hydrocarbon amounts were detected.
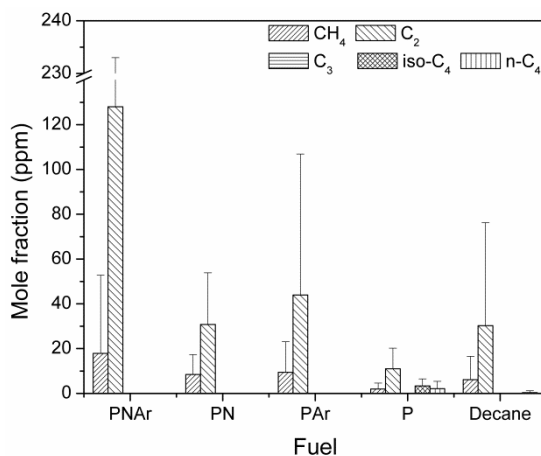

Figure 6.10 Exhaust emission measurements for $\phi = 1$ under 150 W of thermal load at a distance equal to d_{eq}.

Finally, Figure 6.10 presents measurements of hydrocarbon amounts detected at a distance of 1/3 D_{eq}. The signal to noise ratio was not satisfactory, resulting in large errors associated with the measurements. Nevertheless, it was clear, that paraffinic blend yields lower quantities of C_1-C_4 alkanes, appearing mainly as methane and C_2 isomers, with the latter being an order of magnitude higher than methane. On the other hand, the paraffinic blend yielded significantly different unburned hydrocarbons (UHCs) than n-decane. Additionally, the presence of aromatic compounds in the fuel composition seems to affect the UHC levels the most. Overall, the results concerning trends in measured temperatures, CO and CO_2 levels, as well as the unburned hydrocarbon quantities on the simplified premixed utilized configuration, are in good agreement with similar studies in diffusion flames

6.5.   Concluding remarks

The chapter focuses on the characterization of laboratory-scale premixed flames for several FT blends and an n-decane for benchmark purposes. The systematic variation of FT blends composition with respect to paraffinic, naphthenic and aromatic content, made possible the assessment of fuel mixing trends. An analytical methodology was followed in order to assign key thermochemical properties to all blends. Thermochemical properties were calculated from detailed composition and compared against experimental data, with good agreement. A sensitivity analysis was performed in order to assess the effect of the choice of isomers for each constituent class on the heating value of the fuel. An extensive flame stability mapping was realized for all blends, as a function of thermal power and stoichiometry, which provided a set of appropriate operating conditions for the detailed measurements. Temperature profiles were obtained along the burner symmetry axis and species emission measurements were performed at locations representative of flame and post-flame zones. Temperature measurements under same thermal loads and stoichiometry showed similar behaviour for all FT blends, exhibiting constantly higher temperatures than n-decane. Among FT fuels, the neat paraffinic blend results in the lowest temperatures, which increase with increasing aromatic content. Species measurements highlighted the similar behavior among all examined FT blends. It was also shown that the fully paraffinic blend results in the lowest UHC levels, whereas blends with aromatic and naphthenic content show the opposite tendency. Further comparison between the theoretically determined CO_2 levels reveals that fully synthetic paraffinic blends also result higher conversion rates and blends with aromatic, naphthenic, and naphthenic and aromatic compounds following with this order. Additionally, the results concerning trends in measured temperatures, CO and CO_2 levels, as well as the unburned hydrocarbon quantities on the simplified premixed utilized configuration, came in good agreement with similar studies in diffusion flames (Saffaripour *et al*., 2013). Finally, it has been demonstrated that simple laboratory scale combustion equipment, when used in a carefully controlled environment, can provide useful information about combustion characteristics of novel fuel. Overall, the present chapter underlines that the proper utilization of the combustion diagnostic tools developed in previous chapters, along with the knowledge of fundamental physical properties of the mixtures under study, can successfully extend their applicability in the research field of complex fuel mixtures, as far as their operational performance in laboratory scale burners is concerned.

Chapter references

Abu-Jrai A, Rodriguez-Fernandez J, Tsolakis A, Megaritis A, Theinmoi K, Cracknell RF and Clark RH, Performance, combustion and emissions of a diesel engine operated with reformed EGR. Comparison of diesel and GTL fuelling. Fuel 2009:88;1031-1041.

Abu-Jrai A, Tsolakis A, Theinmoi K, Cracknell RF, Megaritis A, Wyszynski ML and Golunski SE. Effect of Gas-to-Liquid Diesel Fuels on Combustion Characteristics,Engine Emissions, and Exhaust Gas Fuel Reforming. Comparative Study. Energ Fuel 2006:20;2377-2384.

Aksit IM and Moss JB. Model fuels to reproduce the sooting behavior of aviation kerosene. Fuel. 2005:84;239–245

Azimov U and Kim KS, Visualization of Gas-to-Liquid (GTL) Fuel Liquid Length and Soot Formation in the Constant Volume Combustion Chamber. J Therm Sci Tech-JPN 2008:3;461-473

Benson SW. Thermochemical Kinetics, John Wiley and Sons, N.Y. 1976

Blakey S, Rye L, Wilson CW, Aviation gas turbine alternative fuels: A review. Proc. Combust. Inst. 2011:33;2863-2885

Bruno TJ and Smith BL. Evaluation of the Physicochemical Authenticity of Aviation Kerosene Surrogate Mixtures. Part 1: Analysis of Volatility with the Advanced Distillation Curve. 2010:24;4266–4276.

Bruno TJ and Smith BL. Evaluation of the Physicochemical Authenticity of Aviation Kerosene Surrogate Mixtures. Part 2: Analysis and Prediction of Thermophysical Properties. 2010:24;4277–4284.

Cooke JA, Bellucci M, Smooke MD, Gomez A, Violi A, Faravelli T and Ranzi E. Computational and experimental study of JP-8, a surrogate, and its components in counterflow diffusion flames. Proc Combust Inst 2005:30;439-446.

Corporan E, DeWitt MJ, Belovich V, Pawlik R, Lynch AC, Gord JR and Meyer TR. Emissions Characteristics of a Turbine Engine and Research Combustor Burning a Fischer–Tropsch Jet Fuel. Energ Fuel 2007:21(5); 2615–2626.

CRC, Handbook of Aviation Fuels, Society of Automotive Engineers, 2004

Dagaut P and Cathonnet M. The ignition, oxidation, and combustion of kerosene: A review of experimental and kinetic modeling. Prog Energy Combust Sci 2006:32(1);48–92

Dagaut P, El Bakali A and Ristori A. The combustion of kerosene: Experimental results and kinetic modeling using 1- to 3-component surrogate model fuels. Fuel. 2006:85;944–956.

Dagaut P and Gail S. Chemical Kinetic Study of the Effect of a Biofuel Additive on Jet-A1 Combustion J Phys Chem A 2007:111;3992-4000.

Dewitt MJ, Corporan E, Graham J and Minus D. Effects of Aromatic Type and Concentration in Fischer–Tropsch Fuel on Emissions Production and Material Compatibility Energ Fuel 2008:22;2411–2418.

Edwards T and Maurice LQ. Surrogate mixtures to represent complex aviation and rocket fuels. J Propul Power 2001:17(2);461-466

Gökalp I. and Lebas E. Alternative fuels for industrial gas turbines (AFTUR) Appl. Therm. Eng. 2004:24;1655-1663.

Gokulakrishnan P, Kazakov, A and Dryer FL. Comparison of numerical and experimental kinetic data for flow reactor systems: Mixing effects. The Combustion Institute (2003) *Proceedings of the Third Joint Meeting*

Heitor MV and Moreira ALN. Thermocouples and sample probes for combustion studies. Prog. Energy Combust. Sci. 1993:19;259-278

Humer S, Frassoldati A, Granata S, Faravelli T, Ranzi E, Seider R and Seshadri K. Experimental and kinetic modeling study of combustion of JP-8, its surrogates and reference components in laminar nonpremixed flows. Proc Combust Inst 2007:31;393–400.

Kahandawala MSP, DeWitt MJ, Corporan E and Sidhu SS. Ignition and Emission Characteristics of Surrogate and Practical Jet Fuels. Energ Fuel 2008:22;3673–3679.

Kick Th, Herbst J, Kathrotia T, Marquetand J, Braun-Unkhoff M, Naumann C and Riedel U. An experimental and modeling study of burning velocities of possible future synthetic jet fuels. Energy 2012;43:111-123.

Kumar K and Sung CJ. A comparative experimental study of the autoignition characteristics of alternative and conventional jet fuel/oxidizer mixtures. Fuel 2010:89;2853–2863.

Kumar K, Sung CJ and Hui X. Laminar flame speeds and extinction limits of conventional and alternative jet fuels. Fuel 2011:90;1004–1011.

Linstrom PJ and Mallard WG. Eds., NIST Chemistry WebBook, NIST Standard Reference Database Number 69, June 2005, National Institute of Standards and Technology, Gaithersburg MD, 20899, (http://webbook.nist.gov)

Maurice LQ, Lander H, Edwards T and Harrison WE. Advanced aviation fuels: a look ahead via a historical perspective. Fuel 2001:80;747-756.

Moses CA and Roets PNJ. Properties, Characteristics, and Combustion Performance of Sasol Fully Synthetic Jet Fuel. J Eng. Gas Turb Power 2009:131;041502-17.

Moss JB and Aksit IM. Modelling soot formation in a laminar diffusion flame burning a surrogate kerosene fuel. Proc. Combust. Inst 2007:31(2);3139–3146

Naik CV, Puduppakkam KV, Modak A, Meeks E, Wang YL, Feng Q and. Tsotsis TT. Detailed chemical kinetic mechanism for surrogates of alternative jet fuels. Combust. Flame 2011:158;434-445.

Nguyen DN, Ishida H and Shioji M. Ignition and Combustion Characteristics of Gas-to-Liquid Fuels for Different Ambient Pressures. Energ Fuel 2010:24;365-374

Poling BE, Prausnitz JM and O'Connell JP. The Properties of Gases and Liquids, McGraw-Hill, 2001

Rye L, Blakey S and Wilson C. Sustainability of supply or the planet: a review of potential drop-in alternative aviation fuels. Energ Environ Sci. 2010:3;17-27

Rye L and Wilson C. The influence of alternative fuel composition on gas turbine ignition performance. Fuel 2012:96;277–283

Saffaripour M, Zabeti P, Kholghy M and Thomson MJP. An experimental comparison of the sooting behaviour of synthetic jet fuels. Energ Fuel 2011:25(12);5584–5593

Saffaripour M, Kholghy M, Dworkin SB and Thomson MJP. A numerical and experimental study of soot formation in a laminar coflow diffusion flame of a Jet A-1 surrogate. Proc. Combust. Inst. J.proci.2012.06.176

Sarathy SM, Westbrook CK, Mehl M, Pitz WJ, Togbe C, Dagaut P, Wang H, Oehlschlaeger MA, Niemann U, Seshadri K, Veloo PS, Ji C, Egolfopoulos FN and Lu T. Comprehensive chemical kinetic modeling of the oxidation of 2-methylalkanes from C_7 to C_{20}. Combust Flame 2012;158:2338-2357.

Takeshita T and Yamaji K. Important roles of Fischer– Tropsch synfuels in the global energy future. Energy Policy 2010:36;2773–2784.

Timko MT, Yu Z, Onasch TB, Wong HW, Miake-Lye RC, Beyersdorf AJ, Anderson BE, Thornhill KL, Winstead EL, Corporan E, DeWitt MJ, Klingshirn CD, Wey C, Tacina K, Liscinsky DS, Howard R and Bhargava A. Particulate Emissions of Gas Turbine Engine Combustion of a Fischer–Tropsch Synthetic Fuel. Energ Fuel 2010:24(11);5883–5896.

Wang H and Oehlschlaeger MA Autoignition studies of conventional and Fischer–Tropsch jet fuels Fuel (2012) dx.doi.org/10.1016/j.fuel.2012.03.041

Wu T, Huang Z, Zhang WG, Fang JH and Yin Q. Physical and Chemical Properties of GTL - Diesel Fuel Blends and Their Effects on Performance and Emissions of a Multicylinder DI Compression Ignition Engine. Energ Fuel 2007:21;1908-1914

Chapter 7

Experimental characterization of a porous inert medium burner with intrusive and nonintrusive diagnostic techniques

Combustion domain augmentation by heat recirculation, on the concept of excess enthalpy burning has been acknowledged over the past as an effective, epoch-making technique (Weinberg, 1971). Since an intense flame of high temperature can be achieved through this energy transfer, it has been widely adopted in numerous practical applications with various configurations (Mujeebu *et al.* 2009a). In particular, instead of the conventional combustion in a pure gas flow, combustion in porous burner occurs within a porous inert structure, hence increasing the heat transport process in comparison to free flames. (Babkin *et al.*, 1991 and 1993). When a porous inert medium (PIM) is inserted in a flame, its conductive and radiative heat transfers to the pre-flame zone, rendering capabilities of high burning rate, extended flammability limits and low pollutant emissions to the flame (Wood and Harris, 2008). It also known that the flame can survive in porous inert media having a mean pore diameter less than the classical quenching diameter (Lee and Maruta, 2012).

The flame stabilizes inside the porous media by energy recirculation over a wide mixture velocity range up to several times as high as the burning velocity of the flame in free space. From the a view point of combustion augmentation, the structure of radiation-controlled flame in the porous media, results in a strong energy feedback by radiation through the reaction zone, yielding an excess enthalpy flame. (Hanamura *et al.*, 1991). Heat recirculating systems from hot combustion products to cold reactants, involving convective heat exchange, thermal conduction and radiation transfer in porous medium have been demonstrated to be efficient over the past decades. As a systematic methodological approach dictates, after validating the diagnostic techniques in fundamental applications, they are implemented for characterizing a complex combustor, as is the porous inert medium burner. In this context, the porous inert medium combustor is the state-of-the-art burner of choice, for implementing all diagnostic tools and methods developed and analyzed in the previous chapters of the present thesis. Hereon, the burner is characterized primary by means on nonintrusive techniques and then its operation with respect to nominal thermal load, equivalence ratio and fuel variation, is investigated, also utilizing intrusive diagnostic tools.

7.1.   The porous inert medium burner technology

The increasing need for more efficient, less emissive and less energy consuming technologies has shifted the focus of combustion research towards technologies involving flameless applications (Wunning and Wunning, 1997). Flameless or mild combustion (Cavaliere and de Joannon, 2004) is winning its place among cutting-edge, emission reduction and energy saving technologies. Numerous techniques have been employed in order to utilize inlet mixture preheating to reduce NO_x emissions (e.g. Choi and Katsuki, 2001). Excess enthalpy combustion or heat recirculation from burned products to unburned mixture, has been proposed as a fuel flexible technology, with reduced emissions and enhanced efficiency (Hanamura *et al.*, 1991 and 1993), which also finds application in porous media combustion. Porous burner combustion fulfills the aforementioned requirements since it is characterized by low pollutant emissions, high power density, high turn-down ratio, enhanced combustion stability (Malico *et al.*, 2000), high radiant efficiency (Bouma and de Goey, 1999) and the potential to operate in ultra-lean combustion regimes.

The porous inert medium burners operate on the principle that the premixed fuel/air mixture burns within the cavities of a solid porous matrix with superior heat transfer properties, serving as a means of internal heat recirculation. The incoming mixture is thus preheated leading to excess enthalpy burning, also commonly referred as super-adiabatic combustion (Takeno *et al.*, 1981). In the case of super-adiabatic combustion in porous media, the flame is stabilized at the interface of the preheating section and the ceramic foam with superior heat transfer properties and can be operated with a wide range of gaseous fuels (Mishra *et al.*, 2006). Combustion in a porous medium is also characterized by increased flame speeds, extended flammability limits and stability across a wide range of conditions and it continuously improves its place in numerous combustion applications utilizing these advantages which have started to be systematically examined over the last decades (Sathe *et al.*, 1991), such as combined burner and heat exchanger systems, off gas burners, partial oxidation reformers and household heating (Mujeebu *et al.*, 2009b).

Porous matrix stabilized combustion along with the associated burner technology development and the materials used, have been thoroughly described in the past (Pickenäcker *et al*. 1999 a; Trimis and Durst, 1996) and it is not in the scope of the present thesis, hence only a brief review will be given here. Porous burner design considerations include the length and orientation of the porous matrix or matrices in the case of multiple stages, the shape and the porosity. As far as the porosity is concerned, small-pored materials exhibit better conductive and convective and rather poor radiative heat transfer. Additionally, small pored foams act in favour of thermal dispersion effects, or in other words, enhanced heat transfer due to hydrodynamic mixing of the gas within the pore cavities (Fend *et al*. 2005). Moreover, high permeability are desirable in order to minimize the pressure drop and decrease the required preheating time during start up (Mößbauer *et al*., 1999).

However, the most critical consideration is the material selection. The type of the material has a dramatic effect on the ability of a burner element to resist melting and on its resistance to thermal cracking fatigue. Since the increase of the convective heat transfer coefficient leads to stronger heat recirculation (Barra *et al*., 2003), ceramic materials are highly appropriate for combustion inside porous matrix. Ceramic materials are suitable for porous burners because of their high usage temperatures, chemical stability and resistant to corrosion and wear (Bowen, 1980). While porous ceramic foams have good temperature resistance, their durability suffers from cracking caused by thermal stresses due to differential expansion during start up and shutdown. The most commonly used ceramic materials in porous combustors are alumina (or aluminium oxide, Al_2O_3), silicon carbide (SiC) or silicon impregnated silicon carbide (SiSiC) and zirconia (or zirconium dioxide, ZrO_2), which are typically met either as reticulated foams, lamella structures or packed beds. Alumina has high application temperature and resistance to wear, but has a large thermal expansion coefficient, poor thermal shock resistance and moderate thermal conductivity and emissivity. It is however the most popular, mostly met in packed beds and lamella structures. On the other hand, although zirconia based ceramics offer a very high application temperature, they present low thermal conductivity and moderate thermal shock resistance and emissivity. Finally, silicon carbide based materials present lower application temperatures, but they have higher thermal conductivity and emissivity and very good resistance to thermal shock and they are mostly used in reticulated foams (Pickenäcker *et al*., 1999b).

The combustion process inside porous media is quite complex, requiring a coupled solution of the heat and mass transfer and chemical kinetics occurring locally in the medium. Moreover, the effects of conduction and radiation heat transfer as well as convective interactions between the gas phase and the solid matrix must also be taken into account. The chemical kinetics can be simplified even to one step reaction process, or extended to account for a more complete detailed reaction set. In either case, the resulting equation is extremely stiff, because of the temperature dependence of the chemical reactions and solutions for the temperature, the flame speed and the species concentration inside porous media is highly uncertain (Howell *et al*., 1996). There is an important amount of studies describing analytically or numerically the phenomena inside the porous media (Pereira *et al*., 2005; Shi et al., 2011), using varying methodological approaches (Keshtkar and Nassab, 2009) and different models (Zhou and Pereira, 1998), analysing the influence of multidimensionality (Hackert *et al*., 1999) and parameterizing model uncertainties (Mendes *et al*., 2011). Most studies describe and analyse flame stabilization (Catapan *et al*., 2011) and burner

characterization in terms of temperature (Rumminger *et al.*, 1996) and emissions (Brenner *et al.*, 2000), focusing also on NO_x (Afsarvahid et al, 2008) and their formation mechanism (Gauthier *et al.*, 2008). There are also studies calculating maximum superadiabatic temperatures for laminar stationary lean premixed flames within porous inert media (Pereira et al., 2011) and flammability limits (Di Mare *et al.* 2000) and recently incorporating surface reactions (Machado, 2012).

In the present chapter, a porous burner with geometrical and physical characteristics as described in section 7.1.1 is examined in terms of flame stabilization, emissions, solid and gaseous phase temperatures and fuel interchangeability. In the following paragraphs the burner is firstly tested with nonintrusive means, namely Laser Induced Fluorescence, and the flame shape, height and location inside the matrix are parametrically determined. This investigation has been carried out using methane and the effects of nominal thermal load and stoichiometry variation as well as the sampling probe positioning on the flame are discussed. After the flame behaviour inside the porous matrix is determined, the investigation deals with the burner characterization and fuel interchangeability. Sections 7.2 and 7.3 deal with the burner characterization, when operated with conventional (e.g. natural gas and LPG) and alternative (biogas) gaseous fuels respectively. The latter investigation is realised utilizing a variety of diagnostic techniques, described in detail in the respective paragraphs.
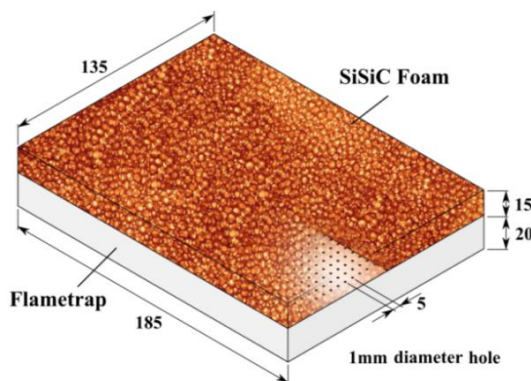
Figure 7.1 The burner configuration

7.1.1.   The burner configuration

For the needs of the present chapter, burners with identical characteristics were considered, for consistency reasons. The burner has a two layer, flat, rectangular porous geometry. It consists of a mixing tube with two supplies for air and fuel connected to a distribution chamber. The mixing chamber is connected to the first layer, namely the flame trap, made of alumina (Al_2O_3). The geometry of the flame trap consists of a hole-pattern with 1 mm holes in a non-staggered arrangement with 5 mm spacing. Thermal quenching of the flame is accomplished within the flame trap at low thermal loads, while at high thermal loads the flow velocity within the holes is significantly higher than the burning velocity additionally to thermal quenching. The flame trap prevents the flashback into the mixing section through the small drillings, affecting thermal quenching of the flame. In more detail, the low heat conductivity of the flame trap material

(< 0.2 W/mK at ambient conditions) prevented the upstream propagation of a thermal wave, which could lead to a flashback in the flow distributor. The second layer is the porous matrix, made out of silicon infiltrated silicon carbide foam (SiSiC) with a pore size of 10 ppi (pores per inch) and serves as the combustion zone. Furthermore, the SiSiC ceramic material combines high mechanical stability with being chemically inert even at high temperatures. Dimension-wise, the burner is 185 mm long and 135 mm wide and hereon the long axis is referred as x axis. The inert porous matrix and the flame trap have a height of 15 mm and 20 mm, respectively, as shown in Figure 7.1.

7.2. PIM burner operation characterization using nonintrusive diagnostic techniques

Although burners of this type have been characterized over the past years, nonintrusive experimental methods are needed to describe the actual processes taking place inside the porous structure. In the present section, the technique of laser induced fluorescence is employed to visualize the flame zone, utilizing the excitation of the hydroxyl radical. A pumped Nd:YAG, frequency doubled dye laser was utilized for this purpose. Hydroxyl radical is the most widely examined species with the LIF technique on the combustion field, because it gives a good understanding of the flame zone and hence it was used in the present study. In order to perform LIF measurements inside the porous combustion zone, optical access along the porous structure for the laser beam to reach the probe volume and furthermore, to allow a sufficient amount of fluorescence to reach the detector was realized by a thin gap of a similar size as the porous cavity size. A parametric study for the optical gap size and positioning was performed, yielding the most suitable configuration for a sufficient signal to noise ratio without significant disturbance of the combustion process in the porous reaction zone. The experiments were conducted over a range of various thermal loads and excess air ratios for methane-air combustion. The main scope of this section is to demonstrate how appropriate optical access in a porous combustion zone can be achieved, hence demonstrating the capabilities of the methodology described in paragraph 3. Besides this, an experimental characterization of the wide, stable operating conditions of the porous burner is given, along with the description of the flame zone inside the porous matrix.

7.2.1. Experimental investigation of flame structure inside the reaction zone using LIF

The advantages of porous burners have started to be systematically examined over the last decades as mentioned earlier, but the actual processes taking place within the porous inert structure could not be investigated experimentally by means of nonintrusive optical methods, due to the difficulties in achieving optical access inside of the porous matrix. Most of the experimental campaigns carried out in the past, concerned concentration measurements at the exhaust of the burner, or intrusive temperature measurements by utilizing thermocouples in the porous matrix. In the case of slow partial oxidation reforming processes in inert porous media also concentration measurements by gas sampling through probes placed inside the porous matrix were performed (Al-Hamamre *et al.*,

2009). However in the case of lean combustion the reaction zone is not thick enough to allow resolving it by gas sampling.

Only recently, a similar burner with the one described above was tested with nonintrusive techniques. The experiments concerned nonintrusive gas-phase temperature and hydrogen concentration measurements, along the burner symmetry axis temperature measurements inside the porous burner, facilitating the Coherent Anti-Stokes Raman Scattering (CARS) technique (Kiefer *et al.*, 2009). The same group extended the work providing advanced measurements with an improved setup by using Dual-Pump Dual-BroadBand Coherent anti-Stokes Raman Scattering spectroscopy (DP-DBB-CARS), presenting also measurements with variation of the radial position within one pore, (Weikl *et al.*, 2010). However, in these measurements the optical access was provided axially along the burner axis by guiding the laser beam through a hole in the flame trap structure and by creating an empty cylindrical path in the porous reaction zone downstream. Thus, the measuring volume was always lying within a single jet exiting the flame trap structure and was not representative for a random position in the porous structure.

The depiction of the combustion process within the porous structure supports the understanding of the complex local physico-chemical phenomena. The scope of the present section is to examine the methane-air combustion inside a porous burner operating under lean combustion regimes, by means of Planar Laser Induced Fluorescence (PLIF) and clarify the aforementioned issues. The planar LIF technique, as explained at section 3.1, has been used in the combustion field for qualitative (Dryer and Crosley, 1982) and quantitative measurements of species concentrations (Yamamoto *et al.*, 2009), as well as for determining mixing efficiency (Yip *et al.*, 1994) and temperature in reacting flows (Hartlieb *et al.*, 2000). Among its various advantages, the LIF technique provides a more intense signal compared to other nonintrusive techniques, such as Raman spectroscopy, and thus, can be also used as a planar technique. Moreover, the signal intensity is essential for the current study, because the fluorescence signals are received at a small solid angle from within the glowing radiating porous structure of the porous burner.

Experimental determination of the flame front location is based on measurement of quantities, which show a large spatial gradient at the flame front boundary. The hydroxyl radical, OH, is an important intermediate species and, since it is formed in the high-temperature regions, it is commonly employed as a flame front indicator as stated in paragraph 3.2. As documented earlier in the present thesis, besides acting as a flame front indicator, OH holds important advantages for the LIF technique, that makes it the most widely examined species in the combustion field, such as well-established structure and distribution of the energy levels, along with the possible transitions and transition probabilities. Due to these reasons the hydroxyl radical was selected as the species to be detected for the present study. Its normalized distribution was visualized for various thermal loads and excess air ratios in order to support the understanding of the flame zone structure and behavior over the operational range in the porous reaction zone.

Optical access through the porous structure cannot be achieved in a fully nonintrusive way, due to the opacity of the employed ceramic porous material and the relatively low optical thickness, which allow only a direct optical path up to a few porous cavity sizes distance inside the inner part of the foam with a lot of shadowed regions from the matrix itself. In the present work, appropriate optical

182

access has been created for the sending (planar laser light sheet) and for the receiving optics by cutting two slices from the foam (Stelzner *et al.*, 2010). The slice gap for the sending optics had to ensure sufficient space for the parallel light sheet thickness, whereas the detector opening had to provide a solid angle allowing a sufficient amount of fluorescence to reach the detector. Since the experiments focused on describing the actual phenomena in a random place inside the porous structure, the gap width for the optical paths had to be less than the characteristic length of the porous structure, which is considered to be the porous cavity size/diameter. Possible disturbances of the combustion process in the porous matrix due to the gap size and position were investigated in the current work by parametrically varying the size and positioning of the gap. Moreover, the structure of the reaction zone over the burner operating condition was examined and an extensive stability mapping was performed, establishing the range of operation in terms of thermal loads and mixture equivalence ratios.

7.2.1.1.   Sampling probe and burner coupling with the LIF system

The fundamentals of Laser Induced Fluorescence (LIF) have been described in detail in paragraph 3.1.1, hence a short overview of the system utilized is given here for reader's convenience. In order to facilitate the measurements, a frequency doubled Nd:YAG laser was used, pumping a frequency doubled dye laser (Quantel Brilliant B/TDL90), with a Rhodamine 6G dye, solved in ethanol, providing a wavelength at the UV region near 283 nm, exciting the $Q_1(6)$ line of the OH (1,0) band. The mean energy of the OH LIF beam was approximately 8mJ per pulse and the signal of the OH (0,0) transition has been selectively filtered to observe the two dimensional LIF images.
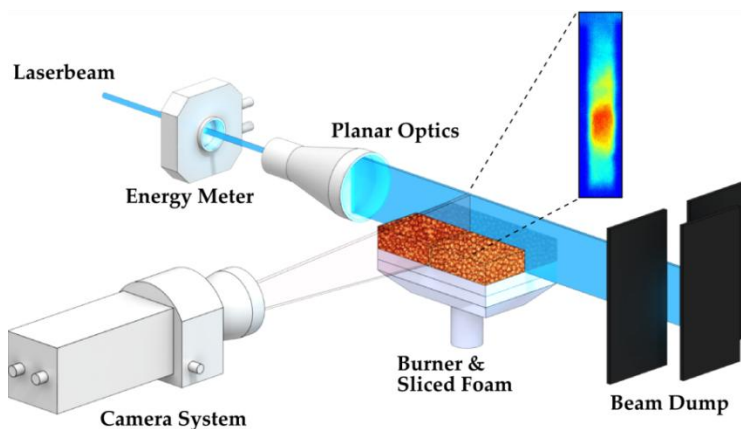
Figure 7.2 Schematic illustration of laser beams and receiving optics

The scope of the work here is to capture the flame front and depict its characteristics inside the porous matrix. The OH radical is one of the most important flame markers holding an important share on combustion research. The OH radical was one of the first and most commonly used radicals in combustion diagnostics from the beginning of the application of LIF in this field due to the strong signal and the advanced possibilities for a thorough physicochemical interpretation of the results. Here, for the excitation of the OH radical, the transition between the ground and the first energy state, which is described as $A^2\Sigma \rightarrow X^2\Pi_i$, is chosen for the high probability of transition, the relatively same nuclear distance and the relatively low energy needed for excitation. The

influence of collisions is the most troublesome aspect of making accurate profile measurements of minor species with LIF and for this reason a proper selection of the excitation transition is crucial. As described earlier in paragraph 3.2.1, the rotational level of the OH radical (1-0) band chosen from the excitation spectrum is the $Q_1(6)$ near 283 nm, because it appears to be temperature independent, providing a good depiction of the species population, eventually resembling realistically the flame front inside the combustion zone of the porous matrix.

The burner main features and operational characteristics have been described earlier in the present chapter, however it is important to note that the characteristic length scale of the porous cavity with an equivalent diameter for the 10 ppi SiSiC foam structure, is slightly less than 5 mm as elaborated in previous studies (Pan *et al.*, 2003). Since achieving optical access in the porous structure is a compromise between the disturbances of the actual phenomena taking place and obtaining the required optical characteristics, all parametric studies conducted concerned gap sizes smaller than 5 mm. The laser beam was passed through a cylindrical lens to formulate a planar laser sheet profile. For obtaining the fluorescence of the excited OH radical an intensified CCD camera with receiving optics was placed perpendicular to the laser light sheet in front of another slice gap created in the foam for this purpose. The paths were made in a way that allowed the width of the cut in the foam to be adjustable, so that their effect upon the actual process could be evaluated (Figure 7.2).

The results presented hereon, concern average mean pictures made from hundred single shots. The fluctuation of the beam energy was recorded for each shot and equalized. The background noise from the radiating foam and from the detector (ICCD-camera) was subtracted. The thermal radiation of the foam, according to Planck's law, was lower than expected in the receiving band of the OH fluorescence signal (FWHM~300-330nm). In a different case, conflict between foam radiation and fluorescence would arise, thus compromising the experiment, since the effective emission coefficient for SiSiC foams, could reach that of a black body (Mach, 2007). The burner was assembled over a traversing system for the fine tuning of the beam path alignment, as well as for the detector side. The arrangement of the optical access pathway gap sizes was achieved using length prototype specimens in order to satisfy the minimum tolerance demand.
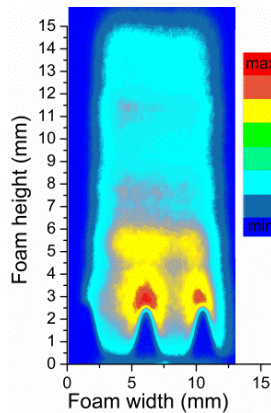

Figure 7.3 Flame visualization inside porous media with misplaced optical pathway positioning and sizing

Optics positioning inside porous media

Before dealing with the gap size for the optical access, the positioning of the optical path above the flame trap itself is of great importance. The random structure of the porous matrix induces a uniform flame front along the foam and the optical path has to maintain this feature. Positioning the optical path above a raw of flame-trap holes disturbs the randomness inside the foam by leaving a shortcut to some small jets or breaking the *isotropic* heat transfer inside the matrix. An extreme example with misplaced optical pathway positioning and sizing, is shown in Figure 7.3, where besides applying large width of the optical path, the positioning is lying above a series flame-trap holes (see Figure 7.1), maintaining a Bunsen-like shape, as the ones from a single jet, in chapter 5.

The optically accessible position in relation to the hole pattern of the flame trap is of great importance, since the flame structures resulting from the interaction between the exiting jets and the SiSiC foam are going to be different in the axial direction depending on the relative position of the optically accessed area to the holes pattern. Since an optical access just above the holes could lead to channeling of the flow, the position of the optical pathway was placed between four flame trap holes. Alternatively, one can visualize the jets issuing by the flame trap. During this parametric investigation, it was observed that, if the optical access opening was made above a flame trap hole, the issuing jet -depending on the gap size- could even maintain the familiar Bunsen-like structure, which was disappearing for gap widths less than 3 mm. In order to get a better picture of the porous foam influence upon the flame zone, without the interaction with jets possibly directly exiting the combustion zone, due to the channel formed by the gap, the optical access was finally adjusted in a way so that the optical pathway was not overalping with flame trap holes.
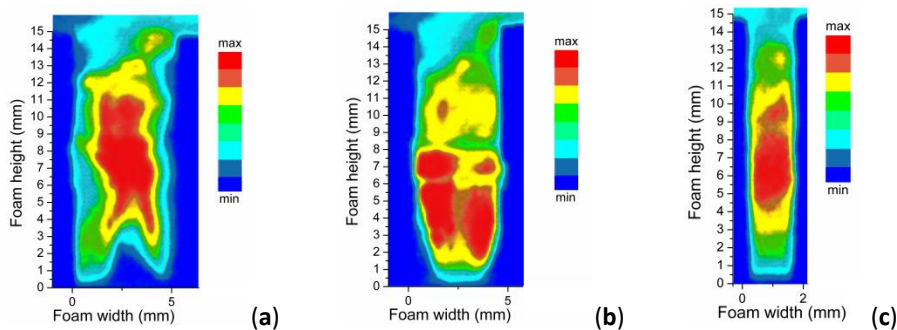
Figure 7.4 OH LIF images inside porous media for the same conditions (a) above the flame trap jet, (b) above two neighbor flame trap jets (CCD gap width of 5 mm) and (c) between the jets (CCD gap width of 2 mm)

Supporting previous discussion, Figure 7.4 depicts the difference in the OH concentrations with respect to the discussed scenarios above, under the same thermal load (600 kW/m²) and excess air ratio $\lambda = 1.2$ ($\varphi = 0.83$) condition, for gap widths of 2 and/up to 5 mm. The visualized area included firstly the area of a single jet exiting a flame trap hole as shown in case (a), the interaction area between two jets exiting two neighboring flame trap holes as shown in case (b) and the area around the middle distance among four neighboring jets and at a gap width of 2 mm, thus without axial free paths as shown in case (c). The flame jet is clearly seen in the first picture, whereas in the second one, the nearby jets seem to start interacting towards creating a unified zone. It can be also seen that the 5 mm gap width significantly disturbs the flow phenomena taking place. In conclusion, the parametric studies established the optimum configuration to describe the homogeneous interaction in the random porous matrix, is between nearby flame trap jets, as presented below.

Optical pathway parametrical sizing inside porous media

Since the configuration for achieving optical access could influence the processes taking place inside the porous matrix, the gap width for both the detector (side A) and laser light side (side B) are crucial factors. The final optical setup is shown in Figure 7.5.
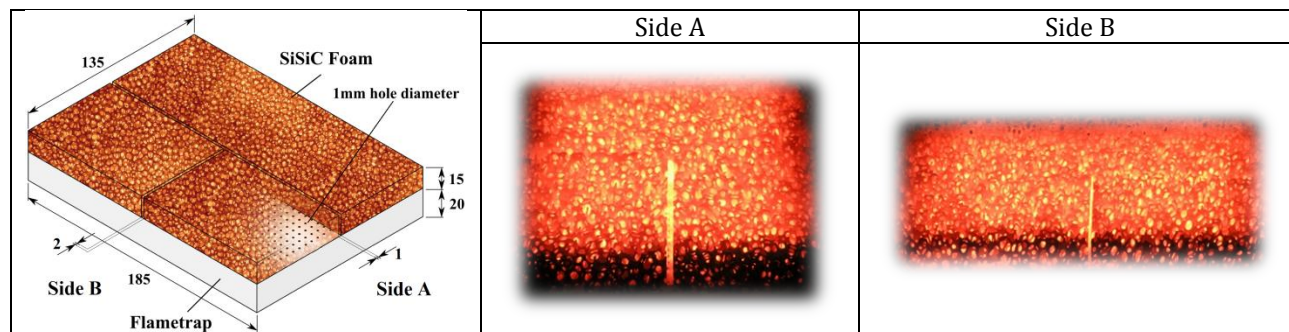
Figure 7.5 Configuration for achieving optical access inside the burner

The probe volume was set near the center of the burner where the influence of heat losses is minimized. In order to attain optical access near the probe volume, the foam was precisely cut in three pieces. The first cut, parallel to the laser beam, served as a path for the planar laser sheet. This path was made along the main burner axis to ensure that the beam would pass through the probe volume in order to avoid reflections from the random porous structure. The second cut was created with the purpose of allowing, as much fluorescence amount as possible, to reach the detector. The modifications needed for the optical access might influence the combustion process taking place inside the porous media. In order to minimize this effect, the influence of the foam structure disturbance on combustion process was investigated through a parametric study with a varying gap width. The gap size for the laser beam cannot be smaller than the largest beam width in the foam region, while the beam focus is located in the central foam region. As a result, a gap size of 1mm was chosen. Fluorescence signal power is proportional to the detection solid angle (see section 3.1.1.1), hence a parametric study for the gap size from the detector side was also conducted, in order to clarify, which is the minimal width for achieving sufficient amount of fluorescence signal. The gap width for the detector side was gradually reduced down from 5 mm, which as mentioned above, is considered to be the characteristic length of a 10 ppi foam. In the results presented here, a gap size of 2 mm from the detector side allowed a sufficient amount of fluorescence to reach the CCD camera. The 2 mm gap yielded a sufficient signal to noise ratio, and did not disturb significantly the actual phenomena inside of the porous reaction zone. This configuration is demonstrated in Figure 7.5 and was set and kept for all further experiments in this work, namely 2 mm gap width for detector side and 1 mm for laser sheet, focusing the probe volume in the middle distance among four flame trap holes.

Flame structure without porous matrix

The comparison between the flame structure with or without the porous matrix delivers valuable information about the effect of the heat and mass transfer of the porous structure on the flame structure. In an attempt to compare the flame structure with the free flame formed under the same

conditions, a comparison with burner operating without the porous matrix was made, serving as a reference case related to the results presented in paragraph 5.2.1 of the thesis.

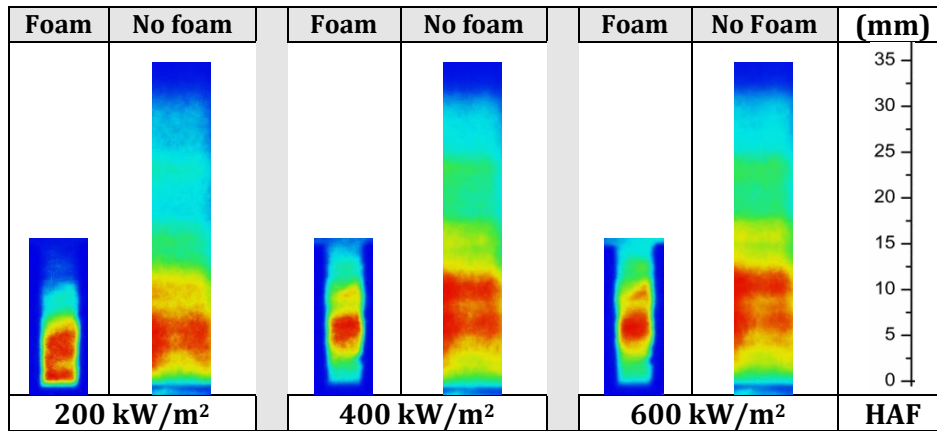| Foam	No foam		Foam	No foam		Foam	No Foam	(mm)
200 kW/m²			400 kW/m²			600 kW/m²		HAF

Figure 7.6 Comparison of flame front structure as a function of the Height Above the Flame-trap (HAF) with and without foam under varying thermal loads and constant stoichiometry (iso-scaled).

In burner operation without the porous matrix, the resulting structure appeared as a free flame carpet consisting of connected individual small flames. In order to facilitate these measurements, the burner was enclosed in a confined environment to avoid air entrainment and reduce flame instability. This configuration can only serve as an indicative measure for the difference in the flame length and structure, since the laser sheet cannot be focused homogeneously at a distant position above the flame-trap. Figure 7.6 presents measurements performed in both cases with the optical paths laying in the middle distance of neighboring flame trap jets, hence revealing the uniform flame carpet in both cases. Images presented are normalized with their maximum intensity in order to clearly represent the flame front spatial characteristics. The latter investigation clarified that the presence of the porous matrix, stabilized the flame in up to 6 times less distance from the flame-trap and furthermore reduced flame blow-off effects. It was also shown that with increasing thermal load, as shown in Figure 7.6, the flame was stabilized in the middle of the foam whereas without the porous matrix instability effects occurred with blow-off cases increasing dramatically. A detailed investigation, concerning the flame behavior inside the porous matrix with variation of thermal load and stoichiometry is given in section 7.2.1.2.

7.2.1.2.   Parametric investigation and operating regimes

<u>Influence of the thermal load on the flame front inside inert porous media</u>
The influence of the nominal thermal load on the flame structure was parametrically investigated by varying the latter from 200 to 800 kW/m², with steps of 100 kW/m². The excess air ratio was kept constant at $\lambda = 1.4$ ($\varphi = 0.71$), corresponding to typical industrial application conditions operating in the lean combustion regime. The aim was to visualize combustion inside the porous media demonstrating flame stabilization over a wide range of mass flows.

Figure 7.7 presents normalized OH concentration profiles obtained with the configuration described earlier. The normalization was made with the maximum fluorescence value for each case in order to obtain a comparable and clear picture of the flame front inside the foam and the position

where the reaction zone is more intense. The depicted stars (left figure) correspond to the maximum fluorescence value, calculated for each case through spatial integration of the signal distribution as a function of foam height (right figure) along the receiver side. The latter serves as an indicator for the flame front intensity and stability inside the porous matrix. As far as the maximum OH position is concerned, it is observed that its position does not significantly move over a wide range of thermal loads. For the lower thermal loads studied (200 to 300 kW/m²), combustion takes place directly after the flame trap. For thermal loads of 400 to 700 kW/m², the flame stabilizes approximately in the middle of the porous media, whereas, for higher loads, the flame moves further downstream. This behavior seems to be in agreement with previous numerical observations (Kiefer et $al.$, 2009). The latter results show the wide range of stable operating conditions of a porous burner and prove the advantages of internal heat recirculation. The results also show that the starting position of the flame zone is almost independent of the thermal load for thermal loads higher than 400 kW/m². Besides the trend of the maximum OH concentration position, the flame zone length remains almost constant for 200 to 600 kW/m².
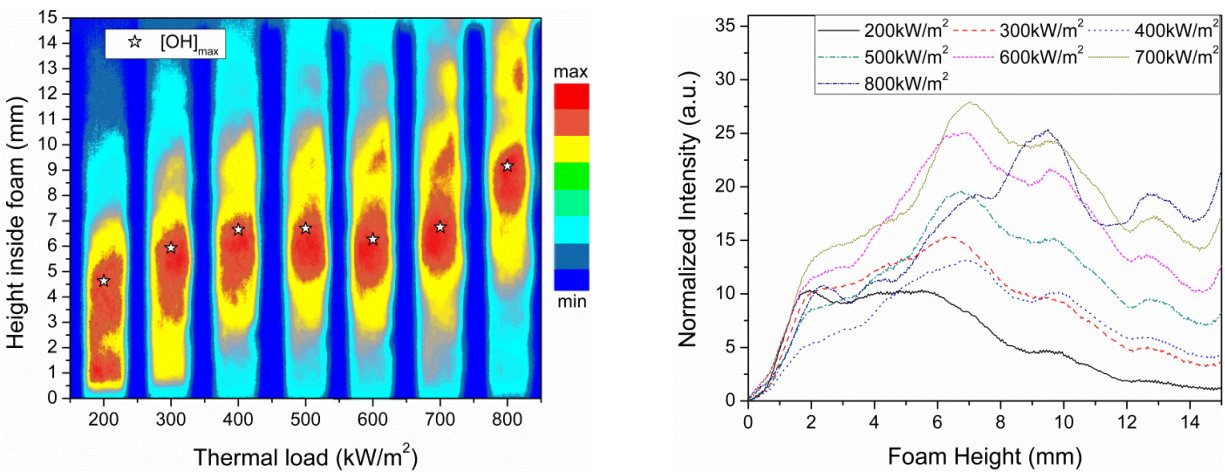
Figure 7.7 Position of maximum OH concentration for various thermal loads and constant excess air ratio (left). Normalized OH profiles inside porous media for various thermal loads (right)

On the basis of the aforementioned observations it can be anticipated that the flame stabilization can be divided into three regimes. In the first regime (200 to 300 kW/m²), the flame front starts directly above the flame trap. The flame speed is much higher than the flow speed and the flame trap acts to stop the flashback by thermal quenching. The second regime can be found for thermal loads from 300 to 700 kW/m². In this operational range, a balance between the heat released from the combustion process and the forced convection of the incoming unburned air/fuel mixture is achieved. In this range the flame maintains an almost constant height and a similar structure. In the third regime (higher than 800 kW/m²), the reaction zone moves further downstream and the flame is at the point of crossing over to blow off conditions, since the combustion zone has a depth of only 15 mm. This behaviour is in agreement with the conducted experiments, where at a thermal load of approximately 1000 kW/m², a blow-off of the flame was observed. This process is noticeable by low levels of OH radicals at the exit of the porous structure. The reason for this behaviour is either the lower residence times in the porous medium due to increased mass supply or due to the reduced preheating of the unburned gas by the solid foam, which leads to lower burning velocities,

eventually resulting reduced heat release These findings are in good agreement with the related numerical studies (Mendes *et al.*, 2008; Nemoda *et al.*, 2004).

<u>Influence of the excess air ratio on the flame front inside inert porous media</u>

In order to extent the previous investigation in order to determine the influence of the excess air ratio on the flame structure, a parametric study was conducted for three different thermal loads namely 200, 400 and 600 kW/m^2. The excess air ratio was varied in a range of $1.2 \leq \lambda \leq 1.8$ ($0.83 \leq \varphi \leq 0.56$). Here, as in the previous paragraph, normalized OH concentration profiles are presented normalized for each case to the respective maximum fluorescence value, in order to obtain a clear picture of the flame zone location inside the porous matrix. The depicted stars at the lesft side of the figures below correspond to the maximum fluorescence value as a function of foam height as depicted at the right side if the figure, calculated as well, for each case through spatial integration of the signal distribution along the receiver side. Figure 7.8 presents the flame front measurement as a function of the excess air ratio ($\lambda = 1/\varphi$). It is evident, that the flame front does not significantly move downstream by varying the excess air ratio up to values of 1.6, while afterwards a clear movement downstream can be observed. In the case of a thermal load of 200 kW/m^2 the maximum OH concentration can be found at a height of approximately 5 mm within the porous structure for all investigated excess air ratios. It can be noted that the flame stabilizes just downstream the flame trap, for most excess air ratios. It is clear that for lower excess air ratios, the flame peak has a horizontal flat shape at approximately 1mm height above the flame trap, creating a homogeneous flat flame. This distance is relatively low compared with the optical path width (2 mm) and the distance between two neighboring jets (5 mm). It can be argued that the incoming gas is preheated and ignites immediately expanding in the horizontal axis due to the temperature rise and the higher pressure loss in the foam structure. Increasing the excess air ratio causes the flame to start to lift up and to stabilize in the porous inert combustion zone while the flame peak zone starts to compress. This is obvious in both figures either through monitoring the OH radical profiles distribution (left) or by noticing the oscillating lines of the air excess ratios of $\lambda = 1.7$ or $\lambda = 1.8$ (right). It is also clear that no OH radicals reach the exit of the foam.

Figure 7.8 OH distribution for various excess air ratios at a thermal load of 200 kW/m^2 (left). Normalized OH profiles inside porous media for various excess air ratios (right)

It is here noted that the slightly inhomogeneous energy profile of the laser sheet, induced lower excitation energies at around 2 mm and 8 mm heights, which are not to be mistakenly correlated with the flame front intensity.

Figure 7.9 OH distribution for various excess air ratio at a thermal load of 400 kW/m^2 (left). Normalized OH profiles inside porous media for various excess air ratios (right)

Similar measurements for the cases of higher loads, namely 400 and 600 kW/m^2, as shown in Figure 7.9 and Figure 7.10 respectively, indicated that a fully developed, stabilized flame inside the porous inert media is achieved over the total excess air ratio range. In both cases the normalized OH concentration peak can be found in almost the same position for all excess air ratios (6.5 mm to 7 mm). The starting point of the lifted flame moves slightly downstream in the porous media while increasing the total mass flow, whereas this change is more significant with the increase of the excess air ratio. The comparison shows that the flame zone shrinking follows the same trend on the lower and upper part of the flame peak zone. When the total mass flow increased by changing the thermal load or excess air ratio, the starting point of the lifted flame moves slightly downstream in the porous media.
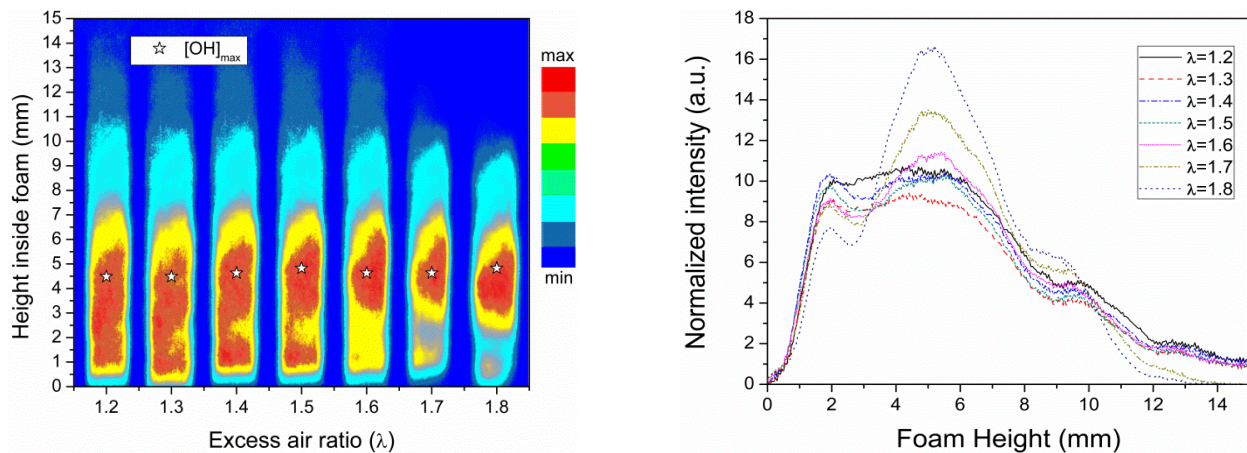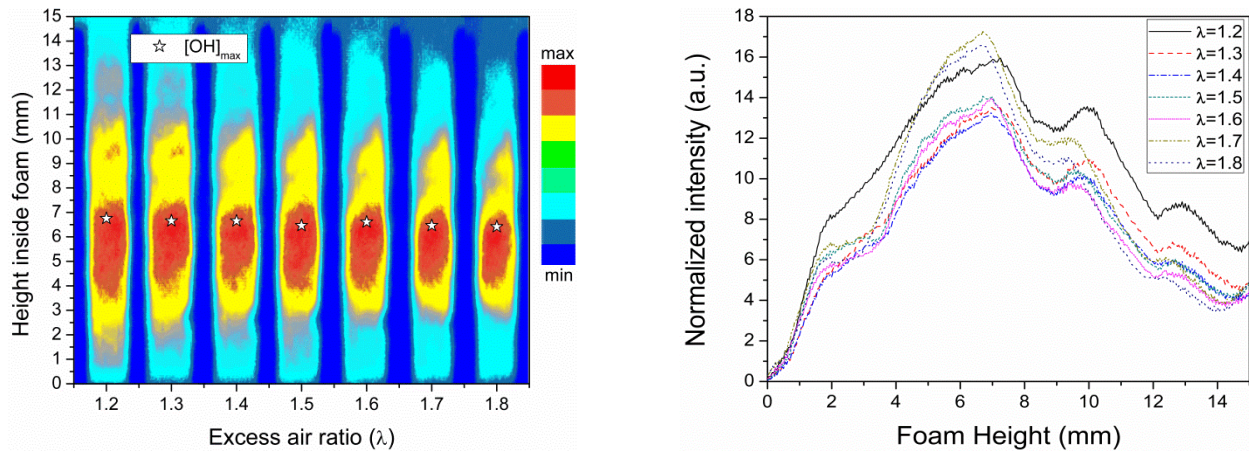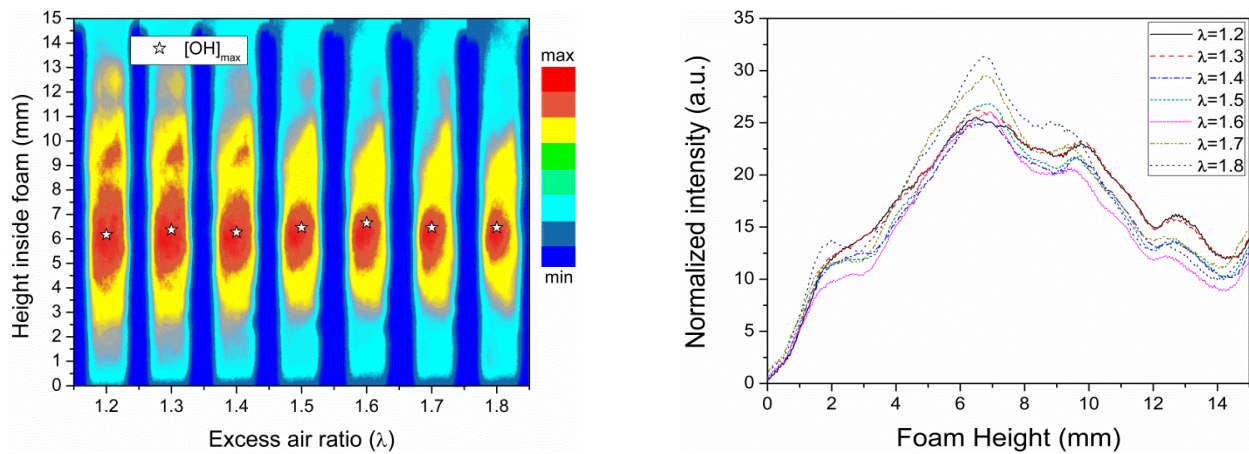

Figure 7.10 OH distribution for various excess air ratio at a thermal load of 600 kW/m^2 (left). Normalized OH profiles inside porous media for various excess air ratios (right)

The latter investigation for thermal loads, 400 and 600 kW/m^2, also reveals that the flame zone length is independent of the actual flame position inside the porous matrix, when the flame zone is located completely inside the foam. The total length of peak OH concentration increases marginally with the thermal load in these operation conditions. Summarizing, the present section revealed the critical limits for the flame stability, *i.e.* blow-off under the condition of higher mixture velocity than the burning velocity, flame extinction under extremely low mixture velocity and flashback when the range of mixture velocity is lower than the burning velocity according to a flame temperature decrease by heat losses through energy conversion from gas enthalpy to radiant energy emitted from the porous medium. Moreover the flame zone appeared to shrink with increasing each excess air ratio under the same thermal load, and as marked through the OH radical maximum concentration profiles, remained almost at the same position for varying excess air ratios at approximately in the middle of the porous medium.

7.3. Burner characterization using intrusive combustion diagnostic tools

Following the burner operation characterization conducted in the previously, the objective of the present paragraph is to perform a comprehensive experimental characterization of the state-of-the-art porous burner described, in terms of thermal efficiency and pollutant emissions and assess its operating limits. The burner is operated with methane and LPG, as representative gaseous fuels for most conventional systems and an extensive stability mapping is performed in terms of thermal loads and mixture equivalence ratios. Gas phase temperature profiles were measured using thermocouples and the solid phase temperature distribution was obtained using an IR camera. Gaseous emissions are quantified using an online gas analyser sampling system and the results confirmed the homogeneous temperature distribution, low NO_x and CO emissions and wide flexibility with respect to fuels and thermal loads. The effects of fuel interchange on efficiency and emissions are also analysed, as well as the relative impact of thermal load on temperature and emission values, with respect to equivalence ratio or fuel type.

7.3.1. Burner characterization using conventional gaseous fuel mixtures

Porous media combustion offers significant advantages against free flame burners, concerning pollutant emissions, power density, turndown ratio, combustion stability and the potential to operate in ultra-lean combustion regimes. These advantages explained in detail in previous sections, have started to be systematically examined over the last decades. There are numerous studies employing intrusive methods to provide experimental data for porous burner operation and compare it with different types of burners (Rørtveit *et al.*, 2002). Most studies focus on maximum temperature and maximum CO and NO_x concentration measurements at the exhaust of the burner (Liu and Hsieh, 2004), or parameterizing operating conditions such as preheating temperatures (Huang *et al.*, 2002). However, there are only few studies examining the burner behaviour over different thermal loads and equivalence ratios (Smucker and Ellzey, 2004) but without focusing on the temperature and species concentration distribution. A parametric

experimental assessment of the temperature and species distribution along the burner, addressing also the issue of fuel interchangeability, over a wide operational range has not been performed, to the authors' knowledge.

In the present section, the rectangular two-layer porous burner considered in paragraph 7.1.1, was operated without air confinement, over a wide range of operational conditions representative of all combustion regimes, from back-flash to marginally blow-off conditions, as stated in the previous section. Measurements were obtained over a range of nominal thermal loads from 200 to 1000 kW/m^2 under varying lean combustion regimes, namely of $1.2 \leq \lambda \leq 1.6$ ($0.83 \leq \varphi \leq 0.625$), within its stability limits. The burner was operated with methane and propane-based typical low-calorific value fuels. Gas phase temperature profiles were obtained using S-type thermocouples and the solid phase temperature distribution was obtained using an IR camera. Gaseous emissions were quantified using an online gas analyser (UV and IR sensor, Paramagnetic) coupled with an in-house developed ceramic gas sampling system. Temperature and species distribution above the burner are also presented, serving as a means of experimental evaluation of the porous burner homogeneous distribution with respect to low emission characteristics, operational range and fuel interchangeability.

7.3.2. Burner assembly and coupling with diagnostic test rig

The measurements performed concerned continuous monitoring of the burner performance in terms of temperature and emission profiles. The diagnostic methodology followed in this chapter in described in detail in chapter 2.2, hence a short description is given for chapter consistency and continuity. Species sampling was realized directly at the burner exhaust, through a non-cooled, in-house Al_2O_3 probe with an inner diameter of 2 mm, which led the exhaust gas samples to the gas analysis system. A humidity trap was connected between the sampling system and the gas analyser. Along with the probe, a ceramic insulated S-type thermocouple was located at the same measuring position, to allow real time monitoring of the temperature. A simplified equation for correcting the thermocouple temperature values based on the semi-empirical Nusselt functions was implemented (Baehr and Stephan, 1998) and the temperature dependences of the thermocouple emissivity coefficient was also taken into account (Deemyad and Silvera, 2008). Additional solid phase temperature measurements were performed using two infrared cameras (FLIR PM 595 and InfraTec-VarioCAM hr) with a maximum range near 2000 ^{o}C and nominal accuracy ± 10% of the local temperature. These measurements served for monitoring solid phase temperature, in order to depict clearly the homogeneous temperature distribution and to correct the S-type thermocouple values for radiation losses as in similar studies (Zheng et al., 2011). During the IR thermo-graphic measurements, both the burner and the camera were rotated by a slight angle less than 10° to prevent the exhaust gas stream damaging the sensor, but still maintaining that the sensor and the burner surface were perpendicular to each other. The utilised gas analysis system (see section 2.2) incorporated a UV spectrometer (ABB Limas11) calibrated for detecting NO and NO_2 at a range of 0 to 1000 ppm with 2% accuracy per volume, an IR spectrometer (ABB Uras26) calibrated for detecting CO at a range of 0 to 10000 ppm and CO_2 at a range of 0 to 25% (vol.) with 2% accuracy per volume and, finally, for O_2 concentration measurements, an electrochemical cell and a

paramagnetic detector (ABB Magnos206) were utilized. Finally, additional measurements for detecting hydrocarbon emissions were performed for selected cases with the gas chromatographic (GC) system described in paragraph 2.1. All detectors were calibrated close to the expected operational range to ensure a linear response. The GC sampling system incorporated a two-way sampling valve which introduced the sample into the GC. The sample was sucked through the GC system by a peristaltic pump connected at its exit. The GC system was equipped with an FID detector, analyzing C_1-C_4 alkanes and alkenes, calibrated close to the expected range to ensure a linear response. Calibration uncertainty was less than 1% for all hydrocarbons analyzed. The overall accuracy of the gas sampling measurements is estimated to be ±5%. The presented gas measurements are absolute and have not been corrected to reference oxygen concentration.
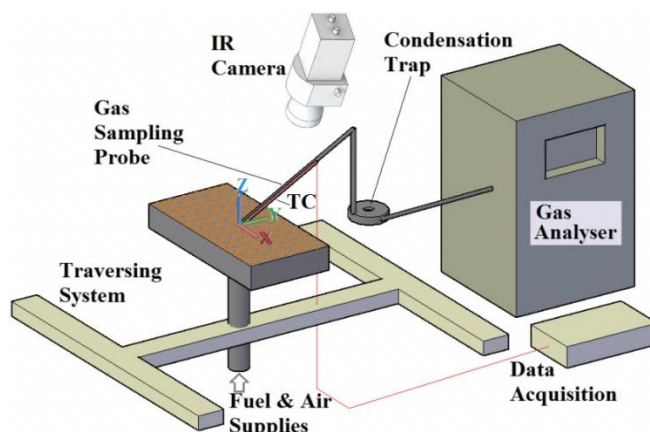
Figure 7.11 The experimental setup for coupling the burner with the test rig

The burner assembly (Figure 7.11) was placed on a traversing system that allowed measurements in the two horizontal directions above the burner. The sampling was realized at 1mm height above the burner, through a non-cooled, in-house Al_2O_3 probe with an inner diameter of 2 mm, which led the exhaust gas samples to the continuous gas analysis system. Along with the probe, a ceramic insulated S-type thermocouple was located at the same measuring position, to allow real time monitoring of the temperature. A humidity trap was connected between the sampling system and the gas analyser. Fuel and air flows were monitored through mass flow controllers (Bronkhorst MFCs) with total capacity of 1600 slpm for air (two separate MFCs connected in series) and 120 slpm for the fuel stream. For CO_2 supply (section 7.3.3) a methane-calibrated MFC was used with a correction factor (approx.1.04 according to the manufacturer). The CO_2 stream was mixed with methane at a distant position (more than 40 diameters downstream) and then introduced as the fuel stream at the burner inlet.

7.3.2.1. Temperature and emission measurements using methane and liquefied petroleum gas

The burner was tested with methane and Liquefied Petroleum Gas (LPG) and temperature and emission data were obtained. Methane was chosen as representative fuel for natural gas operation and LPG as a typical commercial gaseous fuel with higher carbon content. The burner was tested over a range of nominal thermal loads from 200 to 1000 kW/m² under various lean combustion

conditions, within its stability limits. These conditions correspond from flashback up to blow off operational conditions and it was revealed that the flame stabilizes inside the porous structure providing high turn down ratio and enhanced combustion stability. On the basis of previous observations (section 7.2.1.2), the flame stabilization inside porous media can be divided into three major regimes. In the first regime, occurring at ca. 200 kW/m^2 for the specific burner, the flame speed is much higher than the flow speed and the flame trap acts to prohibit flashback via thermal quenching. The second regime corresponds to the burner operating conditions where the flame stabilizes inside the porous structure. In the third regime (above 1000 kW/m^2), the reaction zone moves downstream and the flame towards the point of crossing over to blow off conditions.

Temperature measurements

Temperature distributions along the centrelines of the two main axes of the rectangular burner considered are presented in this section. The measurements shown in Figure 7.12, were performed at 1mm height above the burner for excess air ratios between $\lambda = 1.2$ and $\lambda = 1.6$, under thermal loads of 200 and 400 kW/m^2 with methane as fuel. The two-dimensionality of the temperature field is confirmed when comparing the x-axis with the y- axis measurements. Systematic and random errors (due to positioning, repeatability) of 2% and 3% respectively have been calculated for the thermocouple measurements. The overall error of ±5% justifies the measured differences in the local temperatures when comparing temperature distribution in X and Y axis.
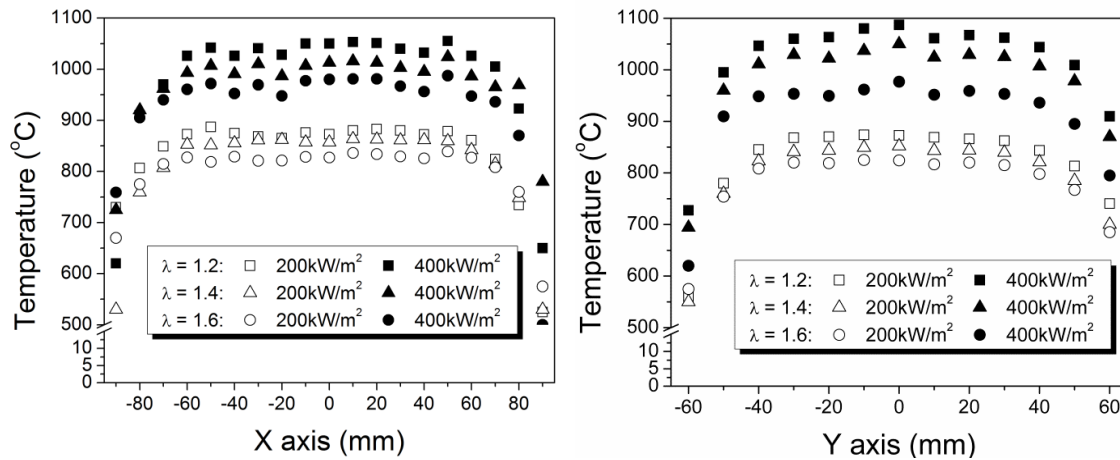
Figure 7.12 Temperature distribution along the X (left) and Y (right) symmetry axes line of the burner

The profiles reveal homogeneous temperature distribution along both burner main axes. The observed abrupt temperature drop at the edges of the burner corresponds to measuring points above the burner housing. As expected, increasing the thermal load from 200 to 400 kW/m^2 leads to higher peak temperatures (from 850 to 1050 ^{o}C). The opposite trend is observed with increasing the excess air ratio. Overall, the operational performance of the burner is more sensitive to the variation of the thermal load, where the mean peak temperature is increased by ca. 200 ^{o}C when increasing the thermal load by 200 kW/m^2 rather than the excess air ratio. The variation of the latter from $\lambda = 1.2$ to $\lambda = 1.6$ revealed changes in the peak mean temperature of less than 100 ^{o}C, independent of the power

Solid phase temperature measurements were performed with the IR camera with methane as fuel. They confirmed the constant and homogeneous temperature distribution on the burner surface over various conditions. Furthermore, the IR measurements were used to improve the accuracy of the correction for radiation losses of the gas phase measurements obtained with the thermocouple.
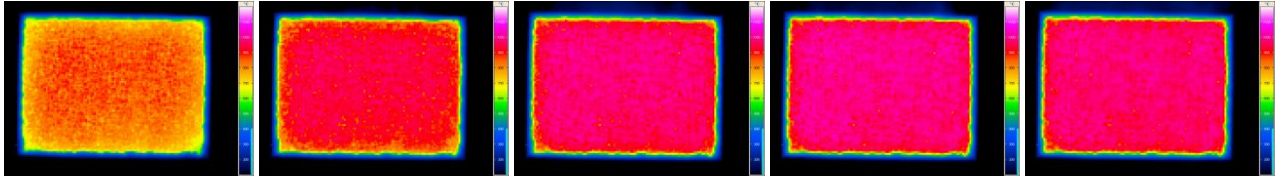
Figure 7.13 Burner surface temperature for λ=1.5 (φ=0.67). Thermal loads (a) to (e) stand for 200, 400, 600, 800 and 1000W/m². Temperature scale (indicated at the right side) 0-1200°C.

It is known that the radiation emission coefficient of the SiSiC in the range of 1000 °C is higher than ε = 0.9 (Mach, 2007). For SiSiC porous structures the use of an effective emission coefficient is suggested (Modest, 2003), which at the latter temperature range, leads to an emission coefficient of ε = 0.99, a value very close to black body behaviour. Temperatures presented in Figure 7.13 have been obtained with ε = 0.99.
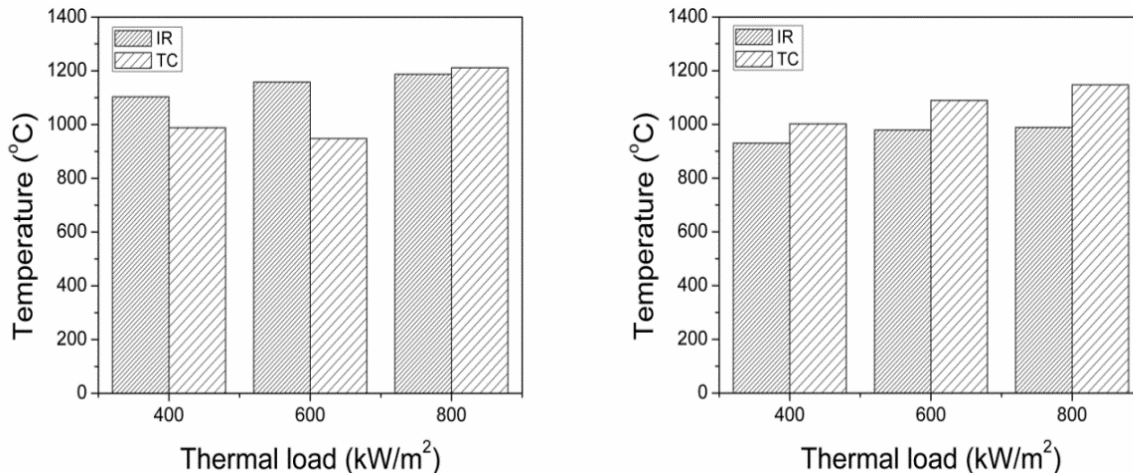
Figure 7.14 Maximum temperature values obtained for λ=1.2 (left) and λ=1.6 (right) with IR and TC

Figure 7.14 presents the maximum temperatures measured with the IR camera and the thermocouple (placed 1mm above the surface). The comparison between the two techniques allows the establishment of the expected maximum temperature differences and consequently the range of random errors. It can be observed that random errors in temperature measurements, with both techniques, range from ± 2% to ± 20%, with an average of ± 10%. It can be expected that thermal losses are more significant at the lower power range, thus affecting the measurement accuracy. Furthermore, the accuracy of the IR-temperature measurements is affected by cooling effects of the foam as a result of flow rate increase. For example, at λ = 1.6 the foam characteristics are expected to diverge from black body behavior, as a consequence of the above effect. Hence, the assumed value of ε = 0.99 may not be accurate enough, thus affecting the measured temperatures. Finally, the thermocouple correction for radiation losses influences the accuracy of the results because the

emission coefficient for Platinum alloys is also temperature dependant. Nevertheless, both techniques depict the temperature at the exhaust of the burner, which are expected to be significantly lower than temperatures reported inside the porous media.

Emission measurements

Emission measurements are presented along the burner surface at 1mm height above the burner, for different thermal loads and excess air ratios. Figure 7.15 depicts the CO distributions along the centreline of the two main burner axes, for excess air ratios of $\lambda = 1.2$, $\lambda = 1.4$ and $\lambda = 1.6$ under nominal thermal loads of 200 and 400 kW/m². CO emissions are consistently below 30 ppm for $1.2 < \lambda < 1.6$ and 200 kW/m² thermal load. CO levels are relatively higher at the burner edges due to the heat losses and consequently lower local temperatures. Small inconsistencies and hence higher CO values can be observed at some points far from the burner edges. This can be due to some small jet flames from the flame trap holes which may find an "easier/shorter" way through the porous structure, due to the randomized distribution of the porous cavities. For the higher thermal load, the CO values are in the range of 50 - 100 ppm with high scatter.

In general, CO levels increase with thermal load, near stoichiometric conditions. Under these conditions, the measured temperatures are higher and the reaction zone provided by the porous foam is not sufficient. It can be anticipated, and confirmed from measurements not presented here, that the respective CO levels downstream are significantly lower, since CO still converts to CO_2. However, as the burner is not confined, presenting the systematic emission measurements downstream the burner, would have limited value due to air entrainment effects.
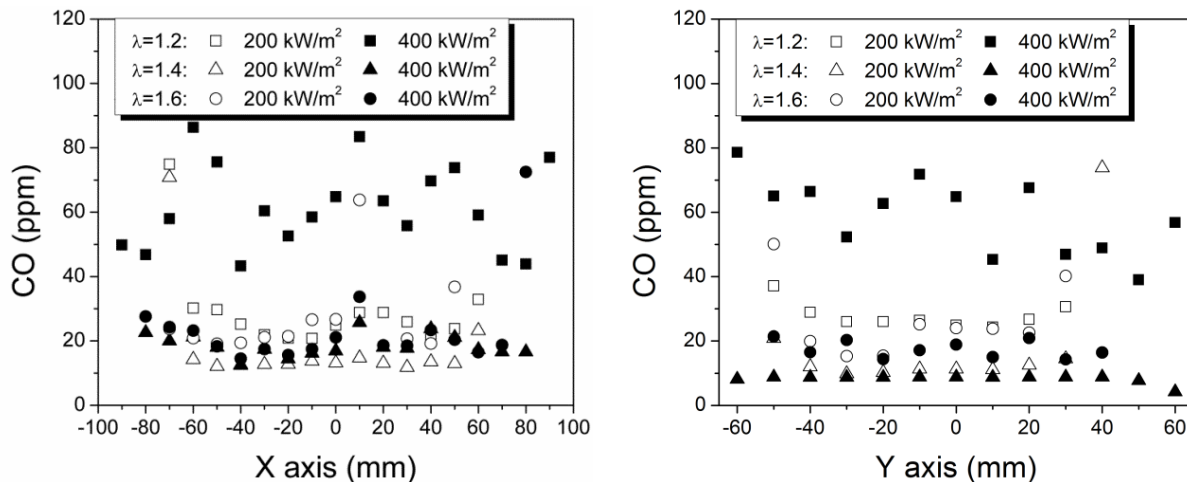
Figure 7.15 CO distribution along the X (left) and Y (right) centreline of the burner

In order to evaluate the influence of the excess air ratio upon the NO_x emissions, Figure 7.16 present the distribution for the same cases along the burner centrelines. NO_x emissions appear to increase around 30% when increasing the thermal load by 200 kW/m² for the same excess air ratios. However, the NO_x emissions in high excess air ratios are of the order of few ppm, whereas only in high power and low excess air ratios are of the order of 10 - 25 ppm. Finally, both figures show the trend of reducing the thermal NO_x formation by decreasing the equivalence ratios and

therewith the gas temperature. As expected, the thermally generated NO_x emission distribution above the burner follows the temperature homogeneous distribution, shown in previous figures.
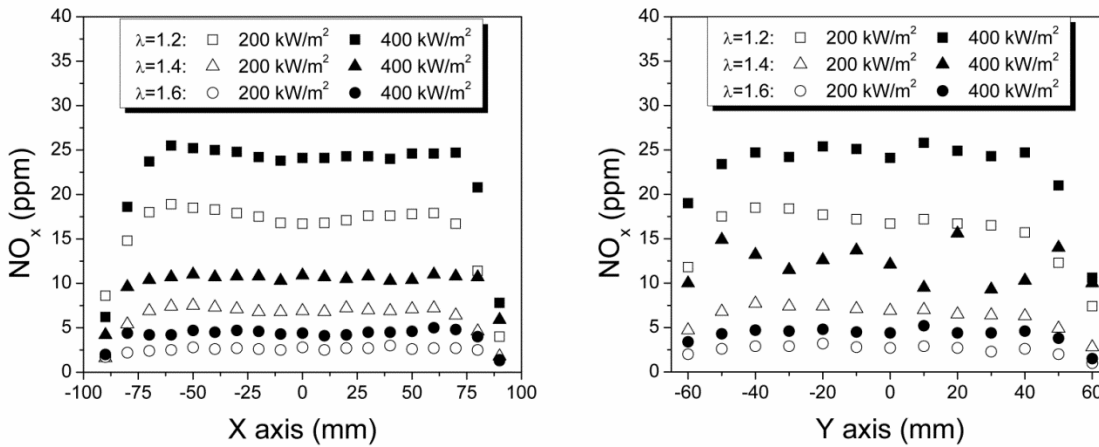
Figure 7.16 NO_x distribution along the X (left) and Y (right) centreline of the burner

Fuel interchangeability

Temperature and emission distribution measurements verified the capability of the burner operating in a wide range of thermal loads and excess air ratios. A homogeneous behaviour over the entire burner surface was confirmed. Therefore, it can be assumed that a sampling point at the burner centre is representative of the burner behaviour under the current conditions. In the present section, the results of the burner performance operating with methane and LPG (a mixture of 60% propane and 40% butane, volumetrically, is considered) are compared, under different equivalence ratios and thermal loads.
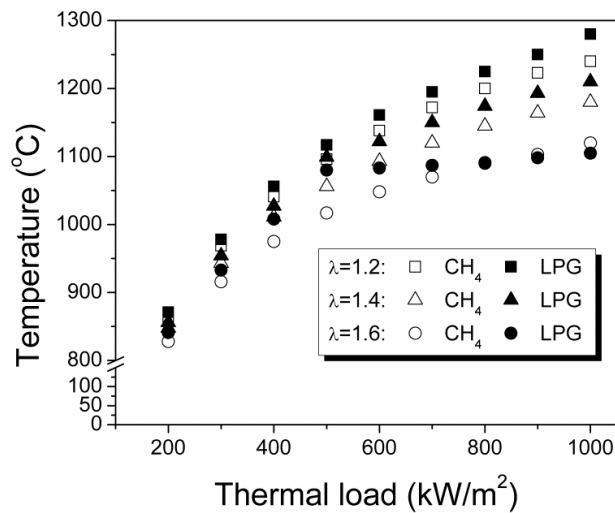
Figure 7.17 Gas phase temperature as a function of thermal load for different excess air ratios

Figure 7.17 presents the temperature values at the burner centre for excess air ratios of λ = 1.2, λ = 1.4 and λ = 1.6, for thermal loads varying from 200 to 1000 kW/m², for both fuels. Temperature

measurements suggest that thermal load variation is of higher importance than equivalence ratio, probably associated with the more significant relative heat losses at lower thermal loads. Furthermore, measured temperatures indicate that the excess air ratio holds more important role than the operating fuel.
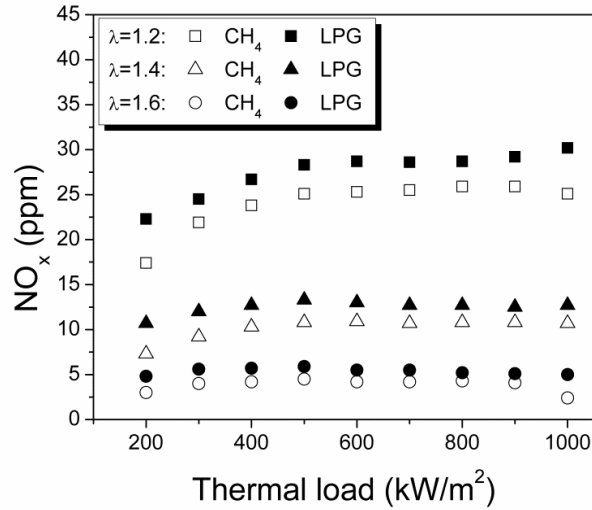
Figure 7.18 NO_x concentration as a function of thermal load for different excess air ratios

The NO_x concentration measurements (Figure 7.18) reveal that, at lower excess air ratios where temperature values are higher, the NO_x values rise with increasing of thermal load. An interesting feature is that, for higher excess air ratios, NO_x values remain constant, independently of the thermal load. It can be anticipated that this behavior is due to the reduced thermal NO_x production, at higher excess air ratios where temperatures are lower, with relatively small effect of the fuel. NO_x values appear to be systematically about 20% higher for LPG operation. It is here noted that NO_2 formation was an order of magnitude less than NO.
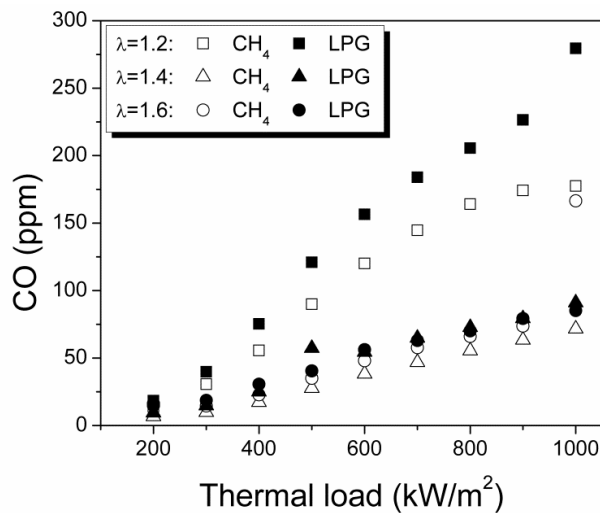
Figure 7.19 CO concentration as a function of thermal load for different excess air ratios

Finally, Figure 7.19 shows that CO emissions exhibit increased values with increasing thermal load, since the residence time in the porous matrix is reduced, leading to higher unconverted CO emissions. The results indicate that burner operation under lean combustion regimes, with excess air ratios higher than $\lambda = 1.2$, can lead to CO values around 50 ppm. The measurements indicate slightly higher CO values for the LPG operation, which can be, up to a point, justified by the higher carbon content of the LPG mixture.

Overall, the present section presents a detailed account of temperature and emission measurements, aiming at the experimental multi-parametric assessment of a porous inert medium burner operation. The constant and homogeneous species and temperature distribution along the two main burner axes and the burner flexibility with respect to fuel interchangeability is demonstrated. It is finally noted that the CO and NO_x emissions can meet the high legislative standards that apply for modern combustion devices (RAL gGmbH - Blue angel). For instance, for $\lambda = 1.4$ under $400\,kW/m^2$ with methane as fuel, the NOx emission levels are approximately 31 mg/kWh and CO levels approximately 29 mg/kWh. Accordingly, CO and NOx levels, for the same conditions, are 40 mg/kWh and 47 mg/kWh, respectively, under LPG operation.

7.3.3. Burner characterization using alternative fuel mixtures. The biogas case

Excess enthalpy burning concept was originally proposed for low calorific fuels combustion (Weinberg, 1975). Porous media combustion constitutes a particularly attractive technology, allowing operation in ultra-lean combustion regimes with excellent fuel interchangeability and low levels of pollutant emissions. In the previous chapters the burner stability in terms of thermal load and stoichiometry has been established when the burner was operated with conventional gaseous fuels. It is also a fact that most experimental studies focused on conventional gaseous fuels, such as methane or natural gas operation. Nevertheless, there are references for vaporised liquid fuel operation in porous reactors (Wu *et al*., 2012), mainly for hydrogen (Pedersen *et al*., 2005) or synthesis gas production (Pastore and Mastorakos, 2011), in slightly different design configurations (Loukou *et al*, 2012). Moreover, most studies focus on temperature, CO and NO_x concentration measurements at the burner exhaust, using methane as fuel (Hsu *et al*., 1993) or liquefied petroleum gas (LPG) (Muthukumar and Shyamkumar, 2012; Liu and Hsieh, 2004). Studies examining the burner stability and behaviour over different thermal loads and equivalence ratios, focusing also on temperature and species concentration distribution and addressing the issue of fuel inter-changeability, over a wide operational range are really scarce (Keramiotis *et al*., 2011).

In the case of low caloric fuels, the combustible domain shifts to a richer environment. The internal heat recirculation in a porous media is expected to maintain the capability of operating under fuel lean regimes, even in the case of low calorific fuels. However, there is scarce experimental experience concerning porous burner operation with low-calorific value fuels, such as coke oven gas (COG) (Cho *et al*., 2001) and gaseous mixtures emitted by landfills and pyrolytic processes (Al Hamamre *et al,* 2009). The effect of CO_2 addition to methane mixtures is of particular importance since it is related to the increasing interest of using biogas mixtures in practical

applications (Xuan et al., 2009). A two layer packed bed burner has been recently shown the ability to operate on biogas (Gao *et al.*, 2011), with good results. Although the mean porosity of the upper layer of the packed bed burner is similar to the current porous medium structure, there are important design differences, such as the total length of the combustion matrix which is made of packed balls rather than an actual porous matrix.

This section demonstrates a comprehensive experimental characterization of the described state-of-the-art porous burner fuelled with a simulated biogas mixture, in terms of thermal efficiency and pollutant emissions. An extensive stability mapping is performed in order to establish the range of operation in terms of thermal loads and mixture equivalence ratios. The burner is operated without air confinement, over a wide range of operational conditions representative of regimes, from flashback to blow-off conditions. The range of nominal thermal loads varied from 200 to 1000 kW/m^2 under lean combustion regimes, within its stability limits. The burner is operated with a methane and carbon dioxide mixture in a 60:40 molar ratio respectively as a typical biogas composition.

7.3.3.1.   Burner stability mapping for biogas fueled PIM burner

The formulation of the stoichiometry of a biogas mixture in not unambiguous and poses several difficulties since carbon dioxide, although contained in the fuel stream, does not contribute to the nominal thermal load. Moreover, the methane/air ratio remains the same (namely 1:2) in both, biogas and pure methane, air combustion. According to the strict definition of the equivalence ratio, the CO_2 percentage should be incorporated in the fuel stream mass fraction, since it is a constituent of the fuel. Such an approach would apparently result in nominal equivalence ratio values corresponding to fuel rich regimes, which are not representative of the particular burner operation. Overall, the latter approach does not represent the essence of the equivalence ratio, especially in the case where CO_2 acts more like a diluent. It is also a fact that, the total volumetric supply with biogas, increases by approximately 5%, when compared to the same thermal load and air supply with pure methane operation, respectively resulting in lower residence times in the porous matrix. The effects of the latter are demonstrated in the current work and will be discussed in the last section of the paper. In order to avoid mis-representation of results, it was decided not to include the contribution CO_2 presence in the calculation of equivalence ratios. Hereafter, all equivalence ratio (or air excess ratio) calculations do not include CO_2 as a constituent of the fuel stream. The justification for this is further discussed in the last section of this work. Typically, calculated local excess air values presented here correspond to ca. 40% lower ones according to the strict definition of the global equivalence ratio, namely $\lambda = 1$ without accounting CO_2 in the calculation corresponds to $\lambda = 0.61$ when CO_2 fraction is considered, $\lambda = 1.1$ without accounting CO_2 corresponds to $\lambda = 0.67$ with it etc. Moreover, the latter approach facilitates the comparison between biogas and pure methane operation under the same conditions.

An extensive stability mapping, as a function of the fuel and air supply, was performed in order to define the stable burner operation regime and the flame extinction limits. The results of the burner performance operating with a mixture of 60% methane and 40% carbon dioxide volumetrically, under different equivalence ratios and thermal loads are presented in Figure 7.20. The burner stability map was based on visual observations and recorded CO values, with thermal load steps of

40 to 50 kW/m² and for excess air ratios varying between stoichiometric to λ=1.5, as discussed earlier. The tested range of nominal thermal loads from 200 to 1000 kW/m² under various lean combustion conditions, covers the burner's operational limits, from flashback up to blow-off operational conditions. Visual observations confirmed that the flame stabilizes inside the porous structure providing high turn down ratio and enhanced combustion stability. Blue colours in Fig. 2 correspond to stable operating regime being characterized by low CO emissions. Green colour characterizes the regime of flame stabilization inside porous matrix but with increased CO levels, indicative of behaviour closer to blow-off and finally, red areas point towards or even represent the blow-off regime. Exploiting previous results (7.2.1.2), the flame stabilization inside porous media can be divided in three major regimes. In the first major regime, occurring at ca. 200 kW/m², for the specific burner, the flame speed is much higher than the flow speed and the flame trap acts to prohibit flashback via thermal quenching (area I). The second major regime corresponds to the burner operating conditions where the flame stabilizes inside the porous structure. The aforementioned regime can be further divided in three minor ones, being characterized respectively by low CO emissions (area III) or areas within stable operation but with increased CO emissions closer to blow-off conditions due to increased flow rates, areas II and IV respectively. In the third regime (above 1000 kW/m²), the reaction zone moves downstream and the flame towards the point of crossing over to blow-off conditions (area V).
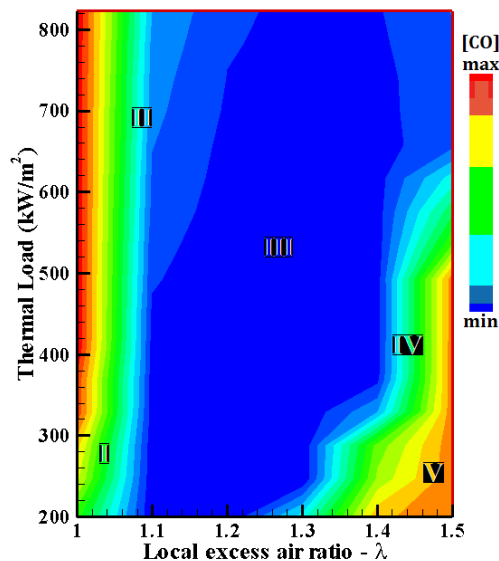
Figure 7.20 Burner stability map for biogas operation. Blue colour correspond to stable operating regime, characterized by low CO emissions, green colour characterizes the regime of flame stabilization inside porous matrix with increased CO levels and red areas point towards or even represent the blow-off.

The flame stability mapping performed with the biogas mixture indicated that the burner was capable of operating under stoichiometric and fuel lean conditions, maintaining low carbon monoxide emissions with complete fuel consumption. However, with increasing nominal thermal load it was rather difficult to maintain a stable flame under stoichiometric regimes, hence the presented measurements start from a local excess air ratio higher than λ ≥ 1.1. For lean fuel-air mixtures with local excess air ratio higher than λ ≥ 1.5, small diffusion flames started forming, indicating that the burner was in blow-off mode. Apparently, high CO values are indicative of

unstable burner operation. Consequently, the presented temperature and emission measurements correspond to local excess air ratios from $\lambda = 1.1$ to $\lambda = 1.4$.

Temperature and emission measurements

The burner homogeneous behaviour over the entire burner surface and consequently the respective relatively flat temperature and emission profiles were confirmed in the previous paragraph. Therefore, it can be assumed that a sampling point at the burner centre is representative of the burner behaviour under the current conditions; hence all measurements were performed likewise. Furthermore, it can be anticipated that, as the burner is not confined, presenting the systematic emission measurements downstream of the burner, would be of limited value due to air entrainment effects.
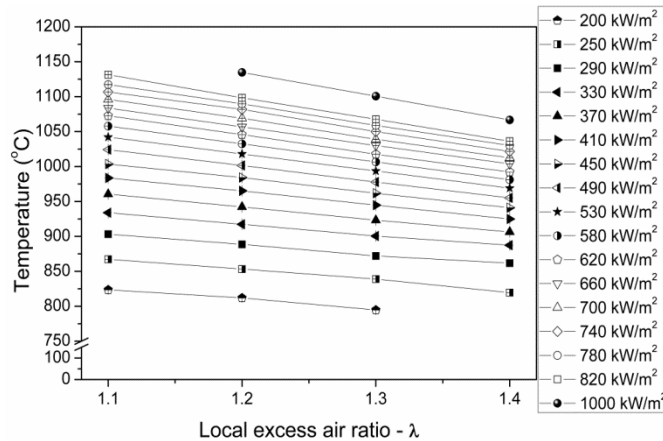
Figure 7.21 Gas phase temperature as a function of local excess air ratio for different thermal loads

Figure 7.21 presents the measured temperature values at the burner center. The presented values include the thermocouple measurement correction (TC) for radiation losses. Additional infrared (IR) thermography measurements for the solid phase temperature were used, to improve the accuracy of the radiation losses correction method. Systematic and random errors (due to positioning, repeatability) have been calculated for both techniques to averagely range about ± 5%. An interesting feature is that with increasing mixture's air content, IR values come closer to TC systematically. As expected, increasing the thermal load leads to higher temperatures and the opposite trend is observed with increasing the excess air ratio. Overall, the operational performance of the burner in terms of temperatures, suggest that thermal load variation is of higher importance than equivalence ratio, probably associated with the more significant relative heat losses at lower thermal loads. At low nominal thermal loads e.g. from 200 to 350 kw/m, a 50 kW/m^2 step increase results in ca. 60 $^\circ$C higher temperatures, for each stoichiometry. At higher values of applied thermal load, namely from ca. 500 kW/m^2 to 800 kW/m^2, temperature values are concentrated within a 100 $^\circ$C window for all stoichiometries.

Carbon monoxide emission measurements are presented in Figure 7.22. CO levels increase with increasing thermal load, since the residence time in the porous matrix is reduced, leading to a higher percentage of unconverted CO emissions. The results indicate that CO emissions are systematically minimized when the air excess ratio is between $1.2 < \lambda < 1.3$, always maintaining

values of the order 300ppm even under the maximum nominal thermal load tested in the present study (1000 kW/m^2). The stepwise increase of nominal thermal load by 40 - 50 kW/m^2 induces a linear increase on CO emission levels of 10 to 15 ppm. It is also noted that elevated values for low thermal load applied and at local excess air ratio of $\lambda = 1.4$ correspond area IV presented at Figure 7.20, pointing towards unstable burner operation. However, CO levels are more than 60% higher in comparison to pure methane operation in their common stable operational regime, as shown in Figure 7.23, especially under high excess air ratios. This trend could be mostly attributed to the reduced residence time of the mixture in the porous matrix due to the increased total flow rate, which also results in lower temperatures. However, it can be anticipated that the increased carbon content of the mixture is also partially responsible for the difference between biogas and pure methane operation at the exhaust CO levels, although such a statement carries high risk without investigating the phenomena inside the combustion matrix.
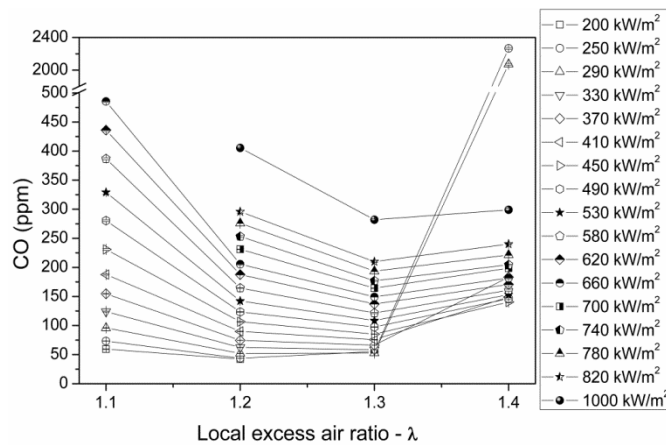
Figure 7.22 CO concentration as a function of local excess air ratio for different thermal loads
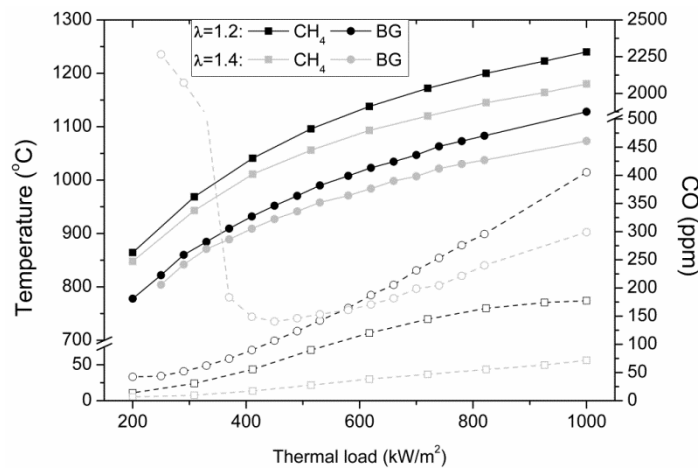
Figure 7.23 Comparison of temperature (solid line) and CO concentration levels (dots) between biogas pure methane operation as a function of nominal thermal load for local excess air ratios of $\lambda = 1.2$ and $\lambda = 1.4$

In order to get a clear picture of the difference between pure methane and biogas burner operation, Figure 7.23 presents comparative experimental results for temperature and CO levels under the same thermal load and air supply (same local excess air ratio). It is obvious that temperature values

are in general of the order of 10% lower than the respective ones with pure methane as fuel, under the same nominal thermal load and air supply, which obviously correlates with the 5% volumetric flow rate increase when using biogas contrary to pure methane under the same conditions. The only inconsistency concerning CO levels in Figure 7.23 can be seen under low thermal loads and higher excess air ratios, where, as Figure 7.20 suggests, the burner stable regime in these conditions is characterized by high CO concentration levels.
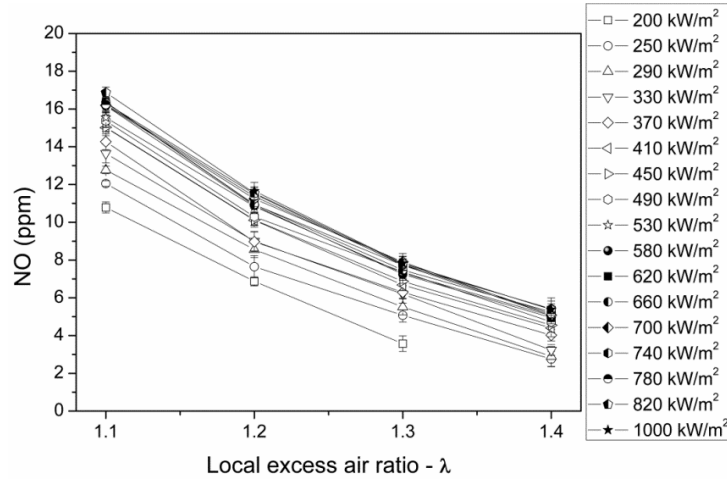
Figure 7.24 NO concentration as a function of local excess air ratio for different thermal loads
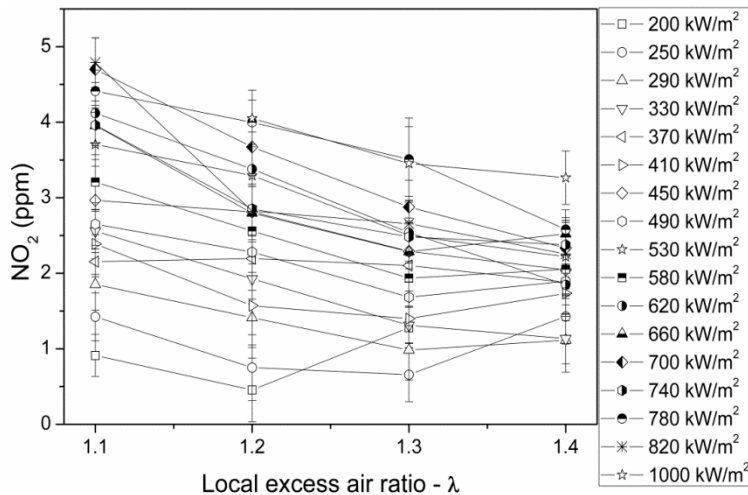
Figure 7.25 NO_2 concentration as a function of local excess air ratio for different thermal loads

Figure 7.24 reveals that variation of of thermal load is of negligible importance since NO concentrations, which reach a threshold depending only on the excess air ratio. NO values are of the order of 10 to 16 ppm for excess air ratio of λ = 1.1 and up to 7 ppm under excess air ratio of λ = 1.4. Accordingly, Figure 7.25 presents NO_2 concentration measurements where the same trend is noted with small exceptions within the experimental uncertainty under low nominal thermal loads. However, the values remain extremely low and they are 60% lower than the respective ones under the same methane and air flows. Finally, both figures show the trend of reducing the thermal NO_x formation by decreasing the equivalence ratios and therewith the gas temperature. As expected, the

thermally generated NO_x emission distribution above the burner follows the temperature trend, shown in Figure 7.21.
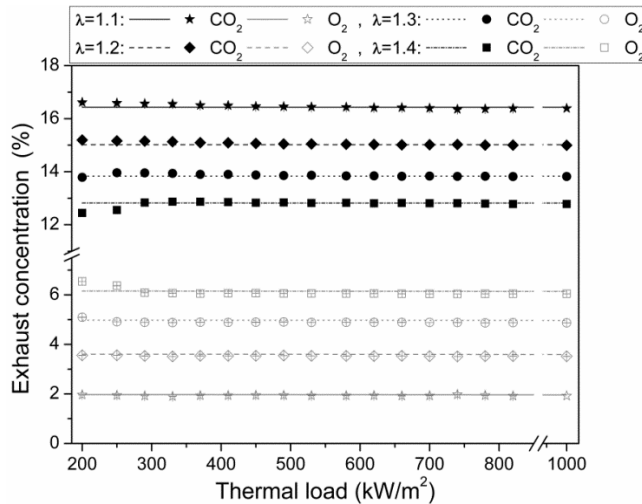
Figure 7.26 CO_2 and O_2 dry basis concentration levels as a function of local excess air ratio for different thermal loads. Lines correspond to theoretical equilibrium and symbols to experimental data.

Finally, selected experiments were also performed with GC, within the burner's stable operating regime, namely $\lambda = 1.2$ and $\lambda = 1.3$ under thermal loads up to $600\,\text{kW/m}^2$, in order to evaluate hydrocarbon emissions. However, the measurements showed that such species were absent or below detectability range. As a concluding remark, Figure 7.26 presents CO_2 and O_2 measurements against the respective theoretical equilibrium values. The continuous lines correspond to dry basis equilibrium numerical results and symbols correspond to experiments. It is obvious that the experimental values are in total agreement with theoretical predictions. Some inconsistencies are shown only at lower thermal loads close to stoichiometry, where as discussed on the burner stabilization section, the burner behaviour is close to instability. This fact builds up the argument that the small flame scale inside the porous media are subjected to the local conditions representative of equivalence ratio calculated without incorporating CO_2 in the fuel stream.

Overall gas and solid phase temperature profiles measured reveal the wide stability with respect to thermal loads, low NO_x and CO levels. The effects of CO_2 addition on burner operation and efficiency showed its relative impact in temperature and emission values with respect to equivalence ratio and thermal load variation. The comparably strong physical effect of the CO_2 addition against its chemical impact on the processes was also discussed.

7.4.   Summary

The porous burner constitutes the state-of-the-art combustor of choice to implement the experimental diagnostic techniques developed in previous chapters. The present chapter examines the porous inert medium burner stability and performance, with a variety of intrusive and nonintrusive combustion diagnostic techniques, with respect to fuel and operating conditions variation. A two stage porous burner, incorporating materials and geometries representative of

modern industrial porous burner applications, with an Al_2O_3 flame trap and a 10 ppi SiSiC foam was considered. Measurements of the hydroxyl radical in a combustion environment inside porous inert media were performed for the first time, and a methodology for visualizing the flame front inside a porous inert media by planar laser induced fluorescence was proposed. OH concentration monitoring, allowed the determination of the flame front intensity and spatial stabilization position for various excess air ratios at different thermal loads. It was shown that the thermal radiation could be separated from the fluorescence signal of detected hydroxyl radicals for the operating temperature range of a porous burner's glowing foam. Additionally, a study about the flame disturbance, induced by creating the optical access, was carried out. The configuration used in order to overcome technical difficulties was presented and useful parametric studies were conducted in such a way as to facilitate future theoretical and numerical studies. In the context of burner operation, it was observed that the position of the maximum OH concentration is almost independent of the excess air ratio for the same thermal loads in the stable operation regime. The results revealed that the flame zone length decreases with higher excess air ratios. For lower excess air ratios and thermal loads of the order of 200 kW/m², the flame stabilizes directly downstream of the flame trap, whereas for higher thermal loads (up tp 800 kW/m²), the flame moved further downstream at high excess air ratios. It total, the burner stable operation was demonstrated over a wide operational range and this range becomes the basis for the experimental characterization of the burner in terms of emission and performance.

The experimental campaign concerning burner performance extended to exhaust emission measurements with online continuous analyzers and a gas chromatographic system, along with solid and gaseous phase measurements, when the burner was operated with methane and LPG. The results revealed a stable burner operation for wide power ranges with low emissions for different fuels, thermal loads and stoichiometry. Mean CO emissions were of the order of 50 ppm and NO_x emissions were around 25 ppm at 1 mm height above the burner, under high power and low excess air ratios, where the high temperature range is in favor of thermal NO_x formation. In addition, the comparison between methane and LPG operation revealed very good fuel interchangeability concerning emissions and burner operation. In the latter case, temperature measurements indicate that thermal load variation is of higher importance than equivalence ratio, for both methane and LPG operation. In the context of burner operation, the results suggest that the burner provides a wide flexibility when operated at lean combustion regimes with excess air ratio higher than $\lambda = 1.2$ providing low emissions and constant thermal potential

Finally, a detailed account of temperature and emission measurements, aiming at experimental multi-parametric assessment as well as burner stability mapping and characterization, were performed, when the burner was operated with a typical biogas mixture. Exhaust gas measurements revealed that the CO_2 presence in the fuel mixture leads to higher CO levels at the burner exhaust. This behavior could be either attributed to the chemical impact of CO_2 or to the fact that it also acts as a diluent leading to lower residence times in the porous matrix and lower temperatures in comparison with pure methane combustion. This observation suggests that residence times versus kinetic scales in the porous matrix of the particular burner are long enough to overcome any kinetic effect. Overall, the work indicates that the CO_2 addition had eventually small chemical impact at the exhaust of the burner, although this statement may not be valid for

phenomena inside the combustion zone. Considering this finding and also for direct comparison with pure methane combustion, the mixture's stoichiometry were presented calculating excess air ratios bypassing the strict definition of the equivalence ratio, without taking into consideration the percentage of CO_2 in the fuel stream. This approach results to a phenomenal fuel rich combustible domain, whereas the actual local conditions correspond to fuel lean regime. The burner stable operation was tested for thermal loads varying from 200 to 1000 kW/m², with local excess air ratios (calculated as discussed) from $\lambda = 1.1$ to $\lambda = 1.4$. It is here noted that the global definition would result excess air ratios from $\lambda = 0.6$ to $\lambda = 0.9$. The studied cases covered operating conditions from flashback up to marginally blow-off operational conditions. The results revealed stable burner operation for wide power ranges with low emissions and complete fuel consumption (methane constituent) for different thermal loads and stoichiometries. The stable operation domain was slightly shifted to the richer domain in comparison to pure methane operation. Temperature values reached 1100 °C under the highest applied thermal load and were systematically 10% lower compared to pure methane operation under the same fuel and air supply. Carbon monoxide levels reached 300 ppm under 1000kW/m² of nominal thermal load and $\lambda = 1.3$ and total NO_x levels were never above the threshold of 20 ppm. CO emissions were around 50% increased, in comparison to pure methane operation, whereas total NO_x values were reduced by 50 to 60%. Overall, the burner characterization in terms of operation, performance, emission reduction and fuel interchangeability, reveals that the porous inert medium burner constitutes a particularly attractive technology that meets modern requirements (Richards *et al.*, 2001), resolving important issues for fuel-flexible environmental friendly combustors.

Chapter References

Afsharvahid S, Ashman PJ, Dally BB. Investigation of NOx conversion characteristics in a porous medium. Combust Flame 2008;152:604–615.

Al-Hamamre Z, Diezinger S, Talukdar P, Von Issendorff F, Trimis D. Combustion of Low Calorific Gases from Landfills and Waste Pyrolysis Using Porous Medium Burner Technology. Process Saf Environ Prot 2006;84:297–308.

Al-Hamamre Z, Voss S, Trimis D. Hydrogen production by thermal partial oxidation of hydrocarbon fuels in porous media based reformer. Int J Hydrogen Energ 2009;34:827-32.

Babkin VS, Korzhavin AA and Bunev VA. Propagation of Premixed Gaseous Explosion Flames in Porous Media. Combust Flame 1991;87:187–192.

Babkin VS, Filtrational combustion of gases. Present state of affairs and prospects, Pure Appl.Chem. 1993;65: 335–344.

Barra AJ, Diepvens G, Ellzey JL, Henneke MR. Numerical study of the effects of material properties on flame stabilization in a porous burner. Combust Flame 2003;134:369–79.

Baehr HD, Stephan K. Heat and mass transfer, Berlin, Heidelberg, Springer; 1998.

Bouma PH and de Goey LPH. Premixed combustion on ceramic foam burners. Combust Flame 1999;119:133–143.

Bowen HK. Basic research needs on high temperature ceramics for energy applications. Mater Sci Eng 1980;44:1–56.

Brenner G, Pickenäcker K, Pickenäcker O, Trimis D, Wawrzinek K, Weber T. Numerical and experimental investigation of matrix-stabilized methane/air combustion in porous inert media. Combust Flame 2000;123:201–13.

Catapan RC, Oliveira AAM, Costa M. Non-uniform velocity profile mechanism for flame stabilization in a porous radiant burner Exp Therm Fluid Sci 2011;35:172–179.

Cavaliere A, de Joannon M. Mild combustion. Prog. Energy Combust. Sci. 2004;30:329–36.

Cho KW, Han K, Lee YK, Noh DS, Yoon HM, Riu KJ, Lee KH. Premixed combustion of coke oven gas in a metallic fibre mat. Fuel 2001;80:1033–1036.

Choi GM, Katsuki M. Advanced low NOx combustion using highly preheated air. Energ Convers Manage 2001;42:639–652Modest MF. Radiative heat transfer. Academic Press; 2003

Deemyad S, Silvera IF. Temperature dependence of the emissivity of platinum in the IR. Rev Sci Instrum 2008;79:086105.

Di Mare L, Mihalik TA, Continillo G and Lee JHS. Experimental and numerical study of flammability limits of gaseous mixtures in porous media. Exp Therm Fluid Sci 2000;21:117-123.

Dyer M.J., Crosley D.R., Two-dimensional imaging of OH laser-induced fluorescence in a flame, Optics Letters, 1982:7;No 8

Eckbreth A., Laser Diagnostics for Combustion Temperature and Species, 2nd Edition, Gordon & Breach, Amsterdam 1996

Fend T, Trimis D, Pitz-Paal R, Hoffschmidt B, Reutter O. Thermal properties. In: Scheffler M, Colombo P, editors. Cellular ceramics: structure, manufacturing, properties and applications. Weinheim: Wiley; 2005. p. 342–60.

Gao H, Qu Z, Tao W, He Y, Zhou J. Experimental Study of Biogas Combustion in a Two-Layer Packed Bed Burner. Energ Fuel 2011;25:2887–2895.

Gauthier S, Nicolle A and Baillis D. Investigation of the flame structure and nitrogen oxides formation in lean porous premixed combustion of natural gas/hydrogen blends. Int J Hydrogen Energ 2008:33;4893-4905.

Hackert CL, Ellzeya JL and Ezekoyea OA, Combustion and heat transfer in model two-dimensional porous burners. 1999;116:177–191.

Hanamura K, Echigo R. An analysis of flame stabilization mechanism in radiation burners. Wärme-Stoffubertragung 1991;26:377–83.

Hanamura K, Echigo R, Zhdanok SA. Superadiabatic combustion in a porous medium. Int J Heat Mass Transfer, 1993;36(13):3201–9.

Hartlieb A.T., Atakan B., Kohse-Höinghaus K., Temperature measurement in fuel-rich non-sooting low-pressure hydrocarbon flames, Appl Phys B 2000:70;435–445

Hsu PH, Evans WD, Howell JR. Experimental and Numerical Study of Premixed Combustion within Nonhomogeneous Porous Ceramics. Comb Sci Tech 1993;90:149–72.

Howell JR, Hall MJ and Ellzey JL. Combustion of hydrocarbon fuels within porous inert media, Prog. Energy Combust. Sci. 1996;22:121–145.

Huang Y, Chao CYH and Cheng P. Effects of preheating and operations conditions on combustion in a porous medium. Int J Heat Mass Transfer, 2002;45:4315–4324.

Keramiotis Ch, Stelzner B, Trimis D, Founti MA. Porous burners for low-emission combustion: An experimental investigation. dx.doi.org/10.1016/j.energy.2011.12.006.

Keshtkar MM and Gandjalikhan Nassab SA. Theoretical analysis of porous radiant burners under 2-D radiation field using discrete ordinates method. J Quant Spectrosc Ra 2009;110:1894-1907

Kiefer J, Weikl MC, Seeger T, Von Issendorff F, Beyrau F, Leipertz A. Non-intrusive gas-phase temperature measurements inside a porous burner using dual-pump CARS. Proc Comb Institute 2009;32:3123-9.

Kohse Höinghaus K., Jeffries J.B. (Eds.), Applied Combustion Diagnostics, Taylor Francis, New York, 2002

Lee DK and Maruta K. Heat recirculation effects on flame propagation and flame structure in a mesoscale tube. Combustion Theory and Modelling 2012;16: 507–536.

Liu JF, Hsieh WH. Experimental investigation of combustion in porous heating burners. Combust Flame 2004;138:295–303.

Loukou A, Frenzel I, klein J and Trimis D. Experimental study of hydrogen production and sootparticulate matter emissions from methane rich-combustion in inert porous media. dx.doi.org/10.1016/j.ijhydene.2012.02.041

Machano R. Numerical simulations of surface reaction in porous media with lattice Boltzmann. Chem Eng Sci 2012;69:628-643

Mach Al. Entwicklung eines kompakten Heizsystems für Heizöl EL auf Basis der Verbrennung in porösen Keramiken, [dissertation]. Aachen, Germany: Universität Erlangen-Nürnberg; 2007.

Malico I, Zhou XY and Pereira JCF. Two dimensional numerical study of combustion and pollutants formation in porous burners. Combust Sci Tech. 2000:152;57-79

Mendes MAA, Pereira JMC, Pereira JCF. A numerical study of the stability of one-dimensional laminar premixed flames in inert porous media. Combust Flame 2008;153:525–539.

Mendes MAA, Pereira JMC, Pereira JCF. Calculation of premixed combustion within inert porous media with model parametric uncertainty quantification. Combust Flame 2011;158: 466–476.

Mishra SC, Steven M, Nemoda S, Talukdar P, Trimis D, Durst F. Heat transfer analysis of a two-dimensional rectangular porous radiant burner. Heat Mass Transfer 2006;33:467–474.

Mößbauer S, Pickenäcker O, Trimis D. Application of the porous burner technology in energy- and heat-engineering, In: Proceedings of the fifth international conference on technologies combustion for a clean environment (Clean Air V), Lisbon, 1999. p. 519–23.

Modest MF. Radiative heat transfer. Academic Press; 2003.

Mujeebu MA, Abdullah MZ, Bakar MZA, Mohamad AA, Abdullah MK. Applications of porous media combustion technology - A review. Appl Energ. 2009;86:1365–1375.

Mujeebu MA, Abdullah MZ, Bakar MZA, Mohamad AA, Abdullah MK. Combustion in porous media and its applications - A comprehensive survey. J Environ Manage. 2009;35: 216–230.

Muthukumar P, Shyamkumar PI. Development of novel porous radiant burners for LPG cooking applications. Fuel (2011), doi:10.1016/j.fuel.2011.09.006.

Nemoda S., Trimis D., Zivkovic G., Numerical simulation of porous burners and hole plate surface burners, Thermal Science, Vol. 8, No. 1, pp. 3-17, 2004

Pan HL., Pickenäcker O and Trimis D. Characterization of pore diameters in highly porous media, in Proceedings of 2003 ASME Summer Heat Transfer Conference, Las Vegas, Nevada, USA, July 2003

Pastore A, Mastorakos E. Syngas production from liquid fuels in a non-catalytic porous burner. Fuel 2011;90:64–76.

Pedersen-Mjaanes H, Chan L, Mastorakos E. Hydrogen production from rich combustion in porous media. Int J Hydrogen Energ 2005;30:579–592.

Pereira JCF, Malico I, Hayashi TC and Raposo J. Experimental and numerical characterization of the traverse dispersion at the exit of a short ceramic foam inside a pipe. Int J Heat Mass Tran 2005:48;1-14

Pereira FM, Oliveira, AAM and Fachini FF. Maximum superadiabatic temperature for stabilized flames within porous inert media. Combust Flame 2011;158:2283-2288.

Pickenäcker O, Pickenäcker K, Wawrzinek K, Trimis D, Pritzkow WEC, Müller C, et al. Innovative ceramic materials for porous-medium burners. Interceram 1999;48:326–30.

Pickenäcker O, Pickenäcker K, Wawrzinek K, Trimis D, Pritzkow WEC, Müller C, et al. Innovative ceramic materials for porous-medium burners II. Interceram 1999;48:424–33.

RAL gGmbH, Low-emission and Energy-saving Gas-fired Calorific-Value Heating Devices, RAL-UZ 61, Sankt Augustin, Deutschland, 2011.

Richards GA, McMillian MM, Gemmen RS, Rogers WA and Cully SR. Issues for low emission, fuel flexible power systems. Prog Energy Combust Sci 200;27:141–169.

Rørtveit GJ, Zepter K, Skreiberg Ø, Fossum M, Hustad JE. Comparison of low-NOx burners for combustion of methane and hydrogen mixtures. Proc Comb Institute 2002;29:1123–9.

Rumminger MD, Dibble RW, Heberle NH, Crosley DR. Gas temperature above a porous radiant burner: Comparison of measurements and model predictions. Symp (Int) Comb 1996;26:1755–62.

Sathe SB, Kulkarni MR, Peck RE, Tong TW. An experimental and theoretical study of porous radiant burner performance. Symp (Int) Comb 1991;23:1011–8.

Shi JR, Xie MZ, Liu H, Liu HS, Zhang XS and Xu YN. Two-dimensional numerical study of combustion and heat transfer in porous media combustor-heater. Proc Comb Institute 2011;33:3309-3316.

Smucker MT, Ellzey JL. Computational and experimental study of a two section porous burner. Comb Sci Tech 2004;176:1171–89.

Stelzner B, Keramiotis Ch, Voß S, Werner M, Founti MA, Trimis D. Experimental Study of the Flame Structure inside a Porous Inert Medium Burner using Planar Laser Induced Fluorescence. In: Adrian RJ, Durão DFG, Hishida K, Moreira ALN, Tropea C, editors. Proceedings of the 15th International Symposium on Applications of Laser Techniques to Fluid Mechanics; 2010 July 05-08; Lisbon, Portugal.

Takeno T, Sato K and Hase K. A theoretical study on an excess enthalpy flame. Symp (Int) Comb 1981;18:465–472.

Trimis D, Durst F. Combustion in a Porous Medium-Advances and Applications. Comb Sci Tech 1996;121:153–68.

Vourliotakis G, Skevis G, Founti MA. A detailed kinetic modelling study of benzene oxidation and combustion in premixed flames and ideal reactors. Energ Fuel 2011; 25: 1950–1963.

Weinberg FJ. Combustion Temperatures: The Future?. Nature. 1971:233;239–241.

Weinberg FJ. The first half million years of combustion research and today's burning problems Symp (Int) Comb 1975;1:1–17

Weikl MC, Tedder SA, Seeger T, Leipertz A. Investigation of porous media combustion by coherent anti-Stokes Raman spectroscopy. Exp Fluids 2010;49:775–81.

Wood S, Harris AT. Porous burner for lean-burn applications. Prog Energy Combust Sci 2008;34:667–84.

Wu D, Liu H, Xie M, Liu M and Sun W. Experimental investigation on low velocity filtration combustion in porous packed bed using gaseous and liquid fuels. Exp Therm Fluid Sci 2012;36:169-177.

Wunning JA, Wunning JG. Flameless oxidation to reduce thermal NO-formation. Prog Energy Combust Sci, 1997;29:81–94.

Xuan J, Leung MKH Leung DYC, Meng N. A review of biomass-derived fuel processors for fuel cell systems. Renew. Sust. Energ. Rev. 2009; 13: 1301–1313.

Yamamoto K., Ozeki M., Hayashi N., Yamashita H., Burning velocity and OH concentration in premixed combustion, Proc Comb Institute 2009:32;1227–1235

Yip B., Miller M. F., Lozano A., Hanson R. K., A combined OH/acetone planar laser-induced fluorescence imaging technique for visualizing combusting flows, Exp Fluids, 1994:17;330-336

Zheng C, Cheng L, Saveliev A, Luo Z, Cen K. Gas and solid phase temperature measurements of porous media combustion. Proc Comb Institute 2011;33:3301–3308.

Zhou XY, Pereira JCF. Comparison of Four Combustion Models for Simulating the Premixed Combustion in Inert Porous Media. Fire Mater 1998;22:187–97.

Chapter 8

Summary and conclusions of the thesis

Progress to develop and apply conventional as well as laser-based diagnostics to combustion applications is proceeding at a rapid pace. Combustion diagnostics improve the understanding of a variety of phenomena, leading to improved efficiencies in and cleanliness reduced emissions from practical systems. Currently, there are three distinct, but overlapping scientific directions in the area of development and application of diagnostic techniques (Alden *et al.*, 2011). In a first level, the combustion research targets in developing novel diagnostic techniques, as well as improving the precision and accuracy of existing ones, through fundamental studies. This category may involve rather fundamental aspects of atomic, molecular and laser physics and may not necessarily aim for a deepened understanding of combustion itself, rather the measurement techniques. In a second level, the aim is to employ mature techniques in tightly-controlled, laboratory-scale configurations, in order to enrich the understanding of certain combustion-related, dynamic phenomena (Candel, 2002), such as turbulent-chemistry interaction, combustion and pollutant formation. Such studies require multidisciplinary fields of expertise, such as chemical kinetics and fluid mechanics. The third level is the application of mature techniques for characterization, optimization and control of industrial processes, such as *in situ* measurements in engines, gas turbines or furnaces. This work deals to a certain extent with all these levels as summarized here.

8.1.   Summary and final conclusions

A number of intrusive as well as nonintrusive diagnostic tools were developed, evaluated and finally combined to characterize a porous burner with an increased level of complexity and design sophistication. As stated earlier, the main axes of combustion diagnostic research, relate to the development and implementation of novel and existing diagnostic methodologies in fundamental applications, so as to improve the knowledge concerning the methodology itself, as well as the phenomena under study. As the degree of complexity of both the experimental technique and the studied application increases, a number of fruitful combinations of methods allow the simultaneous measurement of different parameters, leading eventually to a more comprehensive investigation.

The first part of the thesis presented the basic scientific background along with the essential instrumentation concerning the techniques used with intrusive means. This included continuous gas analysis and gas chromatographic systems. A novel gas chromatographic method was developed and used and additional measurements were performed with a previously validated methodology (Esarte *et al.*, 2012). In order to obtain a clearer picture, the operating principles and the respective uncertainty analysis for both systems were also discussed. Subsequently, the gas chromatographic systems were utilized in the study of various methane-based mixtures under pyrolytic conditions and high temperature ranges. In the context of the latter, novel experimental data concerning minor species and polycyclic aromatic compounds were presented in chapter 4. Additionally, the gas chromatographic technique was utilized, in chapter 6, for the study of premixed flames of complex Fischer-Tropsch fuels with a systematic variation of their paraffinic, aromatic and naphthenic content. This is one of the very few studies in the literature dealing with premixed Fischer-Tropsch fuel blends, trying to assess their combustion performance to their constituent species. Finally, both continuous gas analysis and gas chromatographic systems were used in chapter 7, in order to facilitate detailed measurements at a porous burner exhaust, hence providing novel experimental data with respect to fuel and operating conditions variation.

In the context of the rapidly increasing incorporation of lasers in combustion research, the thesis examined the technique of the laser induced fluorescence as the nonintrusive diagnostic tool of choice. Chapter 3 provided the fundamental background knowledge in molecular structure and spectroscopic concepts, followed by an exhaustive discussion concerning laser induced fluorescence measurement strategies. Specifically, the scheme for the flame zone visualization through monitoring the hydroxyl radical was demonstrated. The utilized system was presented, including laser excitation and tuning sources as well as signal collection units. Accordingly, the adopted strategies were tested in simple laboratory-scale flame and a complex combustor. Hydroxyl radical–laser induced fluorescence measurements were obtained in a simple cross-flow premixed flame in chapter 5, where additional experiments with acetone-tracer laser induced fluorescence, served the further support of the results. Lastly, the technique was employed in chapter 7, in order to visualize the evolution and spatial characteristics of the flame inside a porous medium burner. The latter, constitutes the first study with nonintrusive diagnostic in the literature, which deals with the parametrical flame stabilization inside porous media with respect to nominal thermal load and stoichiometry.

As far as the choice of fuel is concerned, this study primarily focused in the conventional, methane based mixtures, since natural gas and biogas is expected to remain the cornerstone of existing combustion infrastructure. In this context, methane-based mixtures pyrolysis was firstly studied in a flow reactor, so as to examine fuel conversion and pollutant and soot formation mechanisms. The work was extended to quantify the influence of CO_2 environment under pyrolytic conditions, as far as the latter mechanisms were concerned. In order to assess the influence of CO_2 addition in a more practical environment, the biogas combustion in a porous burner was subsequently examined in chapter 7. In this way, the physical versus chemical impact of the CO_2 addition in the fuel stream was discussed with respect to combustor performance and emission levels. The natural gas feedstock can be additionally exploited in order to produce liquid fuels, fully compatible with existing engines, through the Fischer-Tropsch process. In this context, a chapter was devoted to the study of alternative cutting-edge fuels, produced via the Fischer-Tropsch process. The composition of the Fischer-Tropsch blends was systematically varied in order to allow the assessment of fuel mixing trends. Mixture thermochemical properties were calculated from detailed composition and compared against experimental data, with good agreement. As a result, the work provided a basic methodology for addressing fuel interchangeability with respect to fuel analysis and combustion performance.

Table 8-1 Summary of performed investigations with respect to innovative research in fuels, flames and combustion diagnostic methodologies. Research exploitation capabilities are also shown.

Chapter	Fuels	Flames	Diagnostics	Exploitation	Research directions
4	CH_4 CH_4/C_2H_6 CH_4/CO_2	methane, NG & biogas synergies in flames	GC &GC/MS for gaseous and PAH formation in PFRs	H_2/CO & soot yield in reformers / numerical model validation	Development, optimization and application of diagnostic techniques for fundamental studies in controlled, laboratory-scale configurations, in order to enrich the understanding of combustion-related, dynamic phenomena
5	H_2	cross flow mixing flames	OH-LIF / acetone tracer-LIF	nonintrusive assessment of mixing efficiency	
6	FT blends (C_xH_y)	constituent species synergies in FT flames	GC study in premixed lab-scale burner	alternative aviation fuels	
7	CH_4 C_3H_8/C_4H_{10} CH_4/CO_2	flame structure inside porous medium / emission formation with respect to fuels and operating conditions	LIF inside porous media / CGA & GC for emissions investigation	lean, mild combustion / fuel interchange-ability / heat distribution systems	Application of mature diagnostic techniques for characterization, optimization and control of industrial processes using *in situ* measurements

Table 8-1 presents the experimental investigations conducted in the frame of the thesis, with respect to the diagnostic research main directions. In addition, Table 8-1 summarizes the studied cases with reference to the innovation of the work as far as fuels, flames and diagnostic techniques are concerned. The field of application of each case study is also given regarding the exploitation and expansion of the research conducted. The latter are discussed in detail in the next paragraphs.

In more detail, in the fourth chapter the pyrolysis of atmospheric pressure methane mixtures has been experimentally investigated in an isothermal flow reactor in the temperature range of 1000-1200 ^{o}C with gas chromatographic means. Different methane mixtures, representative of natural gas and biogas operation, were tested in pure nitrogen and mixed N_2/CO_2 atmospheres. The studied cases were also relevant to the fuel reforming process in fuel cell systems, broadening the prospects of the work towards practical applications. The results were reproduced with two comprehensive detailed kinetic mechanisms, resulting in close agreement with experimental results. Experimental results for fuel conversion, H_2 and CO levels as well as concentration levels of key species, were presented and critically analyzed. It was shown that methane and natural gas pyrolysis yielded hydrogen of the order of 20% at the highest temperatures, whereas for the case of N_2/CO_2 atmosphere, hydrogen production was suppressed and CO was also present at the exhaust. Trends in exhaust gaseous species levels as a function of temperature and initial mixture composition were identified. In particular, the chemical effect of CO_2 was demonstrated. The results pointed towards the enhanced physical over chemical effect of the CO_2 addition; a 30% increase of the mixture carbon content, when CO_2 was introduced in the flow reactor, affected the mixture reactivity in temperatures higher than 1150 ^{o}C, where soot, water and CO were also present, hence also affecting minor species concentration levels. The higher carbon content and reactivity of the natural gas mixture were reflected in soot measurements and the temperature threshold for soot formation was measured. Furthermore, in order to assess the synergistic effects appearing in soot formation processes of the different mixtures, selected PAH species measurements were also performed.

The implementation of the laser induced fluorescence system for monitoring flame shape characteristics of a cross-flow flame was demonstrated in the fifth chapter. The potential of imaging diagnostics in studies of combustion phenomena is readily apparent, with significant potential to impact combustion research, for example in surveying complex flows and in guiding development of realistic flow models. The configuration studied comprised a laminar premixed flame, where the hydroxyl radical imaging can reveal mixing flow characteristics, hence constituted an ideal flame for introducing the methodology of the parametric study followed latter on, in the seventh chapter. In the frame of the chapter, the anisotropic flame structure was sufficiently captured by employing the OH-LIF technique. A parametric study with respect to stoichiometry and thermal load revealed a virtual confinement of the flame with increasing air content and an enhanced reaction zone intensity with increasing flame power. Overall, the results captured the OH radical distribution and revealed the inhomogeneous mixing induced from the cross-jet mixing configuration. This was also confirmed by supplementary investigations with acetone-tracer LIF experiments. Additionally, this work also has considerable linkage with practical fuels cell systems for automotive applications, especially as a part of an integrated mixing-flame trap stage of a porous burner (Voß *et al.*, 2011), similar to the one studied in the seventh chapter.

As also stated in the introductory chapter of the thesis, there is an increased research interest for alternative fuels. Combustion diagnostics should be employed in fundamental devices so as to correlate combustion performance to fuel characteristics, avoiding complexities introduced from the setup. Aviation fuels are probably the most challenging from the viewpoint of physical as well as thermochemical properties (Hui *et al.*, 2012). As premixed flames of Fischer-Tropsch fuels are relatively scarce in the literature, the sixth chapter of the thesis used a laboratory-scale premixed flame burner in order to test several Fischer-Tropsch blends and an n-decane for benchmark purposes. An extensive flame stability mapping was realized, as a function of thermal power and stoichiometry, and temperature profiles were obtained along the burner symmetry axis and species emission measurements were performed at locations representative of flame and post-flame zones. Although the Fischer-Tropsch blends revealed similar temperature values, the neat paraffinic blend exhibited the lowest temperatures, which increased with increasing aromatic content in the fuel. Through emission measurements it was also shown that the fully paraffinic blend results in the lowest unburnt hydrocarbon quantities, whereas blends with aromatic and naphthenic content show the opposite tendency. Overall, the findings were in good agreement with results from diffusion flame studies (Saffaripour *et al.*, 2013). It was demonstrated that simple laboratory scale combustion equipment, when used in a carefully controlled environment, can provide useful information about combustion characteristics of novel fuel mixtures.

The diagnostic methodologies developed, analyzed and implemented in fundamental configurations are combined in the seventh chapter of the thesis, in order to assess the operation, performance and fuel interchangeability of a porous inert medium burner. The burner characteristics, its principle of operation and its advantages are discusses in the opening section of the seventh chapter. A two-stage porous burner design with an Al_2O_3 flame trap and a 10 ppi SiSiC foam was considered, in order to resemble leading-edge porous burners utilized in industrial applications (Wood and Harris, 2008). The experimental characterization of the burner incorporated three major stages. Initially, the burner operation was examined through visualizing the flame zone inside the porous media. As the burner stability mapping was established, an extensive temperature and emission characterization with conventional as well as alternative fuels was performed. The conducted experimental campaign covered operating conditions from flashback up to marginally blow-off operational conditions.

In order to capture the flame shape and characteristics, the hydroxyl radical concentration was monitored by planar laser induced fluorescence measurements, for various nominal thermal loads and stoichiometries. Measurements of the hydroxyl radical in a combustion environment inside porous inert media have never been performed before, due to the high difficulty of obtaining optical access in such an environment. A study concerning the flame disturbance, induced by creating the optical pathway, was carried out. In the context of burner operation, it was observed that the position of the maximum OH concentration was almost independent of the stoichiometry for the same thermal loads in the stable operation regime. The results revealed that the flame zone length decreases with higher excess air ratios. For a near stoichiometric regime and low applied thermal loads, the flame stabilized directly downstream the flame trap, whereas for thermal loads up to $800 \, kW/m^2$, the flame moved further downstream at high excess air ratios. In total, the burner

stable operation was demonstrated over a wide operational range and this range formed the basis for the experimental characterization of the burner in terms of temperature and emissions.

In order to fully characterize the burner performance, the experimental campaign was extended to exhaust emission measurements with online continuous analyzers and a gas chromatographic system, along with gaseous and solid phase measurements obtained with thermocouples and infrared thermography respectively. The burner was initially tested with methane and liquefied petroleum gas, as the most commonly applied gaseous fuels. The burner's homogeneous distribution of temperature and emission profiles along its surface was confirmed and detailed measurements were parametrically conducted. Mean CO emissions were of the order of 50 ppm and NO_x emissions were around 25 ppm, under high power and low excess air ratios, where the high temperature range acted in favor of thermal NO_x formation. In the context of burner operation, the results suggested that the burner provides a wide flexibility when operated at lean combustion regimes with excess air ratio higher than $\lambda = 1.2$ providing low emissions and constant thermal potential for both tested fuels. Finally, the considered porous burner was operated with a typical biogas mixture. Exhaust gas measurements revealed that the CO_2 presence in the fuel mixture led to higher CO levels at the burner exhaust. This behavior could be either attributed to the chemical impact of CO_2 or to the fact that it also acted as a diluent leading to lower residence times in the porous matrix and lower temperatures in comparison with pure methane combustion. This observation suggested that residence times versus kinetic scales in the porous matrix of the particular burner were long enough to overcome any kinetic effect. Overall, the work indicated that the CO_2 addition had eventually small chemical impact at the exhaust of the burner, although this statement may not be valid for phenomena inside the combustion zone. In biogas operation the burner's stable operation domain was slightly shifted to the richer domain in comparison to pure methane operation. Temperature values reached 1100 ^{o}C under the highest applied thermal load and were systematically 10% lower compared to pure methane operation under the same fuel and air supply. Carbon monoxide levels reached 300 ppm under 1000 kW/m^2 of nominal thermal load and $\lambda = 1.3$ and total NO_x levels were never above the threshold of 20 ppm. CO emissions were around 50% increased, in comparison to pure methane operation, whereas total NO_x values were reduced by 50 to 60%. Overall, the burner characterization in terms of operation, performance, emission reduction and fuel interchangeability, revealed that the porous inert medium burner constitutes a particularly attractive technology that meets modern requirements, resolving important issues for fuel-flexible environmental friendly combustors.

8.2.   Publications related to framework of the thesis

The majority of the work presented in the present thesis has been accepted and published in four scientific journals and six international conferences and therefore has been submitted in extensive reviewing process. The conducted experimental campaigns included the fruitful cooperation of eighteen coworkers from four European. These papers are listed below.

Publications in International Scientific Journals

I.   Ch. Keramiotis, M.A. Founti, An experimental investigation of stability and operation on a biogas fueled porous burner. Fuel (2013) Volume 103, Pages 278–284.

II.   Ch. Keramiotis, G. Zannis, G. Skevis, M.A. Founti Performance investigation of Fischer-Tropsch kerosene blends in a laboratory-scale premixed burner. Experimental Thermal Fluid Science (2013) Volume 44, Pages 868–874.

III.   Ch. Keramiotis, G. Vourliotakis, G. Skevis, M.A. Founti, C. Esarte, N.E. Sánchez, A. Millera, R. Bilbao, M.U. Alzueta, Experimental and computational study of methane pyrolysis in a flow reactor under atmospheric pressure, Energy (2012) Volume 43, Issue 1, Pages 103–110.

IV.   Ch. Keramiotis, B. Stelzner, D. Trimis and M. Founti, Porous burners for low-emission combustion: An experimental investigation, Energy (2012) Volume 45, Issue 1, Pages 213–219.

Publications in International Conferences

V.   Ch. Keramiotis, L. Leon, G. Vourliotakis, G. Skevis, M.A. Founti, F. Mauss. Performance and emission characterization of a laboratory-scale swirl burner operating with methane mixtures. COST CM0901, 3rd annual meeting, 5th – 7th September 2012, Sofia, Bulgaria.p.172

VI.   Ch. Keramiotis, M.A. Founti, Experimental characterization of a two layer porous inert medium burner operating with a biogas-like CO_2/CH_4 mixture. COST CM0901, 3rd annual meeting, 5th – 7th September 2012, Sofia, Bulgaria. p.137

VII.   Ch. Keramiotis, G. Vourliotakis, G. Skevis, M.A. Founti, C. Esarte, M.U. Alzueta, Experimental and computational study of methane pyrolysis in a Flow Reactor under atmospheric pressure, Cleaner Combustion 2011, 7th – 9th September 2011, Zaragoza, Spain. p.162

VIII. Ch. Keramiotis, B. Stelzner, D. Trimis and M. Founti, Porous burners for low-emission combustion: An experimental investigation, Proceedings of ECOS 2011, 920-930

IX.   Ch. Keramiotis, G. Zannis, G. Skevis, A. Tsalavoutas, K. Mathioudakis, M.A. Founti, An experimental assessment of combustion and emission characteristics of alternative aviation fuels, The 5th European Combustion Meeting 2011, p.156

X.   B. Stelzner, Ch. Keramiotis, S. Voss, M. Werner, M.A. Founti, D. Trimis, Experimental Study of the Flame Structure inside a Porous Inert Medium Burner using Planar Laser Induced Fluorescence, 15th International Symposium on Applications of Laser Techniques to Fluid Mechanics, p. 1.1.3

8.3.   Future work

The present work could be further extended in a number of aspects, which could integrate and complete the research carried out. Here, a few point-wise suggestions are made for future work.

Fuel characterization

A more erudite investigation of methane-based mixtures in a flow reactor setup could provide valuable experimental data concerning the synergistic effects of various additives, such as ethane, propane and hydrogen, which would resemble natural gas composition and in turn uncover its chemical pathways. Additional experimental campaigns should take place, choosing additives that resemble biogas-like mixture compositions. Such investigations should be accompanied with an in depth analysis of intermediates formed during the process, as well as with polycyclic aromatic compounds speciation data. Specifically, polycyclic aromatic compounds hold an important role in soot formation and their chemistry should be thoroughly understand, in order to develop more accurate numerical models. The preliminary work presented in the fourth chapter could provide an indicative guideline for future work.

Moreover, expanding the alternative fuels investigation attempted in the frame of the thesis, more Fischer-Tropsch blends could be tested. Although, aviation demands the usage of additives for improvement of physical fuel properties, or their blending mixed with conventional kerosene, the same process may be drafted to reproduce lighter fuel blends for automotive industry. Following the same methodology presented in the sixth chapter, more Gas-to-Liquid or Biomass-to-Liquid fuels could be investigated with respect to their combustion performance characteristics.

Flame/Burner characterization

The conducted experimental campaign, which covered a several areas of the porous burner characterization, could be further enriched with additional key investigations. For example, following the proposed methodology, further measurements inside the porous media could be conducted, with respect to thermal load, stoichiometry and fuel. For instance, the hydroxyl radical, chosen here as a marker for the flame zone, may be combined with formaldehyde measurements (CH_2O-LIF). Such a study can produce interesting results concerning, besides the flame zone, the heat release rate inside the porous media as it does in free flames (Fayoux, 2005). This investigation may be even realized with the usage of the third harmonic Nd: YAG generator and a detection band around 420 nm, given a similar scheme to the one followed in the fifth chapter for acetone tracer laser induced fluorescence measurements. In the same direction with OH-LIF measurements, CH-LIF could provide extra information for reaction zone visualization and heat release rates.

In line with the previous proposal, laser induced fluorescence measurements may be utilized in order to measure burning velocity inside the porous media as followed in the literature of open flames (Yamamoto *et al.*, 2011). Furthermore, measurements with laser induced fluorescence for the detection of nitric monoxide could be conducted at the burner exhaust and calibrated with measurements obtained with intrusive techniques. Such studies would either require a different dye such as coumarin or the incorporation of the mixing-after-doubling technique as described in the third chapter. This methodology could provide quantitative speciation information, which could, in principle, be further employed for measurements inside porous media. In conclusion the porous burner design could be slightly modified, maintaining its principal characteristics, so as for instance to incorporate a porous flame trap, rather than a drilled one. This configuration may extinguish any flowfield disturbances and provide even more realistic flame zone visualization.

Chapter References

Aldén M, Bood J, Li Z and Richter M. Visualization and understanding of combustion processes using spatially and temporally resolved laser diagnostic techniques. Proc. Combust. Inst. 2011;33:69-97.

Candel S. Combustion dynamics and control: Progress and challenges. Proc. Combust. Inst. 2002;29:1-28.

Esarte C, Abián M, Millera A, Bilbao R and Alzueta MU. Gas and soot products formed in the pyrolysis of acetylene mixed with methanol, ethanol, isopropanol or n-butanol. Energy 2012;43:37-46

Fayoux A, Zähringer K, Gicquel O and Rolon JC. Experimental and numerical determination of heat release in counterflow premixed laminar flames. Proc. Combust. Inst. 2005;30:251–257.

Hui X, Kumar K, Sung C, Edwards T and Gardner D. Experimental studies on the combustion characteristics of alternative jet fuels. Fuel 2012;98:176-182.

Saffaripour M, Kholghy M, Dworkin SB and Thomson MJP. A numerical and experimental study of soot formation in a laminar coflow diffusion flame of a Jet A-1 surrogate. Proc. Combust. Inst. J.proci.2012.06.176

Voß S, Steinbrück R, Kautz M, Schießwohl E, Arendt M, Tom Felde J, Volkert J and Trimis D. Premixed hydrogen-air combustion system for fuel cell systems. Int. J. Hydrogen Energy 2011;36:3697-3703

Wood S and Harris AT. Porous burner for lean-burn applications. Prog Energy Combust Sci 2008;34:667–84.Yamamoto K, Ozeki M, Hayashi N and Yamashita H. Burning velocity and OH concentration in premixed combustion. Proc. Combust. Institute 2009;32:1227-1235.

Yamamoto K, Isii S and Ohnishi M. Local flame structure and turbulent burning velocity by joint PLIF imaging. Proc. Combust. Inst. 2011;33:1285-1292.

Summary of Bibliography

[1]   Abián M, Esarte C, Millera A, Bilbao R and Alzueta MU. Oxidation of acetylene-ethanol mixtures and their interaction with NO. Energy Fuel 2008;22:3814–3823

[2]   Abián M, Giménez-López J, Bilbao R, Alzueta MU. Effect of different concentration levels of CO_2 and H_2O on the oxidation of CO: Experiments and modeling. Proc. Combust. Inst. 2011; 33: 317–323.

[3]   Abián M, Millera A, Bilbao R, Alzueta MU. Experimental study on the effect of different CO2 concentrations on soot and gas products from ethylene thermal decomposition. Fuel 2012; 91: 307-312.

[4]   Abu-Jrai A, Rodriguez-Fernandez J, Tsolakis A, Megaritis A, Theinmoi K, Cracknell RF and Clark RH, Performance, combustion and emissions of a diesel engine operated with reformed EGR. Comparison of diesel and GTL fuelling. Fuel 2009:88;1031-1041.

[5]   Abu-Jrai A, Tsolakis A, Theinmoi K, Cracknell RF, Megaritis A, Wyszynski ML and Golunski SE. Effect of Gas-to-Liquid Diesel Fuels on Combustion Characteristics,Engine Emissions, and Exhaust Gas Fuel Reforming. Comparative Study. Energy Fuel 2006:20;2377-2384.

[6]   Afsharvahid S, Ashman PJ, Dally BB. Investigation of NOx conversion characteristics in a porous medium. Combust Flame 2008;152:604–615.

[7]   Agafonov GL, Borisov AA, Smirnov VN, Troshin KY, Vlasov PA, Warnatz J. Soot formation during pyrolysis of methane and rich methane/oxygen mixtures behind reflected shock waves. Comb. Sci. Technol. 2008; 180: 1876–1899

[8]   Aksit IM and Moss JB. Model fuels to reproduce the sooting behavior of aviation kerosene. Fuel. 2005:84;239–245

[9]   Al-Hamamre Z, Diezinger S, Talukdar P, Von Issendorff F, Trimis D. Combustion of Low Calorific Gases from Landfills and Waste Pyrolysis Using Porous Medium Burner Technology. Process Saf Environ Prot 2006;84:297–308.

[10]   Al-Hamamre Z, Voss S, Trimis D. Hydrogen production by thermal partial oxidation of hydrocarbon fuels in porous media based reformer. Int J Hydrogen Energ 2009;34:827-32.

[11]   Aldén M, Wallin S and Wendt W. Applications of two-photon absorption for detection of CO in combustion gases, Appl. Phys. B 1984;33:205-208.

[12]   Aldén M, Bood J, Li Z and Richter M. Visualization and understanding of combustion processes using spatially and temporally resolved laser diagnostic techniques. Proc. Combust. Inst. 2011;33:69-97.

[13]   Alzueta MU, Glarborg P, Dam-Johansen K. Low temperature interactions between hydrocarbons and nitric oxide: An experimental study. Combust. Flame 1997; 109: 25–36.

[14]   Alzueta MU, Oliva M, Glarborg P. Parabenzoquinone pyrolysis and oxidation in a flow reactor. International J. Chem. Kinet. 1998; 30: 683–697.

[15]   Alzueta MU, Glarborg P, Dam-Johansen K. Experimental and kinetic modeling study of the oxidation of benzene. International J. Chem. Kinet. 2000; 32: 498–522.

[16]   Alzueta MU, Hernández JM. Ethanol oxidation and its interaction with nitric oxide. Energy Fuels 2002; 16: 166–171.

[17]   Alzueta MU, Borruey M, Callejas A, Millera A, Bilbao R. An experimental and modeling study of the oxidation of acetylene in a flow reactor. Combust. Flame 2008; 152: 377–386.

[18]   Appel J, Bockhorn H, Frenklach M. Kinetic modeling of soot formation with detailed chemistry and physics: laminar premixed flames of C2 hydrocarbons. Combust. Flame 2000; 121: 122–136.

[19]   Appleby AJ. Fuel cell technology: Status and future prospects. Energy. 1996; 21: 521-653

[20]   Arutyunov VS, Vedeneev VI. Pyrolysis of the methane in the temperature range 1000-1700K. Uspekhi Khimii Russian Chemical Reviews 1991; 60: 2663-2684.

[21]   Axelsson B, Collin R and Bengtsson PE. Laser-induced incandescence for soot particle size measurements in premixed flat flames Appl Opt 2000;39:3683-3690.

[22]   Azimov U and Kim KS, Visualization of Gas-to-Liquid (GTL) Fuel Liquid Length and Soot Formation in the Constant Volume Combustion Chamber. J Therm Sci Tech-JPN 2008:3;461-473

[23]   Babkin VS, Korzhavin AA and Bunev VA. Propagation of Premixed Gaseous Explosion Flames in Porous Media. Combust Flame 1991;87:187–192.

[24]   Babkin VS, Filtrational combustion of gases. Present state of affairs and prospects, Pure Appl.Chem. 1993;65: 335–344.

[25]   Baehr HD, Stephan K. Heat and mass transfer, Berlin, Heidelberg, Springer; 1998.

[26]   Bakali AEl, Mercier X, Wartel M, Acevedo F, Burns I, Gasnot L, Pauwels JF and Desgroux P. Modeling of PAHs in low pressure sooting premixed methane flame. Energy 2012;43:73-84.

[27]   Balès-Guéret C, Cathonnet M, Boettner JC and Gaillard F. Experimental study and kinetic modeling of higher hydrocarbons oxidation in a jet-stirred flow reactor. Energy Fuel 1992;6:189-194.

[28]   Ball M and Wietchel M. The future of hydrogen – opportunities and challenges. Int J Hydrogen Energy 2009;34:615-627

[29]   Barra AJ, Diepvens G, Ellzey JL, Henneke MR. Numerical study of the effects of material properties on flame stabilization in a porous burner. Combust Flame 2003;134:369–79.

[30]   Barry EF and Grob RL. 2007. Columns for gas chromatography, Performance and selection. Hoboken, New Jersey. John Wiley & Sons, Inc.

[31]   Baulch DL, Bowman CT, Cobos CJ, Cox RA, Just T, Kerr JA et al. J, Evaluated Kinetic Data for Combustion Modeling: Supplement II. J. Phys. Chem. Ref. Data 2005; 34: 757-1359.

[32]   Benson SW. Thermochemical Kinetics, John Wiley and Sons, N.Y. 1976

[33]   Bermúdez V, Lujan JM, Pla B, Linares WD. Effects of low pressure exhaust gas recirculation on regulated and unregulated gaseous emissions during NEDC in a light-duty diesel engine. Energy 2011; 36: 5655-5665.

[34]   Bessler WG and Schulz C. Quantitative multi-line NO-LIF temperature Imaging, Appl. Phys. B 2004;78:519–533.

[35]   Bessler WG, Schulz C, Lee t, Jeffries JB and Hanson RK. Strategies for laser-induced fluorescence detection of nitric oxide in high-pressure flames. I. A–X (0,0) excitation. Appl Opt 2002;41:3547-3557.

[36]   Bessler WG, Schulz C, Lee t, Jeffries JB and Hanson RK. Strategies for laser-induced fluorescence detection of nitric oxide in high-pressure flames. I. A–X (0,0) excitation. Appl Opt 2003;42:2031-2042.

[37]   Bessler WG, Schulz C, Lee t, Jeffries JB and Hanson RK. Strategies for laser-induced fluorescence detection of nitric oxide in high-pressure flames. III. Comparison of A–X excitation schemes. Appl Opt 2002;42:4922-4936

[38]   Bilbao R, Millera A, Alzueta MU, Prada L. Evaluation of the use of different hydrocarbon fuels for gas reburning. Fuel 1997; 76: 1401–1407.

[39]   Blakey S, Rye L, Wilson CW, Aviation gas turbine alternative fuels: A review. Proc. Combust. Inst. 2011:33;2863-2885

[40]   Bockhorn H, D'Anna A, Sarofim AF and Wang H (Eds.) Combustion generated fine carbonaceous particles. Karlsruher Institut für Technologie-KIT Scientific Publishing 2012.

[41]   Böckle S, Kazenwadel J, Kunzelmann T, Shin D-I, Schulz C. Single-shot laser-induced fluorescence imaging of formaldehyde with XeF excimer excitation. Applied Physics B 2000;70:733-735.

[42]   Borman GL and Ragland KW. Combustion engineering. McGraw Hill (1998)

[43]   Bouma PH and de Goey LPH. Premixed combustion on ceramic foam burners. Combust Flame 1999;119:133–143.

[44]   Bowen HK. Basic research needs on high temperature ceramics for energy applications. Mater Sci Eng 1980;44:1–56.

[45]   Brenner G, Pickenäcker K, Pickenäcker O, Trimis D, Wawrzinek K, Weber T. Numerical and experimental investigation of matrix-stabilized methane/air combustion in porous inert media. Combust Flame 2000;123:201–13.

[46]   Brockhinke A, Lenhard U, Bulter A and Kohse-Hoinghaus K, Energy transfer in the OH $A^2\Sigma^+$ state: The role of polarization and of multi-quantum energy transfer, Phys. Chem. Chem. Phys 2005;7:874-881.

[47]   Brockhinke A and Kohse-Hoinghaus K, Energy transfer in combustion diagnostics: Experiment and modelling. Faraday Discuss. 2001;119:275-286.

[48]   Bruno TJ and Smith BL. Evaluation of the Physicochemical Authenticity of Aviation Kerosene Surrogate Mixtures. Part 1: Analysis of Volatility with the Advanced Distillation Curve. 2010:24;4266–4276.

[49]   Bruno TJ and Smith BL. Evaluation of the Physicochemical Authenticity of Aviation Kerosene Surrogate Mixtures. Part 2: Analysis and Prediction of Thermophysical Properties. 2010:24;4277–4284.

[50]   Burke MP, Chaos M, Ju Y, Dryer FL and Klippenstein SJ. Comprehensive H_2/O_2 kinetic model for high-pressure combustion. Int J Chem Kinet 2012;44:444-474

[51]   Burns IS, MercierX, Wartel M, Chrystie RSM, Hult J and Kaminski CF. A method for performing high accuracy temperature measurements in low-pressure sooting flames using two-line atomic fluorescence Proc. Combust. Inst. 2011:33;799-806.

[52]   Bülter A, Lenhard U, Rahmann U, Kohse-Höinghaus K, Brockhinke A. LASKIN: Efficient simulation of spectra affected by energy transfer. In: Proceedings of LACEA 2004 (Laser Applications to Chemical and Environmentel Analysis). 2004.

[53]   Candel S. Combustion dynamics and control: Progress and challenges. Proc. Combust. Inst. 2002;29:1-28.

[54]   Catapan RC, Oliveira AAM, Costa M. Non-uniform velocity profile mechanism for flame stabilization in a porous radiant burner Exp Therm Fluid Sci 2011;35:172–179.

[55]   Cavaliere A, de Joannon M. Mild combustion. Prog. Energy Combust. Sci. 2004;30:329–36.

[56]   Cazes J and Scott RPW. 2002. Chromatography theory. Marcel Dekker, INC. New York Basel

[57]   Chen CJ, Back MH, Back RA. The Thermal Decomposition of Methane. I. kinetics of the Primary Decomposition to C_2H_6 + H_2; Rate Constant for the Homogeneous Unimolecular Dissociation of Methane and its Pressure Dependence. Can J. Chem. 1975; 53: 3580–3590.

[58]   Chen CJ, Back MH, Back RA. The thermal decomposition of methane. II. Secondary reactions, autocatalysis and carbon formation; non-Arrhenius behavior in the reaction of CH3 with ethane. Can. J. Chem. 1976; 54: 3175–3184.

[59]   Chen YC, Petters N, Schneemann GA, Wruck N Renz U and Mansour MS. The detailed flame structure of highly stretched turbulent premixed methane-air flames. Combust Flame. 1996;107:223–224

[60]   Cheng TS. Yuan T, Lu CC and Chao YC. The application of spontaneous vibrational raman scattering for temperature measurements in high pressure laminar flames. Combust Sci Technol 174;5-6:111-128

[61]   Cheskis S. Quantitative measurements of absolute concentrations of intermediate species in flames. Prog. Energy Combust. Sci. 1999;25:233-252

[62]   Chigier N (Ed.). 1991. Combustion Measurements. Hemishpere Publishing Corporation, USA

[63]   Cho KW, Han K, Lee YK, Noh DS, Yoon HM, Riu KJ, Lee KH. Premixed combustion of coke oven gas in a metallic fibre mat. Fuel 2001;80:1033–1036.

[64]   Choi GM, Katsuki M. Advanced low NOx combustion using highly preheated air. Energ Convers Manage 2001;42:639–652Modest MF. Radiative heat transfer. Academic Press; 2003

[65]   Cooke JA, Bellucci M, Smooke MD, Gomez A, Violi A, Faravelli T and Ranzi E. Computational and experimental study of JP-8, a surrogate, and its components in counterflow diffusion flames. Proc Combust Inst 2005;30;439-446.

[66]   Cooper CS, Ravikrishna RV and Laurendeau NM. Comparisons of laser-saturated, laser-induced, and planar laser-induced fluorescence measurements of nitric oxide in a lean direct-injection spray flame. Appl. Opt. 1998;37:4823-483

[67]   Corporan E, DeWitt MJ, Belovich V, Pawlik R, Lynch AC, Gord JR and Meyer TR. Emissions Characteristics of a Turbine Engine and Research Combustor Burning a Fischer–Tropsch Jet Fuel. Energ Fuel 2007:21(5); 2615–2626.

[68]   CRC, Handbook of Aviation Fuels, Society of Automotive Engineers, 2004

[69]   Daily JW. Laser Induced Fluorescence Spectroscopy in Flames, Prog. Energy Combust. Sci., 1997;23: 133-199.

[70]   Dagaut P and Nicolle A. Experimental and detailed kinetic modeling study of hydrogen-enriched natural gas blend oxidation over extended temperature and equivalence ratio ranges. Proc Combust Inst 2005;30:2631–2638.

[71]   Dagaut P and Cathonnet M. The ignition, oxidation, and combustion of kerosene: A review of experimental and kinetic modeling. Prog Energy Combust Sci 2006:32(1);48–92

[72]   Dagaut P, El Bakali A and Ristori A. The combustion of kerosene: Experimental results and kinetic modeling using 1- to 3-component surrogate model fuels. Fuel. 2006:85;944–956.

[73]   Dagaut P and Gail S. Chemical Kinetic Study of the Effect of a Biofuel Additive on Jet-A1 Combustion J Phys Chem A 2007:111;3992-4000.

[74]   Dagaut P. Kinetics of jet fuel combustion over extended conditions: Experimental and modeling. Transactions of ASME 2007;129:394-403.

[75]   Dagaut P and Nicolle A. Experimental study and detailed kinetic modeling of the effect of exhaust gas on fuel combustion: mutual sensitization of the oxidation of nitric oxide and methane over extended temperature and pressure ranges. Combust Flame 2005;140:161-171.

[76]   Day M, Tachibana S, Bell J, Lijewski M, Beckner V and Cheng RK. A combined computational and experimental characterization of lean premixed turbulent low swirl laboratory flames I. Methane flames. Combust Flame 2012;159:275-290

[77]   Deemyad S, Silvera IF. Temperature dependence of the emissivity of platinum in the IR. Rev Sci Instrum 2008;79:086105.

[78]   Deschamps BM, Smallwood GJ, Prieur J, Snelling DR and Gülder ÖL. Surface density measurements of turbulent premixed flames in a spark-ignition engine and a Bunsen-type burner using planar laser-induced fluorescence. Symposium (Int) on Combustion 1996;26:427-435

[79]   Dewitt MJ, Corporan E, Graham J and Minus D. Effects of Aromatic Type and Concentration in Fischer–Tropsch Fuel on Emissions Production and Material Compatibility Energ Fuel 2008:22;2411–2418.

[80]   Di Mare L, Mihalik TA, Continillo G and Lee JHS. Experimental and numerical study of flammability limits of gaseous mixtures in porous media. Exp Therm Fluid Sci 2000;21:117-123.

[81]   Docquier N and Candel S. Combustion control and sensors: a review. Prog Energy Combust Sci 2002;28:107-150

[82]   Dreier T and Rakestraw DJ. Degenerate Four-Wave Mixing Diagnostics on OH and NH Radicals in Flames. Appl. Phys. B 1990;50:479-485

[83]   Dryer AJ and Crosley DR. Two-dimensional imaging OH laser-induced fluorescence in a flame.Opt. Letter 1982;7:382-384

[84]   Du DX, Axelbaum RL, Law CK. The influence of carbon dioxide and oxygen as additives on soot formation in diffusion flames. Symposium (International) on Combustion 1991; 23: 1501-1507.

[85]   Dyer M.J., Crosley D.R., Two-dimensional imaging of OH laser-induced fluorescence in a flame, Optics Letters, 1982:7;No 8

[86]   Eckbreth AC, Bonczyk PA and Verdieck JF. Combustion diagnostics by laser Raman and fluorescence techniques. Prog. Energy Combust. Sci. 1979;5:253-322.

[87]   Eckbreth AC. Recent advances in laser diagnostics for temperature and species concentration in combustion. Symposium (Int) Combust. 1981;18:1471-1488.

[88]   Eckbreth A.1996. Laser Diagnostics for Combustion Temperature and Species, 2nd Edition, Gordon & Breach, Amsterdam

[89]   Edwards T and Maurice LQ. Surrogate mixtures to represent complex aviation and rocket fuels. J Propul Power 2001:17(2);461-466

[90]   Esarte C, Abián M, Millera A, Bilbao R and Alzueta MU. Gas and soot products formed in the pyrolysis of acetylene mixed with methanol, ethanol, isopropanol or n-butanol. Energy 2012;43:37-46

[91]   Esarte C, Millera Á, Bilbao R, Alzueta MU, Gas and soot products formed in the pyrolysis of acetylene–ethanol blends under flow reactor conditions, Fuel Process. Technol. 2009;90:496–503.

[92]   Esarte C, Callejas A, Millera A, Bilbao R, Alzueta MU. Influence of the concentration of ethanol and the interaction of compounds in the pyrolysis of acetylene and ethanol mixtures, Fuel 2011;90: 844–849.

[93]   Esarte C, Peg M, Ruiz MP, Mellera Á, Bilbao R, Alzueta MU. Pyrolysis of ethanol: Gas and soot products formed. Ind Eng Chem Res 2011;50:4412-4419

[94]   Etzkorn T, Muris S, Wolfrum J, Dembny C, Bockhorn H, Nelson PF, Attia-Shahin A and Warnatz J. Destruction and formation of no in low pressure stoichiometric CH_4/O_2 flames. Symposium (Int) on Combustion 1992;24:925–932

[95]   Farhad S, Yoo Y and Hamdullahpur F. Developing fuel map to predict the effect of fuel composition on the maximum efficiency of solid oxide fuel cells. J Power Sources 2009;193:632–638.

[96]   Farhad S, Yoo Y and Hamdullahpur F. Effects of fuel processing methods on industrial scale biogas-fuelled solid oxide fuel cell system for operating in wastewater treatment plants. J Power Sources 2010;195:1446–1453.

[97]   Fayoux A, Zähringer K, Gicquel O and Rolon JC. Experimental and numerical determination of heat release in counterflow premixed laminar flames. Proc. Combust. Inst. 2005;30:251-257.

[98]   Fend T, Trimis D, Pitz-Paal R, Hoffschmidt B, Reutter O. Thermal properties. In: Scheffler M, Colombo P, editors. Cellular ceramics: structure, manufacturing, properties and applications. Weinheim. Wiley 2005 p.342–60.

[99]   Feynman RP, Leighton RB and Sands M. 2005. The Feynman Lectures on Physics including Feynman's Tips on Physics: The Definitive and Extended Edition (2nd Ed.) Addison-Wesley, Boston

[100]   Fischer K, Rzepka M, Stimming U, Biermann JW, Johannaber M and Wallentowitz H. Performance of gasoline fuel cell cars – a simulation study. Proc. IMechE Part D: J Automob Eng 2005;219:889-896

[101]   Freitag R and Allington RW (Eds). 2002. Modern Advances in Chromatography. Springer Verlag Berlin Heidelberg

[102]   Fryda L, Panopoulos K, Vourliotis P, Pavlidou E and Kakaras E. Experimental investigation of fluidised bed co-combustion of meat and bone meal with coals and olive bagasse. Fuel 2006;85:1685–1699

[103]   Gao H, Qu Z, Tao W, He Y, Zhou J. Experimental Study of Biogas Combustion in a Two-Layer Packed Bed Burner. Energ Fuel 2011;25:2887–2895.

[104]   Garman JD and Dunn-Rankin D. Spatial averaging effects in CARS thermometry of a nonpremixed flame. Combust Flame 1998;115:481-486

[105]   Gauthier S, Nicolle A and Baillis D. Investigation of the flame structure and nitrogen oxides formation in lean porous premixed combustion of natural gas/hydrogen blends. Int J Hydrogen Energ 2008:33;4893-4905.

[106]   Gazi A, Vourliotakis G, Skevis G, Founti MA. A modelling study of allene and propyne combustion in flames, in: Fifth European Combustion Meeting ECM2011, Cardiff, UK, 2011.

[107]   Gibaud C, Snyder JA, Sick V and Lindstedt R.P. Laser-induced fluorescence measurements and modeling of absolute CH concentrations in strained laminar methane/air diffusion flames. Proc. Combust. Institute 2005;30:455-463

[108]   Giakoumis EG, Rakopoulos CD, Dimaratos AM, Rakopoulos DC. Exhaust emissions of diesel engines operating under transient conditions with biodiesel fuel blends. Prog. Energy Combust Sci 2012;38:691–715

[109]   Glarborg P, Alzueta MU, Dam-Johansen K, Miller JA. Kinetic modeling of hydrocarbon/nitric oxide interactions in a flow reactor. Combust. Flame 1998; 115: 1–27.

[110]   Ghosh S, De S. Energy analysis of a cogeneration plant using coal gasification and solid oxide fuel cell. Energy. 2003; 31: 345-363.

[111]   Gökalp I. and Lebas E. Alternative fuels for industrial gas turbines (AFTUR) Appl. Therm. Eng. 2004:24;1655-1663.

[112]   Gokulakrishnan P, Kazakov, A and Dryer FL. Comparison of numerical and experimental kinetic data for flow reactor systems: Mixing effects. The Combustion Institute (2003) *Proceedings of the Third Joint Meeting*

[113]   Goldman A and Cheskis S. Intracavity laser absorption spectroscopy of sooting acetylene/air flames. Appl. Phys. B 2008;92:281–286.

[114]   Gordon RL, Masri AR and Mastorakos E. Simultaneous Rayleigh temperature, OH- and CH_2O-LIF imaging of methane jets in a vitiated coflow. Combust Flame 2008;155:181–195

[115]   Gorte RJ, Vohs JM. Novel SOFC anodes for the direct electrochemical oxidation of hydrocarbons. J. Catal. 2003; 23: 477–486.

[116]   Granovskii M, Dincer I and Rosen MA. Economic and environmental comparison of conventional, hybrid, electric and hydrogen fuel cell vehicles. J Power Sources 2006;159:1186–1193

[117]   Grob RL and Barry EF (Eds.). 2004. Modern practice of gas chromatography (4th Ed.) Hoboken, New Jersey. John Wiley & Sons, Inc.

[118]   Guiochon G and Guillemin CL. Gas chromatography. Rev. Sci. Instrum. 1990:61;3317-3339.

[119]   Gülder ÖL, Smallwood GJ Wong R Snelling DR, Smith R, Deschamps BM and Sautet JC. Flame Front Surface Characteristics in Turbulent Premixed Propane/Air Combustion. Combust Flame 2000;120:407-416

[120]   Hackert CL, Ellzeya JL and Ezekoyea OA, Combustion and heat transfer in model two-dimensional porous burners. 1999;116:177–191.

[121]   Hanamura K, Echigo R. An analysis of flame stabilization mechanism in radiation burners. Wärme-Stoffubertragung 1991;26:377–83.

[122]   Hanamura K, Echigo R, Zhdanok SA. Superadiabatic combustion in a porous medium. Int J Heat Mass Transfer, 1993;36(13):3201–9.

[123]   Hancock RD, Bertagnolli KE and Lucht RP. Nitrogen and Hydrogen CARS Temperature Measurements in a Hydrogen/Air Flame Using a Near-Adiabatic Flat-Flame Burner. Combust. Flame 1997;109:323-331.

[124]   Hansen N, Miller JA, Klippenstein SJ, Westmoreland PR. and Kohse-Höinghaus K. Exploring Formation Pathways of Aromatic Compounds in Laboratory-Based Model Flames of Aliphatic Fuels. Combust.Expl. Shock Wave 2012;48:508–515.

[125]   Hanson RK. Combustion diagnostics: Planar imaging techniques. Symposium (int) combust. 1986;21:1677-1691.

[126]   Hardalupas Y and Orain M. Local measurements of the time-dependent heat release rate and equivalence ratio using chemiluminescent emission from a flame. Combust Flame 2004;139:188–207.

[127]   Hardaloupas Y, Orain M, Panoutsos CS, Taylor AMKP, Olofsson J, Seyfried H, Richter M, Hult J, Aldén M, Hermann F and Klignmann J. Chemiluminescence sensor for local equivalence ratio of reacting mixtures of fuel and air (FLAMESEEK). Appl Therm Eng 2004;241619–1632

[128]   Harris WE and Habgood HW. 1966Programmed Temperature Gas Chromatography (2nd Ed.) New York. John Wiley & Sons, Inc

[129]   Harrington JE and Smyth KC. Laser-induced fluorescence measurements of formaldehyde in a methane/air diffusion flame. Chem Phys Lett 1993;202:196-202

[130]   Hartlieb AT, Atakan B and Kohse-Höinghaus K, Temperature measurement in fuel-rich non-sooting low-pressure hydrocarbon flames, Appl. Phys. B 2000;70:435–445.

[131]   Handa T, Masuda M, Kashitani M and Yamaguchi Y. Measurement of number densities in supersonic flows using a method based on laser-induced acetone fluorescence. Exp Fluids 2011;50:1685–1694

[132]   Hassel EP and Linov S. Laser diagnostics for studies of turbulent combustion. Meas. Sci. Technol. 2000;11:37-57.

[133]   Heitor MV and Moreira ALN. Thermocouples and sample probes for combustion studies. Prog. Energy Combust. Sci. 1993:19;259-278

[134]   Hidaka Y, Sato K, Henmi Y, Tanaka H, Inami K. Shock-Tube study of methane pyrolysis and oxidation. Combust. Flame 1999; 118: 340–358.

[135]   Hilborn RC. Einstein coefficients, cros sections, f values, dipole moments, and all that. Am.J. Phys. 1982;50:982-986

[136]   Hollis OL. Separation of gaseous mixtures using porous polyaromatic polymer beads. Anal. Chem. 1966;38:309-316.

[137]   Hollis OL and Hayes WV. Water analysis by gas chromatography using porous polymer columns. J Gas Chromatogr 1966;4:235-239.

[138]   Holtappels P, Stimming U. Solid Oxide Fuel Cells (SOFC). In Handbook of Fuel Cells - Fundamentals, Technology and Applications, edited by W. Vielstich, A. Lamm and H.A. Gasteiger. Wiley 2003.

[139]   Holm T. Mechanism of the flame ionization detector II. Isotope effects and heteroatom effects. J Chromatograph A 1997;782:81-86.

[140]   Holm T. Mechanism of the flame ionization detector. J Chromatograph A 1999;842:221-227.

[141]   Hsu PH, Evans WD, Howell JR. Experimental and Numerical Study of Premixed Combustion within Nonhomogeneous Porous Ceramics. Comb Sci Tech 1993;90:149–72.

[142]   Howell JR, Hall MJ and Ellzey JL. Combustion of hydrocarbon fuels within porous inert media, Prog. Energy Combust. Sci. 1996;22:121–145.

[143]   Huang Y, Chao CYH and Cheng P. Effects of preheating and operations conditions on combustion in a porous medium. Int J Heat Mass Transfer, 2002;45:4315–4324.

[144]   Hui X, Kumar K, Sung C, Edwards T and Gardner D. Experimental studies on the combustion characteristics of alternative jet fuels. Fuel 2012;98:176-182.

[145]   Humer S, Frassoldati A, Granata S, Faravelli T, Ranzi E, Seider R and Seshadri K. Experimental and kinetic modeling study of combustion of JP-8, its surrogates and reference components in laminar nonpremixed flows. Proc Combust Inst 2007:31;393–400.

[146]   Ingle JDJ and Crouch SR. 1988. Spectrochemical Analysis, Prentice Hall, New Jersey

[147]   Jennings W, Mittlefehldt E and Stremple P. 1997. Analytical gas chromatography (2nd Ed.) Academic Press Ltd. San Diego California

[148]   Joensen F, Rostrup-Nielsen JR. Conversion of hydrocarbon and alcohols for fuel cells. J. Power Sources 2005; 105: 195–201.

[149]   Johnson MR, Kostiuk LW and Cheng RK. A Ring Stabilizer for Lean Premixed Turbulent Flames. Combust Flame 1998;114: 594–596

[150]   Jönsson JA (Ed). 1987. Chromatographic Theory and Basic Principles. Dekker

[151]   Jörg A, Meier U, Kienle R and Kohse-Höinghaus K. State-specific rotational energy transfer in OH ($A_2\Sigma+$, v'=0) by some combustion relevant Collision partners. Appl. Phys. B 1992;55:305-310.

[152]   Juchmann W, Latzel H, Shin DI, Peiter G, Dreier T, Volpp HR, Wolfrum J, Lindstedt RP and Leung KM. Absolute radical concentration measurements and modeling of low-pressure $CH_4/O_2/NO$ flames. Symposium (Int) on Combustion 1998;27:469–476

[153]   Kahandawala MSP, DeWitt MJ, Corporan E and Sidhu SS. Ignition and Emission Characteristics of Surrogate and Practical Jet Fuels. Energ Fuel 2008:22;3673–3679.

[154]   Kállai M, Veres Z and Balla, J. Response of flame ionization detectors to different homologous series. Chromatographia. 2001;54;511-517.

[155]   Kállai M and Balla, J. The effect of molecular structure upon the response of the flame ionization detector. Chromatographia. 2002;56;357-360.

[156]   Kállai M, Máté, V and Balla, J. Effects of experimental conditions on the determination of the effective carbon number. Chromatographia. 2003;57;639-644.

[157]   Keating EL.2007. Applied Combustion 2nd Ed. Taylor & Francis Group

[158]   Kee RJ, Rupley FM, Miller JA. Chemkin-II: A fortran chemical kinetics package for the analysis of gas-phase chemical kinetics. Sandia National Laboratories Report SAND 1991; 87-8215.

[159]   Kee RJ, Zhu H, Goodwin DG. Solid-oxide fuel cells with hydrocarbon fuels. Proc. Combust. Inst. 2005; 30: 2379–2404.

[160]   Kee RJ, Zhu H, Sukeshini AM, Jackson GS. Solid oxide fuel cells: operating principles, current challenges, and the role of syngas. Combust. Sci. Technol. 2008; 180: 1207–1244.

[161]   Keramiotis Ch, Vourliotakis G, Skevis G, Founti MA, Esarte C, Sánchez NE, Millera A, Bilbao R and Alzueta MU. Experimental and computational study of methane pyrolysis in a flow reactor under atmospheric pressure. Energy. 2012;43(1):103–110.

[162]   Keramiotis Ch, Stelzner B, Trimis D, Founti MA. Porous burners for low-emission combustion: An experimental investigation. Energy. 2012;45(1): 213–219.

[163]   Keshtkar MM and Gandjalikhan Nassab SA. Theoretical analysis of porous radiant burners under 2-D radiation field using discrete ordinates method. J Quant Spectrosc Ra 2009;110:1894-1907

[164]   Kiefer J, Weikl MC, Seeger T, Von Issendorff F, Beyrau F, Leipertz A. Non-intrusive gas-phase temperature measurements inside a porous burner using dual-pump CARS. Proc Comb Institute 2009;32:3123-9.

[165]   Kick Th, Herbst J, Kathrotia T, Marquetand J, Braun-Unkhoff M, Naumann C and Riedel U. An experimental and modeling study of burning velocities of possible future synthetic jet fuels. Energy 2012;43:111-123.

[166]   Kirchhoff and Bunsen. On chemical analysis by spectrum-observations. (Quarterly Journal of the Chemical Society of London) Q. J. Chem. Soc. 1861;13:270-289

[167]   Kiefer J, Tröger JW, Li Z, Seeger T, Alden M and Leipertz A. Laser-induced breakdown flame thermometry. Combust Flame (2012) dx.doi.org/10.1016/j.combustflame.2012.08.005

[168]   Kiefer J and Ewart P. Laser diagnostics and minor species detection in combustion using resonant four-wave mixing. Prog Energy Combust Sci 2011;37:525-564

[169]   Kienle R, Jörg A and Kohse-Höinghaus K. State to state rotational energy transfer in OH ($A_2\Sigma+$, $v'=1$) Appl. Phys. B 1993;56:249-258

[170]   Kohse Höinghaus K. Quantitative Laser-Induced Fluorescence: Some recent developments in combustion diagnostics. Appl. Phys. B 1990;50:455-461.

[171]   Kohse-Höinghaus K and Brockhinke A, Experimental and numerical methods for studying the flame structure Combust Expl. Shock Wave 2009;45:349–364.

[172]   Kohse Höinghaus K. and Jeffries JB. 2002. (Eds.), Applied Combustion Diagnostics, Taylor Francis, New York,

[173]   Kohse Höinghaus K., Laser techniques for the quantitative detection of reactive intermediates in combustion systems, Prog. Energy Combust. Sci. 1994;20:203-279

[174]   Kohse Höinghaus K, Barlow RS, Alden M and, Wolfrum J, Combustion at the focus: Laser Diagnostics and Control, Proc. Comb. Inst. 2005;30:89-123.

[175]   Kumar K and Sung CJ. A comparative experimental study of the autoignition characteristics of alternative and conventional jet fuel/oxidizer mixtures. Fuel 2010:89;2853–2863.

[176]   Kumar K, Sung CJ and Hui X. Laminar flame speeds and extinction limits of conventional and alternative jet fuels. Fuel 2011:90;1004–1011.

[177]   Kuo KK and Parr TP. 1994. Non-Intrusive Combustion Diagnostics. Begell House

[178]   Knaus DA, Sattler SS and Gouldin FC. Three-dimensional temperature gradients in premixed turbulent flamelets via crossed-plane Rayleigh imaging. CombustFlame 2005;141:253–270

[179]   Lacour C, Honore D, Boukhalfa A and Hauguel R. Stabilization mechanisms of laminar partially premixed from domestic like burner. Combust. Sci Tech. 2007;180-156-175

[180]   Lakshmanarao A, Renfro MW, King GB and Laurendeau NM. Acetone as a tracer for mixture fraction time-series measurements in turbulent non-reacting jets Exp Fluids 2001;30:595-596

[181]   Lammel G, Schweizer S and Renaud P. MEMS infrared gas spectrometer based on a porous silicon tunable filter. The 14th IEEE International Conference on Micro Electro Mechanical Systems, 2001:578-581.

[182]   Laurendeau NM. Temperature measurements by light-scattering methods. Prog. Energy Combust. Sci. 1988;14:147-170.

[183]   Lee DK and Maruta K. Heat recirculation effects on flame propagation and flame structure in a mesoscale tube. Combustion Theory and Modelling 2012;16: 507–536.

[184]   Linstrom PJ and Mallard WG. Eds., NIST Chemistry WebBook, NIST Standard Reference Database Number 69, June 2005, National Institute of Standards and Technology, Gaithersburg MD, 20899, (http://webbook.nist.gov)

[185]   Liso V, Olesen AC, Nielsen MP, Kær SK. Performance comparison between partial oxidation and methane steam reforming processes for solid oxide fuel cell (SOFC) micro combined heat and power (CHP) system. Energy 2011; 36: 4216-4226

[186]   Liu F, Guo H, Smallwood GJ, Gulder O. The chemical effects of carbon dioxide as an additive in an ethylene diffusion flame: Implications for soot and NOx formation. Combust. Flame 2001; 125: 778–787.

[187]   Liu JF, Hsieh WH. Experimental investigation of combustion in porous heating burners. Combust Flame 2004;138:295–303.

[188]   Lindstedt RP, Skevis G. Chemistry of acetylene flames. Combust. Sci. Technol. 1997;125: 73–137.

[189]   Lindstedt RP, Skevis G. Molecular growth and oxygenated species formation in laminar ethylene flames. Proc. Combust. Inst. 2000; 28: 1801-1807.

[190]   Loukou A, Frenzel I, Klein J and Trimis D. Experimental study of hydrogen production and sootparticulate matter emissions from methane rich-combustion in inert porous media. 2012;37:16686-16696

[191]   Lozano A, Yip B and Hanson RK. Acetone: a tracer for concentration measurements in gaseous flows by planar laser-induced fluorescence Exp Fluids 1992;13:369-376

[192]   Luft KF. Infrared techniques for the measurement of carbon monoxide. Ann. Occup. Hyg. 1975;18:45-51

[193]   Luque J and Crosley DR. "LIFBASE: Database and spectral simulation (version 1.5)", SRI International Report MP 99-009 (1999)

[194]   Mach Al. Entwicklung eines kompakten Heizsystems für Heizöl EL auf Basis der Verbrennung in porösen Keramiken, [dissertation]. Aachen, Germany: Universität Erlangen-Nürnberg; 2007.

[195]   Machano R. Numerical simulations of surface reaction in porous media with lattice Boltzmann. Chem Eng Sci 2012;69:628-643

[196]   Mahallawy FE and Habik SED 2002. Fundamentals and technology of combustion. Elsevier Science Ltd

[197]   Malico I, Zhou XY and Pereira JCF. Two dimensional numerical study of combustion and pollutants formation in porous burners. Combust Sci Tech. 2000:152;57-79

[198]   Mati K, Ristori A, Gail S, Pengoloan G and Daguat P. The oxidation of a diesel fuel at 1-10 atm experimental study in a JSR and detailed chemical kinetic modeling. Proc. Combust. Inst. 2007;31:2939-2946.

[199]   Mansour MS, Chen YC and Peters N. Highly Strained Turbulent Rich Methane Flames Stabilized by Hot Combustion Products. Combust Flame 1999;116:136-153

[200]   Masri AR, Dibble RW and Barlow RS. The structure of turbulent nonpremixed flames revealed by Raman-Rayleigh-LIF measurements. Prog. Energy Combust. Sci. 1996;22:307-362.

[201]   Marrocco M. Vibration–rotation interaction in time-resolved coherent anti-Stokes Raman scattering for gas-phase thermometry. J. Raman Spectrosc. 2012;43:621–626.

[202]   Martin AJP and Synge RLM. A new form of chromatogram employing two liquid phases. Biochem J. 1941;35:1358–1368

[203]   Mayunger F and Feldmann O (Eds.). 2001. Optical Measurements: Techniques and Applications, 2nd Edition, Springer- Verlag Berlin Heidelberg,

[204]   Maurice LQ, Lander H, Edwards T and Harrison WE. Advanced aviation fuels: a look ahead via a historical perspective. Fuel 2001:80;747-756.

[205]   McAllister S, Jyh-Yuan C and Fernandez-Pello AC. 2011. Fundamentals of combustion processes. Springer New York

[206]   McNair HM and Miller JM. 1998. Basic gas chromatography. New York. John Willey & Sons, Inc.

[207]   McWilliam IG and Dewar RA, Nature 1958;181:760

[208]   Medwell PR, Kalt PAM, Dally BB. Simultaneous imaging of OH, formaldehyde, and temperature of turbulent nonpremixed jet flames in a heated and diluted coflow. Combustion and Flame 2007;148:48-61.

[209]   Mendes MAA, Pereira JMC, Pereira JCF. A numerical study of the stability of one-dimensional laminar premixed flames in inert porous media. Combust Flame 2008;153:525–539.

[210]   Mendes MAA, Pereira JMC, Pereira JCF. Calculation of premixed combustion within inert porous media with model parametric uncertainty quantification. Combust Flame 2011;158: 466–476.

[211]   Mendiara MT, Oxidación de hollín (soot) obtenido por pirólisis de hidrocarburos gaseosos y su interacción con NO, Doctoral Thesis, Zaragoza, Spain, 2006

[212]   Mercier X, Therssen E, Pauwels F and Desgroux P. Quantitative Features and Sensitivity of Cavity Ring-Down. Combust. Flame 2001;125:656 – 667.

[213]   Mercier X, Wartel M, Pauwels JF and Desgroux P. Implementation of a new spectroscopic method to quantify aromatic species involved in the formation of soot particles in flames. Appl. Phys. B 2008;91:387–395.

[214]   Micka DJ and Driscoll JF. Stratified jet flames in a heated (1390 K) air cross-flow with autoignition. Combust Flame 2012;159:1205-1214

[215]   Migliorini F, De Iuliis S, Cignoli F and Zizak G. How "flat" is the rich premixed flame produced by your McKenna burner?. Combust Flame 2008;153:384-393

[216]   Miller JA and Bowman CT. Mechanism and modeling of nitrogen chemistry in combustion. Prog. Energy Combust Sci 1989;15:287-338.

[217]   Mishra SC, Steven M, Nemoda S, Talukdar P, Trimis D, Durst F. Heat transfer analysis of a two-dimensional rectangular porous radiant burner. Heat Mass Transfer 2006;33:467–474.

[218]   Mishra TK, Datta A and Mukhopadhyay A. Comparison of the structures of methane-air and propane-air premixed flames. Fuel 2006;85:1254-1263

[219]   Mishra TK, Datta A and Mukhopadhyay A. Concentration measurements of selected hydrocarbons in methane/air partially premixed flames using gas chromatography. Int. J. Therm. Sci. 2005;44:1078-1089

[220]   Momirlan M, Veziroglu TN. Current status of hydrogen energy. Renew. Sustain. Energy Rev. 2002; 6: 141–179.

[221]   Moses CA and Roets PNJ. Properties, Characteristics, and Combustion Performance of Sasol Fully Synthetic Jet Fuel. J Eng. Gas Turb Power 2009:131;041502-17.

[222]   Moss JB and Aksit IM. Modelling soot formation in a laminar diffusion flame burning a surrogate kerosene fuel. Proc. Combust. Inst 2007:31(2);3139–3146

[223]   Mößbauer S, Pickenäcker O, Trimis D. Application of the porous burner technology in energy- and heat-engineering, In: Proceedings of the fifth international conference on technologies combustion for a clean environment (Clean Air V), Lisbon, 1999. p. 519–23.

[224]   Moffat RJ. Describing the uncertainties in experimental results. Exp Therm Fluid Sci 1988;1:3-17

[225]   Modest MF. Radiative heat transfer. Academic Press; 2003.

[226]   Mokhov AV and Levinsky HB. A LIF and CARS study of the effects of upstream heat loss on NO formation from laminar premixed burner-stabilized natural-gas/air flames. Symposium (Int) on Combustion 1996;26:2147–2154

[227]   Mokhov AV and Levinsky HB. NO formation in a burnout region of a partially premixed methane-air flame with upstream heat loss. Combust Flame 1999;118:733-740

[228]   Mujeebu MA, Abdullah MZ, Bakar MZA, Mohamad AA, Abdullah MK. Applications of porous media combustion technology - A review. Appl Energ. 2009;86:1365–1375.

[229]   Mujeebu MA, Abdullah MZ, Bakar MZA, Mohamad AA, Abdullah MK. Combustion in porous media and its applications - A comprehensive survey. J Environ Manage. 2009;35: 216–230.

[230]   Muthukumar P, Shyamkumar PI. Development of novel porous radiant burners for LPG cooking applications. Fuel (2011), doi:10.1016/j.fuel.2011.09.006.

[231]   Naik CV, Puduppakkam KV, Modak A, Meeks E, Wang YL, Feng Q and. Tsotsis TT. Detailed chemical kinetic mechanism for surrogates of alternative jet fuels. Combust. Flame 2011:158;434-445.

[232]   Natelson RH, Johnson RO, Kurman MS, Cernansky NP, Miller DL. Comparison of reactivity in a flow reactor and a single cylinder engine. Exp. Therm. Fluid. Sci. 2010; 34: 928–932.

[233]   Nau P, Krüger J. Lackner A, Letzgus M and Brockhinke A. On the quantification of OH*, CH*, and C_2* chemiluminescence in flames. Appl Phys B 2012;107:551–559.

[234]   Nguyen DN, Ishida H and Shioji M. Ignition and Combustion Characteristics of Gas-to-Liquid Fuels for Different Ambient Pressures. Energ Fuel 2010:24;365-374

[235]   Nemoda S., Trimis D., Zivkovic G., Numerical simulation of porous burners and hole plate surface burners, Thermal Science, Vol. 8, No. 1, pp. 3-17, 2004

[236]   Nogenmyr KJ, Kiefer J Li ZS Bai XS and Aldén M. Numerical computations and optical diagnostics of unsteady partially premixed methane/air flames. Combust Flame 2010;157:915-924

[237]   Norton TS, Smyth KS , Miller JH and Smooke MD. Comparison of Experimental and Computed Species Concentration and Temperature Profiles in Laminar, Two-Dimensional Methane/Air Diffusion Flames Combust Sci Technol 1993;90:1-34

[238]   Olsvik O, Rokstad, Holmen A. Pyrolysis of methane in the presence of hydrogen. Chem. Eng. Technol. 1995; 18: 349–358.

[239]   Pan HL., Pickenäcker O and Trimis D. Characterization of pore diameters in highly porous media, in Proceedings of 2003 ASME Summer Heat Transfer Conference, Las Vegas, Nevada, USA, July 2003

[240]   Paschotta R. 2008. Encyclopedia of Laser Physics and Technology. John Willey & Sons. New York.

[241]   Pastore A, Mastorakos E. Syngas production from liquid fuels in a non-catalytic porous burner. Fuel 2011;90:64–76.

[242]   Pedersen-Mjaanes H, Chan L, Mastorakos E. Hydrogen production from rich combustion in porous media. Int J Hydrogen Energ 2005;30:579–592.

[243]   Penner SS, Wang CP and Bahadori MY. Laser diagnostics applied to combustion systems. Symposium (Int) Combust. 1984;20:1149-1176.

[244]   Pereira JCF, Malico I, Hayashi TC and Raposo J. Experimental and numerical characterization of the traverse dispersion at the exit of a short ceramic foam inside a pipe. Int J Heat Mass Tran 2005:48;1-14

[245]   Pereira FM, Oliveira, AAM and Fachini FF. Maximum superadiabatic temperature for stabilized flames within porous inert media. Combust Flame 2011;158:2283-2288.

[246]   Pitz RW, Wehrmeyer JA, BowlingJM and Cheng TS. Single pulse vibrational Raman scattering by a broadband KrF excimer laser in a hydrogen/air flame. Appl. Opt. 1990;29:2325–2332.

[247]   Pfadler S, Löffler M, Dinkelacker F and Leipertz A. Measurement of the conditioned turbulence and temperature field of a premixed Bunsen burner by planar laser Rayleigh scattering and stereo particle image velocimetry. Exp Fluids 2005;39: 375–384

[248]   Pickenäcker O, Pickenäcker K, Wawrzinek K, Trimis D, Pritzkow WEC, Müller C, et al. Innovative ceramic materials for porous-medium burners. Interceram 1999;48:326–30.

[249]   Pickenäcker O, Pickenäcker K, Wawrzinek K, Trimis D, Pritzkow WEC, Müller C, et al. Innovative ceramic materials for porous-medium burners II. Interceram 1999;48:424–33.

[250]   Pitz RW, Wehrmeyer JA, BowlingJM and Cheng TS. Single pulse vibrational Raman scattering by a broadband KrF excimer laser in a hydrogen/air flame. Appl. Opt. 1990;29:2325–2332.

[251]   Plessing T, Terhoeven P, Peters N and Mansour MS. An experimental and numerical study of a laminar triple flame. Combust Flame. 1998;115:335–353

[252]   Poddar NB, Thomas S and Wornat MJ. Polycyclic aromatic hydrocarbons from the co-pyrolysis of 1,3-butadiene and propyne. Proc. Comb. Inst. (2012) doi:10.1016/j.proci.2012.05.013

[253]   Poling BE, Prausnitz JM and O'Connell JP. The Properties of Gases and Liquids, McGraw-Hill, 2001

[254]   Rabenstein G, Hacker V. Hydrogen for fuel cells from ethanol by steam-reforming, partial-oxidation and combined auto-thermal reforming: A thermodynamic analysis. J. Power Sources 2008; 185: 1293–1304.

[255]   RAL gGmbH, Low-emission and Energy-saving Gas-fired Calorific-Value Heating Devices, RAL-UZ 61, Sankt Augustin, Deutschland, 2011.

[256]   Richards GA, McMillian MM, Gemmen RS, Rogers WA and Cully SR. Issues for low emission, fuel flexible power systems. Prog Energy Combust Sci 200;27:141–169.

[257]   Rye L, Blakey S and Wilson C. Sustainability of supply or the planet: a review of potential drop-in alternative aviation fuels. Energ Environ Sci. 2010:3;17-27

[258]   Rye L and Wilson C. The influence of alternative fuel composition on gas turbine ignition performance. Fuel 2012:96;277–283

[259]   Rørtveit GJ, Zepter K, Skreiberg Ø, Fossum M, Hustad JE. Comparison of low-NOx burners for combustion of methane and hydrogen mixtures. Proc Comb Institute 2002;29:1123–9.

[260]   Rothe EW and Andersen P. Application of tunable excimer lasers to combustion diagnostics: a review. Appl. Opt. 1997;36:3971-4033.

[261]   Ruiz MP, Guzmán de Villoria R, Millera A, Alzueta MU, Bilbao R. Influence of different operation conditions on soot formation from C2H2 pyrolysis, Ind Eng Chem Res 2007;46:7550–7560.

[262]   Rumminger MD, Dibble RW, Heberle NH, Crosley DR. Gas temperature above a porous radiant burner: Comparison of measurements and model predictions. Symp (Int) Comb 1996;26:1755-62.

[263]   Saffaripour M, Zabeti P, Kholghy M and Thomson MJP. An experimental comparison of the sooting behaviour of synthetic jet fuels. Energ Fuel 2011:25(12);5584–5593

[264]   Saffaripour M, Kholghy M, Dworkin SB and Thomson MJP. A numerical and experimental study of soot formation in a laminar coflow diffusion flame of a Jet A-1 surrogate. Proc. Combust. Inst. J.proci.2012.06.176

[265]   Sánchez NE, Callejas A, Millera Á, Bilbao R and Alzueta MU. Determination of Polycyclic Aromatic Hydrocarbons (PAH) Absorbed on Soot Formed in Pyrolysis of Acatylene at Different Temperatures, Chemical Engineering Transactions 2010;22:131–136

[266]   Sánchez NE, Callejas A, Millera Á, Bilbao R and Alzueta MU. Formation of PAH and soot during acetylene pyrolysis at different gas residence times and reaction temperatures. Energy. 2012;43(1):30–36.

[267]   Sánchez NE, Callejas A, Millera Á, Bilbao R and Alzueta MU. Polycyclic Aromatic Hydrocarbon (PAH) and Soot Formation in the Pyrolysis of Acetylene and Ethylene: E ff ect of the Reaction Temperature. Energy Fuels 2012;26:4823-4829.

[268]   Sarathy SM, Westbrook CK, Mehl M, Pitz WJ, Togbe C, Dagaut P, Wang H, Oehlschlaeger MA, Niemann U, Seshadri K, Veloo PS, Ji C, Egolfopoulos FN and Lu T. Comprehensive chemical kinetic modeling of the oxidation of 2-methylalkanes from C_7 to C_{20}. Combust Flame 2012;158:2338-2357.

[269]   Sathe SB, Kulkarni MR, Peck RE, Tong TW. An experimental and theoretical study of porous radiant burner performance. Symp (Int) Comb 1991;23:1011–8.

[270]   Schießwohl E, von Unwerth T, Seyfried, F, Brüggemann D. Experimental investigation of parameters influencing the freeze start ability of a fuel cell system. J Power Sources 2009;193:107-115

[271]   Schmid U, Seidel H, Mueller G and Becker Th. Theoretical considerations on the design of a miniaturized paramagnetic oxygen sensor. Sensors Actuators B 2006;116:213–220.

[272]   Schneider Ch, Dreizler A, Janicka J and Hassel EP. Flow field measurements of stable and locally extinguishing hydrocarbon-fuelled jet flames. Combust Flame 2003;135:185–190

[273]   Schwar MJR and Weinberg FJ. Laser techniques in combustion research. Combust. Flame. 1969;13:335–374

[274]   Schulz C and Sick V. Tracer-LIF diagnostics: quantitative measurement of fuel concentration, temperature and fuel/air ratio in practical combustion systems. Prog Energ Combust Sci 2005;31:75–121

[275]   Schulz W, Weber H and Poprawe R. 2008. Laser Physics and Applications–B: Laser Systems. Springer-Verlag, Berlin, Heidelberg, New York

[276]   Schneider Ch, Dreizler A, Janicka J and Hassel EP. Flow field measurements of stable and locally extinguishing hydrocarbon-fuelled jet flames. Combust Flame 2003;135:185–190

[277]   Schwar MJR and Weinberg FJ. Laser techniques in combustion research. Combust. Flame. 1969;13:335–374

[278]   Scott RPW. 1996. Chromatographic detectors; Design, function and operation. Marcel Dekker, INC. New York Basel

[279]   Scott RPW. 1998. Introduction to Analytical Gas Chromatography (2nd Ed.) Marcel Dekker, INC. New York Basel

[280]   Scott RPW. 2003. Principles and practice of chromatography. Chrom-Ed Book Series, *Libraryforscience, LLC.*

[281]   Scott RPW. 2003. Gas chromatography Detectors. Chrom-Ed Book Series, *Libraryforscience, LLC.*

[282]   Schofield K. The enigmatic mechanism of the flame ionization detector: Its overlooked implications for fossil fuel combustion modeling. Prog Energ Combust Sci. 2008;34:330-350

[283]   Seeger T and Leipertz A. Experimental comparison of single-shot broadband vibrational and dual-broadband pure rotational coherent anti-Stokes Raman scattering in hot air. Appl Optics 1996;35:2665-2671.

[284]   Sepman AV, van Essen VM, Mokhov AV and Levinsky HB. The effects of hydrogen addition on Fenimore NO formation in low-pressure, fuel-rich-premixed, burner-stabilized $CH_4/O_2/N_2$ flames Int J Hydrogen Energy 2008;331957–1964

[285]   Shaddix CR and Smyth KC. Laser-induced incandescence measurements of soot production in steady and flickering methane, propane, and ethylene diffusion flames. Combust. Flame 1996; 107:418-452.

[286]   Sheng CY and Dean AM. Importance of gas-phase kinetics within the anode channel of a solid-oxide fuel cell. J Phys Chem A. 2004;108:3772-3783

[287]   Shi JR, Xie MZ, Liu H, Liu HS, Zhang XS and Xu YN. Two-dimensional numerical study of combustion and heat transfer in porous media combustor-heater. Proc Comb Institute 2011;33:3309-3316.

[288]   Singhal SC, Kendall K. High-Temperature Solid Oxide Fuel Cells: Fundamentals, Design and Applications. Elsevier Science, Amsterdam (2004).

[289]   Slavinskaya N, Frank P. A modelling study of aromatic soot precursors formation in laminar methane and ethene flames. Combust. Flame 2009; 156: 1705–1722.

[290]   Slemr J, Slemr F, D'Souza H and Partiridge R. Study of relative response factors of various gas chromatograph-flame ionization detector systems for measurements of C2-C9 hydrocarbons in air. J Chromatograph A 2004;1061:75-84

[291]   Smucker MT, Ellzey JL. Computational and experimental study of a two section porous burner. Comb Sci Tech 2004;176:1171–89.

[292]   Smyth KC, Miller JH, Dorfman RC, Mallard WG and Santoro RJ. Soot inception in a methane/air diffusion flame as characterized by detailed species profiles. Combust Flame 1985;62:157-181

[293]   Smyth KC. NO production and destruction in a methane/air diffusion flame. Combust Sci Tech 1996;115:151-176

[294]   Stelzner B, Hunger F, Voss S, Keller J, Hasse C and Trimis D. Experimental and numerical study of rich inverse diffusion flame structure. Proc. Combust. Institute 2012 dx.doi.org/10.1016/ j.proci.2012.06.153

[295]   Stelzner B, Keramiotis Ch, Voß S, Werner M, Founti MA, Trimis D. Experimental Study of the Flame Structure inside a Porous Inert Medium Burner using Planar Laser Induced Fluorescence. In: Adrian RJ, Durão DFG, Hishida K, Moreira ALN, Tropea C, editors. Proceedings of the 15th International Symposium on Applications of Laser Techniques to Fluid Mechanics; 2010 July 05-08; Lisbon, Portugal.

[296]   Stuke M. (ed.), 1992. Dye lasers: 25 Years. Springer Verlag Berlin Heidelberg

[297]   Sun Qi, Tang Y, Gavalas GR. Methane pyrolysis in a hot filament reactor. Energy Fuels 2000; 14: 490– 494.

[298]   Supina WR. 1974. The packed column in gas chromatography, Supelco, Inc., Bellefonte, PA

[299]   Sutton G, Levick A, Edwards G and Greenhalgh D. A combustion temperature and species standard for the calibration of laser diagnostic techniques. Combust Flame 2006;147;39–48

[300]   Sutton JA Williams BA and Fleming JW. Laser-induced fluorescence measurements of NCN in low-pressure $CH_4/O_2/N_2$ flames and its role in prompt NO formation. Combust. Flame 2008;153:465-478.

[301]   Suvernev AA, Dreizler A, Dreier T and WolfrumJ. Polarization-spectroscopic measurement and spectral simulation of OH ($A^2\Sigma$-$X^2\Pi$) and NH($A^3\Sigma$-$X^3\Pi$) transitions, Appl. Phys. B 1995;61:421–427

[302]   Takeno T, Sato K and Hase K. A theoretical study on an excess enthalpy flame. Symp (Int) Comb 1981;18:465–472.

[303]   Takeshita T and Yamaji K. Important roles of Fischer– Tropsch synfuels in the global energy future. Energy Policy 2010:36;2773–2784.

[304]   Taylor JR. 1997. Introduction to error analysis (2nd ed.) University Science Books. Sausalito California

[305]   Tan Y, Dagaut P, Cathonnet M, Boettner JC. Pyrolysis, oxidation and ignition of C1 and C2 hydrocarbons - Experiments and modeling. J. Chim. Phys. PCB 1995; 92:726–746.

[306]   Tan Y, Dagaut P, Cathonnet M, Boettner JC. Oxidation and ignition of methane-propane and methane-ethane-propane mixtures: Experiments and modeling. Comb. Sci. Technol. 1994; 103:133–151.

[307]   Thurber MC, Grisch F, Kirby BJ, Votsmeier M and Hanson RK, Measurements and Modeling of Acetone Laser-Induced Fluorescence with Implications for Temperature-Imaging Diagnostics. Appl Opt 1998;37:4963-4978

[308]   Thurber MC and Hanson RK, Pressure and composition dependences of acetone laser-induced fluorescence with excitation at 248, 266, and 308 nm. Appl Phys B 1999;69:229–240

[309]   Timko MT, Yu Z, Onasch TB, Wong HW, Miake-Lye RC, Beyersdorf AJ, Anderson BE, Thornhill KL, Winstead EL, Corporan E, DeWitt MJ, Klingshirn CD, Wey C, Tacina K, Liscinsky DS,

Howard R and Bhargava A. Particulate Emissions of Gas Turbine Engine Combustion of a Fischer–Tropsch Synthetic Fuel. Energ Fuel 2010:24(11);5883–5896.

[310]   Träger F (Ed.). 2007. Springer handbook of laser and optics. Springer Science & Business Media, LLC New York.

[311]   Trimis D, Durst F. Combustion in a Porous Medium-Advances and Applications. Comb Sci Tech 1996;121:153–68.

[312]   Tropea C, Yarin AL and Foss JF. (Eds.). 2007. Springer Handbook of Experimental Fluid Mechanics. Springer-Verlag Berlin Heidelberg

[313]   Tswett M. Adsorptionanalyse und chromatographische Methode. Anwendung auf die Chemie des Chlorophylls (Adsorption analysis and chromatographic method. Application to the chemistry of chlorophyll.), *Berichte der Deutschen botanischen Gesellschaft*, 1906:24;384–393.

[314]   Turbiez A, Bakali El, Pauwels JF, Rida A and Meunier P. Experimental study of low pressure stoichiometric premixed methane, methane/ethane, methane/ethane/propane and synthetic natural gas flames. Fuel 2004;83:933-941

[315]   Upatnieks A, Driscoll JF, Rasmussen, CC and Ceccio SL. Liftoff of turbulent jet flames—assessment of edge flame and other concepts using cinema-PIV. Combust Flame 2004;138: 259–272

[316]   Varbanov P, Klemeš J. Analysis and integration of fuel cell combined cycles for development of low-carbon energy technologies. Energy. 2008; 33: 1508-1517

[317]   Videto BD and Santavicca DA. Flame-Turbulence Interactions in a Freely-Propagating, Premixed Flame. Comb Sci Tech. 1990;70:47-73.

[318]   Voß S, Steinbrück R, Kautz M, Schießwohl E, Arendt M, Tom Felde J, Volkert J and Trimis D. Premixed hydrogen-air combustion system for fuel cell systems. Int J Hydrogen Energy 2011;36:3697-3703

[319]   Voß S and Trimis D. Investigation of a combined flame trap- and mixing- system as surface burner support for lean hydrogen air combustion. In: De Azevedo T, Weber R, Tognotti L, editors. Proceedings of the 10th Conference on Energy for a Clean Environment; 2009 July 07-09; Lisbon, Portugal.

[320]   Vourliotakis G. Development and implementation of detailed chemical kinetics tools for performance and emissions assessment of domestic SOFC systems. PhD thesis, Athens 2012

[321]   Vourliotakis G, Skevis G, Founti MA, Al-Hamamre Z, Trimis D. Detailed kinetic modelling of the T-POX reforming process using a reactor network approach. Int J Hydrogen Energy 2008;33:2816–2825

[322]   Vourliotakis G, Skevis G, Founti MA. A detailed kinetic modelling study of benzene oxidation and combustion in premixed flames and ideal reactors. Energy Fuels 2011; 25: 1950–1963.

[323]   Vourliotakis G, Skevis G, Founti MA. Combustion chemistry aspects of alternative fuels reforming for high-temperature fuel cell applications. Int J Hydrogen Energy 2012;37:16649–16662

[324]   Walters KM, Dean AM, Zhu H and Kee RJ. Homogeneous kinetics and equilibrium predictions of coking propensity in the anode channels of direct oxidation solid-oxide fuel cells using dry natural gas. J Power Sources. 2003;123:182-189

[325] Warnatz J, Ulrich Maas U and Dibble RW. 2006. Combustion: Physical and Chemical Fundamentals, Modeling and Simulation, Experiments, Pollutant Formation (4th Ed.). Springer-Verlag Berlin Heidelberg

[326] Wang CH, Crowder JG, Mannheim V, Ashley T, Dutton DT, Johnson AD, Pryce G. and Smith SD. Detection of nitrogen dioxide using a room temperature operation mid-infrared lnSb light emitting diode. Electronics Letters 1998;35:300-301

[327] Wang H and Oehlschlaeger MA Autoignition studies of conventional and Fischer–Tropsch jet fuels Fuel 2012;98:249-258

[328] Werner M. Experimentelle Untersuchungen zur teil-vorgemischten Verbrennung von Wasserstoff-Luftgemischen. Diplomarbeit Technische Universität Bergakademie Freiberg, Freiberg, Deutschland, 2009

[329] Weikl MC, Tedder SA, Seeger T, Leipertz A. Investigation of porous media combustion by coherent anti-Stokes Raman spectroscopy. Exp Fluids 2010;49:775–81.

[330] Weinberg FJ. Combustion Temperatures: The Future?. Nature. 1971:233;239–241.

[331] Weinberg FJ. The first half million years of combustion research and today's burning problems Symp (Int) Comb 1975;1:1–17

[332] Wierzchowski PT and Wieslaw Zatorski L. Determination of Cyclo C_6 and C_7 peroxides and hydroperoxides by gas chromatography. Chromatographia. 2000;51;83-86

[333] Wolfrum J. Lasers in combustion: From basic theory to practical devices. Proc. Combust. Institute 1998;27:1-41

[334] Wolfrum J. Advanced laser spectroscopy in combustion chemistry: From elementary steps to practical devices. Faraday Discuss. 2002;119:1-26.

[335] Wood S, Harris AT. Porous burner for lean-burn applications. Prog Energy Combust Sci 2008;34:667–84.

[336] Wood S, Fletcher DF, Stephen DJ, Dawson A and Harris AT. Design and evaluation of a porous burner for the mitigation of anthropogenic methane emissions. Environ. Sci Technol 2009;43:9329-9334.

[337] Wu T, Huang Z, Zhang WG, Fang JH and Yin Q. Physical and Chemical Properties of GTL - Diesel Fuel Blends and Their Effects on Performance and Emissions of a Multicylinder DI Compression Ignition Engine. Energ Fuel 2007:21;1908-1914

[338] Wu D, Liu H, Xie M, Liu M and Sun W. Experimental investigation on low velocity filtration combustion in porous packed bed using gaseous and liquid fuels. Exp Therm Fluid Sci 2012;36:169-177.

[339] Wunning JA, Wunning JG. Flameless oxidation to reduce thermal NO-formation. Prog Energy Combust Sci, 1997;29:81–94.

[340] Xuan J, Leung MKH Leung DYC, Meng N. A review of biomass-derived fuel processors for fuel cell systems. Renew. Sust. Energ. Rev. 2009; 13: 1301–1313.

[341] Yang B, Li Y, Wei L, Huang C, Wang J, Tian Z, Yang R, Sheng L, Zhang Y, Qi F. Proc Combust Inst 2007;31:555–563.

[342] Yamamoto K, Ozeki M, Hayashi N and Yamashita H. Burning velocity and OH concentration in premixed combustion. Proc. Combust. Institute 2009;32:1227-1235.

[343] Yamamoto K, Isii S and Ohnishi M. Local flame structure and turbulent burning velocity by joint PLIF imaging. Proc. Combust. Inst. 2011;33:1285-1292.

[344]   Yip B., Miller M. F., Lozano A., Hanson R. K., A combined OH/acetone planar laser-induced fluorescence imaging technique for visualizing combusting flows, Exp Fluids, 1994:17;330-336

[345]   Zhang Y, Yoon Y, Kelly P and Kennedy IM. LIF measurements of atomic arsenic in hydrogen and methane diffusion flames. Proc. Combust. Institute 1998;27:1777-1783

[346]   Zhang X, Chan SH, Li G, Ho HK, Li J, Feng Z. A review of integration strategies for solid oxide fuel cells. J. Power Sources 2010; 195: 685-702.

[347]   Zhao H and Ladommatos N. Optical diagnostics for in-cylinder mixture formation measurements in IC engines. Prog. Energy Combust. Sci. 1998;24:297–336

[348]   Zhao FQ and Hiroyasu H. The application of laser Rayleigh scattering to combustion diagnostics. Prog. Energy Combust. Sci. 1993;19:447-485.

[349]   Zheng C, Cheng L, Saveliev A, Luo Z, Cen K. Gas and solid phase temperature measurements of porous media combustion. Proc Comb Institute 2011;33:3301–3308.

[350]   Zhou XY, Pereira JCF. Comparison of Four Combustion Models for Simulating the Premixed Combustion in Inert Porous Media. Fire Mater 1998;22:187–97.

[351]   Zink F, Lu Y, Schaefer L. A solid oxide fuel cell system for buildings. Energy Convers. Manage. 2007; 48: 809–818.